

1985

The Use Of Probabilistic Multiphase Flow Equations In The Study Of The Hydrodynamics And Heat Transfer In Gas-solids Suspensions

Douglas Walter Muzyka

Follow this and additional works at: <https://ir.lib.uwo.ca/digitizedtheses>

Recommended Citation

Muzyka, Douglas Walter, "The Use Of Probabilistic Multiphase Flow Equations In The Study Of The Hydrodynamics And Heat Transfer In Gas-solids Suspensions" (1985). *Digitized Theses*. 1461.
<https://ir.lib.uwo.ca/digitizedtheses/1461>

This Dissertation is brought to you for free and open access by the Digitized Special Collections at Scholarship@Western. It has been accepted for inclusion in Digitized Theses by an authorized administrator of Scholarship@Western. For more information, please contact tadam@uwo.ca, wlsadmin@uwo.ca.

The author of this thesis has granted The University of Western Ontario a non-exclusive license to reproduce and distribute copies of this thesis to users of Western Libraries. Copyright remains with the author.

Electronic theses and dissertations available in The University of Western Ontario's institutional repository (Scholarship@Western) are solely for the purpose of private study and research. They may not be copied or reproduced, except as permitted by copyright laws, without written authority of the copyright owner. Any commercial use or publication is strictly prohibited.

The original copyright license attesting to these terms and signed by the author of this thesis may be found in the original print version of the thesis, held by Western Libraries.

The thesis approval page signed by the examining committee may also be found in the original print version of the thesis held in Western Libraries.

Please contact Western Libraries for further information:

E-mail: libadmin@uwo.ca

Telephone: (519) 661-2111 Ext. 84796

Web site: <http://www.lib.uwo.ca/>

CANADIAN THESES ON MICROFICHE

THÈSES CANADIENNES SUR MICROFICHE



National Library of Canada
Collections Development Branch

Canadian Theses on
Microfiche Service

Ottawa, Canada
K1A 0N4

Bibliothèque nationale du Canada
Direction du développement des collections

Service des thèses canadiennes
sur microfiche

NOTICE

The quality of this microfiche is heavily dependent upon the quality of the original thesis submitted for microfilming. Every effort has been made to ensure the highest quality of reproduction possible.

If pages are missing, contact the university which granted the degree.

Some pages may have indistinct print especially if the original pages were typed with a poor typewriter ribbon or if the university sent us an inferior photocopy.

Previously copyrighted materials (journal articles, published tests, etc.) are not filmed.

Reproduction in full or in part of this film is governed by the Canadian Copyright Act, R.S.C. 1970, c. C-30. Please read the authorization forms which accompany this thesis.

**THIS DISSERTATION
HAS BEEN MICROFILMED
EXACTLY AS RECEIVED**

AVIS

La qualité de cette microfiche dépend grandement de la qualité de la thèse soumise au microfilmage. Nous avons tout fait pour assurer une qualité supérieure de reproduction.

S'il manque des pages, veuillez communiquer avec l'université qui a conféré le grade.

La qualité d'impression de certaines pages peut laisser à désirer, surtout si les pages originales ont été dactylographiées à l'aide d'un ruban usé ou si l'université nous a fait parvenir une photocopie de qualité inférieure.

Les documents qui font déjà l'objet d'un droit d'auteur (articles de revue, examens publiés, etc.) ne sont pas microfilmés.

La reproduction, même partielle, de ce microfilm est soumise à la Loi canadienne sur le droit d'auteur, SRC 1970, c. C-30. Veuillez prendre connaissance des formules d'autorisation qui accompagnent cette thèse.

**LA THÈSE A ÉTÉ
MICROFILMÉE TELLE QUE
NOUS L'AVONS REÇUE**

Canada

THE USE OF PROBABILISTIC MULTIPHASE
FLOW EQUATIONS IN THE STUDY OF THE
HYDRODYNAMICS AND HEAT TRANSFER
IN GAS-SOLIDS SUSPENSIONS

by
Douglas Walter Muzyka
Faculty of Engineering Science

Submitted in partial fulfillment
of the requirements for the degree of
Doctor of Philosophy

Faculty of Graduate Studies
The University of Western Ontario
London, Ontario
January 1985

© Douglas Walter Muzyka 1985

LIST OF FIGURES (continued)

<u>Figure</u>	<u>Description</u>	<u>Page</u>
6.8	Pressure drop versus $\bar{\alpha}_s$: Series B-1	226
6.9	Pressure drop versus $\bar{\alpha}_s$: Series B-2,B-5	227
6.10	Pressure drop versus $\bar{\alpha}_s$: Series B-4,B-7	228
6.11	Pressure drop versus $\bar{\alpha}_s$: Series B-3,B-6	229
6.12	Pressure drop versus $\bar{\alpha}_s$: Series C-1	230
6.13	Pressure drop versus $\bar{\alpha}_s$: Series C-2,C-5	231
6.14	Pressure drop versus $\bar{\alpha}_s$: Glass beads	232
6.15	Slopes of Pressure drop vs. Mean solids concentration curves as a function of gas velocity: SERIES B	237
6.16	Slopes of Pressure drop vs. Mean solids concentration curves as a function of gas velocity: SERIES C	238
6.17	Slopes of Pressure drop vs. Mean solids concentration curves as a function of gas velocity: SERIES D (Glass beads)	239
6.18	Solids flowrate versus Mean solids concentration: SERIES B-3,B-5,B-7	241
6.19	Solids flowrate versus Mean solids concentration: SERIES B-2,B-4,B-6	242
6.20	Solids flowrate versus Mean solids concentration: SERIES C-2,C-3,C-5	243
6.21	Solids flowrate versus Mean solids concentration: Glass bead runs	244
6.22	Mean solids velocity versus Mean gas velocity: Series B and C	246
6.23	Mean solids velocity versus Mean gas velocity: Series D (Glass beads)	247
6.24	Suspension pressure drop as a function of Loading ratio: Typical SERIES B results	249

were independent of the mean solids concentration in dilute flows. This conclusion and an asymptotic analysis of the energy equations allowed the development of a general expression for the variation of fully developed heat transfer coefficients as a function of loading ratio. Heat transfer coefficient ratios were predicted to either increase, decrease, or pass through a minimum and then increase depending on the relative magnitudes of three coefficients which are fully determined by the hydrodynamics of the system. The general predicted variation was confirmed experimentally and numerical values of the hydrodynamic coefficients were determined.

ACKNOWLEDGEMENTS

This work was undertaken at the Département de Genie Chimique, Université de Technologie de Compiègne, France as part of a scientific exchange programme with the University of Western Ontario. Gratitude is expressed to the coordinators of the exchange programme, Professors M.A. Bergougnou (Western) and J.P. Large (Compiègne) who acted as joint thesis supervisors for making this undertaking possible and for their helpful suggestions during the course of the work.

Cette thèse, ainsi que tout mon séjour en France, a été très marquée par l'influence de mon collègue et ami, Yuri Molodtsov. La possibilité de faire sa connaissance a va lu, seule, le voyage.

Dave Young is thanked for his help with some of the early experimental work. Plus tard, Daniel Eschoriheula a effectué de nombreuses expériences. Il est remercié pour cela ainsi que pour l'aide qu'il a apportée à la résolution de problèmes techniques sur l'installation. Pierre Blavier est remercié pour son apport technique.

Marion Birck a tapé et retapé cette thèse dans une langue qui n'est pas la sienne. Ses efforts remarquables ont été très appréciés. Vers la fin, Christiane Mouret a fait l'impossible pour la compléter avant mon départ.

Thanks is owed to the Natural Science and Engineering Research Council of Canada for a post-graduate scholarship. Financial support for the research programme was supplied by the European Economic Community.

Enfin, remerciements à G.C., D.M. et tous les autres qui m'ont soutenu (et supporté) pendant les pénibles mois à la fin de l'année 1984.

TABLE OF CONTENTS

	<u>Page</u>
CERTIFICATE OF EXAMINATION.....	ii
ABSTRACT	iii
ACKNOWLEDGEMENTS.....	v
TABLE OF CONTENTS	vii
LIST OF TABLES	xii
LIST OF FIGURES	xiii
NOMENCLATURE	xviii
CHAPTER 1 - INTRODUCTION	1
CHAPTER 2 - LITERATURE SURVEY : EXPERIMENTAL FINDINGS AND EMPIRICAL AND SEMI-EMPIRICAL CORRELATIONS	7
2.1 Introductory remarks	7
2.2 Vertical Pneumatic Transport Hydrodynamics	17
2.2.1 Early studies	17
2.2.2 Friction factor correlations	17
2.2.3 Other empirical and semi-empirical approaches ...	27
2.2.4 Comments and conclusions	36
2.3 Heat Transfer between Vertically Flowing Gas-Solids Suspensions and Pipe Walls	41
2.3.1 Experimental studies : Methods and data analysis	41
2.3.2 Experimental studies : Operating parameters and results	49
2.3.3 Correlations and models	56
2.3.4 Comments and conclusions	66
2.4 Concluding remarks.....	69

TABLE OF CONTENTS (Continued)

	<u>Page</u>
CHAPTER 3 - GENERAL MULTIPHASE FLOW EQUATIONS : REVIEW OF PREVIOUS WORK	71
3.1 Introduction	71
3.2 Equations derived directly in terms of mean variables.	72
3.3 Averaged equations	92
CHAPTER 4 - GENERAL PROBABILISTIC MULTIPHASE FLOW EQUATIONS ...	103
4.1 Introduction	103
4.2 Basic concepts	107
4.2.1 Phase presence probability	108
4.2.2 Mean variables	109
4.2.3 Differentiation	110
4.2.4 Variations of a quantity ψ_p with respect to time	114
4.3 Continuity	117
4.4 Momentum	118
4.4.1 External forces acting on the fluid phase	120
4.4.2 External forces acting on the solids phase	122
4.4.3 Momentum equations	128
4.5 Energy	131
4.5.1 Heat transfer	132
4.5.2 Work by external forces	135
4.5.3 Energy equations	137
4.6 Concluding remarks	140

TABLE OF CONTENTS (Continued)

	<u>Page</u>
CHAPTER 5 - EXPERIMENTAL INSTALLATION : CHARACTERISTICS, OPERATING PROCEDURE AND VERIFICATIONS	144
5.1 Introduction	144
5.2 Pneumatic transport installation and procedure	146
5.2.1 General description	146
5.2.2 Operating procedure	156
5.2.3 Overall gas flow measurements and pressure drop verification : Moody diagram	161
5.2.4 Return line gas flowrate determination	167
5.2.5 Calculations	173
5.3 Heat transfer installation and procedure	178
5.3.1 Description	178
5.3.2 Operating procedure	183
5.3.3 Test section heat losses and time required to reach thermal steady state	185
5.3.4 Overall heat transfer system verification : Seider-Tate equation	195
5.3.5 Calculations	199
5.4 Gas and solids physical properties	204
5.4.1 Gas properties	204
5.4.2 Solids properties	206
CHAPTER 6 - EXPERIMENTAL RESULTS AND DISCUSSION	211
6.1 Experimental programme	211
6.2 Preliminary pneumatic transport runs	213
6.3 Main series suspension hydrodynamic results	225
6.3.1 Pressure drop as a function of mean solids concentration	225

TABLE OF CONTENTS (Continued)

	<u>Page</u>
6.3.2 Mean solids concentration as a function of solids flowrates	240
6.3.3 Pressure drop as a function of loading ratio ..	248
6.3.4 Solids hold-up particle size distributions:	249
6.4 Suspension to pipe wall heat transfer results	257
6.4.1 Temperature and heat transfer coefficient profiles	257
6.4.2 Variation of heat transfer coefficients as a function of solids loading	262
6.5 Summary of major experimental findings	268
CHAPTER 7 - ANALYSIS OF EXPERIMENTAL RESULTS USING PROBABILISTIC MULTIPHASE FLOW EQUATIONS	269
7.1 Introduction	269
7.2 Analysis of Hydrodynamic results	271
7.2.1 Fully developed flow	271
7.2.2 Pressure drop ; Model for s_{ij} at the pipe wall .	273
7.2.3 Comparison with experimental results	282
7.2.4 Conclusions of the hydrodynamic analysis	291
7.3 Analysis of Heat Transfer results	292
7.3.1 Thermally fully developed flow	292
7.3.2 Asymptotic similar solutions to the energy equations	295
7.3.3 Heat transfer coefficient variations	304
7.3.4 Comparison with experimental results	308
7.3.5 Conclusions of the heat transfer analysis	315

TABLE OF CONTENTS (Continued)

	<u>Page</u>
CHAPTER 8 - CONCLUSIONS AND RECOMMENDATIONS FOR FURTHER STUDY .	316
APPENDIX I - ROTAMETER CALIBRATIONS : METHODS AND RESULTS	321
APPENDIX II - PLATINUM RESISTANCE THERMOMETER CALIBRATIONS	333
APPENDIX III - DIFFERENCE BETWEEN THE INSIDE AND OUTSIDE PIPE WALL TEMPERATURES	335
APPENDIX IV - HYDRODYNAMIC DATA	340
APPENDIX V - HEAT TRANSFER DATA	380
REFERENCES	397
VITA	409

LIST OF TABLES

<u>Table</u>	<u>Description</u>	<u>Page</u>
2.1	Vertical Pneumatic Transport Experimental Studies: Typical Parameter Ranges	16
2.2	Solids Friction Factor Correlations as Decreasing Functions of Solids velocity	22
2.3	Typical Solids Velocity Correlations	27
2.4	Suspensions-Wall Heat Transfer Studies: Experimental Set-ups	46
2.5	Experimental Studies of Heat Transfer between Vertically Flowing Gas-Solids Suspensions and Pipe Walls : Parameter Ranges	50
2.6	Suspension Heat Transfer Correlations Based on a Single or Limited Number of Studies	57
4.1	General Probabilistic Multiphase Flow Equations	142
6.1	Summary of Experimental Programme	214

LIST OF FIGURES

<u>Figure</u>	<u>Description</u>	<u>Page</u>
2.1	Zenz(154) graphical representation of pressure drop in vertical pneumatic conveying	11
2.2	Capes and Kamura (20) Friction Factor correlation	39
2.3	Yang (149) Friction Factor correlation	39
2.4	Experimental Suspension Heat Transfer Coefficients	67
4.1	Surfaces totally enclosing phases contained within a reference volume v	113
4.2	Types of particle collisions involving phase p particles at least partially contained in the control volume v	125
5.1	Vertical Pneumatic Conveying Installation	147
5.2	Fluidized Bed Feeder	150
5.3	Pressure tap configuration and locations	153
5.4	Pneumatic slide valves	155
5.5	Gas inlet positions for Suspension runs and for "Gas only" verifications	163
5.6	Typical transport line pressure profile: "Gas only" runs	165
5.7	Experimental Moody diagram	166
5.8	Return line gas flowrate verification installation	170
5.9	Pressure drop versus gas flowrate down return line: Fixed bed of sand (P.S.D. 2)	172
5.10	Gas flowrate down return line as a function of solids flowrate: Moving bed of sand (P.S.D.)	174
5.11	Maximum errors in mean solids concentration measurements as a function of non-simultaneous slide valve closing times	177

LIST OF FIGURES (continued)

<u>Figure</u>	<u>Description</u>	<u>Page</u>
5.12	Heat Transfer Test Section	180
5.13	Heat loss model	188
5.14	Typical axial temperature profiles obtained during heat loss calibrations	192
5.15	Variation of the effective radial heat transfer coefficient during heat loss correlation experiments	194
5.16	Typical pipe wall temperature profile- Gas only run	197
5.17	Local heat transfer coefficients for Gas only runs	198
5.18	Gas-only asymptotic coefficients versus gas flowrate	203
5.19	Basis for heat transfer coefficient calculation	201
5.20	P.S.D. 1 Sand particle size distribution	208
5.21	P.S.D. 2 Sand particle size distribution	209
5.22	Glass beads particle size distribution	210
6.1	Typical line pressure profiles : Preliminary suspension runs	215
6.2	Typical line pressure profiles : Main hydrodynamic series	217
6.3	Suspension pressure drop as a function of gas velocity; Low solids flowrates	219
6.4	Suspension pressure drop as a function of gas velocity; High solids flowrates	220
6.5	Mean solids concentration as a function of gas velocity (Series A-4)	222
6.6	Mean solids concentration as a function of gas velocity (Series A-5)	223
6.7	Variation of mean solids velocity with mean gas velocity: Series A-4, A-5	224

LIST OF FIGURES (continued)

<u>Figure</u>	<u>Description</u>	<u>Page</u>
6.8	Pressure drop versus $\bar{\alpha}_s$: Series B-1	226
6.9	Pressure drop versus $\bar{\alpha}_s$: Series B-2, B-5	227
6.10	Pressure drop versus $\bar{\alpha}_s$: Series B-4, B-7	228
6.11	Pressure drop versus $\bar{\alpha}_s$: Series B-3, B-6	229
6.12	Pressure drop versus $\bar{\alpha}_s$: Series C-1	230
6.13	Pressure drop versus $\bar{\alpha}_s$: Series C-2, C-5	231
6.14	Pressure drop versus $\bar{\alpha}_s$: Glass beads	232
6.15	Slopes of Pressure drop vs. Mean solids concentration curves as a function of gas velocity: SERIES B	237
6.16	Slopes of Pressure drop vs. Mean solids concentration curves as a function of gas velocity: SERIES C	238
6.17	Slopes of Pressure drop vs. Mean solids concentration curves as a function of gas velocity: SERIES D (Glass beads)	239
6.18	Solids flowrate versus Mean solids concentration: SERIES B-3, B-5, B-7	241
6.19	Solids flowrate versus Mean solids concentration: SERIES B-2, B-4, B-6	242
6.20	Solids flowrate versus Mean solids concentration: SERIES C-2, C-3, C-5	243
6.21	Solids flowrate versus Mean solids concentration: Glass bead runs	244
6.22	Mean solids velocity versus Mean gas velocity: Series B and C	246
6.23	Mean solids velocity versus Mean gas velocity: Series D (Glass beads)	247
6.24	Suspension pressure drop as a function of Loading ratio: Typical SERIES B results	249

LIST OF FIGURES (continued)

<u>Figure</u>	<u>Description</u>	<u>Page</u>
6.25	Suspension pressure drop as a function of Loading ratio: Typical SERIES C results	250
6.26	Suspension pressure drop as a function of Loading ratio: SERIES D (Glass beads)	251
6.27	Variation of the mean particle diameter of the solids hold-up as a function of mean solids concentration	253
6.28	Variation of mean particle diameter of solids hold-up as a function of gas velocity (SERIES B)	255
6.29	Typical wall temperature, suspension mixed mean temperature, and heat transfer coefficient profiles for suspension runs	258
6.30	Heat transfer coefficient axial profiles: (SERIES C-1)	260
6.31	Heat transfer coefficient axial profiles: (SERIES C-2)	260
6.32	Heat transfer coefficient axial profiles: (SERIES C-4)	261
6.33	Heat transfer coefficient axial profiles: (SERIES C-5)	261
6.34	Variation of fully developed heat transfer coefficients as a function of solids flowrate: (SERIES C-1)	263
6.35	Variation of fully developed heat transfer coefficients as a function of solids flowrate: (SERIES C-2)	263
6.36	Variation of fully developed heat transfer coefficients as a function of solids flowrate: (SERIES C-4)	264
6.37	Variation of fully developed heat transfer coefficients as a function of solids flowrate: (SERIES C-5)	265
6.38	Variation of fully developed heat transfer coefficients as a function of solids flowrate: (SERIES C-3)	265

LIST OF FIGURES (continued)

<u>Figure</u>	<u>Description</u>	<u>Page</u>
7.1	Particle-wall collisions	280
7.2	Variation of $(1 + \overline{Ma}_s) / (h_{ss}/h_g)$ as a function of solids loading for the five heat transfer series	310
7.3	Variation of heat transfer coefficients as a function of solids loading for the five heat transfer series	312
7.4	$(1 + \overline{Ma}_s) / (h_{ss}/h_g)$ as a function of solids loading: Data of Depew and Farbar (34) and Tien and Quan (130)	314

NOMENCLATURE

A	Pipe cross-sectional area
A_0	Surface area per unit volume of particles
A_1, A_2	Rotameter constants
A_{pp}	Ratio of pick-up area at the injection point to pipe area
b	Fully developed flow axial temperature gradient (Defined by Eq. 7.34)
B	Displacement factor (Eq. 3.33)
B_{ij}	$= \beta_{ij}$ Fluid velocity fluctuation tensor
C	Dispersion factor (Eq. 3.33)
C_d	Orifice discharge coefficient
C_D	Particle drag coefficient
C_f, C_g, C_s	Fluid, gas, solids' heat capacity
C_1, C_2	Integration constants
d_0	Orifice diameter
d_p	Particle diameter
D	Pipe diameter
D_0	Outside pipe diameter

NOMENCLATURE (continued)

D_1	Inside pipe diameter
D_s	Rotameter scale displacement
E_p	Random internal energy per unit mass of a phase p
f	Reduced solids concentration profile (Defined by Eq. 7.27)
f_1	Two phase friction factor (Defined by Eq. 2.3)
f_2	Two phase friction factor (Defined by Eq. 2.19)
f_g	Gas phase friction factor
f_s	Solids phase friction factor (Defined by Eq. 2.5)
f_{sg}	Solids phase friction factor (Defined by Eq. 2.12)
f_1^{qp}	Random force exerted by a phase q particle on a phase p particle during collision
F_1^{fs}	Mean force exerted by the fluid phase on the solids phase
F_1^{pq}	Mean force exerted by the phase p on the phase q
F_1^{ap}	Mean force exerted by the interface on the phase p
F_1^{cp}	Random force exerted on the phase p contained in a control volume v due to collisions with other particles or the pipe wall
F_1^{sp}	Random force exerted by the solids phases or the wall, contained within the control volume v, on the phase p particles also contained in v

NOMENCLATURE (continued)

Fr	Froude number U_g/\sqrt{gD}
Fr'	Modified Froude number V_t/\sqrt{gD}
g, g_1	Gravitational acceleration
$g(r)$	Reduced solids velocity profile (Defined by Eq. 7.31)
$g(x_1)$	Weighting function (Used in Eq. 3.38 to 3.43)
G_p	Characteristic function describing the spatial extension of collisions involving phase p particles
$G(r)$	Proportionality factor between $\rho_s C_s^{\alpha} b_s$ and Q_{fs}
h	Solids velocity profile (Defined by Eq. 7.28)
h_g	Fully developed gas-wall heat transfer coefficient
h_p	Gas-particle heat transfer coefficient
$h_{ss}(z)$	Local suspension-wall heat transfer coefficient
h_{ss}	Fully developed suspension-wall heat transfer coefficient
h_g^{lm}	Gas-wall heat transfer coefficient based on the log-mean temperature difference
h_{ss}^{lm}	Suspension-wall heat transfer coefficient based on the log-mean temperature difference
H_f	Random enthalpy of the fluid phase

NOMENCLATURE (continued)

k, k_1, k_2	Miscellaneous constants
k_c	Proportionality factor between the mean solids concentration in the vicinity of the wall and the particle-wall collision frequency
k_r	Rotameter constant found experimentally
k_{rm}	Rotameter constant supplied by the manufacturer
K_p	Phase p characteristic function
L	Length
L_{sv}	Distance between the two slide valves
m_p	Mass of a phase p particle
m_{sv}	Mass of solids retained between the two slide valves
\hat{M}_L	Momentum loss of a particle undergoing collision
\overline{M}_s	$\frac{W_s C_s}{W_f C_f}$ $M = (\rho_s \bar{v}_s C_s / \rho_f \bar{a}_f \bar{U}_f C_f)$
n_i	Unit normal vector directed outward from the surface S bounding the control volume v
\overline{n}_i	Unit random normal vector directed outward from the surface bounding the phase p
n_p	Particle concentration by number
N_p	Number of a total of N experiments during which the point in question is occupied by the phase p

NOMENCLATURE (continued)

$O()$	Order of magnitude
P	Pressure
p^p, p^s	Partial pressures of phase p , solids phase
P_{st}	Standard pressure for rotameter calibrations
P_{ro}	Pressure at rotameter outlet
Pe	Peclet number = $RePr$
Pr	Prandtl number = $C_p \mu / \lambda$
ΔP_g	Gas pressure drop
ΔP_{fs}	Pressure drop due to solids-wall friction
ΔP_{ss}	Overall suspension pressure drop
ΔP_{orf}	Pressure drop across orifice meter
q_A	Heat flow in the axial direction
q_p	Heat flow from the pipe toward the exterior (Losses)
q_r	Heat flow in the radial direction
q_T	Total heat dissipated in a discrete length of pipe
q_{ss}	Heat flux from the pipe wall to the suspension
$q_{ss}(z)$	Local heat flux from the pipe wall to the suspension

NOMENCLATURE (continued)

q''	Volumetric heat generation
Q_g	Volumetric gas flowrate
Q_T	Total heat generated electrically
χ_{fp}	Rate of thermal energy transfer from the fluid phase to the solids phase (random)
Q_{fs}	Mean heat flux from the fluid phase to the solids phase
r	Radial coordinate
r_i	Inside pipe radius
r_o	Outside pipe radius
R	Pipe radius.
R_R	Electrical resistance of on-line resistance
Re	Pipe Reynolds number $\rho_g D U_g / \mu$
Re_t	Particles Reynolds number based on the particle terminal settling velocity $\rho_g d_p V_t / \mu$
\tilde{s}_p	Random surface bounding a phase p particle
\tilde{s}_{p1} \tilde{s}_{p2}	Random phase p interfacial surface contained in the control volume v
s_{ij}	Mean stress tensor in the overall solids phase due to collisions with other particles located outside the control volume v

NOMENCLATURE (continued)

s_{ij}^p	Mean stress tensor in the particle phase p due to collisions with other particles located outside the control volume v
S	Surface bounding the control volume v
S_p^a	Random surface formed by the intersection of the phase p and the control volume surface
S_c	Rotameter scale reading
t	Time
Δt_{sv}	Time between the closing of the two slide valves
t^+, t^-	Time discontinuities in phase functions arising from passage across a phase interface
T	Time interval over which time averaging is carried out
T_p	Portion of the time interval T during which a point in question is occupied by the phase p
T_p^a	Random temperature of the phase p
T_p^a	Interfacial mean temperature (Defined by Eq. 4.58)
T_s, T_g, T_f	Mean solids, gas and fluid phase temperatures
T_∞	Ambient temperature
T_{ss}	Suspension mixed mean temperature

Applicable
only in
Chapter 3

NOMENCLATURE (continued)

T_{ss1}, T_{ss2}	Suspension mixed mean inlet and outlet temperatures
ΔT_{ss}^{lm}	Suspension log mean temperature difference (Defined by Eq. 2.25)
T_w	Wall temperature
T_{wi}, T_{wo}	Wall inside and outside temperatures
\bar{T}_w	Mean wall temperature (Defined by Eq. 5.21)
T_{st}	Standard temperature for rotameter calibrations
T_{ro}	Temperature at rotameter outlet
U_i	Mean fluid velocity
U_g	Superficial fluid velocity
U_o	Overall heat transfer coefficient between pipe wall surface and surrounding atmosphere based on outer pipe diameter
U_{mi}	Mixture mean velocity by volume (Defined by Eq. 3.6)
v	Control volume
\tilde{v}_p	Random volume of the phase p contained in v
$v_{p\infty}$	Volume enclosing all points occupied by the phase p over which the weighting function $g(r)$ is applied
V_i	Mean solids velocity vector
V_{mi}	Mass mean velocity of the mixture (Defined by Eq. 3.26)

NOMENCLATURE (continued)

\hat{v}_{pi}	Random phase p velocity vector
\bar{v}_{pi}	$= \overline{\hat{v}_{pi}}$ Phase mean velocity vector for phase p
\hat{v}_p^2	$= \hat{v}_{pi} \cdot \hat{v}_{pi}$
\hat{v}'_{pi}	Arithmetic mean of before and after collision velocities of a phase p particle
\hat{v}_r^i, \hat{v}_r^r	Before and after collision radial velocity components.
V_R	Voltage across on-line resistor
V_s, \bar{V}_s	Mean solids velocity, averaged over pipe cross-section
V_t	Particle terminal settling velocity
V_{to}	Particle terminal settling velocity in an infinitely dilute medium
V_T	Voltage drop across heat transfer test section
\hat{v}_z^i, \hat{v}_z^r	Before and after collision axial velocity components
V_z	Mean solids axial velocity component
W_f, W_g, W_s	Fluid, gas, solids mass flowrate
w_f^{ext}	Random rate of work done by external forces on the fluid phase contained in v
x_i	Space coordinates
Y	Gas expansion factor

NOMENCLATURE (continued)

z	Axial coordinate
Z_i	Force due to particle collisions
α_p	Phase presence probability of the phase p (Defined by Eq. 4.1) Also used in Chapter 3 to denote volume fraction
$\bar{\alpha}_s$	Mean solids volume fraction averaged across the pipe cross-section
$\Delta\bar{\alpha}_s$	Error in solids volume fraction measurement due to non-simultaneous slide valve closing
β	Heat transfer coefficient correlation factor (Defined by Eq. 2.34)
β_{ij}^p	Phase p velocity cofluctuation tensor (Defined by Eq. 4.23)
β_{ij}	Solids phase velocity cofluctuation tensor
Γ_{ij}^{qp}	Random stress tensor created within a phase p particle due to a collision with a phase q particle
Γ_{ij}^p	Random stress tensor created within a phase p particle due to collisions with other particles or the pipe wall
δ_p^y	Random delta distribution which is zero except at the phase p interface where it is infinite
δ_{ij}	Kronecker delta
ϵ	Suspension porosity
ϵ_t	Thermal eddy diffusivity

NOMENCLATURE (continued)

ϵ_i^p	Velocity-temperature co-fluctuation tensor for phase p (Defined by Eq. 4.67)
θ_p	Pipe angle with horizontal
θ_f	$T_f - T_w$
θ_s	$T_s - T_w$
θ_a	$T_a - T_w$
ϵ_{nm}^o	Wall-gas mixed mean temperature difference
ϵ_{nm}	Wall-suspension mixed mean temperature difference (Defined by Eq. 7.58)
Λ_f^o	Fluid flow field perturbation (Defined in Eq. 7.64)
Λ_f^1	Fluid temperature field perturbation (Defined in Eq. 7.65)
Λ_s	Solids temperature field integral (Defined in Eq. 7.66)
$\lambda_f, \lambda_g, \lambda_s$	Fluid, gas, solids thermal conductivity.
λ_T	Pipe wall thermal conductivity
μ	Gas viscosity
ν	Kinematic viscosity
ρ_p	Phase p density
ρ_f, ρ_g, ρ_s	Fluid, gas, solids density

NOMENCLATURE (continued)

ρ_m	Mixture density (Defined by Eq. 3.25)
ρ_{st}	Standard gas density for rotameter calibrations
σ_{ij}	Mean fluid phase shear stress tensor
σ_{ij}^s	Solids phase shear stress tensor
σ_{ij}^m	Mixture shear stress tensor
σ_{ij}^{pm}	Contribution of the phase p to the overall shear stress tensor in the mixture
τ_{ij}^{rp}	Random phase p stress tensor
τ_{ij}^p	Phase p mean stress tensor
τ_{ij}^f	Fluid phase mean stress tensor
τ_{ij}^s	Solids phase mean stress tensor
$\phi_1 \dots \phi_6$	Correlation functions defined by Eq. 2:14
ϕ_{pi}	Random rate of thermal energy received by the phase p in v
ϕ_s	Sphericity
x	Coefficient of restitution
x_t	Tangential coefficient of restitution
x_n	Normal coefficient of restitution

NOMENCLATURE (continued)

ψ_a	Particle surface shape factor
ψ_p	Random physical quantity associated with the phase p
$\bar{\psi}_p$	Phase mean of ψ_p
ω_p	Volume of an individual particle
Ω_i	Body force
Ω_i^m	Body force exerted on the mixture

SUBSCRIPTS

a	At the phase interface
f	Fluid phase
g	Gas phase
i, j, k	Tensor notation
m	Mixture
mm	Mixture mean
p	Phase p
q	Phase q
r	Radial component
s	Solids phase

NOMENCLATURE (continued)

ss Suspension
vw In the vicinity of the wall
w At the wall
z Axial component

SUPERSCRIPTS

a At the phase interface
af |
ap | Between interface and fluid or phase p
cp Collisions involving the phase p particles
i Before collision
lm Log mean
m Mixture
p Phase p
q Phase q
pq Between the phases p and q
r After collision
s Solid phase

NOMENCLATURE (continued)

— Mean, or probabilistic mean

— Phase mean

—_g Weighting function mean

—_v Volume phase mean

—_v Volume intrinsic mean

—_T Time phase mean

~ Random variables

o Reference variables

1 Perturbation variables

CHAPTER 1

INTRODUCTION

Gas-solids suspensions found their first industrial applications in the 19th century when it was discovered that grain suspended in a flowing gas stream could be transported over considerable distances with a minimum of handling. Since these early beginnings, the uses of gas-solids suspensions have multiplied to encompass a wide range of diverse industrial processes: solids suspended by a gas in a fluidized state are employed in a variety of chemical reactors such as catalytic crackers, fluidized bed combustors and iron-ore roasters. Densely conveyed suspensions are now in use as "circulating" bed reactors for alumina roasting and coal combustion and gasification. In more dilute form, gas solids suspensions are routinely used, as in the first grain conveying installation, to pneumatically transport all kinds of granular solids in addition to finding applications in transport-line catalytic reactors and as heat exchange media.

This thesis concerns the study of one type of gas-solids suspension: namely, relatively dilute (less than 1% solids by volume) suspensions flowing upward in a vertical pipe. This particular area was originally chosen for study because of the fact that, while much research has been carried out on dilute gas-solids suspensions since their first 19th century application, many gaps in the knowledge of their basic hydrodynamic and heat transfer behaviour still exist. These gaps manifest themselves on a practical level as uncertainties

2

in such basic design calculations as pressure drops and heat transfer coefficients.

The following chapters describe the research program undertaken in a more or less chronological order. Chapters 2 and 3 served to fully define the objectives of the study : Chapter 2 is a detailed literature review of previous experimental work carried out on the pressure drop and heat transfer characteristics of vertically flowing gas-solids suspensions as well as of the empirical and semi-empirical correlations which have resulted from these studies. In an extensive review of gas solids flow published in 1959 Torobin and Gauvin (132) summarized approaches to these problems as being "still largely empirical and resting heavily on arbitrary friction factors, specific to each application, from which generalization is utterly impossible". The conclusions drawn from Chapter 2, despite 25 years of additional work, were remarkably similar to Torobin and Gauvin's evaluation of the situation : many ambiguities, some resulting from unsound experimental techniques, were found to exist and a colossal number of ungeneralizable correlations based on friction factors and heat transfer coefficient ratios were shown to have been developed.

The sentence immediately following the above-cited Torobin and Gauvin quotation in their 1959 review was : "It is perhaps surprising to report that a large number of workers, currently active in the field, are still following this line of attack". The unfruitful results described in Chapter 2 of the still larger numbers of workers who have pursued this course since 1959 defined the antithesis of the objective of the present study : it was considered futile to undertake

3

another experimental study with the sole objective of developing yet another friction factor or heat transfer coefficient correlation incorporating a limited number of new parameters. A break from the "line of attack" which has characterized research in this area for the last 50 years seemed indispensable if any real progress was to be made.

The lack of a fundamental basis is perhaps the most striking aspect of most correlations developed for gas-solids suspension flows. The forms of proposed correlations generally have no theoretical foundation and instead result from either dimensional analysis or simply random groupings of the parameters varied within a given study. The development of a sound theoretical support based on a rigorous mathematical description of the heat, mass and momentum transfer processes occurring in gas-solids suspension flows seemed therefore to represent the first step in a new direction in research in this area.

Two basic approaches are conceivably possible in order to develop such a mathematical description. It would be possible to treat the fluid phase in an Eulerian fashion typical of single phase fluids and then to combine this with a Lagrangian description of the behavior of the discrete particles in suspension. This would involve approximating the particles as point masses and writing equations relating the accelerations of their centres of mass as functions of all other variables influencing their motion. Resolution to treat a given flow problem would then require solving a number of equations equal to one (for the fluid phase) plus the number of particles present subject to the same number of boundary conditions ; that is :

- the boundary conditions of the fluid phase at time zero and their evolution in time,
- the coordinates and velocity components of each particle at a given instant in time (initial conditions).

Beyond the difficulties arising when there are a large number of particles present, and therefore a large number of equations to solve, resolution of the flow problem is not possible when all boundary conditions are not precisely known. In typical gas-solids suspension flows, while overall boundary conditions are generally imposed and precisely known, individual boundary conditions for each and every particle in suspension are generally unknown. A combined Eulerian-Lagrangian approach is thus generally unfeasible.

A more practical approach to a fully rigorous treatment of suspension flows would then be to consider the suspension as a deformable medium subject to a fully Eulerian description, since resolution of the governing equations would require only knowledge of overall boundary conditions.

The need for a more fundamental approach to gas-solids suspension flows and the advantages of a Eulerian description defined the second phase of the present research programme : the examination of general Eulerian equations which had been proposed to describe multiphase media in hope of later using them to analysis experimental results obtained on gas-solids suspension flows. Chapter 3 presents the results of this examination. It was found that, while a single set of generally accepted equations existed for single phase flows (the

Navier-Stokes and associated energy equations) many different basic equation formulations had been postulated for multiphase flows. The critical analysis of these equations carried out in Chapter 3 showed them all to be either not fully rigorous from a mathematical, conceptual or physical point of view or subject to limitations arising from basic differences between suspensions of macroscopic particles and single phase fluids. Further work on the development of general multiphase flow equations was therefore necessary in order to provide the theoretical support required to advance research on the behavior of gas-solids suspension flows.

The conclusions of Chapters 2 and 3 led then to the definition of the objectives of the present thesis :

- the development of fully rigorous general continuity, momentum and energy equations to describe multiphase media (Chapter 4)
- the design, construction and verification of a flexible experimental installation capable of supplying reliable, unambiguous pressure drop, mean solids concentration and suspension-pipe wall heat transfer coefficient data in vertically flowing gas-solids suspensions. (Chapter 5)
- the use of the above-mentioned installation to obtain experimental results on fully developed dilute suspension flows using a number of different granular solids.
(Chapter 6)

the analysis of the above and of comparable data in the literature using the general multiphase flow equations in order to identify determinant phenomena for pressure drop and heat transfer coefficients.

The research for this thesis was carried out at the Université de Technologie de Compiègne, France as part of a scientific exchange with the University of Western Ontario. The experimental installation was constructed at the Département de Génie Chimique, U.T.C. and all experiments were performed there. The general equation development was jointly undertaken with Yuri Molodtsov to provide a theoretical support for not only the experimental study presented here, but also for a wide range of gas-solids suspension flow problems being studied experimentally in the U.T.C. laboratories. Molodtsov's Thèse de Doctorat d'Etat (93) to which frequent reference will be made in Chapters 4 and 7, provides details of certain derivations not required in the present study as well as applications of the General Probabilistic Multiphase Flow Equations to other suspension flow problems.

CHAPTER 2

LITERATURE SURVEY : EXPERIMENTAL FINDINGS AND EMPIRICAL AND SEMI-EMPIRICAL CORRELATIONS

2.1 Introductory remarks

Compared to the study of the hydrodynamics of vertical pneumatic conveying which began in the early part of the 20th century, investigations of heat transfer between gas-solids suspension and pipe walls are relatively recent, with the first published studies appearing only in the late 1950's. Work in these two areas has nevertheless followed similar paths : many experiments have been carried out with the general orientation being the study of the dependence of factors of immediate practical interest - pressure drops, mean solids concentrations and heat transfer coefficients - on basic operating conditions and geometrical configurations. The results of these experimental investigations have been regrouped in order to develop a wide variety of empirical or semi-empirical correlations to be used in engineering design.

This chapter will be concerned with the review of previous experimental work in these two areas. As the present study is directed toward hydrodynamically fully developed vertically flowing gas-solids suspensions, emphasis will be placed on work carried out under these conditions. It will be shown that, despite the large number of data which exist, many ambiguities still remain concerning the effect of basic flow variables on the hydrodynamics and heat transfer of suspen-

sion flows. As some of these anomalies can be traced to problems in basic experimental techniques, this aspect will be examined in some detail. Weaknesses in traditional empirical and semi-empirical treatments of these two subjects will be examined and the need for a more fundamental approach in dealing with the complex phenomena involved will be demonstrated.

2.2. Vertical Pneumatic Transport Hydrodynamics

2.2.1 Early studies

The earliest published studies on pneumatic transport of solids in pipes appeared in the 1920's with the works of Cramp (25), Cramp and Priestly (26) and Gasterstadt (49). The objectives of these works were to try to provide some guidance in the design of pneumatic grain-conveying installations which had become increasingly preponderant in the years leading up to the First World War. The scope of these early studies, as well as those which appeared in the twenty years following (Eg. Ref. 23, 82, 117, 128), most of which were also directed toward grain conveying, were limited and very practically oriented: injection methods were tested and emphasis was placed on determining "safe" gas velocities for a particular application. Nevertheless, certain trends were elucidated and certain research orientations which would influence later work were established: Cramp and Priestly developed arguments by which the additional pressure drop due to the presence of solids was related to the drag force required to accelerate particles. Gasterstadt was the first to try to correlate the ratio of the pressure drop of the suspension over that of the gas

flowing alone under the same conditions in terms of a simple expression involving the loading ratio (the ratio of the mass flowrate of solids to the mass flowrate of gas). Segler (117) carried out studies to determine the effect of pipe diameter on pressure drops. Chatley (23) first recognized the need to account for particle friction losses at the pipe wall.

The development during the Second World War of catalytic fluidized bed reactors, to and from which solids were transported pneumatically, led to increased interest in this area and to the beginning of more systematic studies which resulted in five significant publications the late 1940's. Farbar (43) investigated the vertical and horizontal transport of cracking catalyst in a 17 mm dia. Pyrex tube. He attempted to correlate his pressure drop results with an expression of the form first proposed by Gasterstadt :

$$\frac{\Delta F_{SS}}{\Delta F_g} = 1 + k (W_c/W_g) \quad (2.1)$$

where k is an empirically determined constant.

A significant result of Farbar's work was his experimental finding that solids having a wide particle size distribution exhibited a considerably different behaviour compared with those of a fixed size.

Zenz (153) presented pressure drop results for rape seed, glass beads and sand transported in a 44.5 mm dia. lucite tube. The major contribution of his work was the graphical representation of pressure drop results which has remained as the qualitative basis for the

interpretation of vertical pneumatic transport behaviour. Figure 2.1 shows Zenz's plot of unit pressure drop as a function of superficial gas velocity for a number of different solids flowrates. The curves are characterized by a minimum pressure drop : at gas velocities in excess of that at which the minimum occurs, the increases in pressure drop are due to increased frictional losses associated with both the gas and solids phases ; at gas velocities below the minimum, particle hold-up, which increases with decreasing gas velocity, becomes predominant and accounts for increasing pressure drops until erratic slugging and choking occurs. Increasing solids flowrates magnify these effects and generally lead to choking at higher gas velocities.

The three other significant studies published in the late 1940's were the first attempts to quantify the effect of different variables on pressure drops over expanded ranges of operating conditions. Vogt and White (137) studied the transport of sand, steel shot, clover seed and wheat in a 12.7 mm dia. steel pipe. They identified what they felt to be the relevant variables affecting pressure drops, namely, pipe diameter, gas velocity, gas density, gas viscosity, particle diameter, particle density, loading ratio, particle roughness and particle shape factor and attempted to group them dimensionlessly in order to correlate pressure drops in terms of the ratio of the suspension pressure drop over that of the gas alone. They arrived at an expression of the form :

$$\frac{\Delta F_{SC}}{\Delta F_g} = 1 + k_1 \left[\frac{D}{d_p} \right]^2 \left[\frac{\rho_g W_s}{\rho_s W_g} \frac{1}{Re} \right]^{k_2} \quad (2.2)$$

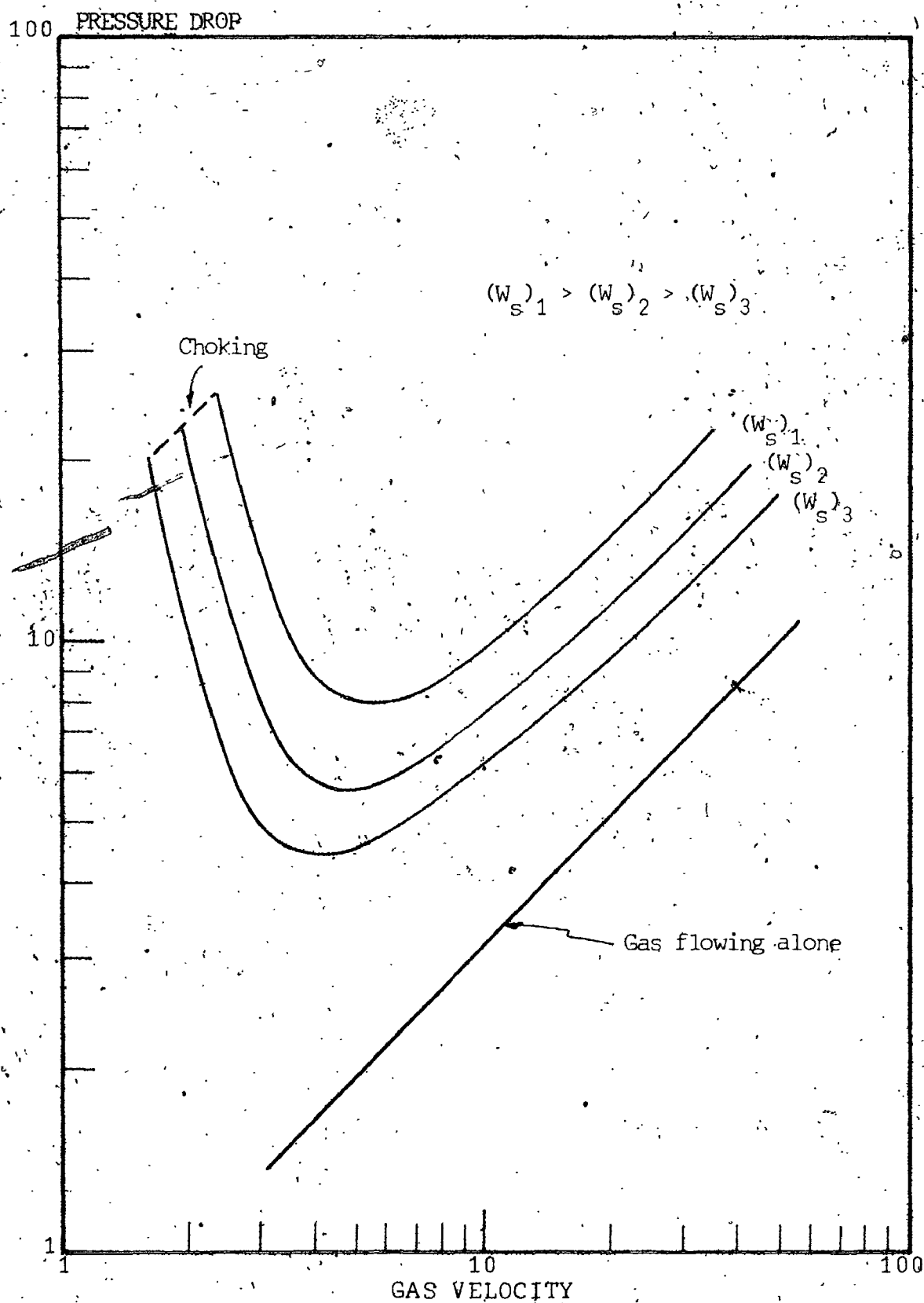


FIGURE 2.1 Zenz (154) graphical representation of pressure drop in vertical pneumatic conveying

where the empirical factors k_1 and k_2 were correlated graphically as a function of $Re\sqrt{C_D}$. While the above expression seemed to correlate their results well, some doubt can be expressed concerning the even limited generality of the proposed correlation. Firstly, from an experimental point of view, Vogt and White's pressure drop measurements were obtained using only two pressure taps in a short (1.83 m) pipe, with one of the pressure taps being placed at only a short distance downstream from an elbow. The measured pressure drops thus may have been influenced by acceleration effects. Secondly, the strong dependence on the pipe to particle diameter ratio was not substantiated by later studies including one published the following year by Belden and Kassel (8). These latter authors studied the transport of catalyst particles in commercial steel pipes having diameters of 12 and 26 mm. They correlated their data by assuming that the overall pressure drop was composed of two contributions: frictional pressure drop involving the gas and solids phases and particle hold-up. The particle hold-up term was determined indirectly assuming the slip velocity between the gas and solids to be equal to the particle terminal settling velocity. The frictional pressure drop was then determined by subtracting the solids hold-up from the measured pressure drop. This was then correlated in terms of a two phase friction factor defined by the following equation:

$$\frac{\Delta P_{fs}}{\Delta L} + \frac{\Delta P_g}{\Delta L} = \frac{2f_1}{D} (\rho_s(1-\epsilon)V_s + \rho_g \epsilon U_g)^2 \quad (2.3)$$

Finally the friction factor correlation was given to be :

$$f_1 (\bar{Re})^{0.2} = 0.049 + 0.22 \left[\frac{(\rho_g \epsilon U_g)(\rho_s (1-\epsilon)V_s)}{(\rho_g \epsilon U_g + \rho_s (1-\epsilon)V_s)^2} \right] \quad (2.4)$$

The above equations were nevertheless found to correlate poorly results obtained at low gas velocities and low D/d_p ratios.

Finally, Hariu and Molstad (56) studied vertical pneumatic conveying over a wider range of variables than previously studied by other workers (see Table 2.1) and were the first to directly measure mean solids concentrations by means of quick closing plug valves inserted in the line. Despite some uncertainties linked to the experimental set-up (gas leaks, a pipe length of only 1.05 m) they did manage to contribute some significant new results based on their solids concentration measurements. They found for instance, that, over the range of variables studied, the slip velocity between the gas and solids tended to increase as gas velocity increased ; slip velocity was found not to vary however as solids loadings were increased.

Hariu and Molstad's work was especially significant in the way they attempted to correlate their results. They were the first to decompose the overall pressure drop into three components and to explicitly define a solids phase friction factor. The overall pressure drop was taken to be the sum of the three terms : the pressure drop due to the gas alone, which was assumed not to be influenced by the presence of the solids and therefore could be calculated using conventional techniques ; the pressure drop due to the solids hold-up based

on the actual particle velocity and a frictional pressure drop due to the solids which was correlated in terms of a friction factor defined in an analogous way to which single phase flow friction factors are defined. Their overall pressure drop expression was :

$$\frac{\Delta P_{SS}}{\Delta L} = \frac{f_g}{2D} (\rho_g \epsilon U_g) + \rho_s (1-\epsilon)g + \frac{f_s}{2D} (\rho_s (1-\epsilon) V_s) \quad (2.5)$$

Hariu and Molstad correlated their data with a constant solids friction factor, f_s equal to 0.004.

2.2.2 Friction factor correlations

Hariu and Molstad's approach in correlating pressure drops in vertical pneumatic conveying was to serve as the basis for correlating results obtained in the vast majority of the numerous similar studies which were to follow. There seem to be several reasons for this : firstly, the approach corresponds to the qualitative behaviour given by the Zenz graphical representation. For a given solids flowrate, as gas velocity increases the suspension solids concentration decreases provided the slip velocity between the gas and solids remains roughly constant. The combination of increasing gas and solids velocities tends to increase the first and third terms in the overall pressure drop expression (Eq. 2.5). As the gas velocity decreases on the other hand, the frictional terms tend to decrease in importance. The suspension becomes more concentrated and the static head of solids expressed by the second term in Eq. 2.5 increases. Hariu and Molstad's pressure drop expression (for constant slip velocity and friction factors) does

then, in fact, pass through a minimum as gas velocity is increased from the choking velocity to high values.

The second reason for the almost universal adoption of this approach is its simplicity. For a designer interested in knowing the variations of pressure drop in a suspension as a function of various operating conditions, the overall calculation is relatively simple. The first term can be determined using the standard Moody diagram. Once a hypothesis is made concerning particle velocity, the overall pressure drop can be directly calculated provided an appropriate solids friction factor is known.

Most studies carried out since the late 1940's were, as a result, directed toward developing friction factor correlations which would be valid over ever-increasing ranges of operating variables. Table 2.1 lists a representative sampling of such studies and summarizes the major parameters which were varied. Except where noted in the table, these experimental investigations followed the same basic procedure, the same basic measurements were made and the same data analysis techniques were employed: solids are introduced at a controlled rate into a flowing gas stream of known velocity and the resulting pressure gradient is measured. In a few cases, mean solids concentrations or mean solids velocities are also measured. The first term in the overall pressure drop expression is determined by prior calibration of the test pipe or via standard tables; the second term is determined either by direct measurement of the solids concentration or is calculated by making an assumption concerning the slip velocity (most often that the slip velocity is equal to the terminal settling

TABLE 2.1
VERTICAL PNEUMATIC TRANSPORT EXPERIMENTAL STUDIES :
TYPICAL PARAMETER RANGES

Author	Pipe length (m)	Pipe diameter (mm)	Gas velocity range (m/s)	Particle type	Particle density (kg/m ³)	Particle size (µm)	Loading ratio	Add. measurements, Observations
VOGT & WHITE (1948) (137)	1.83	12.7	0-30	Sand	2760	203-1173	0-40	.short pipe length, only two functioning pressure taps
				Steel	7200	420		
				Rape seed	1384	1170		
				Wheat	1391	4013		
BELDEN & KASSEL (1949) (8)	4.0	12 26	0-17	Catalyst	860	967 1963	0-13	.experiments also performed with CO ₂ as carrier gas
FARBAR (1949) (43)	2.11	17	15-45	Catalyst	2450	50	0-16	
ZENZ (1949) (153)	1.11	44.5	0-18	Rape seed	1089	1676	0-10	
				Glass	2484	587		
				Sand	2644	929		
				Salt	2099	168		
HARIU & MOLSTAD (1949) (56)	1.05	6.8 13.5	3.6-12	Sand 1	2640	502-356	0-18	.mean solids concentration measured by quick closing valves
				Sand 2	2710	274-213		
				Catalyst	980	109		

TABLE 2.1 (continued)

VERTICAL PNEUMATIC TRANSPORT EXPERIMENTAL STUDIES :
TYPICAL PARAMETER RANGES

Author	Pipe length (m)	Pipe diameter (mm)	Gas velocity range (m/s)	Particle type	Particle density (kg/m ³)	Particle size (µm)	Loading ratio	Add. measurements, Observations
MEHTA et al. (1957) (88)	4	12.7	3-28	Glass	2530	36 97	0-20	.mean solids concentration measured by manually-operated quick closing valves-poor reproductibility
ROSE & BARNACLE (1957) (89)	3.6	32.2	6-18	Mustard seed Glass Steel	1250 2990 7800	2030 515-1288 840		.experiments performed under partial vacuum-blower downstr...
STERMERDING (1962) (1)	10	51	0-15	Catalyst	1600	65	30-90	.some results at high gas pressures
BOOTHROYD (1966) (10)	4.5	25.4 50.8 76.2	6-42	Zinc	7140	10	0-17	.observed drag reduction

TABLE 2.1 (continued)
 VERTICAL, PNEUMATIC TRANSPORT EXPERIMENTAL STUDIES :
 TYPICAL, PARAMETER RANGES

Author	Pipe length (m)	Pipe diameter (mm)	Gas velocity range (m/s)	Particle type	Particle density (kg/m ³)	Particle size (μm)	Loading ratio	Add. measurements, Observations		
JONES et al. (1967) (67, 68)	6.45	7.75	0-30	Glass	2500	200-765	0-6	.solids concentration by quick closing valves .modified terminal velocities measured in air, helium, CO ₂ argon, Freon-12		
		10.2		Alumina						
		22.1		Silica Steel						
KONNO & SAITO (1969) (78)	8	26.5	8-20	Glass	2500	120-1050	0-6	.local air velocities measured with pitot tube .particle velocities measured photographically		
		48.8		Copper						
				Millet						
				Grass						
REDDY & PEI (1969) (106)	3	100	7-14	Glass beads	2590	100 150 200 270	0-0.6	.local air velocities-pitot tube .turbulence-hot wire .local particle velocities-photo-graphs		

TABLE 2.1 (continued)
 VERTICAL PNEUMATIC TRANSPORT EXPERIMENTAL STUDIES :
 TYPICAL PARAMETER RANGES

Author	Pipe length (m)	Pipe diameter (mm)	Gas velocity range (m/s)	Particle type	Particle density (kg/m ³)	Particle size (µm)	Loading ratio	Add. measurements, Observations
ROSE & DUCKWORTH (1969) (110)	9.75	32	0-25	Mustard seed	960	2020		
				Lead	9800	381-2032		
				Steel	6500	3170		
HAIR & SMITH (1972) (55)	4.6	78.7	11-38	Glass	2570-3110	5900-2300	0-10	studied mixtures of different particles
				Sand	2610	211		
CAPES & NAKAMURA (1973) (20)	9.2	76.2	0-30	Glass	2470-2900	470-2900	0-8	mean solids concentration measured by quick-closing valves
				Steel	7500	256-2340		
				Rape seed	1058	1780		
				Poly-ethylene	911	3400		
YOUSFI & GAU (1974) (152)	6	38	0-16	Poly-styrene	1060	290	0-120	mean solids concentration measured by quick closing valves
				Catalyst Glass	850	55-20		
		50			2740	118-143-183		

TABLE 2.1 (continued)
 VERTICAL PNEUMATIC TRANSPORT EXPERIMENTAL STUDIES :
 TYPICAL PARAMETER RANGES

Author	Pipe length (m)	Pipe diameter (mm)	Gas velocity range (m/s)	Particle type	Particle density (kg/m ³)	Particle size (µm)	Loading ratio	Add. measurements, Observations
SHIMIZU et al. (1978) (119)	6.2	28	0-30	Copper	8900	44-172	0-5	studied upward and downward flowing suspensions
TOMITA et al. (1980) (131)	24	41 67	0-30	Cement	2560	30	51-244	examined gas compressibility effects

velocity) ; the solids friction factor is then determined from the difference between the measured pressure drop and the first two terms.

The simplest friction factor correlation resulting from this type of study follows the initial result given by Hariu and Molstad ; that is, the solids friction factor was found to be essentially constant over the operational parameters studied. As mentioned, Hariu and Molstad determined the solids friction factor to be approximately 0.004 in their experiments. Other investigators proposing constant solids friction factor correlations include Stermerding (126) ($f_s = 0.012$ for cracking catalysts), de Jong (31) ($f_s = 0.0048$ for downward flowing glass beads suspensions), Dixon (36) ($f_s = 0.016$ for acrylic spheres and alkathene chips) and Yousfi and Gau (152) ($f_s = 0.006$ for polystyrene particles ; $f_s = 0.012$ for glass beads).

It is common knowledge that friction factors in single phase pipe flows tend to decrease with fluid velocity (or, more precisely, with Reynolds number). This fact seems to have been the stimulus behind several attempts to correlate solids frictions factors by equations of the form :

$$f_s = a v_s^{-b} \quad (2.6)$$

Correlations of this type are summarized in Table 2.2.

More elaborate friction factor correlations have resulted from the work of several other investigators. Hinkle (59), who mainly studied horizontal transport, proposed the following expression which

TABLE 2.2

SOLIDS FRICTION FACTOR CORRELATIONS
AS DECREASING FUNCTIONS OF SOLIDS VELOCITY

Author	Reference	Values of a and b Equation 2.6 *	
		a	b
Razumov	105	0.089	1.5
Reddy and Pei	106	0.046	1.0
Konno and Saito	78	0.025	1.0
Capes and Nakamura	20	0.048	1.22

* Values are given for V_s in m/s.

was held to be also valid for vertical conveying :

$$f_s = 12 (c_s/c_g) \frac{W_s}{U_g} \left[\frac{U_g}{V_s} \right]^{0.2} \quad (2.7)$$

Knowlton and Bachoychin (76) studied vertical pneumatic conveying of siderite ore and Montana lignite in a transport line operating at pressures up to 45 bars. They unsuccessfully attempted to correlate their results with Hinkle's solids friction factor expression and thus subsequently proposed a modified version of their own :

$$f_s = \left[0.10 \left[\frac{W_s}{c_g U_g} \right]^{0.0415} \left[\frac{V_s}{U_g} \right]^{-0.859} \right]^{-0.12} \quad (2.8)$$

Yang (147, 149) suggesting an analogy between pneumatic conveying and the flow of gas across a fixed bed of solids, presented a friction factor expression, the form of which was derived from the Ergun equation for pressure drop in packed beds. Analyzing the data of Hariu and Molstad (56), Capes and Nakamura (20) and Konno and Saito (78) he arrived at the following two expressions which were said to be valid for $U_g/V_t > 1.5$ and $U_g/V_t < 1.5$ respectively :

$$f_s = 0.0504 \frac{(1-\epsilon)}{\epsilon^3} \left[(1-\epsilon) \frac{V_t}{V_s} \right]^{-0.979} \quad (2.9)$$

and

$$f_c = \frac{(1-c)}{\epsilon} \left[(1-c) \frac{V_s}{V_g} \right]^{-1.75} \quad (2.15)$$

All the friction factor correlations presented thus far require knowledge of the mean solids velocity, either explicitly because V_s appears in the friction factor correlation, or implicitly since V_s is a term in the defining equation for the solids friction factor (Eq. 2.5). Experimental studies with direct measurements of this quantity generally use the measured values in developing their correlations; others are required to make an assumption concerning its value.

Four basic approaches have been used to deal with this problem. The first and simplest, as was previously mentioned, is to assume that the mean solids velocity is equal to the difference between the mean gas velocity and the solids ~~terminal~~ settling velocity, where the latter term is calculated based on the mean particle size. This is the method proposed by Leung (83) in reviewing design techniques for dilute vertical pneumatic conveying. Zenz (154) also suggested using the assumption that $V_s = U_g - V_t$ in conjunction with Hinkle's friction factor correlation for vertical pneumatic conveying in general.

There is little experimental evidence in ~~support~~ support of this hypothesis however, except over limited operating ranges. Konno and Saito (78) found it to be approximately ~~correct~~ correct in their experiments at low solids to gas loading ratios. This assumption also allowed

Stermerding (126) to successfully correlate his data on cracking catalyst conveying. Most other workers, on the other hand, have shown that the mean slip velocity between the solids and the gas is, in fact, greater than the solids terminal velocity. The most important parameters affecting the difference have been found to be the loading ratio and the gas velocity, with the latter variable being of prime importance in dilute conveying.

The effect of these two factors on slip velocities has been accounted for either via the determination of modified drag coefficients (eg. Ottjes (98), Jodlowski (65)) or via modified terminal velocities (eg. Razumov (105), Chandock and Pei (21), Reddy and Pei (106)). A popular way of correlating modified drag coefficients or terminal velocities to account for solids loading is to introduce an expression of the form developed by Richardson and Zaki (108) in experiments on fluidization and sedimentation :

$$v_t = v_{to} e^{-k} \quad (2.11)$$

where at the solids concentration levels characteristic of pneumatic conveying, the constant k has a value of 4.7 (88, 139).

The Richardson and Zaki expression is often used as part of a third approach to the solids velocity problem, which is somewhat more rigorous than the others. This consists of writing a force balance for the solids contained in a section of the pipe and equating the drag forces exerted by the gas on the solids to gravitational and wall

friction forces. The particle velocity is then considered to be established as a result of this balance. The above approach has been used by Mehta, Smith and Comings (88) and by Yang (148). The former authors, having found experimentally that, over the range of their experiments, the slip velocity was unaffected by solids loading, introduced no corrective factor in their drag force expression to account for modified drag coefficients ; the latter author, who attempted to correlate a wider range of data, introduced the Richardson and Zaki modification.

The final technique for dealing with the solids velocity problem is to simply develop correlations either in terms of individual parameters or in terms of groups of dimensionless numbers without reference to terminal velocities. Table 2,3 gives a sampling of this type of correlation.

The use of solids friction factors which require knowledge of, or correlations for solids velocities to calculate pressure drops has been criticized on several occasions (41, 54) since it introduces an unnecessary added level of complication and uncertainty in the overall calculation. As a result, a number of solids friction factor correlations have been developed which require only knowledge of the gas velocity. An example of this was presented in the previous section with Belden and Kassel's combined gas-solids friction factor defined by Eq. 2.3. Other authors have retained the decomposition of the overall pressure drop into three components, defining however a solids friction factor based on the gas velocity :

TABLE 2.1
TYPICAL SOLIDS VELOCITY CORRELATIONS

Author	Reference	Correlation
BARTH	5	$\frac{V_s}{U_g} = \frac{1 - (0.05)^{Fr} \{1 - 1.2 (Fr'/Fr) + (Fr'/Fr)k_2^{0.5}\}}{1 - 0.5k_1 Fr'}$
HINKLE	59	$\left(\frac{V_s}{U_g}\right) = 1 - 0.17 \left(\frac{d_p}{D}\right)^{0.5} \left(\frac{\rho_p}{\rho_g}\right)^{0.5}$
JONES et al.	67	$\frac{U_g}{V_s} = \frac{2.40 \left(\frac{\rho_s}{\rho_g}\right)^{0.573} \left(\frac{d_p}{D}\right)^{1.02} \times 0.7}{0.37 \left(\frac{\rho_p}{\rho_g}\right)^{0.347}}$
SCHUCHART	11b	$\frac{V_s}{U_g} = 1 + \left\{ \frac{1}{2} \left(\frac{\rho_s}{\rho_g} - 1 \right) \right\}^{0.66} \left(\frac{d_p}{D} \right)^{0.66} \times \left[1 + \frac{200}{U_g / (gD)^{0.5}} - \frac{U_g}{(gD)^{0.5}} \right]$
CAPES and NAKAMURA	20	$V_s = k_1 U_g + k_2$

$$\frac{\Delta P_{fs}}{\Delta L} = \frac{f_{sg}}{2D} (\rho_g U_g^2) \quad (2.12)$$

Jones et al. (68) proposed the following correlation for the above-defined solids friction factor :

$$f_{sg} = k_1 (W_s/W_g)^{k_2} \quad (2.13)$$

where

$$k_1 = \left[\frac{20700}{A_o} \right]^{1/3}$$

$$k_2 = 5.76 \times 10^{-7} (A_o/\psi_a)$$

where A_o is the surface area of the particles in (m^2/m^3) and ψ_a is the particle surface shape factor.

The same solids friction factor definition appears in the works of Rose and Barnacle (109), Rose and Duckworth (110) and Duckworth and Kakka (42) all of whom studied both gas-solids and liquid-solids conveying. These three pairs of authors used dimensional analysis to group relevant variables and proposed correlations having similar forms. By way of illustration, the Rose and Duckworth result is :

$$f_{sg} = \phi_1 (W_s/W_g) + \phi_2 (d_p/D) + \phi_3 (\chi) + \phi_4 (\rho_s/\rho_g) + \phi_5 (\theta_p) + \phi_6 (U^2/gD) \quad (2.14)$$

where the each of the functions ϕ is given in the form of a graphical correlation.

2.2.3 Other empirical and semi-empirical approaches

In addition to correlations based on solids phase friction factors, there are a number of other important approaches to pressure drop in vertically flowing gas-solids suspensions which range from pure empiricism to more or less elaborate models. The work of Konchesky et al. (77), who studied crushed coal transport in vertical pipelines is an example of the former approach. Their investigation consisted of experimentally determining the minimum air flow-rate required to convey crushed coal at a given flowrate and then correlating the corresponding pressure drop. As a result of their work they were able to develop the following pressure gradient expression:

$$\frac{\Delta P_{SS}}{\Delta L} = 0.031 W_s^{0.791} \rho_s^{0.231} \exp (7.607/D + 0.0957/A_{pp}) \quad (2.15)$$

where W_s has units of tons per hour ; ρ_s is given in g/cm^3 , D is in inches, $\Delta P_{SS}/\Delta L$ is in inches of water per foot and A_{pp} , the ratio of the pickup area at the injection point to the pipe area, is dimensionless.

While this type of empiricism may be criticized for its limited applicability, the basic approach is nevertheless that used by most pneumatic transport line manufacturers who develop similar correlations for a given solid in their test installations for use as a basis for design of commercial installations (65).

Another method follows from the Vogt and White approach (137) presented earlier whereby correlations are developed in terms of the ratio of the pressure drop of the suspension to that of the gas flowing alone. Other than Vogt and White, Boothroyd (10) and Ghosh and Prem Chand (50) are among those who have advanced correlations of this type. The justification for choosing this form of equation to correlate vertical gas-solids pressure drops has been criticized on at least two occasions however (83, 107) based on arguments that the static head of solids, which plays an important role in vertical conveying, as a tenuous connection to the **losses due to gas-wall friction.**

Six final approaches which differ from those presented up until now also required comment. In the preceding section a solids friction factor expression developed by Yang based on an analogy between pneumatic transport and the flow of gas across a packed bed of solids was presented. While Yang made use of the analogy in order to develop the form of his friction factor correlation, Wen (140, 141) carried the analogy further and suggested that the solids friction term in the overall pressure drop expression could be obtained directly from the Ergun equation for pressure drop across a packed bed :

$$\frac{\Delta P_{fs}}{\Delta L} = \frac{150 (U_g - V_s)(1-\epsilon)^2}{d_p^2 \phi_s^2 \epsilon^3} + \frac{1.75(1-\epsilon)c_g(U_g - V_s)^2}{d_p \phi_s \epsilon} \quad (2.17)$$

Solution, in order to calculate the overall pressure drop, requires an additional expression relating the gas and solids velocity and the porosity in the line. Wen and Yu (139) proposed the following empirical expression for this:

$$\frac{\epsilon^{4.7} d_p^3 (\rho_s - \rho_g) g}{\mu} = \frac{18 d_p (U_g - \epsilon V_s)}{\mu} + 2.7 \left[\frac{d_p (U_g - \epsilon V_s) \rho_g}{\mu} \right]^{1.557} \quad (2.18)$$

While Wen's approach was successfully used to correlate some data (in particular, for dense phase transport), the author himself recognized its main practical drawback as being its extreme sensitivity to porosity which is difficult to determine with precision.

Wen's method may also be criticized in that it is based on faulty reasoning concerning the momentum balance on the suspension. Indeed, the pressure drop expression, Eq. 2.5, can be thought of as a momentum balance on the gas and solids in a pipe section with the inertial terms being zero for fully developed flow. If individual momentum balances on both the solids and gas phases were carried out, an interaction term would appear as an external force in each of the two equations. The fixed bed analogy would allow this interaction term to be expressed by the Ergun equation. Examination of the solids momentum

equation would show this term to be equal not just to the particle wall friction term but to the sum of the solids frictional losses plus the solids hold-up. Wen's approach in retaining the original three term expression consists of ~~counting~~ counting the solids hold-up twice.

Mehta, Smith and Comings (88), after trying several other correlation techniques, finally managed to correlate their pressure drop results on glass beads with the following expression :

$$\frac{\Delta P_{fs} + \Delta P_g}{\Delta L} = \frac{f_2 \rho_g U^2}{2D} \left[1 + \left[\frac{\rho_s (1-\epsilon) V_s^2}{\rho_g U^2} \right]^k \right] \quad (2.19)$$

Their work is significant in that they first attempted to correlate their data by the methods described in Sec. 2.2.2. A plot of the solids friction factor as a function of particle Reynolds number, however, showed such scatter that they concluded that the decomposition of pressure drop into three independent components was unjustified; in particular, they felt that the assumption that gas pressure drop (the first term on the LHS of Eq. 2.5) was unaffected by the presence of solids was unfounded. They preferred therefore to define a "suspension" friction factor given in Eq. 2.19 and found it to be essentially constant for a given particle diameter at pipe Reynolds numbers over about 20 000.

The view that the pressure drop in the gas phase is, in fact, affected by the presence of the solids was the starting point for the work of Julian and Dukler (69) who felt not only that it was affected, but also that the resulting modification of the gas flow field was

primarily responsible for the differences in pressure drops for suspensions compared to those in single phase flow. Particle-wall collisions were considered to be unimportant in comparison. Julian and Dukler therefore proposed a model based on turbulent velocity distribution and eddy viscosity equations modified to account for the mass flow of the solids phase. Pressure drop measurements from a number of workers were then used to correlate the Von Karman turbulence constant as a function of loading ratio. They then went on to derive a suspension friction factor correlation similar to that given by Metha and Comings although, unlike the latter authors, their friction factor shows a monotonic decrease as a function of Reynolds number at constant loading ratio. Values increase as the loading ratio increases at constant Reynolds number.

Nakamura and Capes (96) presented two models for vertical pneumatic transport, each of which was held to apply to a particular flow regime. The first, the "uniform flow model" was developed for relatively high gas velocities where it was assumed that gas and solids velocities and solids concentration were uniform across the section of the pipe. An overall momentum balance carried out on the gas and solids phases in a pipe cross-section then resulted in a representation which is similar to that described in the section on solid friction factors. Once a friction factor correlation was developed, their experimental verification of the uniform flow model consisted of comparing experimental and predicted mean solids velocities.

The second Nakamura and Capes model, the "angular flow model", resulted from two experimental observations, one qualitative and one

quantitative. At gas velocities only slightly in excess of the particle terminal velocity, Nakamura and Capes observed particle recirculation near the walls of the transport line. In correlating their pressure drop data, they, like other workers, subtracted the gas-only pressure drop and the solids hold-up from the total measured pressure drop to obtain the frictional pressure loss due to the solids. In cases where solids recirculation was observed visually, the experimental pressure drop due to the presence of the solids was often found to be negative. In order to account for this, Nakamura and Capes proposed that, at low gas velocities, the pipe cross-section be divided into two zones: a central core in which the uniform flow model applied and an annular region where particle recirculation effects were predominant. Momentum exchange between the two zones was assumed to be due only to that which accompanied radial particle movement. As in the case of the uniform flow model, the annular flow model was tested with experimental mean solids velocity results with adjustable parameters being the relative sizes of the two zones and the particle recirculation rate in the annular zone. The additional assumption that the pressure drop in the pipe was such that energy consumption was minimized was necessary to solve the resulting equations.

Arastoopour and Gidaspow (2) and Arastoopour et al. (3) described the hydrodynamics of vertical pneumatic conveying based on the relative velocity model developed by Gidaspow (51, 52) from non-equilibrium thermodynamic considerations. The relative velocity model is based on writing the total energy of a two phase system as a function

of internal energy and potential energy, the latter of which depends on the relative velocity between the two phases. At equilibrium the total energy is minimized keeping internal energies constant. In the case where the velocities of the solids and gas phases differ, the following relation results :

$$(U_g - V_s) \left[\frac{\partial U_g}{\partial z} - \frac{\partial V_s}{\partial z} \right] + g = 0 \quad (2.20)$$

Arastoopour and Gidaspow use the above equation as well as the individual gas and solids phase continuity equations and a momentum balance equation written for the mixture as the basis for interpreting the experimental results of a number of authors. The numerical solutions to their equations confirm the trends found experimentally, in particular, the graphical representation of pressure drop as a function of gas velocity given by Zenz. Their method is of interest however only in the case of accelerating flows. Indeed, the first term on the left hand side of Eq. 2.20 is zero for fully developed flow ; in this case, Arastoopour and Gidaspow's equation reduces to the pressure drop being equal to the solids hold-up plus the gas frictional losses. Solids friction at the wall is neglected. Furthermore, their numerical solutions require knowledge of initial conditions on pressure and solids concentration at a point in the transport line. Such data is not normally available from experimental studies.

Singh (120) recently published a " theoretical " model to describe pressure drop in vertical conveying which was held to be applicable to both gas-solids and liquid-solids systems. His approach is basically the three component approach described earlier but is

original in its dealing with the solids friction factor and in the fallaciousness of its arguments. Dismissing previous approaches involving the use of solids friction factors he suggests that "by analogy with fluidized beds, ΔP_{fs} is always equal to "

$$\Delta P_{fs} = (\rho_s - \rho_g) (1 - \epsilon) \bar{z} \quad (2.21)$$

The overall pressure drop expression then becomes :

$$\frac{\Delta P_{fs}}{\Delta L} = \frac{\Delta P_{fg}}{\Delta L} + 2\epsilon_s (1 - \epsilon)g + \epsilon_s (1 - \epsilon)g \quad (2.22)$$

with the latter two terms representing the solids hold-up and frictional losses and the gas hold-up. The fault in Singh's reasoning lies in the fact that, while the pressure drop across a fluidized bed is indeed that given by Eq. 2.21, this is true only because frictional losses involving particle-wall collisions are negligible. In the case of a fluidized bed the pressure drop is given solely by the solids hold-up term. Singh's approach reduces to neglecting solids frictional losses and counting the solids hold-up twice. The reason for the apparent good agreement between Singh's predicted and experimental results, as has been pointed out by Ieo and Chong (128), remains a mystery.

2.2.4 Comments and conclusions

The most remarkable aspect of the work carried out up to the present time on vertical pneumatic transport is the striking number of correlations having limited applicability which have been developed,

and the dearth of correlations which are sufficiently general to embrace a wide range of system parameters and operating conditions.

Attempts at generalizing correlations have met with only limited success. Khan and Pei (72) analysed eleven pressure drop correlations using data of their own as well as that of a wide range of other investigators in order to attempt to derive a modified correlation with improved generality. Their analysis resulted in the following correlation, which, while being more reliable than the others tested, still showed deviations between predicted and measured values of up to 51 % :

$$\frac{\Delta P_{SC}}{\Delta P_{LG}} = 2.66 \left[\frac{C_D}{f_{LG}} \left[\frac{\rho_L}{\rho_S} \right] \left[\frac{d_p}{D} \right]^2 \left[\frac{Re}{Fr} \right]^{0.5} \left[\frac{W_S}{W_{LG}} \right] \phi_S^{-0.5} \right] \quad (2.23)$$

Incidentally, Khan and Pei's evaluation of other pressure drop correlations should be approached with caution, as the correlations listed in their article differ from those given in the original papers in at least 4 of the 11 cases.

Yang's (48) "unified theory" of dilute phase pneumatic transport was also an attempt to bring together data from numerous investigators to develop an empirical treatment of wider applicability based on a solids friction factor. Examination of the data he used however shows deviations of up to an order of magnitude in the correlated friction factor results. Similar dispersion in the measured solids friction factors was found by Capes and Nakamura (20) in examining correlations based solely on the particle velocity. By way

of illustration, the Capes and Nakamura and Yang original friction factor plots are reproduced in Figure 2.2, and Figure 2.3 respectively.

The difficulty in obtaining reliable friction factor correlations results essentially from two causes. Firstly, the experimental determination of the solids friction factor involves subtracting two large quantities (the sum of the gas pressure drop and the solids hold-up) from the total measured pressure drop to obtain a smaller quantity (the pressure drop due to solids friction). The latter term is then divided by the square of the solids velocity which must also be determined experimentally. There is a natural tendency then toward data dispersion.

The second reason is linked to the inherent limitations of such empirical approaches. The fundamental hypothesis that the total pressure drop can be decomposed into three independent components and that the frictional pressure drop due to the presence of the solids has a mathematical form analogous to that for a single phase fluid has not yet been established theoretically. Furthermore this type of empiricism gives no a priori indication concerning the dependence of friction factors on the physical parameters characterizing the system nor on the system operating conditions. Correlations, as a result, take on a more or less random form incorporating the limited number of parameters varied within a given study.

The net result is a large number of correlations, often with conflicting functional relationships between derived and basic variables. Some of these conflicts have been pointed out by Khan and Pei in their review: in particular, the literature shows ambiguities

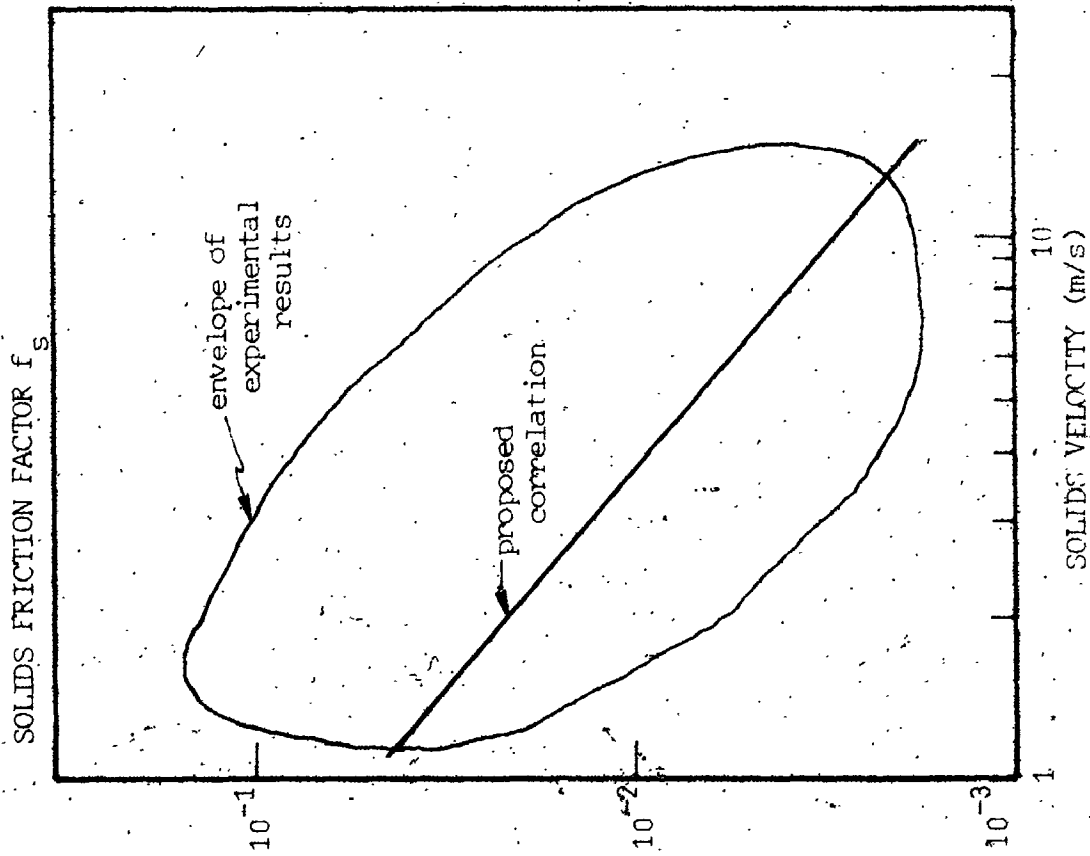


FIGURE 2.2 Capes and Nakamura (20) Friction Factor correlation

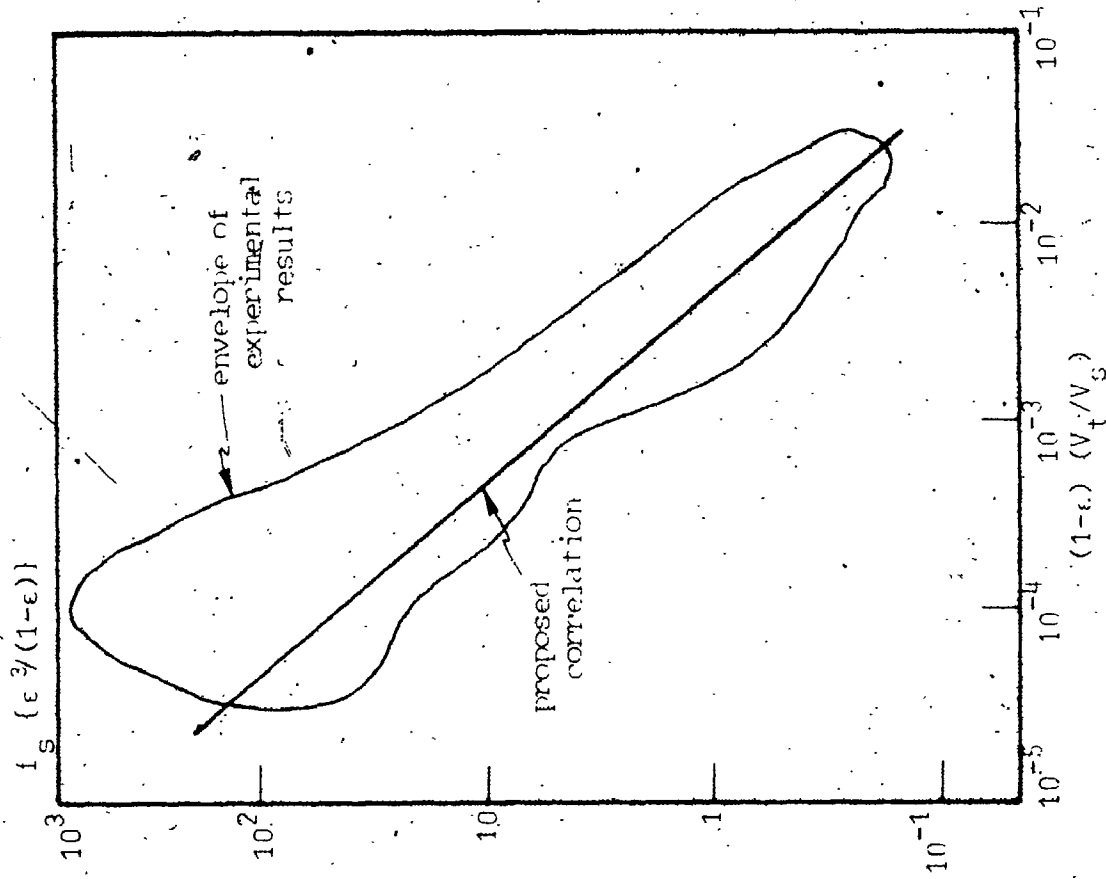


FIGURE 2.3 Yang (149) Friction Factor correlation

in the dependence of pressure drops on particle to pipe diameter, Reynolds number and even loading ratio. This latter point is of particular importance since the traditional three component approaches all make the implicit assumption that pressure drops increase when solids are added to a flowing gas stream; that is, it is assumed that solids friction factors are always positive.

As has already been seen from the work of Capes and Nakamura (Van Swaaij et al. (134) also made a similar observation), at low gas velocities with relatively large particles ($d_p > 50 \mu\text{m}$) pressure losses due to particles friction at the pipe wall can be negative. Similar results under very different experimental conditions (small particles, high gas velocities) have been observed by a number of workers: Soo and Trezek (122), Depew (34), Boothroyd (10, 11), Rossetti and Pfeffer (111) and Kane et al. (70) all observed reductions in pressure drops as the loading ratio was increased from 0 to about 1, followed by increases thereafter.

It can be concluded from this that the situation described by Kraus (80) in 1968 has changed little since: "the theory of pneumatic conveying is still in the development stage.... the formulae and numerical data obtained from the experimentors cannot be extended or applied to the design of pneumatic conveying systems for materials different from those tested". Soo (125) more recently expressed a similar evaluation: "one must recognize the absence of a well-founded theory which would embrace all problems in detail and which has undergone verification in practice".

This state of affairs determines in a large way the strategy for future work. If one is interested only in order of magnitude estimates for industrial design, as proposed by Leung (83) and Govier and Aziz (54), the solution would seem to be to employ a correlation developed under the conditions most closely resembling those of the problem at hand. Simple friction factor correlations (where f_s is constant or a function of a limited number of easily accessible parameters for example) provide quick solutions to this type of problem. From a research and development point of view, the limited success of generalized empirical correlations would seem to argue against further work in this direction: calculations, for practical purposes, become unwieldy (Yang's method, for example, requires iterative solutions for V_s , ϵ and f_s) without a substantial gain in precision nor additional insight into the phenomena determining the flow structure and overall suspension behaviour. Real advances would seem to require a more fundamental approach allowing individual phenomena to be isolated, examined in detail and modeled in cases where they are determinant for specific flow situations.

2.3 Heat Transfer between Vertically Flowing Gas-Solids Suspensions and Pipe Walls

2.3.1 Experimental Studies : Methods and Data Analysis

The earliest published studies on heat transfer between flowing gas-solids suspensions and pipe walls are those of Farbar and Morley (44) and Depew and Farbar (34). The experimental techniques used by these two pairs of authors served as the basis for other experimental

studies which followed. There is however some variation in basic measurement techniques and in subsequent data treatment and, as these differences have considerable influence on the interpretation of phenomena and on the development of correlations, they will be examined in some detail in this section.

Farbar and Morley's experimental set-up consisted of a double-pipe heat exchanger inserted in a pneumatic conveying line. The suspension flowed upward in the inner pipe which had an inner diameter of 17.5 mm. Condensing carbon tetrachloride circulating in the annular section surrounding the test pipe served as the heat source. In this way, Farbar and Morley were able to ensure practically isothermal wall conditions. Assuming the temperature of the gas and solids to be equal at the test section inlet and calculating the suspension "mixed mean" temperature at the outlet from a heat balance on the system, they defined a heat transfer coefficient based on the log mean temperature difference :

$$h_{ss}^{lm} = \frac{q_{ss}}{\Delta T_{ss}^{lm}} \quad (2.24)$$

where :

$$\Delta T_{ss}^{lm} = \frac{(T_1 - T_{ss1}) - (T_2 - T_{ss2})}{\ln \left[\frac{T_1 - T_{ss1}}{T_2 - T_{ss2}} \right]} \quad (2.25)$$

$$T_{ss} = \frac{W_s C_s T_s + W_g C_g T_g}{W_s C_s + W_g C_g} \quad (2.26)$$

and T_1 and T_2 are the inlet and outlet temperatures of the heat source.

The second basic method of determining heat transfer coefficients in flowing gas-solids suspensions consists of passing an electrical current through a steel pipe to heat the suspension flowing inside under more or less constant heat flux conditions. Provided the pipe wall is sufficiently thin so that axial heat conduction can be neglected, the local radial heat flux from the pipe to the suspension can be determined directly from electrical voltage and current measurements. This method has the advantage compared to isothermal wall methods, of allowing the determination of local heat transfer coefficients and thermal entry lengths. Depew and Farbar (34) used this technique with an 18.5 mm ID pipe, 0.9 m in length, and having a wall thickness of 0.5 mm. They defined a local heat transfer coefficient based on measured local wall temperatures and the local mixed mean suspension temperature determined via the measured suspension inlet temperature and a heat balance up to the point under consideration :

$$h_{ss}(z) = \frac{q_{ss}(z)}{T_w(z) - T_{ss}(z)} \quad (2.27)$$

where :

$$T_{ss}(z) = T_{ss1} + \frac{q_{ss} \pi D z}{W_s C_s + W_g C_g} \quad (2.28)$$

and T_{ss1} is the mixed mean suspension inlet temperature.

While these two experimental methods were retained by the majority of workers who followed, some experimental variations have been employed (See Table 2.4). The most important variations in the two basic techniques however concern the way in which temperatures were determined and the definition of heat transfer coefficients. The use of a heat balance to determine the suspension mixed mean temperature, while being convenient from an experimental point of view, is an indirect method and gives neither the real gas temperature nor the real solids temperature except in cases where they are the same (cf. Eq. 2.26). This equivalence rarely holds except where the particles are very small (123). As the general consensus is that the heat transfer process from walls to dilute suspensions involves transfer from the wall to the gas followed by transfer from the gas to the solids (35), some workers have preferred to define the heat transfer coefficient based on the mean gas temperature (See Table 2.4). Coefficients defined in this way generally rely on bare thermocouple measurements to determine the gas temperature. It can be also noted from the table that a number of workers have used thermocouples to measure suspension temperatures at either the outlet of an adiabatic section following the test section or at the point under consideration where the solids and gas are reasoned to be in thermal equilibrium.

Another comment which can be made pertaining to the experimental methods used in previous heat transfer studies concerns the problem of fully developed flow; both from a hydrodynamic and thermal point of view. Clearly, the heat transfer phenomena are dependent on the hydrodynamic structure of the suspension flow. Experimentally deter-

mined heat transfer coefficients would be expected, therefore to be different if the flow was hydrodynamically fully developed or not. Several of the set-ups listed in Table 2.4 had approach sections before the heat transfer section which were very short suggesting that, in some cases, the particles had not been fully accelerated at the test section inlet. Depew and Farbar (34) in their initial study noted a non-linear pressure profile at the test section inlet at loading ratio above three.

Similar uncertainties arise with respect to the length of the heat transfer pipe. As will be shown later thermally fully developed flow can only occur under constant heat flux conditions. In the isothermal-wall set-ups overall coefficients would then depend on the length of the heat transfer section. Even in the uniform heat flux set-ups, the test sections have been found on several occasions (Eg. Ref. 130, 151) not to be long enough for the flow to become thermally fully developed.

These method and definition differences and experimental problems are important to keep in mind when evaluating correlations which have resulted from the various studies cited. Indeed, beyond the obvious differences in measured coefficients which would result from differences in the basic set-ups (isothermal or uniform heat flux), the important deviations in results obtained under similar experimental conditions have often been explained (73, 144) by difference in heat transfer coefficient definitions and in experimental determinations of temperature driving forces.

TABLE 2.4
SUSPENSIONS-WALL HEAT TRANSFER STUDIES: EXPERIMENTAL SET-UPS

Authors	Method	Inside pipe diameter (mm)	Length of heat transfer (m)	Length of approach section (m)	Average wall temperature (°C)	Basis for defining heat transfer coefficients
FARBAR & MORLEY (1957) (44)	heating constant wall temperature condensing CCl_4	17.5	0.84	0.20	81	log mean temperature (suspension) suspension outlet temperature via heat balance
DEPEW & FARBAR (1963) (34)	heating constant heat flux	18.5	0.90	0.55	55	local mixed mean and wall temperatures suspension temperature via heat balance
JEPSON & POLL (1963) (64)	heating double pipe, hot water	38.1	3.65	3.80	80	log mean temperature (gas) gas temperature via thermocouple at exchanger outlet
DANZIGER (1963) (28)	cooling tube banks steam	28.6 38.0	6.70 5.79	N.A.	470	log mean temperature (suspension) suspension outlet temperature via thermocouple
WILKINSON & NORMAN (1967) (144)	heating constant heat flux	53.4	1.52	4.04	540	difference between mean wall temperature and suspension temperature measured via thermocouple

TABLE 2.4. (continued)
SUSPENSIONS-WALL HEAT TRANSFER STUDIES : EXPERIMENTAL SET-UPS

Authors	Method	Inside pipe diameter (mm)	Length of heat transfer (m)	Length of approach section (m)	Average wall Temperature (°C)	Basis for defining heat transfer coefficients
BOOTHROYD & HAQUE (1970) (13, 14)	heating constant heat flux	25.4 50.8 76.2	3.05	1.52	N.A.	local mixed mean and wall temperatures suspension temperature via heat balance
CURIEVICI & HORIA (1970) (27)	heating constant heat flux	30	3.00	1.55	130	local mixed mean and wall temperatures local suspension temperature determined by interpolating between inlet and outlet temperatures measured via thermocouples
YOUSFI & GAU (1974) (151)	heating constant heat flux	38	1.80	3.37	130	average wall and mixed mean temperatures measured by thermocouples
NAG & RAO (1974) (95)	cooling double pipe water	38	1.1	N.A.	N.A.	wall temperatures measured via thermocouples mixed mean temperature via heat balance local coefficient calculated assuming constant heat flux overall coefficient arithmetic mean of local coefficients

TABLE 2.4 (continued).
SUSPENSIONS-WALL HEAT TRANSFER STUDIES : EXPERIMENTAL SET-UPS

Authors	Method	Inside pipe diameter (mm)	Length of heat transfer (m)	Length of approach section (m)	Average wall temperature (°C)	Basis for defining heat transfer coefficients
MATSUMOTO et al. (1978) (87)	heating constant wall temperature condensing steam	26	2.0	4	100	log mean temperature (gas) gas temperature at outlet determined via thermocouple average outlet gas temperature defined by integration of temperature and velocity profiles
KIM & SEADER (1983) (74)	heating constant heat flux downflow	13	0.914	6.7	120	local mixed mean and wall temperatures suspension temperature via heat balance

N.A. = Not available

2.3.2 Experimental Studies: Operating parameters and results

Farbar and Morley's initial exploratory study involved the use of a single solid (alumina-silica catalyst) and investigated only the effects of Reynolds number and loading ratio on a heat transfer coefficient based on the log mean (mixed mean on the suspension side) temperature difference. Their results showed heat transfer coefficients determined in this way to be constant at solids loading ratios less than about 1 after which they increased as a function of $(w_s/w_g)^{0.45}$ and $Re^{0.6}$. These results ~~unambiguously~~ suggested that gas-solids suspensions, in addition to offering higher volumetric heat capacities compared to simple gases, also led to higher heat transfer coefficients and therefore very much increased heat transfer rates. Work in this area then proceeded along three lines: the development of correlations directly applicable to catalyst conveying systems used in transport reactors and transport lines to and from fluidized bed reactors, the development of correlations for, and the study of practical problems associated with the use of fine graphite suspensions for nuclear reactor cooling and academic studies aimed at developing an understanding of the phenomena associated with suspension heat transfer processes. A representative sampling of these studies is detailed in Table 2.5. While managing to elucidate certain general trends, these works, as will be shown in the discussion to follow, have yet to achieve a satisfactory understanding of basic phenomena and many ambiguities continue to exist concerning the effects of basic operating parameters on heat transfer coefficients.

TABLE 2.5

EXPERIMENTAL STUDIES OF HEAT TRANSFER BETWEEN VERTICALLY FLOWING GAS-SOLIDS
SUSPENSIONS AND PIPE WALLS : PARAMETER RANGES

Author	Pipe diameter (mm)	Pipe Reynolds number	Particle type	Particle density (kg/m ³)	Particle size (μm)	Particle heat capacity (J/kgC)	Loading ratio	Notes
FARBAR & MORLEY (1957) (44)	17.5	13500-27000	Alumina-silica catalyst	2450	50	1155	0-10	isothermal pipe wall
BROTZ et al. (1958) (19)	50.3	15000-23000	Glass beads	N.A.	50 300	N.A.	0-4	uniform heat flux
SCHLUDERBERG et al. (1961) (127)	7.95-22.2	1000-60000	Graphite	N.A.	1-5	N.A.	0-14	turbulence promoters present in line He, N ₂ , CF ₄ carrier gases
DEPEW & FARBAR (1963) (34)	18.5	13500-27400	Glass spheres	N.A.	30 200	N.A.	0-8	uniform heat flux
JEPSON & POLL (1963) (64)	38.1	15000-74000	Sand	N.A.	76-104 211-509	N.A.	4.2-16.2	double pipe : water jacket

TABLE 2.5 (continued)
 EXPERIMENTAL STUDIES OF HEAT TRANSFER BETWEEN VERTICALLY FLOWING GAS-SOLIDS
 SUSPENSIONS AND PIPE WALLS : PARAMETER RANGES

Author	Pipe diameter (mm)	Pipe Reynolds number	Particle type	Particle density (kg/m ³)	Particle size (μm)	Particle heat capacity (J/kg°C)	Loading ratio	Notes
TIEN & QUAN (1963) (130)	18.5	15000- 30000	Glass spheres Lead		30 200 30 200	N.A. N.A.	0-3	uniform heat flux
	28.6 38.0	178- 25400	Cracking catalyst	N.A.	50	N.A.	2-446	cooling tube banks
STOCKBURGER (1966) (127)	33.9	13000- 38000	Poly- styrene	1060	280 350 550 770	712	0-30	uniform heat flux
			Calcium carbonate	265	35	760		
WILKINSON & NORMAN (1967) (144)	53.4	17800- 81200	Glass beads	N.A.	40 60 120	N.A.	0-50	high wall temperat- (540°C)
			Graphite	N.A.	74	N.A.		
BOOTHROYD & HAQUE (1970) (13, 14)	25.4 50.8 76.2	35000 53000 80000 100000	Zinc	N.A.	0-40	390	0-17	uniform heat flux

TABLE 2.5 (continued)
 EXPERIMENTAL STUDIES OF HEAT TRANSFER BETWEEN VERTICALLY FLOWING GAS-SOLIDS
 SUSPENSIONS AND PIPE WALLS : PARAMETER RANGES

Author	Pipe diameter (mm)	Pipe Reynolds number	Particle type	Particle density (kg/m ³)	Particle size (μm)	Particle heat capacity (J/kgC)	Loading ratio	Notes
CURIEVICI & HORIA (1970) (27)	30.0	11500-43000	Graphite	N.A.	3	N.A.	0-27	uniform heat flux
YOUSFI (1973) (150)	38.0	2500-38000	Catalyst Glass beads	868 2740	20 180	840 840	0-680	uniform heat flux
MAMEV et al. (1976) (85)	8.0	1000-8000	Corundum	N.A.	60	N.A.	0-25	uniform heat flux
WAH F (1977) (138)	18.0	15000-30000	Glass beads	N.A.	30 62 200	N.A.	0-10	up and down flow
MATSUMOTO (1978) (87)	26.0	12000-24000	Glass beads Copper	2500 8700	72 181 1130 321	770 389	0-10	isothermal pipe wall
KIM & SEADER (1973) (74)	13.0	0-30000	Glass beads	2480	329	N.A.	0-20	down flow

Effect of solids loading ratio

After the initial Farbar and Morley result showing increases in the overall heat transfer coefficient at loading ratios above 2 for 50 μm catalyst particles, other investigations have resulted in less clear trends. Depew and Farbar (34) found no effect on asymptotic coefficients for 30 μm glass beads below loading ratios of 0.5. Using 200 μm glass beads however this observation was extended to loading ratios of up to 7. Their experiments with 30 μm particles showed decreases in the asymptotic heat transfer coefficients for $0.5 < W_s/W_g < 3.0$, followed by large increases thereafter. This latter trend, whereby coefficients pass through a minimum somewhere in the range $0.5 < W_s/W_g < 3.0$ was later substantiated by numerous workers in a wide variety of situations (Eg. Ref. 27, 64, 95, 130, 138). There are exceptions to this to be found however in the works of Danziger (28) who found monotonic increases as a function of loading ratio for cracking catalyst suspensions and Wilkinson and Norman (144) in their work with glass beads, although in the later case, they explained their anomalous results by the difference in their heat transfer coefficient definition (based on the gas temperature) compared to that used by other workers. Kim and Seader (74) using the same coefficient definition as Wilkinson and Norman nevertheless noted decreases in the heat transfer coefficient as a function of loading ratio at high Reynolds numbers in downward flowing suspensions. Constant coefficients were found in Kim and Seader's experiments below Reynolds numbers of about 23,000.

There is general experimental agreement that thermal entry lengths increase with solids loading ratios (27, 74, 130, 138) although the effect seems more pronounced with small particles than with large ones. Depew and Farbar (34) found no significant increase in thermal entry lengths in their experiments with 200 μm glass beads.

Overall, the trends show that, unlike the result suggested by Farbar and Morley's initial experiments, heat transfer coefficients in gas-solids suspension flow are not simple functions of loading ratio.

Effect of particle size

As just mentioned, trends in the variation of heat transfer coefficients as a function of loading ratio appear clearly to be dependent on particle size. Indeed almost all effects, be they decreases in coefficients or increases seem to be more pronounced with small ($< 50 \mu\text{m}$) particles. Large particles tend to exhibit monotonic behaviour with loading ratio although sometimes this translates as monotonic increase, other times by constant coefficients. Small particles tend not to affect coefficients at low loading ratios, then lead to decreases, passage through a minimum and finally increases although the magnitudes of these effects vary considerably. Exceptions to this general behaviour are suggested by Matsumoto et al. (86) who maintain that particle size is of no effect then, curiously propose a correlation (See Sec. 2.3.4) in which particle size appears as a parameter. Jepson and Poll (64) found there to be a critical particle size of about 500 μm which magnified all effects.

Thermal entry lengths systematically have been shown to increase

as particles size decreases.

Effect of Reynolds number (Gas velocity)

Results on the effect of Reynolds number have generally only been results on the effect of gas velocity as, except in a few cases, pipe diameter and gas properties have not been varied. In general, coefficients increase with increasing Reynolds number, although the ratio of suspension coefficients over those for the gas alone flowing under the same conditions tend to remain roughly constant or to decrease slightly. Increasing Reynolds numbers have tended to decrease the effects of other parameters (particle size, loading ratio) on overall coefficients. Again there are some exceptions to these generalizations: Nag (95) found heat transfer coefficient ratios to increase with Reynolds number, Kim and Seader (74) found substantially larger coefficient ratios at high Reynolds numbers than at low.

Thermal entry lengths have been found almost systematically to increase as Reynolds number decreases.

Effect of pipe diameter

The effect of pipe diameter has been examined in some detail by only two investigators, Boothroyd and Haque (13, 14) and Chu (24) with somewhat conflicting results. At similar Reynolds numbers (30000 and 35000) and similar particle sizes (30 μm). Boothroyd and Haque's and Chu's results for 25 mm diameter pipes roughly correspond, both showing decreases in the heat transfer coefficient ratios up to loading ratios of about four. Boothroyd and Haque's data show large

58

increases in coefficient ratios for 51 mm pipes however whereas Chu's do not. The former authors also studied suspension heat transfer in a 76 mm pipe and found very marked increases in coefficient ratios at all loading ratios.

Effect of solids heat capacity

Judging the effect of solids heat capacity on suspension heat transfer coefficients was the primary objective in the work of one pair of investigators. Tien and Quan (130) noted that coefficients were systematically lower with 30 μm lead particles compared with 30 μm glass beads (the glass beads had a volumetric heat capacity of about 6 times that of the lead particles). No perceptible difference was noted in similar experiments with 200 μm particles however.

2.3.3 Correlations and models

Despite the ambiguities in the experimental results cited above a relatively large number of correlations have been developed to predict the variation of suspension heat transfer coefficients on basic flow parameters. These correlations can be divided into three categories: those developed on a strictly empirical basis to be used only within the operating limits of the particular experimental study; those which have resulted from an examination, if only superficial, of the relevant phenomena producing a correlation with improved generality and finally, models which attempt a more or less rigorous treatment of the problem.

Table 2.6 lists a number of examples of the first type of

TABLE 2.6
 SUSPENSION HEAT TRANSFER CORRELATIONS BASED ON A SINGLE OR LIMITED NUMBER OF STUDIES

Authors	Refs	Correlations	Data source	Notes
FARBAR & MORLEY (1957)	44	$\frac{h_{ss}^{lm}}{\lambda_g} = 0.14 Re^{0.6} (W_s/W_g)^{0.45}$ $2.0 < W_s/W_g < 10$	Own	Alumina-silica catalyst
SCHLUDEBERG et al. (1961)	115	$\frac{h_{ss}^{lm}}{\lambda_g} = a Pe^b \{ (W_{Cs}/W_{Cg}) + 1 \}^c$ $0.009 < a < 0.051$ $0.73 < b < 0.97$ $0.45 < c < 0.58$	Own	Graphite suspensions
GORBIS & BAKHTIOZIN (1962)	53	$\frac{h_{ss}^{lm}}{h_g^{lm}} = 1 + 6.3 Re^{-0.3} \left[\frac{\rho_s^d V t}{\mu} \right]^{-0.33} \left[\frac{W_{Cs}}{W_{Cg}} \right]$	Own	Graphite suspensions

TABLE 2.6 (continued)

SUSPENSION HEAT TRANSFER CORRELATIONS BASED ON A SINGLE OR LIMITED NUMBER OF STUDIES

Authors	Refs	Correlations	Data source	Notes																
DANZIGER (1963)	28	$\frac{h_{ss}^{1/4} D}{\lambda_g} = 0.0784 Re^{0.66} (W_s/W_g)^{0.45}$	Own Farbar Morley (9)	Cracking catalyst																
CURIEVICI & HORIA (1970)	27	$\frac{h_{ss}}{h_g} = 0.43 \{ 1 + (W_{sC}/W_g C) \}^{0.75}$	Own	Graphite suspensions																
YOUSFI (1973)	150	$\frac{h_{ss}}{h_g} = 1 + 3.7 \times 10^{-3} Re^{1.09} (W_s/W_g)^{0.81}$	Own	Highly concentrated glass and catalyst suspension																
MAMEV et al. (1974)	89	$\frac{h_{ss}}{h_g} = a Re^b (W_s/W_g)^c$ <table border="1" style="margin-left: auto; margin-right: auto;"> <thead> <tr> <th>Re</th> <th>a</th> <th>b</th> <th>c</th> </tr> </thead> <tbody> <tr> <td>1000 - 2020</td> <td>143.5</td> <td>-0.5</td> <td>0.30</td> </tr> <tr> <td>1700 - 5000</td> <td>1230</td> <td>-0.90</td> <td>0.50</td> </tr> <tr> <td>5000 - 8000</td> <td>8.3</td> <td>-0.30</td> <td>0.47</td> </tr> </tbody> </table>	Re	a	b	c	1000 - 2020	143.5	-0.5	0.30	1700 - 5000	1230	-0.90	0.50	5000 - 8000	8.3	-0.30	0.47	Own	Corundum
Re	a	b	c																	
1000 - 2020	143.5	-0.5	0.30																	
1700 - 5000	1230	-0.90	0.50																	
5000 - 8000	8.3	-0.30	0.47																	

correlation (cf. Table 2.5 for ranges of application). As shown in the table most of these correlations are very simplified and include only the influence of a very limited number of parameters (generally only the Reynolds number and the loading ratio).

An attempt to generalize these correlations was made by Pfeffer and al. (102) who developed the following correlation which regroups data available before 1966 :

$$\frac{h_{ss}}{h_g} = 1 + 4Re^{-0.32} \left(\frac{\bar{w}_s C_s}{w_g C_g} \right) \quad (2.29)$$

Briller and Peskin (18) were the first to try to incorporate reflections on the mechanisms by which heat transfer coefficients are modified by the presence of solids into the development of a correlation. Suggesting that increased heat transfer coefficients are due to particles acting to thin the viscous sublayer established at the pipe wall, they attempted to correlate data via a combination of three parameters. The first was the sublayer thickness calculated from the gas Reynolds number by conventional correlations. The second was the particle concentration by number calculated assuming that the particle and gas velocities were the same (the effect on the viscous sublayer thus being assumed to increase with the number of particles present). The third factor of importance was taken to be the penetration depth of the particles in the sublayer region. This latter term was modeled based on a number of assumptions concerning transverse turbulence intensity and transverse particle motion (See the original paper or Ref. 35). The overall result is a correlation in terms of these three parameters which, expressed in terms of primary flow variables becomes:

$$\frac{h_{ss}}{h_g} = 9.04 \left[\frac{W_s}{W_g} \right]^{0.4} \left[\frac{\rho_s}{\rho_g} \right]^{0.20} \left[\frac{D}{d_p} \right]^{0.18} Re^{-0.105} \quad (2.30)$$

Similar mechanistic arguments were used by Sadek (112) who, also attempted to develop a more general correlation covering the experimental results of Farbar and Depew (45), Wilkinson and Norman (144), Jepson and Pöll (64), Farbar and Morley (44) and Mickley and Trilling (89). Sadek identified what he felt to be the relevant mechanisms affecting suspension heat transfer coefficients as viscous sublayer thinning and modified radial heat transport due to the solids. These two factors were reasoned to be dependent on the pipe Reynolds number, the particle concentration by number and the pipe diameter. He therefore proposed an correlation of the form :

$$\frac{h_{ss} - h_g}{h_g} = a(n_p D^3)^b (d_p/D)^c Re^d \quad (2.31)$$

where, in evaluating the coefficients, he assumed the slip velocity between the gas and solids to be zero (in order to determine the particle number concentration). After examining the available data he later found the Reynolds number effect to be negligible. The resulting correlation was then :

$$\frac{h_{ss} - h_g}{h_g} = 0.20 (n_p d_p^2 D)^{1.19} \quad (2.32)$$

The above correlation was later placed in doubt in a series of caustic letters between Danziger and Sadek (Refs. 29, 30, 113, 114) as it seems the latter made some serious errors in evaluating the data available in the literature. Sadek eventually modified his correlation (114) which took on the new form :

$$\frac{h_{ss} - h_g}{h_g} = 0.5 \left(\frac{n_p d_p^2 D}{\rho_p} \right)^2 / \left(1 + \frac{n_p d_p^2 D}{\rho_p} \right) \quad (2.33)$$

The predicted and experimental results still show large deviations however.

Another general correlation was suggested by Matsumoto et. al. (86) using his own results as well as the data of Farbar and Morley (44), Brötz et. al. (19), Farbar and Depew (45) and Jepson and Poll (64). Using dimensional analysis arguments, they reasoned that the heat transfer coefficients could be correlated in terms of a single factor β which is the "ratio of the heat transfer rate absorbed by solids to that of the gas flow" :

$$\beta = \left[\frac{n_p h_p n_p d_p^2 D}{\rho_p (1-\epsilon) V_s C_s} \right] \left[\frac{W_s C_s}{W_g C_g} \right] \quad (2.34)$$

Matsumoto et. al. treated the available isothermal wall data assuming that the slip velocity between the solids and the gas was equal to the particle terminal settling velocity. The particle-gas heat transfer coefficient was calculated from the Ranz-Marshall equation (103) :

$$\frac{h_d}{\lambda_g} = 2 + 0.6 \text{Re}_t^{0.5} \text{Pr}^{0.3} \quad (2.35)$$

The resulting correlation was

$$\frac{h_{ss}^{lm}}{h_g^{lm}} = 2.5 \beta^{0.5} \quad (2.36)$$

$$0.15 < \beta < 2.0$$

Comparison of this correlation with the others is facilitated by substituting the appropriate relations into Eqs 2.34 and 2.36 to write Eq. 2.36 in terms of primary flow variables

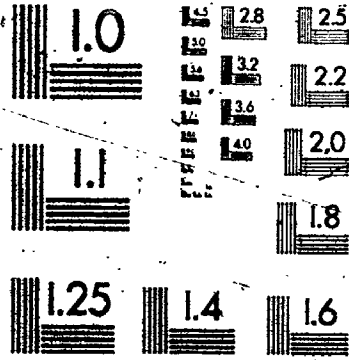
$$\frac{h_{ss}^{lm}}{h_g^{lm}} = 6.12 \left[\frac{\lambda_g DW_s}{\rho_s (U_g - V_t) d_p^2 W C_g} \right]^{0.5} (2 + 0.6 \text{Re}_t^{0.5} \text{Pr}^{0.3}) \quad (2.37)$$

The above form of the Matsumoto et. al. correlation shows a loading ratio dependence, $(W_s/W_g)^{0.5}$, similar to those given by other workers. It also shows an explicit particle size effect.

Finally it can be noted that Matsumoto et. al. were unsuccessful in correlating data from uniform heat flux studies via the above correlation. In addition, as with all the correlations presented here, no minimum as a function of loading ratio is predicted, a fact which runs contrary to many experimental results.

The first theoretical analysis of gas-solids suspension heat

2



transfer problems was that due to Tien (129). The main objective of his work was to apply the Graetz method for single phase heat transfer problems to a two-phase situation in order to predict variations in thermal entry lengths and overall coefficients as a function of solids loading for isothermal wall conditions. He began by writing energy balance equations on the solids and gas phases respectively for steady pipe flow as :

$$V_s \frac{\partial T_s}{\partial z} + \left[\frac{h_p \pi d^2}{\rho_s \omega_p C_s} \right] (T_s - T_g) + \frac{1}{r} \frac{\partial}{\partial r} (r V_s T_s) = 0 \quad (2.38)$$

$$U_g \frac{\partial T_g}{\partial z} = \frac{1}{r} \frac{\partial}{\partial r} \left[r \left[\frac{v}{Pr} + \epsilon_t \right] \frac{\partial T_g}{\partial r} \right] + \left[\frac{n h_p \pi d^2}{\rho_g C_g} \right] (T_s - T_g) = 0 \quad (2.39)$$

The problems with the form of general balance equations of this type will be examined in Chapter 3.

Resolution of Tien's equations required a number of important simplifying assumptions, the most important of which are listed below:

- a) the local mean velocities of the gas and solids are the same
- b) the solids are uniformly distributed throughout the flow field
- c) turbulent diffusion in the solids phase is negligible
- d) the gas flow field is unaffected by the presence of the particles.

These assumptions allow the re-writing of the solids phase equation as :

$$u_g \frac{\partial T_s}{\partial z} + \left[\frac{h_p m d_p^2}{\rho_s w_p C_s} \right] (T_s - T_g) = 0 \quad (2.40)$$

The equations were then solved for the case of an isothermal pipe wall. The results of Tien's analysis predicted longer thermal entry lengths as solids loading increased but asymptotic coefficients which were essentially the same as for the gas flowing alone. Coefficients based on the log mean temperature difference would, as a result, be greater than those in a single phase gas flow. Quantitative verification of Tien's analysis was supplied by Farbar and Morley's data although agreement was satisfactory only at loading ratios below one. Tien reasoned that his assumptions broke down at high loading ratios, in particular, the assumptions concerning the unmodified gas flow field and the uniform solids concentration profile.

Tien's analysis was extended by Depew and Farbar (34) to treat uniform heat flux cases.

Using the same computation techniques as Tien, the latter authors managed to show the local heat transfer coefficient to be dependent on $(W_s C_s)/(W_s C_s + W_g C_g)^2$ which led to a minimum in the local coefficient at loading ratios between 0.5 and 1.5 under the Depew and Farbar experimental conditions. As in the case of Tien, their analysis predicted asymptotic coefficients which were essentially the same as for the gas alone, a prediction which, as was shown earlier, was

not confirmed by their experiments. Furthermore, their treatment predicted bigger dips in the local heat transfer coefficients as a function of loading ratio for larger particles than for small, whereas the opposite behaviour was found experimentally. Like Tien, they suggested the differences in the predicted and experimental results to be due to faulty assumptions concerning solids concentration profiles and unmodified gas flow fields.

Boothroyd (12) using similar equations also attempted to use the Graetz method to determine thermal entry lengths. In his approach to the problem he tried to lift some of the simplifying assumptions used by Tien by introducing distinct gas and solids velocity profiles and an eddy diffusion coefficient in the solids phase. His effort met with computational problems however and he concluded (15) that an empirical approach was preferable.

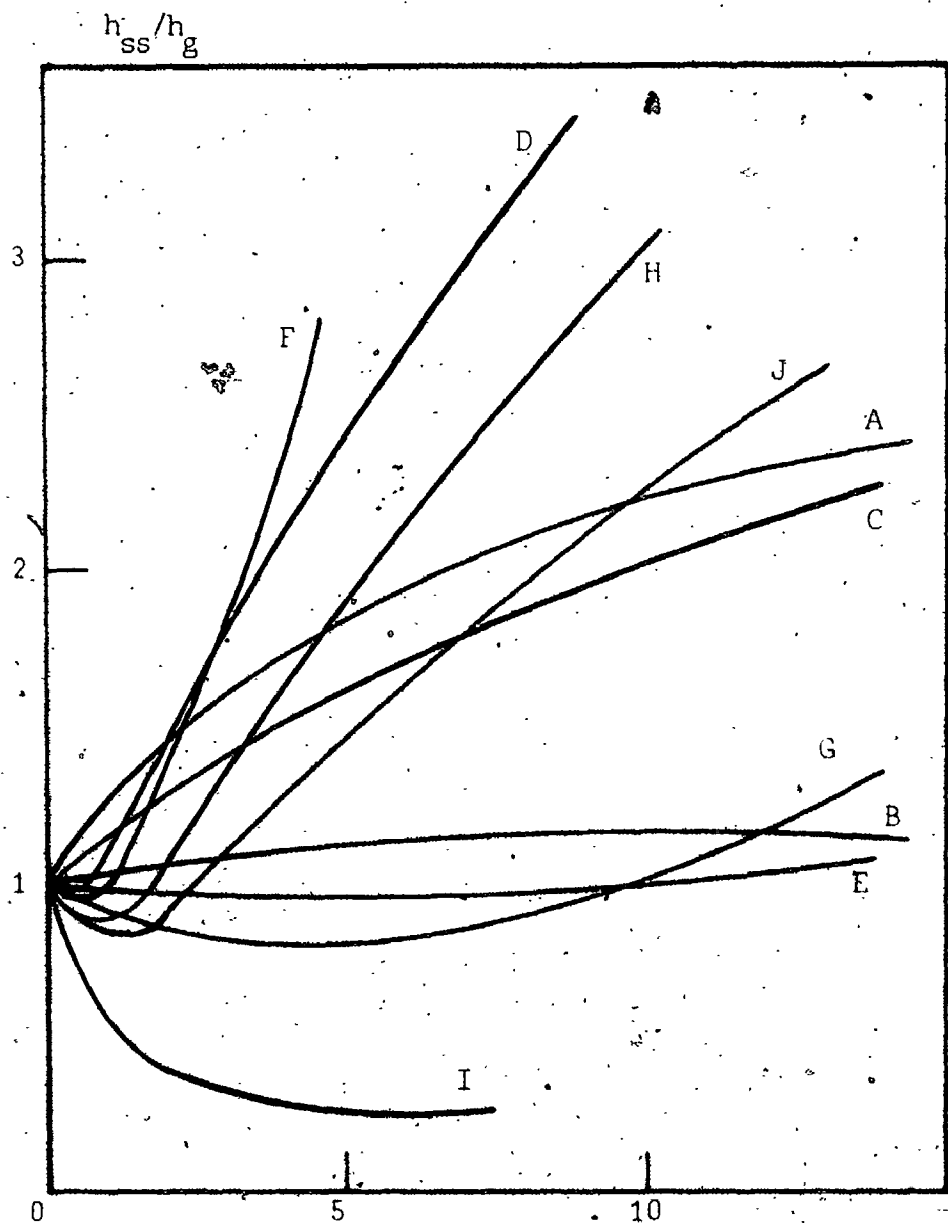
Recently, Matsumoto et. al. (87) proposed two models for heat transfer in suspension flow. The first is somewhat similar to Tien's original analysis in that similar assumptions are made and the basic balance equations are of the same form as Eqs 2.39 and 2.40. The additional assumption that the velocity profiles of both the gas and solids phases were uniform across the pipe cross-section was also made. The major difference in Matsumoto's first model compared with Tien's however is the former author's treatment of eddy diffusivity. Tien assumed that the gas flow field was unaffected by the solids ; Matsumoto assumed the eddy diffusivity to be variable and used it as a parameter to fit measured gas temperature profiles. The fit was

satisfactory at loading ratios of up to two ; beyond this point, measured profiles flattened in the core region and the model was unable to account for this.

The second Matsumoto model is based on the same assumptions as the first with the additional hypothesis that turbulent mixing in the solids phase is so intense as to render the solids radial temperature distribution uniform. While the second model allowed reproduction of measured gas temperature profiles, corresponding results on heat transfer coefficients did not match those found experimentally. The authors explained the differences in both cases as being linked to the assumption of a uniform solids concentration profile and even produced some data showing this not to be the case.

2.3.4 Comments and conclusions

The present situation regarding the study of heat transfer between vertically flowing gas-solids suspensions and pipe walls in many ways parallels vertical pneumatic transport hydrodynamics : a substantial number of data now exist and numerous empirical correlations applicable over narrow ranges of operating conditions have been developed. Many of the existing data, however, show conflicting relationships between primary flow variables and heat transfer coefficient and, while explanations for these ambiguities have been put forth, they have yet to be translated into appropriate mathematical models. This state of affairs is exemplified by Figure 2.4, reproduced from the publication of Maeda (84), showing experimental curves relating heat transfer coefficients to loading ratios. The curves



Curve	Ref.	Re	d_p (μm)	Solid	D (mm)
A	144	18000	60	glass	53.3
B	144	70000	60	glass	53.3
C	144	18000	110	glass	53.3
D	64	19000	220	sand	38.1
E	64	58000	220	sand	38.1
F	64	19000	80	sand	38.1
G	27	15000	65	graphite	7.6
H	13	35000	15	zinc	76.2
I	13	80000	15	zinc	25.4
J	13	35000	15	zinc	50.8

FIGURE 2.4. Experimental Suspension Heat Transfer Coefficients

suggest dramatic differences in overall results with only moderate differences in overall operating conditions.

There are a certain number of points of agreement among workers in this field on the phenomena which lead to these differences. Gas-solids suspensions have the unquestionable advantage of higher volumetric heat capacities compared to gases alone. It is generally recognized that direct heat transfer from pipe walls to particles in suspension is small or negligible due to short contact times and small contact surfaces. The fact that the heat transfer process is consequently from wall to gas and then from gas to solids leads to a temperature lag between the two phases and therefore, to higher thermal entry lengths.

Beyond these generally accepted ideas, there is widespread disagreement concerning other points. The thinning of the viscous sub-layer explanation for increased heat transfer coefficients appears frequently in discussions. It is felt however that this may be a significant mechanism only at low Reynolds number where sub-layers are sufficiently thick for there to be a potential for thinning. This explanation is far from universal however and attempts to quantify the effect have met with only limited success. Matsumoto (86) presents arguments suggesting it not to be important at all.

While many workers suggest that the presence of solids has an important influence on the characteristics of the turbulence in the gas phase it is not clear whether turbulent fluctuations are dampened or enhanced nor under what conditions. None of the proposed models

correctly account for this:

While radial transport in the solids phase has been advanced as a possible mechanism in order to develop correlations for increased heat transfer coefficients (eg. Sadek (112)), most investigators consider this to be of negligible importance.

Yousfi (150) and Mamaev et. al. (85) suggest overall coefficients to be increased, at least at higher solids loadings, due to downflow of solids at the pipe wall. While it is generally held that solids velocity and concentration profiles are very important in the overall heat transfer process, all of the theoretical treatments assume uniform concentration profiles and simplified velocity distributions.

As Depew and Kramer (35) state in conclusion to their 1973 review then, "heat transfer to gas-solids suspension flow is far from being an unified subject". In a similar view, Boothroyd (15) summarized the state of the art in 1971 saying that "despite the extensive experimental data now available it is still difficult to the predict heat transfer rate to an arbitrary suspension... the engineer has little option but to make a full study of the available literature and undertake his own experimental programme".

2.4 Concluding remarks

Traditional empirical and semi-empirical approaches to the hydrodynamics and heat transfer in flowing gas-solids suspensions are remarkable both in their quantity and in their quality. The above review of vertical pneumatic transport showed no fewer than 17 solids

70

friction factor correlations alone, not counting pressure drop correlations based on other methods. Fewer, yet still numerous correlations exist in the heat transfer area but, surprisingly, none accounts for the frequent experimental observation of decreased coefficients at low solids loading.

This chapter has shown some of the reasons for this situation to be related to experimental problems (eg. less than fully developed flows) and to differences in basic definitions (eg. temperature driving forces). More importantly, it has been shown that traditional empirical and semi-empirical approaches are insufficient in explaining the interactions between the complex phenomena which determine basic gas-solids suspension flow behaviour. The lack of success of this line of attack argues in favor of a more rigorous approach to the analysis of these problems.

CHAPTER 3

GENERAL MULTIPHASE FLOW EQUATIONS ;

REVIEW OF PREVIOUS WORK

3.1 Introduction

The preceding chapter showed existing empirical and semi-empirical approaches to be inadequate in dealing with the multiplicity of complex phenomena associated with gas-solids suspension flows. In single phase fluid mechanics, where reliable empirical methods exist in many areas, the Navier-Stokes equations are still of enormous value as they can be used, in a limited number of cases, to provide full solutions to complex flow problems and, more importantly, as the basis for interpretation of particular effects and for modeling of individual phenomena in practically all cases. The understanding of gas-solid suspension flows would seem then to be able to be enhanced by the use of equations analogous to the Navier-Stokes equations for multiphase flow.

Unlike the case of single phase flow however, where the Navier-Stokes and associated energy equations have gained general acceptance for use when the fluid behaves as a continuum, there are many general multiphase flow equation formulations containing widespread differences. These differences relate not only to expressions for phase interaction forces, but also appear in fundamental definitions of flow variables and basic expressions for their variation, with perhaps the most important disagreements arising from complications due to the existence of interfaces between phases.

This chapter will review the different multiphase flow equations which have appeared in the literature. The difficulties which have arisen in previous attempts at formulating such equations will be pointed out. Chapter 4 will present probabilistic multiphase flow equations which overcome many of these problems.

Much of the work carried out in this area has been directed toward gas-liquid flows. While discussion of equations proposed with this particular application in mind will be included, emphasis will be placed on general equation formulations proposed for gas-solids suspensions. The detailed criticism to follow will use momentum equations as an illustration since, where differences in basic formulations arise, they generally appear clearly there, with corresponding differences resulting from the same basic cause occurring in the energy equations.

Note concerning nomenclature

The nomenclature used in the rest of the thesis will, as far as possible, be followed in the present chapter. Given the large number of different approaches to be treated however, there will be some changes in meaning in particular cases. These will be noted as the necessity arises.

3.2 Equations derived directly in terms of mean variables

The simplest approach used in writing equations to describe multiphase mixtures has been to write balance equations directly in terms of mean variables. These variables, while not rigorously defined, are generally taken to be volume averages. Frequent reference is made to the continuum limitations of single phase fluids and the kinetic theory of gases in order to implicitly define average variables for suspensions which are "sufficiently dense, with

particles sufficiently small so that a volume may be considered which on the one hand is so large as to contain a large number of particles and on the other hand is so small that any quantity within this volume may be described by a linear function of the space coordinates " (60).

There are limitations linked to the use of volume averages of this type which will be discussed in detail with other averaging techniques later in this chapter. Nevertheless, a number of notable attempts have been made to directly write general equations starting with intuitively defined volume averaged variables. These approaches consist basically of the following steps :

- Body forces and volumetric terms are written over the part of the overall control volume occupied by the given phase. These expressions are then transformed into integrals over the whole volume by multiplying the integrand by the volume fraction of the phase.
- Surface fluxes and forces are written over the surface enclosing the given phase. The surface integrals are transformed into volume integrals over the part of the control volume occupied by the phase via Gauss' theorem and then over the entire volume by multiplying by the phase volume fraction.

Typical of this approach and historically one of the first attempts to write basic equations for gas-solids suspension flows are the equations of Van Deemter and Van der Laan (134). To derive their momentum equation for the fluid for example, they begin with :

$$\int_{V_f} \left[\frac{\partial}{\partial t} (\rho_f U_i) + \frac{\partial}{\partial x_j} (\rho_f U_i U_j) \right] dv = \int_{V_f} \rho_f g_i dv + \int_{S_f} \tau_{ij} n_j dS \quad (3.1)$$

where V_f is the part of the control volume occupied by fluid which is entirely enclosed by the surface S_f . The volume integrals are then transformed into integrals over the entire volume via multiplication of the integrand by α_f , the volume fraction of fluid in the control volume. The surface integral is re-written as:

$$\int_{S_f} \tau_{ij} n_j dS = \int_C \tau_{ij} n_j dS + \int_{S_{p1} + S_{p2}} \tau_{ij} n_j dS \quad (3.2)$$

where $S_{p1} + S_{p2}$ is the particle-fluid interface within the control volume and S is the overall control volume surface. This latter surface is not just the part of the overall control volume surface in contact with the fluid since Van Deemter and Van der Laan explicitly neglect particles at the control volume surface as secondary effects.

This has two important consequences: firstly, the fluid stress tensor in the fluid and overall suspension equations is of the form $\partial \tau_{ij} / \partial x_j$ and not either $\partial (\alpha_f \tau_{ij}) / \partial x_j$ nor $\alpha_f \partial \tau_{ij} / \partial x_j$ as are found in other general equation formulations. Secondly, the assumption that there are no particles at the control volume surface eliminates the stress tensor in the particle equations, both that due to particle-external medium interaction and that which is due to particle collisions.

The fluid and solids momentum equations given by Van Deemter

and Van der Laan are thus :

$$\rho_f \alpha_f \left[\frac{\partial}{\partial t} U_i + U_j \frac{\partial}{\partial x_j} U_i \right] = \frac{\partial}{\partial x_j} \tau_{ij} + \rho_f \alpha_f g_i - F_i^{fs} \quad (3.3)$$

and :

$$\rho_s \alpha_s \left[\frac{\partial}{\partial t} V_i + V_j \frac{\partial}{\partial x_j} V_i \right] = \alpha_s \rho_s g_i + F_i^{fs} \quad (3.4)$$

where

$$\int_V F_i^{fs} dv = - \int_{S_{p1} + S_{p2}} \tau_{ij} n_j ds$$

A similar difference arising from neglecting particles at the boundary arises in their mechanical energy balance. They make reference to the possibility of including turbulent stress terms but give no explicit expression for them.

This latter point was taken up by Hinze (60) who, starting with Van Deemter and Van der Laan's equations, applied the Reynolds procedure to the gas and solids velocities in order to express "turbulent" stresses of the form :

$$\frac{\partial}{\partial x_j} \rho_f \alpha_f \overline{U_i U_j} \quad \text{for the gas and}$$

$$\frac{\partial}{\partial x_j} \rho_s \alpha_s \overline{V_i V_j} \quad \text{for the solids}$$

which are similar in form to the velocity fluctuation tensors in single phase turbulent flow. No discussion of the time period over which averaging takes place is given by Hinze. This important point will be taken up later in this chapter.

Hinze also pursues further the work of Van Deemter and Van der Laan by giving expressions for the fluid stress tensor and the gas-solids interaction force. He proposes the following expression for the fluid stress tensor :

$$\tau_{ij} = -P\delta_{ij} + \mu \left(\frac{\partial}{\partial x_j} U_{mi} + \frac{\partial}{\partial x_i} U_{mj} \right) - \frac{2}{3} \mu \frac{\partial}{\partial x_k} U_{mk} \delta_{ij} \quad (3.5)$$

where U_{mi} is the mean velocity by volume for the mixture :

$$U_{mi} = \alpha_f U_{fi} + \alpha_s V_{si} \quad (3.6)$$

The above equation for the fluid stress tensor contains an explicit expression for the effect of the presence of the particles on the fluid deformation. Hinze offers no justification for this effect resulting in the particular expression given above. As has been pointed out elsewhere (1) there seems to be little likelihood that this would be true in the general case.

As mentioned, Hinze's starting point is the equations of Van Deemter and Van der Laan. He also neglects therefore particles on the boundary of the control volume. This gives rise to the same absence of α_f in the fluid stress tensor expression as well as to the absence of a solids phase stress tensor. Neglecting particles at the

boundary of the control volume also allows Hinze to define a fluid-particle interaction force in terms of an implied relationship between the volume fraction and the number of particles per unit volume. Clearly, if there are no particles straddling the control volume surface, the number of particles within the control volume is related to the volume fraction via the following expression:

$$n_p \omega_p = \alpha_p \tag{3.7}$$

where n_p = number of particles per unit volume in a volume v

ω_p = volume of an individual particle

If this equality was generally true, it would be possible to express the force of the fluid acting on the particle phase as simply n_p times the force on an individual particle. In general, however, some of the particles will be partly outside the control volume. Even if n_p is taken as the number of particles whose centroid is within the control volume, the product $n_p \omega_p$ is, as has been shown by Fortier (48) generally greater than α_p , with the difference depending on the relative characteristic dimensions of the particles and the control volume.

Finally, as has been pointed out before by Anderson and Jackson (1) and Murray (94), Hinze has inconsistently included a virtual mass term as part of the fluid-particle interaction force in the fluid equation without a corresponding term in the solids equations.

Equations similar to those of Van Deemter and Van der Laan and Hinze, although presented quite differently, are proposed by Rao (20),

also for gas-solids suspensions. Rao begins by postulating the form of the overall gas and solids momentum equation as :

$$\begin{aligned} \frac{\partial}{\partial t} \rho_f^\alpha U_i + \frac{\partial}{\partial x_j} \rho_f^\alpha U_i U_j + \frac{\partial}{\partial t} \rho_s^\alpha V_i + \frac{\partial}{\partial x_j} \rho_s^\alpha V_i V_j \\ = - \frac{\partial P}{\partial x_i} + \frac{\partial}{\partial x_j} \sigma_{ij}^m + \rho_s^\alpha g_i + \rho_f^\alpha g_i + \Omega_i \end{aligned} \quad (3.8)$$

where Ω_i are body forces. From this he extends Hinze's use of the Reynolds procedure by considering that there are fluctuations not only in the local values of the phase velocities but also in the gas and solids volume fractions. This gives rise to a number of additional terms involving mean values of the product of fluctuating volume fractions and velocities.

Rao's solid phase equation is given by :

$$\frac{\partial}{\partial t} \rho_s^\alpha V_i + \frac{\partial}{\partial x_j} \rho_s^\alpha V_i V_j = F_i^{fs} \quad (3.9)$$

While not explicitly stated, the assumptions leading to these two equations are clearly the same as those involved in the equations of Van Deemter and Van der Laan.

The problem of stability and predicting the onset of bubbling in fluidized beds has elicited a number of derivations of fundamental equations for multiphase media. In general these attempts begin by deriving fundamental equations for gas-solids flow and then the resulting equations are simplified to treat the specific fluidization problem. An example of this is Murray (94) who, like Van Deemter and

Van der Laan and Hinze, writes basic equations directly in terms of implicit volume averages.

Murray's gas and solids phase momentum equations are :

$$\rho^u \left[\frac{\partial u_i}{\partial t} + u_j \frac{\partial}{\partial x_j} u_i \right] = - \frac{\partial p}{\partial x_i} + \alpha_f \frac{\partial}{\partial x_j} \sigma_{ij} + \rho^u s_i^f - \rho^u s_i^f \quad (3.10)$$

and :

$$\rho^s \left[\frac{\partial v_i}{\partial t} + v_j \frac{\partial}{\partial x_j} v_i \right] = \rho^s s_i^s + \alpha_s \frac{\partial}{\partial x_j} \sigma_{ij}^s + \rho^s s_i^s \quad (3.11)$$

The major difficulties in Murray's equations arise from his treatment of the surface forces. In deriving the overall momentum equation for the mixture Murray writes the surface forces acting on the gas and the solids as :

$$\text{Surface forces} = \int_{s_f} t_{ij}^f n_j dS + \int_{s_s} t_{ij}^s n_j dS$$

where s_f and s_s represent the entire fluid and solids interfacial surface respectively within the control volume. The above surface integrals are transformed into volume integrals over v_f and v_s respectively using Gauss' theorem and then to volume integrals over the entire control volume by multiplying the integrands by α_f and α_s respectively. For the fluid phase this procedure amounts to writing :

$$\begin{aligned}
\text{Mean fluid surface forces} &= \int_{S_f} \tau_{ij} n_j dS \\
&= \int_{V_f} \frac{\partial}{\partial x_j} \tau_{ij} dv \\
&= \int_V \alpha_f \frac{\partial}{\partial x_j} \tau_{ij} dv
\end{aligned}$$

The volume average of τ_{ij} is usually defined as (see Section 3.3) :

$$\overline{\tau_{ij}} = \frac{1}{V} \int_V \tau_{ij} dv \tag{3.12}$$

Murray's formulation of the mean surface forces thus implies that :

$$\frac{\partial \overline{\tau_{ij}}}{\partial x_j} = \overline{\frac{\partial \tau_{ij}}{\partial x_j}} \tag{3.13}$$

which is generally untrue. As will be shown later in this chapter and in more detail in Chapter 4 the volume mean of the derivative is not equal to derivative of the mean variable, but equal to the derivative of the mean variable plus a term representing the interfacial forces.

An analogous problem arises in Murray's energy equations which have heat transfer terms of the form :

$$\alpha_f \frac{\partial}{\partial x_j} Q_{fs} \quad \text{and} \quad \alpha_s \frac{\partial}{\partial x_j} Q_{sf}$$

for the gas and solids respectively.

Having written his overall momentum equations in this way Murray then equates the individual terms corresponding to each phase to the fluid-solids interaction forces to arrive at his individual phase momentum equations. For the fluid, this amounts to writing :

$$\rho_f \alpha_f \left[\frac{\partial}{\partial t} U_i + U_j \frac{\partial}{\partial x_j} U_i \right] - \alpha_f \frac{\partial}{\partial x_j} \tau_{ij}^f - \rho_f \alpha_f F_i = F_i^{fs} \quad (3.14)$$

In the initial formulation of the surface forces exerted on the fluid phase however, the surface integral was taken over the entire surface bounding the fluid within the control volume, including the surface which is in contact with the solids. The expression :

$$\int_{S_f} \tau_{ij} n_j dS$$

therefore already accounts for the gas-solids interaction at the surface. Drew and Segal (40) have shown that, in cases where proper account of the interaction forces are taken via the above surface integral, Murray's F_i^{fs} term is zero.

Murray's separation of stress tensors into pressure and shear forces also requires comment. He presents the general forms of the fluid and solids stress tensors respectively as :

$$\tau_{ij}^f = -P\delta_{ij} + \sigma_{ij} \quad (3.15)$$

and

$$\tau_{ij}^s = -P^s\delta_{ij} + \sigma_{ij}^s \quad (3.16)$$

He then goes on to argue that, for his particular application (fluidized beds), the physical evidence suggests that the particle collisions are of negligible importance. The particle "pressure" is thus zero and "to be consistent" $\alpha_f(\partial P/\partial x_i)$ should be replaced by $\partial P/\partial x_i$ in the fluid equation.

The consistency point amounts to being able to sum the individual equations and arrive at an overall pressure term multiplied by one instead of by α_f in the overall momentum equation. This aspect has already been criticized by Anderson and Jackson (1). Murray's interpretation of the stress field in the particle phase is more important however. As will be shown in Chapter 4, the stress in the particle phase arises from two different physical origins: that due to particles outside the control volume colliding with particles inside the control volume and that due to hydrodynamic interaction with the surrounding medium. The absence of particle collisions would effectively result in the absence of a stress field from this cause. The second effect would nevertheless still be present however.

Apart from Van Deemter and Van der Laan, Hinze and Murray, at least two other notable attempts have been made to write fundamental

equations directly in terms of implicitly defined mean variables. Jackson (63) and Klinzig and Peters (16,101) have treated gas-solids suspensions in this way, but using a method somewhat different than the one cited above. This second approach consists of :

- writing the Navier-Stokes equations for the gas and adding an interaction term directly to the equation in the same way as one might include an additional body force,
- writing a momentum balance on a single particle and extending it over the entire suspension by multiplying the resulting equation through by the particle concentration by number.

This method leads to a fluid phase momentum equation of the form :

$$\rho_f \left[\frac{\partial}{\partial t} U_i + U_j \frac{\partial}{\partial x_j} U_i \right] = - \frac{\partial}{\partial x_j} \tau_{ij}^f + \rho_f g_i - F_i^{fs} \quad (3.17)$$

There is a fundamental problem associated with this type of approach. In un-averaged form the fluid phase variables and the equations which relate them to each other are generally defined in suspensions at points which are occupied, at a given time, by the fluid. One of the purposes of averaging is to extend these definitions over all points occupied by the suspension and in so doing integrate local boundary conditions directly into the final equations. As has already been shown, averaging the equations cannot be rigorously carried out by multiplying through by the volumetric concentration of a particular species due to complications arising from the treatment

of the phase interfaces. Jackson's and Klinzig and Peter's fluid phase equation, for example, multiplied by α_f , takes on the same form as Murray's fluid equation with the stress term written as $\alpha_f \partial \tau_{ij} / \partial x_j$.

It can be noted here that it is not inconsistent to write the fluid phase momentum equations in the exact same form as the classic Navier-Stokes equations for single phase fluids:

$$\rho_f \left[\frac{\partial}{\partial t} U_i + U_j \frac{\partial}{\partial x_j} U_i \right] = \frac{\partial}{\partial x_j} \tau_{ij}^f + \rho_f g_i \quad (3.18)$$

where the variables are defined when the fluid is present at a given point at a given time. Solution of the flow problem would then be possible by solving the fluid equation subject to all local boundary conditions. Indeed, this is the approach adopted in most rheological studies. Einstein's result for the apparent viscosity of dilute suspensions, for example, is carried out on this basis. Except in very simple cases, however, local boundary conditions are such complicated functions of time and space coordinates that this approach is impractical.

In addition to the above-mentioned problem in the fluid phase momentum equations, several difficulties also appear in Jackson's and Klinzig and Peter's solids phase momentum equations. Jackson's solids phase equation is:

$$\begin{aligned}
 m_p n_p \left[\frac{\partial}{\partial t} V_i + V_j \frac{\partial}{\partial x_j} V_i \right] &= n_p \omega_p \rho_f \left[\frac{\partial}{\partial t} U_i + U_j \frac{\partial}{\partial x_j} U_i \right] \\
 &+ n_p m_p g_i + f(n_p)(U_i - V_i) \\
 &- n_p \omega_p \rho_f g_i \quad (3.19)
 \end{aligned}$$

where the terms on the right hand side are described as the effect of the acceleration forces on the fluid displaced by the particles, gravitational, drag and buoyancy forces respectively. At first glance there are major differences between the above equation and the others presented thusfar. The first three terms on the right hand side can be replaced using Jackson's fluid phase equation multiplied through by α_f to give :

$$\begin{aligned}
 m_p n_p \left[\frac{\partial}{\partial t} V_i + V_j \frac{\partial}{\partial x_j} V_i \right] &= - n_p m_p \frac{\partial}{\partial x_i} P + \alpha_f f(n_p)(U_i - V_i) \\
 &+ n_p m_p g_i \quad (3.20)
 \end{aligned}$$

The only remaining difficulties involve the number concentration problem already discussed and the absence of velocity fluctuation tensors. The stress tensor τ_{ij}^f is taken by Jackson to be $-P\delta_{ij}$ since he explicitly neglected shear forces in the gas phase for his particular fluidization application.

Klinzig and Peter's solids momentum equation is :

$$n_p \left[\frac{\partial}{\partial t} V_i + V_j \frac{\partial}{\partial x_j} V_i \right] = n_p g_i + \frac{n_p}{\omega_r} (U_i - V_i) \quad (3.21)$$

The origin of this equation is a force balance on a single particle considering drag as the fluid force, followed by multiplication by the number of particles per unit volume. All the previous comments concerning number densities, treatment of particle collisions, and particle phase stress tensors apply here but there is an additional problem concerning the compatibility of their solids and gas equations. Klinzig and Peter's gas equation is :

$$\rho_f \left[\frac{\partial}{\partial t} U_i + U_j \frac{\partial}{\partial x_j} U_i \right] = \frac{\partial}{\partial x_j} \tau_{ij}^f + \rho_f g_i + \frac{n_p m_p}{\omega_r} (U_i - V_i) \quad (3.22)$$

Clearly the interaction (drag) terms must cancel in the overall momentum equation. This can be accomplished by multiplying their solids equation by the mass of an individual particle and adding the gas and solids equations to give :

$$\rho_f \left[\frac{\partial}{\partial t} U_i + U_j \frac{\partial}{\partial x_j} U_i \right] + n_p m_p \left[\frac{\partial}{\partial t} V_i + V_j \frac{\partial}{\partial x_j} V_i \right] = \frac{\partial}{\partial x_j} \tau_{ij}^f + \rho_f g_i + n_p m_p g_i \quad (3.23)$$

The inconsistency here involves the momentum variation expressions. Whereas the solids momentum is weighted by $n_p m_p$ to account for the part of the control volume occupied by the fluid, a similar weighting is not present in the fluid momentum expression. If, by

adding the two equations, the fluid equation was multiplied through by α_f to account for this, the interaction expressions would not cancel. Indeed there is no way to re-work the equations in such a way as to allow the correct expression for the fluid momentum variation to be written and have the interaction forces cancel out when the gas and solids equations are added together.

Most formulations of general multiphase equations, whether they are derived directly in terms of mean variables as discussed thus far in this section or based on rigorous averaging techniques to be discussed in the following section, begin by developing individual phase equations and then add them to arrive at the overall equation for the mixture. An alternative formulation of the problem is to begin from the hypothesis that the overall equations for the mixture should be of the same form as that for a single phase fluid. This is the approach adopted in the numerous publications by Soo and co-workers (Eg. 22, 118, 123, 124) who cite as a priori evidence in its favor, the fact that the Navier-Stokes equations apply to gas mixture such as air as well as to single component gases (22). Soo's overall momentum equation for the mixture is then :

$$\rho_m \frac{\partial}{\partial t} V_{mi} + \rho_m V_{mj} \frac{\partial}{\partial x_j} V_{mi} = - \frac{\partial}{\partial x_i} P + \frac{\partial}{\partial x_j} \sigma_{ij}^m + \Omega_i^m \quad (3.24)$$

where :

$$\rho_m = \sum_p \alpha_p \rho_p \tag{3.25}$$

$$\rho_m V_{mi} = \sum_p \rho_p \alpha_p V_{mi} \tag{3.26}$$

and P is the total pressure in the mixture ; σ_{ij}^m represents the shear stresses in the mixture and Ω_i^m the overall body force. Momentum equations for the individual components are then obtained by decomposing the overall momentum equation. For a component p in the mixture, the individual momentum equation becomes :

$$\begin{aligned} \rho_p \frac{\partial}{\partial t} V_{pi} + \rho_p V_{pj} \frac{\partial}{\partial x_j} V_{pi} - \frac{\partial}{\partial x_j} \left[\rho_p \alpha_p (V_{pi} - V_{mi})^2 \right] \\ = - \frac{\partial}{\partial x_i} P^p + \frac{\partial}{\partial x_j} \sigma_{ij}^{pm} + \sum_q F_i^{pq} + \Omega_{pi} \end{aligned} \tag{3.27}$$

where P^p is partial pressure of component P in the mixture, σ_{ij}^{pm} is the contribution of the component P to the shear stresses in the mixture, F_i^{pq} is the interaction force between the component p and the other components in the mixture and Ω_{pi} represents the body force on the component p . The partial pressure term can be re-written as :

$$- \frac{\partial}{\partial x_i} P^p = - \frac{\partial}{\partial x_i} \alpha_p P = - \alpha_p \frac{\partial}{\partial x_i} P - P \frac{\partial}{\partial x_i} \alpha_p \tag{3.28}$$

The unique feature in the above equations is the third term on the left hand side of the individual phase momentum equation, a term which Soo describes as an inertial coupling force. Its origin is

linked to the choice of the reference frame when carrying out the momentum balance : the two terms on the left hand side of the overall momentum balance represent the overall momentum variation of the mixture in a control volume moving at the mass mean or barycentric velocity of the mixture with respect to fixed coordinates. Likewise, the three terms on the left hand side of the individual phase momentum equation represent the momentum variation of the component p in a control volume moving at the mixture mass mean velocity ; the first two terms represent the momentum variation for a control volume moving at the mass mean velocity of component p and the inertial coupling terms arise from the difference between the two reference frames.

In this way Soo's approach is very similar to the use of the kinetic theory of gases in treating the hydrodynamics of multi-component gas mixtures where momentum fluxes are generally expressed relative to a reference frame moving at the mass mean velocity of the mixture. By way of example, the Enskog equation (61) can be applied to the momentum variation of one of the components in a multicomponent gas mixture, neglecting for simplicity shear and body forces to give (in the case of one-dimensional flow) :

$$\alpha_p \rho_p \frac{\partial}{\partial t} U_p + \alpha_p \rho_p U_p \frac{\partial}{\partial x} U_p - \frac{\partial}{\partial x} \left[\rho_p \alpha_p (U_p - U_m)^2 \right] + \sum_q F^{pq} = \frac{\partial}{\partial x} \left[n_p m_p \overline{V'_p V'_p} \right] \quad (3.29)$$

where V'_p is the diffusion velocity defined as :

$$V'_p = U'_p - U_m \quad (3.30)$$

and

$$U_p = \overline{U'_p} = \frac{1}{n_p} \int U'_p f_p dU'_p \quad (3.31)$$

(m_p is the mass of molecules of component p ; $\sum_p n_p m_p$ gives the partial density $\alpha_p \rho_p$ and f_p defines the phase p velocity distribution function). The partial pressure in the above equation originates in the normal velocity fluctuations of the component p gas molecules about the mass mean velocity of the mixture. As in Soo's equations there are inertial coupling terms in the above equation.

An exactly equivalent equation can be derived however from the Enskog equation in terms of the linear velocity U'_p of the component p :

$$\rho_p \frac{\partial U'_p}{\partial t} + \rho_p U'_p \frac{\partial U'_p}{\partial x} + \sum_q F^{pq} = - \frac{\partial}{\partial x} \sum_p n_p m_p \overline{U'_p U'_p} \quad (3.32)$$

In this case inertial coupling terms are not present since the term on the right hand side represents the normal velocity fluctuations of the component p gas molecules about the mass mean velocity of the given phase.

The former equation is convenient in treating multicomponent gas mixtures in so far as each component in the mixture makes an exactly analogous contribution to the overall pressure in the mixture and the

overall pressure defined in this way corresponds to that which would be measured experimentally. This type of definition is less useful when components in the mixture have fundamentally different behaviours as is generally the case in multiphase flow problems. For this reason it seems more appropriate to define fluxes with respect to the mass mean velocities of the individual phases; it is not generally possible to define an overall pressure in a multiphase mixture in the same way as in a multicomponent gas mixture.

To account for the basic behavioural differences between multiphase mixtures and multicomponent gases, in more recent publications (124), Soo introduces corrective factors. With these factors, his individual phase momentum equations become :

$$\begin{aligned} & \rho_p^\alpha \frac{\partial}{\partial t} V_{pi} + \rho_p^\alpha V_{pj} \frac{\partial}{\partial x_j} V_{pi} - C \frac{\partial}{\partial x_j} \left[\rho_p^\alpha (V_{pi} - V_{mj})^2 \right] \\ & = - \alpha_p \frac{\partial}{\partial x_i} P - (1-B)P \frac{\partial}{\partial x_i} \alpha_p + \frac{\partial}{\partial x_j} \sigma_{ij}^{pm} - \sum_q F_i^{pq} + \Omega_{pi} \end{aligned} \quad (3.33)$$

where B is the "displacement factor" depending on the flow configurations and C is the "dispersion factor" depending on "suspension homogeneity, local isotropy, relative sizes within a system and the relative magnitudes of inertia within a phase and due to interaction with other phases". He cites values of $B = 0$ and $C = 1$ for Brownian diffusion. This would be expected since suspensions susceptible to Brownian diffusion closely approach the multi-component gas mixture case. For particle suspensions B and C vary between 0 and 1.

3.3 Averaged equations

All the general equation formulations presented up to this point have been seen to be incomplete, based on less than fully rigorous derivations or founded on questionable analogies with single phase flows. The major difficulties have been shown to be due to :

- neglecting particles at the control volume surface,
- unrigorous attempts to develop definitions of particle concentration by number,
- inconsistent treatment of surface forces,
- problems associated with mean values of derivatives,
- incomplete accounting of the origins of the stress fields in particle phases,
- inconsistencies in defining domains for fluid and particle phase variables,
- choices of reference frames and definitions of overall pressures,

as well as a number of inconsistent mathematical manipulations.

Many of the problems encountered in the previous section by authors deriving basic multiphase equations directly in terms of implicitly defined mean variables were avoided by later workers using more rigorous averaging techniques which, among other things, offer the major advantage of allowing consistent formulations of interfacial terms.

This section will review the more important averaging techniques and their resulting general equation formulations.

The basic purpose of averaging is to extend definitions of variables, which are initially defined only when a particular phase is present, over the entire suspension thereby defining a number of continua corresponding to the number of phases present co-existing at all points in the suspension at all times. In the process of averaging, local boundary conditions relative to individual phase interfaces are integrated directly into individual phase equations as interaction terms. Finally, averaging "smooths out" fluctuations in multiphase flow equations in the same way as in turbulent single phase flows.

The use of rigorous averaging techniques as the basis for developing general multiphase flow equations has been especially prevalent in treating gas-liquid flows. The approach consists basically of :

- assuming the Navier-Stokes equations to be locally valid for all phases in the mixture,
- applying an averaging operator to extend the local equations over the entire mixture.

The major types of averaging operators which have been applied to multiphase flows include :

- spatial averaging (volume or area),
- time averaging,
- combinations of time and space averaging,
- probability (or as it is sometimes called, statistical or ensemble) averaging, which will be considered in detail in Chapter 4.

The two main types of averages which have been used to define volume-averaged mean variables can be expressed as :

$$\bar{\psi}_p^v = \frac{1}{V} \int_{V_p} \psi_p dv \tag{3.34}$$

and

$$\bar{\psi}_p^i = \frac{1}{V_p} \int_{V_p} \psi_p dv \tag{3.35}$$

Whitaker (143) has termed these, respectively, the phase average and the intrinsic phase average. It will be noted that, whereas the function ψ_p is defined only when the phase is present, its associated mean values are defined everywhere in the multiphase mixture.

The use of volume averages encounters the problem of the choice of a suitable reference volume. This problem is analogous to the continuum limitations of the kinetic theory of gases: the mean values at a point in gas configuration space correspond to the mean values in a volume surrounding the corresponding point in the real gas when the volume is chosen such that its characteristic dimension is within a well-defined interval. The lower limit of the interval is given by the mean free path of the gas molecules while the upper limit is given by the distance over which large macroscopic changes begin to occur. Examples of where the continuum approximation breaks down are dilute gases where the mean free paths of the gas molecules are very large and shock waves where macroscopic changes in gas properties occur over very small distances.

In the same way, values of volume averages which are independent of the choice of the reference volume require that there exist volumes having characteristic dimensions larger than the distance over which local fluctuations take place yet smaller than the length over which macroscopic changes occur. Clearly, for a given volumetric concentration the lower limit decreases as the particle size decreases. For this reason volume averages have been mainly applied in gas-liquid flows to cases where one phase is well-dispersed in the other (Eq. 32, 155). In general the lower and upper limits of such volumes are fixed by the characteristic dimensions of the particles making up the suspension and the characteristic dimension of the experimental installation, respectively (39, 143). Solbrig and Hughes (121) discuss this problem in more detail as it relates to gas-liquid flows; Fortier (47) presents a similar discussion concerning gas-solids flows.

Even if a suitable averaging volume for a given problem does not exist, it is still possible to average over a specific volume. There is an accompanying loss in generality associated with the resulting equations and all experimental work must make reference to the volume in question. Delhaye and co-workers (16, 32, 33) use this approach in presenting equations based on the volume of a pipe (and, by letting the pipe axial dimension tend toward zero, based on the area-averaging across the pipe cross-section).

Volume averaged equations derived rigorously result in general balance equations of the form (using the momentum equation as an example):

$$\frac{\partial}{\partial t} \overline{\rho_p V_{pi}^v} + \frac{\partial}{\partial x_j} \overline{\rho_p V_{pi}^v V_{pj}^v}$$

$$= \frac{\partial}{\partial x_j} \overline{\tau_{ij}^p} + \frac{1}{v} \int_{s_{p1} + s_{p2}} \tau_{ij}^p n_j dS + \overline{\rho_p}^v \varepsilon_1 \quad (3.36)$$

in terms of phase volume averages, or :

$$\frac{\partial}{\partial t} v \alpha_p \overline{\rho_p V_{pi}^v} + \frac{\partial}{\partial x_j} v \alpha_p \overline{\rho_p V_{pi}^v V_{pj}^v}$$

$$= \frac{\partial}{\partial x_j} v \alpha_p \overline{\tau_{ij}^p} + \int_{s_{p1} + s_{p2}} \tau_{ij}^p n_j dS + \alpha_p \overline{\rho_p}^v \varepsilon_1 \quad (3.37)$$

in terms of intrinsic phase volume averages, where phase change effects in both cases have been neglected. The second term on the right hand side of the above equations represents the action of the interface on the given phase contained in the averaging volume v . Mathematically this term originates directly from the difference between the mean value of the derivative $\overline{\partial \tau_{ij}^p / \partial x_j}^v$ and the derivative of the mean value of the stress tensor $\overline{\partial \tau_{ij}^p}^v / \partial x_j$.

A novel spatial averaging technique is used by Anderson and Jackson for gas-solids suspensions (1). The technique involves averaging over the entire region occupied by the suspension by the use of a weighting function $g(r)$ which is defined for $r > 0$. Average values are thus given by :

$$\alpha_p \overline{\psi'_p(x_1, t) g} = \int_{V_{p\infty}} \psi'_p(y_1, t) g(x_1 - y_1) dv_y \quad (3.38)$$

where $V_{p\infty}$ includes all the points occupied by phase p at a time t.

This type of averaging has the advantage when dealing with gas-solids suspension flow of allowing a clear definition of particle concentration by number :

$$n_p(x_1, t) = \frac{1}{\omega_{pV}} \int_{V_{p\infty}} g(x_1 - y_1) dv_y \quad (3.39)$$

The number concentration so defined and the volume fraction are directly related by :

$$n_p(x_1, t) \omega_{pV} = \alpha_p(x_1, t) \quad (3.40)$$

It will be recalled that for other types of averaging which require the introduction of a control volume at some point in the derivation it is not possible to write the above equation since, in general, there are particles straddling the control volume surface.

Anderson and Jackson derive averaged equations by averaging the Navier-Stokes equations for the fluid phase and by averaging the equation of motion of a single particle for the solids phase. This results in :

$$\begin{aligned} \frac{\partial}{\partial t} \overline{\alpha_f \rho_f U_i^g} + \frac{\partial}{\partial x_j} \overline{\alpha_f \rho_f U_i U_j^g} \\ = \frac{\partial}{\partial x_j} \overline{\rho_f U_{ij}^g} - n_p^* f_i + \overline{\alpha_f \rho_f F_i} \end{aligned} \quad (3.41)$$

for the fluid phase, and :

$$\frac{\partial}{\partial t} \overline{\alpha_s \rho_s V_i^g} + \frac{\partial}{\partial x_j} \overline{\alpha_s \rho_s V_i V_j^g} = n_p f_i + n_p Z_i + \overline{\alpha_s \rho_s F_i} \quad (3.42)$$

where n_p is the number concentration of the solids particles and Z_i is the force due to particle collisions. These equations have a similar form to those discussed earlier where particles at the control volume surface had been neglected. This is to be expected since averaging is carried out over the entire volume occupied by the suspension and weighted in such a way as the surface enclosing the volume has no effect on the contents.

Anderson and Jackson's averaging technique has the disadvantage of not uniquely determining local mean variables since these values would generally depend on the exact weighting function and, in particular, on its radius. The radius r_0 of the weighting function determines the effective volume over which the averaging is carried out. It is defined by :

$$4\pi \int_0^{r_0} g(r) r^2 dr = 4\pi \int_{r_0}^{\infty} g(r) r^2 dr = \frac{1}{2} \quad (3.43)$$

Anderson and Jackson suggest however that the local mean variables will be "insensitive to the radius or detailed form of the weighting function provided the radius is large compared with the particle spacing and small compared with the scale of macroscopic variation from point to point in the system". The mean values are thus independent of the weighting function under the same conditions as ordinary volume averages were independent of the choice of the averaging volume. It can be noted that ordinary volume averaging can be thought of as a particular case of averaging via a weighting function: in ordinary volume averaging the weighting function takes on a value of 1 at every point occupied by the phase in question within the averaging volume and a value of zero at all points beyond. This would seem to be the only choice of $g(r)$ which leads to the definition of mean variables having a clear physical significance.

Similar in methodology with volume averaging is time averaging. Here mean values are given via integration of the form:

$$\overline{\psi_p(x_1, t)}^T = \frac{1}{T} \int_{T_p(t)} \psi_p(x_1, t') dt' \quad (3.44)$$

where T is the time interval over which averaging is carried out; $T_p(t)$ is the portion of the interval during which the point in question is occupied by phase p .

This type of averaging is routinely carried out in single phase flow equations to isolate turbulent fluctuations from terms involving mean variables. In single phase fluid turbulence the time interval over which the averaging takes place is large compared to the time

scale of turbulence and small compared to the interval in time over which significant changes take place in the bulk flow. The appropriate time interval in multiphase flow is limited in the same way except that the constraints are more severe, especially with respect to the lower limit: the time interval must be large enough to smooth out not only inherent turbulence associated with each of the phases but also local variations in properties arising from the passage of different phases at particular points in the flow. As in the case of volume averaging then, there are inherent restrictions in time averaging and it is possible to find practical situations for which a suitable time interval doesn't exist.

Rigorously derived time-averaged equations have been presented by Delhay and Achard (33) and by Ishii (62) who arrive at identical results although with somewhat different approaches with respect to the interfaces between phases. Delhay and Achard consider the interface as a density discontinuity surface; Ishii considers the interface as a zone of finite thickness, derives balance equations for each zone including the interface and then allows the thickness of the interface to tend toward zero. The resulting general balance equation for a phase p , using the momentum equation as an illustration and neglecting phase changes, is, in both cases:

$$\frac{\partial}{\partial t} \alpha_p \bar{c}_p = \frac{\partial}{\partial t} \alpha_p \bar{c}_p + \sum_{\text{disc}} \left[\frac{\partial}{\partial x} \tau_{i,j}^+(x_i, t^+) - \frac{\partial}{\partial x} \tau_{i,j}^-(x_i, t^-) \right] \quad (3.45)$$

where $\alpha_p = (T_p)/(T)$ is defined as the residence time fraction of the phase p at a given point. The final term of the right hand side represents the action of the interface on the phase in question. In the derivations presented by Delhaye and Achard and by Ishii, the above form originates in the Leibnitz rule expansion of the integral of functions with first order discontinuities over the averaging period.

In addition to the problem of finding a suitable time interval over which to carry out the averaging process, there is an additional disadvantage associated with simple time averaging over a finite time interval. As just noted the residence time fraction is defined as: $\alpha_p = T_p/T$. In terms of the characteristic function K_p' this can be written as: $\alpha_p = \overline{K_p' T}$. The time derivative of α_p is discontinuous in that it can only take on values of 0, $1/T$ and $-1/T$. To overcome this difficulty, Delhaye and Achard and Drew (39) have introduced double time averaging which allows, with the first integrations, the definition of continuous mean values of functions and, with the second integration, the definition of mean values of functions having continuous time derivatives.

In order to smooth out both spatial and temporal fluctuations, equations averaged over both space and time have been presented by several investigators. Drew and Segal (39, 40) perform two volume integrations followed by two time integrations to obtain mean variables with continuous first time and space derivatives. Panton (99) considers the case of one-dimensional pipe flow of a gas-solids suspension in presenting area/time averaged equations across the section of a pipe. Delhaye and co-workers (16, 33) consider the case of gas-liquid pipe flow and average their time-averaged equations across the cross-section of a pipe.

The resulting equations are of the same form as the simple volume and simple time averaged equations. Delhaye (33) has also shown that space and time averaging operators are commutative.

GENERAL PROBABILISTIC MULTIPHASE FLOW EQUATIONS

4.1 Introduction

The preceding chapter reviewed numerous attempts which have been made at deriving general multiphase flow equations. Two basic approaches to the problem were outlined: Section 3.2 discussed general equations derived directly in terms of implicitly defined mean flow variables. A variety of problems were found to be associated with this type of approach and none of the equation formulations discussed was fully rigorous from a mathematical and conceptual point of view. Many of the difficulties encountered with the former approach were overcome using the rigorous time and/or space averaging discussed in Section 3.3. Definitions of local mean variables using these techniques were shown however to be dependent on the existence of an appropriate averaging interval, a constraint which is much more limiting in multiphase flows than in single phase flows where these techniques are routinely used in the treatment of turbulence.

Probabilistic (or as it is sometimes called ensemble) averaging makes it possible to overcome this remaining difficulty. The probabilistic approach to multiphase flow problems is based on the observation that such flows are fundamentally random in nature. Local mean variables are defined in an unambiguous fashion as expected values of phase presence and physical quantities associated with different phases in suspension. Spatial and temporal variations of these

variables can then be used to derive fully rigorous general mass, momentum and energy equations for multiphase flows.

Probabilistic averaging has the "logical advantage" (6) of being applicable where time and space averaging are not, in addition to leading to similar results compared to the latter two methods where suitable averaging intervals can be defined.

Its most important advantage is conceptual, however and originates in the fundamentally random nature of suspension flows. The significance of this random nature can be illustrated by considering a large number of identical experiments carried out on a flowing gas-solids suspension. The experiments are termed "identical" if their overall boundary conditions, as well as the evolution of these boundary conditions in time, are strictly the same for all experiments. If a particular point at a particular time after the start of one of these experiments is examined, it is possible to observe the presence of either the fluid phase or any one of the solids phases making up the overall mixture. The reason for this stems from the fact that, while the overall initial and boundary conditions in a suspension may be fixed and precisely known, the individual boundary conditions for each and every particle making up the suspension are generally unknown. Furthermore, the initial and boundary conditions of a given particle are dependent on the initial conditions of all of the other particles in the mixture and on the interactions between particles and between particles and the fluid. The distribution of phases in space, as well as the succession of phases at each point and the physical quantities associated with each phase at each point is consequently random: the

most appropriate mathematical description of such systems is therefore probabilistic.

Probabilistic descriptions of multiphase flows have been introduced on at least three occasions to treat gas-liquid flows. The early work by Delhaye (32) is of interest essentially for its introduction of the concept of phase presence probability for gas-liquid mixtures flowing in pipes. His approach consisted of writing balance equations for each of a total of N experiments carried out on a gas-liquid mixture. The averaged form of the equations was then developed by summing the equations, valid for each individual experiment, over all N experiments. His local equations however, were only valid when the point being considered was entirely surrounded by one particular phase. Phase interaction forces were not therefore present in the final equations.

Delhaye and Achard (33) and Fitremann (46) present derivations for "statistically" averaged general equations for gas-liquid flows which are similar to one another. Their approaches consist of assuming the Navier-Stokes equations to be locally valid for all individual phases at all points. An averaging operator is then applied to the local form of the equations in order to extend the definitions of the local variables and equations over the entire mixture.

While the resulting equations are formally similar to those to be derived here for the fluid phase, their assumption that all phases are governed by the same basic balance equation to which they apply an averaging operator does not allow full consideration of fundamental

differences between particle and fluid phases. The present approach examines all external forces acting on all phases and leads to the definition of two stress tensors in solids phases, one resulting from hydrodynamic interaction with surrounding medium and another due to collisions between particles. Fitremann also introduces an "interface density distribution" function which is not required in the present derivation.

Fortier (48) was the first to introduce the notion of phase presence probability in the treatment of gas-solids suspension flows. Having initially written equations in terms of volume averages for fine particles in suspension (47) he recognized that, when the average particle diameter becomes non-negligible with respect to the characteristic dimension of the installation in which the suspension is flowing, this approach can no longer be followed; that is, an appropriate averaging interval no longer exists and it is necessary to work in terms of the "rate of presence" of a particular phase at a particular point. Fortier's objective was to treat a specific gas-solids suspension flow application; namely, dense phase pneumatic transport. His treatment of the external forces acting on a given phase was, as a result, limited to this particular application. While he didn't attempt a general probabilistic description of suspension flows, his work in showing the necessity of this kind of approach prompted another effort by Molodtsov (90) who developed probabilistic expressions for mass, momentum and kinetic energy variations but who stopped short of a fully rigorous description of external force and heat transfer terms.

This chapter presents fully rigorous probabilistic multiphase flow equations based on concepts initially outlined in Fortier's and Molodtsov's early work. The development of the probabilistic multiphase flow equations was undertaken jointly with Y. Molodtsov and has been published by Molodtsov and Muzyka in Ref. 91. ~~Certain~~ derivations which are attributable exclusively to the former worker as well as some results pertaining to gas-liquid flows (surface tension and phase change phenomena) are presented only briefly here with appropriate references being made either to Ref. 91 or to Molodtsov's thesis (93).

4.2 Basic concepts

Multiphase media are heterogeneous mixtures of non-miscible components or phases often belonging to different fundamental states of matter. In order to rigorously describe the behaviour of multiphase media it is necessary to be able to consider each component individually since the interaction between components in suspension and therefore the behaviour of the suspension as a whole will depend on the physical characteristics of each component present.

The general equations to be developed here will consider a "phase" to be defined as a component which is mechanically separable from the other components in the mixture. Particle phases are consequently distinguishable by particle shape (separable by sorting), particle diameter (sieving) or particle density (flotation). Equations will be written for a general phase "p" where p may be either the fluid phase or any one of the particle phases making up the mixture. Where desirable, particle phases will be re-grouped to form one overall "solids" phase.

The fundamental hypothesis upon which the probabilistic multiphase flow equations are based follows from the random nature of suspension flows:

The phase presence and physical quantities associated with phases are, at all points and instants in time, random variables subject to laws of probability defined by the overall boundary conditions of the system.

4.2.1. Phase presence probability

General probabilistic multiphase flow equations are derived in terms of a basic variable called the "phase presence probability". Consider N identical experiments carried out on a suspension as described in Section 4.1. Out of the total number of experiments, a given phase p will be present at the point x_i at time t after the beginning of the experiment a number, N_p times. As the number of experiments N approaches infinity, the quotient N_p/N approaches a finite limit $\alpha_p(x_i, t)$ defined as the probability of presence of the phase p at the point x_i at time t . Over the entire time and space domain $\alpha_p(x_i, t)$ forms a scalar field which can be expressed in terms of the characteristic function of the phase p , R_p . At all times and points where the phase p is present during one of the identical experiments R_p takes on a value of 1; in all other cases it takes on a value of zero. The phase presence probability is the probabilistic mean or the expected value of R_p :

$$\alpha_p(x_i, t) = \overline{R_p(x_i, t)} = \lim_{N \rightarrow \infty} \frac{1}{N} \sum R_p(x_i, t) \quad (4.1)$$

where the tilde superscript indicates a random variable; the overbar indicates the operation of taking the probabilistic mean.

The phase presence probability $\alpha_p(x_1, t)$ is assumed to be continuous and differentiable with respect to time and space coordinates over the entire time and space domain.

4.2.2 Mean variables

Mean variables associated with individual phases are defined in an analogous way to which the phase presence probability was just defined. Re-consider the point x_1 at time t during one of the previously defined N identical experiments. If the phase p is present, any physical quantity associated with it (velocity, temperature, internal energy, etc...) will have, as a result of the random nature of the suspension, a random value, $\tilde{\psi}_p$. The "phase mean" value of $\tilde{\psi}_p$ will be defined as the probabilistic mean of all the values taken on by $\tilde{\psi}_p$ calculated over all experiments during which the phase p is present at the point considered:

$$\bar{\tilde{\psi}}_p(x_1, t) = \lim_{N \rightarrow \infty} \frac{1}{N_p} \sum_{N_p} \tilde{\psi}_p(x_1, t) = \psi_p(x_1, t) \quad (4.2)$$

The "partial" mean value of the random variable $\tilde{\psi}_p$ can be similarly defined as the probabilistic mean calculated over all N experiments provided $\tilde{\psi}_p$ is assumed to take on a value of zero for experiments where the phase p is not present at the point in question:

$$\overline{\psi_p(x_i, t)} = \lim_{N \rightarrow \infty} \frac{1}{N} \sum_{N_p} K_p \psi_p \quad (4.3)$$

It can be easily shown that the partial and phase mean variables are related to each other via the phase presence probability :

$$\overline{\psi_p^2} = \alpha_p \psi_p \quad (4.4)$$

4.2.3 Differentiation

As was shown in Chapter 3, one of the main causes of inconsistencies in previous general equation formulations arose from the unwarranted assumption that derivatives of mean variables were equal to mean values of derivatives of locally-defined variables. This section considers the relationship between the two in the probabilistic formulation.

Consider the definition of the probabilistic mean value of the derivative of the random variable ψ_p :

$$\overline{\frac{\partial \psi_p}{\partial x_i}} = \lim_{N \rightarrow \infty} \frac{1}{N} \sum_{N_p} K_p \frac{\partial \psi_p}{\partial x_i} \quad (4.5)$$

Expanding the quantity under the sum sign gives :

$$\begin{aligned} \overline{\frac{\partial \psi}{\partial x_i}} &= \lim_{N \rightarrow \infty} \frac{1}{N} \sum \frac{\partial}{\partial x_i} \psi_p - \lim_{N \rightarrow \infty} \frac{1}{N} \sum \psi_p \frac{\partial \psi_p}{\partial x_i} \\ &= \overline{\frac{\partial \psi}{\partial x_i}} - \overline{\psi_p \frac{\partial \psi_p}{\partial x_i}} \end{aligned} \quad (4.6)$$

Thus the mean value of the derivative is not equal to the derivative of the mean value. The difference between the two can be shown to be due to the existence of interfaces between phases in two ways. Firstly, it can be noted that the second term on the right hand side of Equation 4.6 is identically zero whenever the point under consideration is entirely contained within the phase p or entirely within one of the other phases since $\partial \psi_p / \partial x_i$ is zero at all points which meet this condition. The vector $\partial \psi_p / \partial x_i$ is non-zero at the interface however and can be shown to be given by :

$$\frac{\partial \psi_p}{\partial x_i} = \delta_p \tilde{n}_i^p \quad (4.7)$$

where δ_p is a delta distribution which is zero everywhere except at the interface ; \tilde{n}_i^p is the projection of the unit vector normal to the interface directed outward from p . The non-zero second term in Equation 4.6 thus arises from jump discontinuities in ψ_p as the interface is crossed.

This can also be shown by examining the derivative of the function $\tilde{\psi}_p$ summed over the portion of a reference volume v occupied by the phase p :

$$\int_{\tilde{v}_p} \frac{\partial \tilde{\psi}_p}{\partial x_i} dv$$

The surfaces \tilde{S}_p , \tilde{S}_{p1} and \tilde{S}_{p2} totally enclose the volume \tilde{v}_p (See Figure 4.1). The above integral can therefore be transformed using Gauss' theorem into a surface integral as :

$$\int_{\tilde{v}_p} \frac{\partial \tilde{\psi}_p}{\partial x_i} dv = \int_{\tilde{S}_p} \tilde{\psi}_p n_i dS + \int_{\tilde{S}_{p1} + \tilde{S}_{p2}} \tilde{\psi}_p n_i^p dS \quad (4.8)$$

The integral on the left hand side and the first integral on the right hand side of the above equation can be transformed into integrals over v and S respectively by multiplying the integrands by K_p :

$$\int_v K_p \frac{\partial \tilde{\psi}_p}{\partial x_i} dv = \int_S K_p \tilde{\psi}_p n_i dS + \int_{\tilde{S}_{p1} + \tilde{S}_{p2}} \tilde{\psi}_p n_i^p dS \quad (4.9)$$

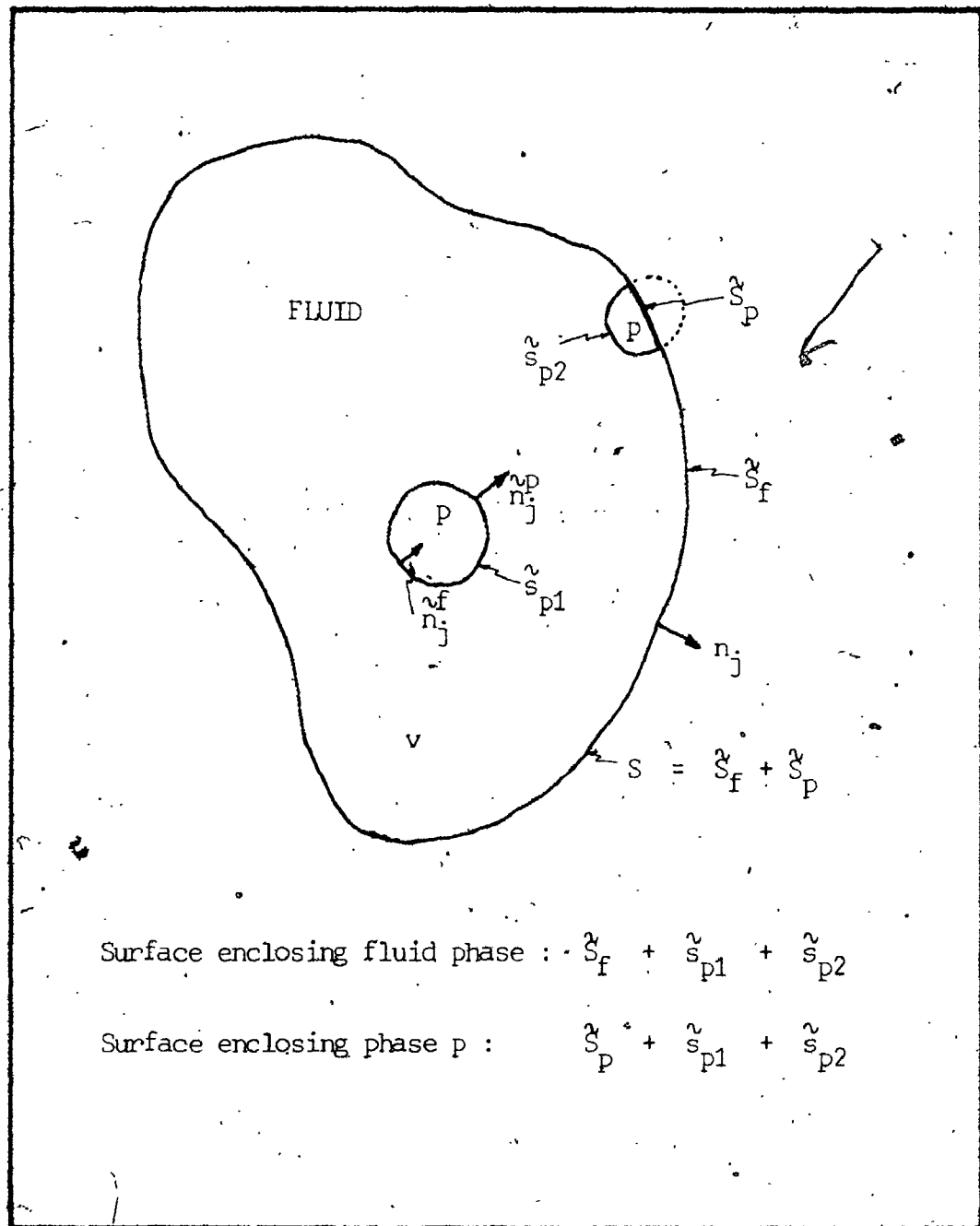


FIGURE 4.1 Surfaces totally enclosing phases contained within a reference volume v

Re-transforming the integral over S into a volume integral and taking the probabilistic mean of the above equation leads to :

$$\int_v \overline{\frac{\partial \Psi_p}{\partial x_i}} dv = \int_v \frac{\partial \overline{\Psi_p}}{\partial x_i} dv + \overline{\int_{S_{p1} + S_{p2}} \Psi_p n_i^D dS} \quad (4.10)$$

Comparing Equations 4.6 and 4.10 shows that :

$$\int_v \overline{\Psi_p \frac{\partial \overline{\Psi_p}}{\partial x_i}} dv = - \overline{\int_{S_{p1} + S_{p2}} \Psi_p n_i^D dS} \quad (4.11)$$

This equation shows that the integral over the reference volume of the mean values taken on by $\overline{\Psi_p}$ at the interface is equal (with a sign change) to the mean value of the integral of Ψ_p along the oriented interfacial surface contained in v (Hence Equation 4.7).

As will be shown in later sections this mathematical result concerning the difference between mean values of derivatives and derivatives of mean values manifests itself physically in terms of interaction forces, heat transfer and phase changes at the interface:

4.2.4 Variations of a quantity Ψ_p with respect to time

The development of general continuity, momentum and energy equations for each phase requires the development of expressions for

the time variations of mass, momentum and internal and kinetic energy which will be used in statements of the principle of mass conservations, Newton's second law and the first law of thermodynamics. The present section will be concerned with the development of a general expression for the time variation of a quantity $\tilde{\psi}_p$ per unit volume in a control volume moving at the velocity of the phase p with respect to fixed space coordinates.

Consider such a volume v . The amount of $\tilde{\psi}_p$ in the volume at time t during one of the identical experiments is given by :

$$\int_{\tilde{v}_p} \tilde{\psi}_p(x_i, t) dv \quad (4.12)$$

Similarly at time $t + dt$ the amount of $\tilde{\psi}_p$ in v is given by :

$$\int_{\tilde{v}_p} \tilde{\psi}_p(x_i, t+dt) dv \quad (4.13)$$

If no phase changes occur $\tilde{\psi}_p$ can be transported out of the control volume with its associated mass only across the external surface bounding the control volume v . The amount transported in this way over the time period dt is given by :

$$\int_{S_P} \psi_P \hat{V}_{PJ} n_j dS dt \quad (4.14)$$

The rate of change of ψ_P within v over dt will thus be given by the sum of expressions 4.13 and 4.14 minus expression 4.12 :

$$d \int_{v_P} \psi_P^2 dv = \int_{v_P} \{\psi_P(x_i, t+dt) - \psi_P(x_i, t)\} dv + \int_{S_P} \psi_P \hat{V}_{PJ} n_j dS dt \quad (4.15)$$

which is equivalent to :

$$\begin{aligned} d \int_v \hat{K}_{PP} \psi_P dv \\ = \int_v \{\hat{K}_{PP} \psi_P(x_i, t+dt) - \hat{K}_{PP} \psi_P(x_i, t)\} dv + \int_S \hat{K}_{PP} \hat{V}_{PJ} n_j dS dt \end{aligned} \quad (4.16)$$

Dividing through by dt and transforming the surface integral into a volume integral leads to :

$$\frac{d}{dt} \int_v \tilde{\rho}_p \tilde{\psi}_p dv = \int_v \left[\frac{\partial}{\partial t} \tilde{\rho}_p \tilde{\psi}_p + \frac{\partial}{\partial x_j} \tilde{\rho}_p \tilde{\psi}_p \tilde{v}_{pj} \right] dv \quad (4.17)$$

Taking the probabilistic mean of both sides of the above equation gives :

$$\overline{\frac{d}{dt} \int_v \tilde{\rho}_p \tilde{\psi}_p dv} = \int_v \left[\frac{\partial}{\partial t} \alpha_p \overline{\tilde{\psi}_p} + \frac{\partial}{\partial x_j} \alpha_p \overline{\tilde{\psi}_p \tilde{v}_{pj}} \right] dv \quad (4.18)$$

It should be noted that the above result holds only when the phase p is conservative : if phase changes (boiling, for example in gas-liquid flows) or phase mutation (attrition or agglomeration in gas-solids flows) occur flux across the surface bounding the volume v_p contained in v will occur across the phase interfaces as well as the surface S_p (Expression 4.14). This latter case is treated in Reference 91.

4.3. Continuity

When no phase changes occur the general continuity equation for a phase p in the suspension is derived by substituting the phase density for $\tilde{\rho}_p$ in Equation 4.17 and equating it to zero. In terms of random variables this gives :

$$\frac{\partial}{\partial t} \overline{\rho_p \tilde{v}_p} + \frac{\partial}{\partial x_j} \overline{\rho_p \tilde{v}_p v_{pj}} = 0 \quad (4.19)$$

The integral signs have been removed since Equation 4.17 is valid for any control volume v .

Note that, in principle, the phase density ρ_p is a random variable. In most cases however, even if the phase under consideration is compressible, density fluctuations will be small. Throughout the rest of the discussion means of the form $\overline{\rho_p \tilde{\psi}_p}$ will be considered to be equal to $\rho_p \overline{\tilde{\psi}_p}$. Later on, the phase p thermal conductivity λ_p will be similarly assumed not to fluctuate.

The probabilistic mean of Equation 4.19 follows from Equation 4.18 :

$$\frac{\partial}{\partial t} \alpha_p \rho_p + \frac{\partial}{\partial x_j} \alpha_p \rho_p v_{pj} = 0 \quad (4.20)$$

4.4 Momentum

The rate of change of momentum for a phase p in the mixture is obtained by substituting $\rho_p \tilde{v}_{pi}$ for $\tilde{\psi}_p$ into Equation 4.17 :

$$\frac{\partial}{\partial t} K_{pp}^{\alpha} \bar{v}_{pi} + \frac{\partial}{\partial x_j} K_{pp}^{\alpha} \bar{v}_{pi} \bar{v}_{pj} \quad (4.21)$$

The probabilistic mean of the above expression is :

$$\frac{\partial}{\partial t} \rho_p^{\alpha} \bar{v}_{pi} + \frac{\partial}{\partial x_j} \rho_p^{\alpha} \overline{\bar{v}_{pi} \bar{v}_{pj}} \quad (4.22)$$

The quantity under the overbar is not generally equal to the product of the two mean velocity vectors. This is analogous to turbulent fluctuations in single phase flows and arises from the fact that, in suspension flows, even stationary overall boundary conditions impose only mean velocities.; instantaneous local velocities are random.

The second term in the above expression can be written in terms of the velocity cofluctuation tensor β_{ij}^P defined as :

$$\beta_{ij}^P = \overline{(\bar{v}_{pi} - v_{pi})(\bar{v}_{pj} - v_{pj})} \quad (4.23)$$

Expression 4.22 then becomes :

$$\frac{\partial}{\partial t} \rho_p^{\alpha} \bar{v}_{pi} + \frac{\partial}{\partial x_j} \rho_p^{\alpha} \bar{v}_{pi} \bar{v}_{pj} + \frac{\partial}{\partial x_j} \rho_p^{\alpha} \beta_{ij}^P \quad (4.24)$$

The development of general momentum equations for individual phases requires equating the above expression to the probabilistic mean of the external forces acting on each phase. As the external forces acting on the fluid phase are somewhat different than those acting on the solids phases, the two derivations will be considered separately in the following two sections.

4.4.1 External forces acting on the fluid phase

The external forces acting on the fluid phase contained in a control volume v are of two types: body forces and surface forces. The former include, under normal circumstances, only gravitational forces but could also be considered to include forces due to electric or magnetic fields. The latter include forces acting on the fluid located at the control volume surface, as well as forces acting on the fluid interfaces contained in v .

The random gravitational force acting on the fluid phase contained in the control volume v is given by:

$$\int_v \rho_f \mathbf{g}_i \, dv \quad (4.25)$$

The probabilistic mean of which is:

$$\int_v \alpha_f \rho_f \mathbf{g}_i \, dv \quad (4.26)$$

The surface bounding the fluid phase is made up of two components : the intersection of the fluid phase and the control volume surface and the surface at the fluid-particle interface (see Figure 4.1). The total of random surface forces exerted on the fluid phase can be expressed as the internal stress tensor in the fluid phase evaluated over these two surfaces :

$$\int_{\partial V} \mathbf{t} \cdot \mathbf{n} \, dA + \int_{\partial V} \mathbf{t} \cdot \mathbf{n} \, dA \quad (4.27)$$

The first integral can be transformed into an integral over V by multiplying the integrand through by \mathbf{K}_0 and then transformed into a volume integral over V using Gauss' theorem. The probabilistic mean of the entire expression can then be taken to yield :

$$\frac{1}{V} \int_V \mathbf{t} \cdot \mathbf{n} \, dV + \int_V \mathbf{t} \cdot \mathbf{n} \, dV \quad (4.28)$$

The first term in expression 4.28 represents the probabilistic mean force exerted by the fluid outside the control volume on the fluid inside ; the second term was obtained by applying the result given by Equation 4.11. It expresses the mean force per unit volume exerted by the fluid interface on the fluid itself in V . This force will be noted as :

$$F_i^{af} = - \frac{\tau_{ij}^{af}}{\tau_{ij}^{af}} \frac{\partial k_f}{\partial x_j} \quad (4.29)$$

4.4.2 External forces acting on the solids phases

Gravitational forces on a given solids phase p in suspension are treated in the same way as for the fluid phase. The probabilistic mean gravitational force acting on a solids phase p in v is given by :

$$\int_v \alpha_p \rho_p g_i \, dv \quad (4.30)$$

Surface forces acting on the particle phases arise from the hydrodynamic interaction between particles and the surrounding medium. As in the case of the fluid phase these forces are composed of two parts : the hydrodynamic effect of the medium external to the control volume transmitted via the surface formed by the intersections of the particles and the control volume surface and forces at particle phase interfaces located in the control volume. These forces result in the creation of a stress tensor within individual particles τ_{ij}^p .

Hydrodynamic forces on solids phases can be treated in the same way as the external surface forces in the fluid phase. The random surface force on the phase p in v is given by :

$$\int_{S_p} \tau_{ij}^{fp} n_j \, dS + \int_{S_{p1} + S_{p2}} \tau_{ij}^{pd} n_j \, dS \quad (4.31)$$

The corresponding probabilistic mean expression is :

$$\int_V \frac{\partial}{\partial x_j} \alpha_p \tau_{ij}^p dv + \int_V F_i^{ap} dv \quad (4.32)$$

where F_i^{ap} is defined as for the fluid phase :

$$F_i^{ap} = - \tau_{ij}^{ap} \frac{\partial k_p}{\partial x_j} \quad (4.33)$$

The above forces are exerted on each of the particle phases in suspension continuously with respect to time and include indirect interaction between the particles and the surrounding medium. In addition to these effects, the suspension motion is affected by direct interaction forces which act intermittently in time due to particles colliding with one another and with solid boundaries enclosing the suspension flow.

Consider for example a phase p particle in collision with a phase q particle. At the instant the collision takes place, the phase q particle exerts a force f_i^{qp} on the phase p particle. This force gives rise to a stress tensor τ_{ij}^{qp} within the phase p particle which is related to f_i^{qp} by :

$$f_i^{qp} = \int_{S_p} \tau_{ij}^{qp} n_j^p dS \quad (4.34)$$

where \tilde{s}_p is the surface bounding the phase p particle. As the force exerted is applied only at the contact point, the vector $\tilde{r}_{ij}^{qp} \tilde{n}_j^p dS$ is zero everywhere on \tilde{s}_p except at the contact point where it is equal to \tilde{r}_i^{qp} .

The treatment of interparticle collisions to formulate a probabilistic mean stress tensor in the particle phases to account for these effects is due to Molodtsov and is discussed in full detail in Reference 91. It consists of examining three types of collisions which differ according to their relative locations with respect to the control volume boundary (see Figure 4.2).

The first type of collision involves particles of the phase p entirely contained in the control volume entering into contact with phase q particles at least partially contained in v. The random force exerted on these particles is given by :

$$\int_{\tilde{s}_{p1}} \tilde{r}_{ij}^{qp} \tilde{n}_j^p dS \quad (4.35)$$

The second type of collision involves phase p particles straddling the control volume surface in contact with phase q particles at least partially contained in v with the contact point also contained in v. The force exerted on the portions of the phase p particles within v is given by :

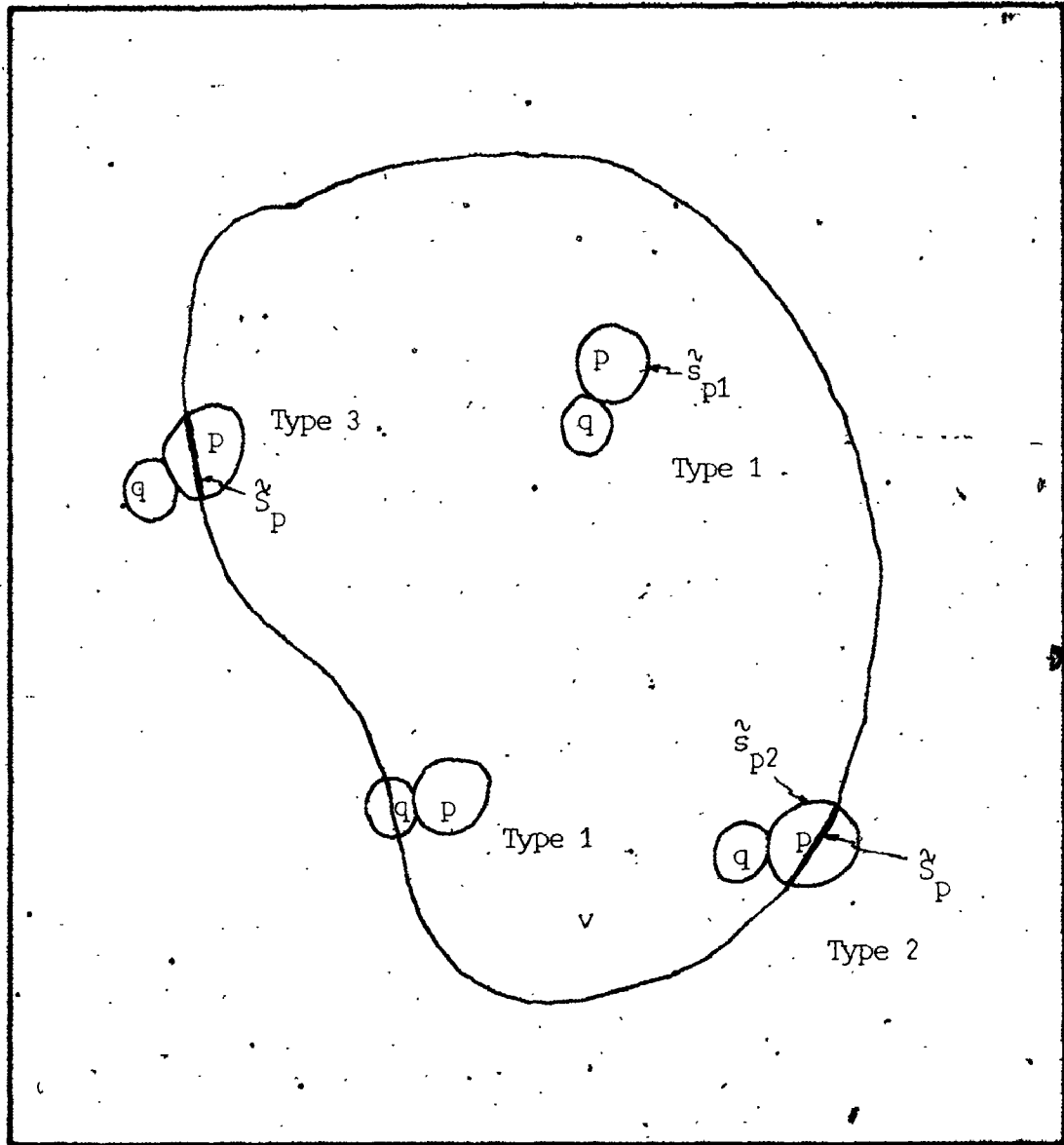


FIGURE 4.2 Types of particle collisions involving phase p particles at least partially contained in the control volume v

$$\int_{S_p} \bar{r}_{ij}^{qp} n_j dS + \int_{\tilde{S}_{p2}} \bar{r}_{ij}^{qp} \tilde{n}_j^p dS \quad (4.36)$$

When the collisions occur between phase p particles straddling the control volume boundary and phase q particles with the contact point outside the control volume (Type 3 collisions) the result is similar to that given above except that the second integral is zero since $\bar{r}_{ij}^{qp} \tilde{n}_j^p dS$ is zero all along \tilde{S}_{p2} in this case.

The resultant force exerted by the phase q on the phase p located in v is thus formed of sums over the surfaces \tilde{S}_p , \tilde{S}_{p1} and \tilde{S}_{p2} which, collectively, entirely enclose p in v which are in contact with phase q particles :

$$\int_{\tilde{S}_p} \bar{r}_{ij}^{qp} n_j dS + \int_{\tilde{S}_{p1}} \bar{r}_{ij}^{qp} \tilde{n}_j^p dS + \int_{\tilde{S}_{p2}} \bar{r}_{ij}^{qp} \tilde{n}_j^p dS \quad (4.37)$$

The overall force exerted on the phase p in the control volume is obtained by summing the above expressions for all phases q in the suspension and for collisions involving solid boundaries.

Transforming the surface integrals in Expression 4.37 into volume integrals in order to develop a probabilistic mean expression for forces due to particle collisions requires the definition of the characteristic function \bar{G}_p to describe the spatial extension of the collisions involving phase p particles. This function takes on a value

of 1 within the entire region occupied by a phase p particle which is in collision with another particle or the walls bounding the flowing suspension at the instant t ; G_p takes on a value of zero everywhere else. The overall random force on the phase p in v due to particle collisions can thus be written as :

$$\begin{aligned}
 F_i^{CP} &= \int_{S_p} \dot{M}_{ij}^p n_j dS + \int_{S_{p1} + S_{p2}} \dot{M}_{ij}^p n_j^p dS \\
 &= \int_{V_p} \frac{\partial}{\partial x_j} \dot{M}_{ij}^p dv \\
 &= \int_V G_p \frac{\partial}{\partial x_j} \dot{M}_{ij}^p dv \\
 &= \int_V \frac{\partial}{\partial x_j} G_p \dot{M}_{ij}^p dv - \int_V \dot{M}_{ij}^p \frac{\partial G_p}{\partial x_j} dv \quad (4.38)
 \end{aligned}$$

The first integral in the above equation is the force exerted on phase p particles in the control volume due to collisions with particles outside the control volume ; the second is an interaction force between phase p particle inside v colliding with other particles also inside v. Letting :

$$F_i^{sp} = - \overline{F_{ij}^{sp}} \frac{\partial G_p}{\partial x_j} \quad (4.39)$$

and

$$s_{ij}^p = \overline{G_p F_{ij}^{sp}} \quad (4.40)$$

the probabilistic mean of the collision forces exerted on the phase p in v can be written as :

$$F_i^{cp} = \int_v \left[\overline{F_i^{sp}} + \frac{\partial}{\partial x_j} s_{ij}^p \right] dv \quad (4.41)$$

4.4.3 Momentum equations

The general probabilistic momentum equations can now be written by equating probabilistic mean expressions for momentum variation with the probabilistic mean of the external forces acting on a given phase. For the fluid phase this amounts to writing :

$$\text{Momentum variation} = \text{Fluid-Fluid Surface forces} + \text{Interfacial forces} + \text{Gravitational forces}$$

In terms of the results derived in this section the above equation can be written as :

$$\frac{\partial}{\partial t} \rho_f^\alpha U_i + \frac{\partial}{\partial x_j} \rho_f^\alpha U_i U_j + \frac{\partial}{\partial x_j} \rho_f^\alpha B_{ij} = \frac{\partial}{\partial x_j} \alpha_f^f \tau_{ij} + F_i^af + \rho_f^\alpha g_i \quad (4.42)$$

where in order to simplify notation U_i is defined as V_{fi} and B_{ij} as B_{ij}^f

For a single solids phase in suspension the momentum equation is :

- Rate of change of Momentum = Hydrodynamic stress due to external medium)
- + Particle collision forces with solids inside v
- + Particle collision forces with solids outside v
- + Interfacial forces
- + Gravitational forces

Mathematically this can be written as :

$$\frac{\partial}{\partial t} \rho_P^\alpha V_{Pi} + \frac{\partial}{\partial x_j} \rho_P^\alpha V_{Pi} V_{Pj} + \frac{\partial}{\partial x_j} \rho_P^\alpha \beta_{ij}^P = \frac{\partial}{\partial x_j} \alpha_P^P \tau_{ij}^P + F_i^{aP} + F_i^{SP} + \frac{\partial}{\partial x_j} s_{ij}^P + \rho_P^\alpha g_i \quad (4.43)$$

When the solids phase is considered as a whole a single momentum equation can be written in simplified form in the case where the density of the solids are all the same. Overall solids phase variables are defined as:

$$\bar{K}_s \bar{\psi}_{si} = \sum_{p \in S} \bar{K}_p \bar{\psi}_{pi} \quad (4.44)$$

$$\alpha_s = \sum_{p \in S} \alpha_p \quad (4.45)$$

$$\alpha_s \beta_{ij} = \sum_{p \in S} \alpha_p \beta_{ij}^p + \sum_{p \in S} \alpha_p V_{pi} (V_j - V_{pj}) \quad (4.46)$$

$$F_i^{as} = \sum_{p \in S} F_i^{ap} \quad (4.47)$$

$$s_{ij} = \sum_{p \in S} s_{ij}^p \quad (4.48)$$

The particle interaction force F_i^{sp} becomes zero in this case since the forces involved in collisions inside the control become internal forces when the solids are considered as a whole.

The solids phase momentum equation can thus be written :

$$\begin{aligned}
& \frac{\partial}{\partial t} \rho_s^\alpha V_i + \frac{\partial}{\partial x_j} \rho_s^\alpha V_i V_j + \frac{\partial}{\partial x_j} \rho_s^\alpha s_{ij} \\
& = \frac{\partial}{\partial x_j} \alpha_s^r s_{ij} + F_i^{as} + \frac{\partial}{\partial x_j} s_{ij} + \rho_s^\alpha g_i \quad (4.49)
\end{aligned}$$

Finally it can be noted that the interfacial interaction forces F_i^{af} and F_i^{as} are equal in magnitude and opposite in direction in the case where there is continuity in the stress fields across the fluid-solids interface ; that is, when surface tension effects are not present. The case of gas-liquid flows where surface tension plays an important role is discussed in Reference 91.

4.5 Energy

The development of general probabilistic energy equations is based on the First Law of Thermodynamics :

Rate of work done by
external forces

Rate of external heat
transfer

= Internal energy
variation

+ Kinetic energy
variation

Their mathematical formulation requires developing random variable expressions for each of the above terms and then taking their probabilistic means. The internal and kinetic energy variation expres-

sions follow directly from the general results obtained in Section 4.2.4 and are the same regardless of whether the phase p under consideration is fluid or one of the solids phases.

The internal energy variation of a phase p contained in a control volume v is given by substituting $\rho_p \tilde{E}_p$ for $\tilde{\psi}_p$ in Equation 4.17 :

$$\frac{d}{dt} \int_v \tilde{K}_{pp} \rho_p \tilde{E}_p dv = \int_v \left[\frac{\partial}{\partial t} \tilde{K}_{pp} \rho_p \tilde{E}_p + \frac{\partial}{\partial x_j} \tilde{K}_{pp} \rho_p \tilde{E}_p \tilde{V}_{pi} \right] dv \quad (4.50)$$

Similarly, the kinetic energy variation is given by substituting $\rho_p (\tilde{V}_p^2/2)$ into Equation 4.17 :

$$\begin{aligned} \frac{d}{dt} \int_v \tilde{K}_{pp} \rho_p (\tilde{V}_p^2/2) dv \\ = \int_v \left[\frac{\partial}{\partial t} \tilde{K}_{pp} \rho_p (\tilde{V}_p^2/2) + \frac{\partial}{\partial x_i} \tilde{K}_{pp} \rho_p (\tilde{V}_p^2/2) \tilde{V}_{pi} \right] dv \end{aligned} \quad (4.51)$$

where $\tilde{V}_p^2 = \tilde{V}_{pi} \tilde{V}_{pi}$.

The next two sections will be concerned with the development for expressions for the other two terms in the First Law equation.

4.5.1 Heat transfer

Heat flows into a phase p contained in the control volume across the surface bounding the phase within v . As in the case of the discussion of external forces. This surface is composed of two parts :

the intersection of the phase p and the surface bounding the control volume S and the phase p interfaces contained in v . Expressing the heat flux vector as $\vec{\phi}_{pi}$ the rate of thermal energy received by the phase p in v is given by integrals over these two surfaces :

$$\int_{S_p} \vec{\phi}_{pi} \cdot \vec{n}_i \, dS + \int_{S_{p1} + S_{p2}} \vec{\phi}_{pi} \cdot \vec{n}_i^p \, dS \quad (4.52)$$

As before the first integral can be transformed into an integral over S by multiplying the integrand by K_p and then into a volume integral by application of Gauss' theorem. It represents the heat flow within the phase p across the control volume surface. The second integral, using the techniques outlined in Section 4.2.3, can be written as :

$$\int_{S_{p1} + S_{p2}} \vec{\phi}_{pi} \cdot \vec{n}_i^p \, dS = - \int_v \vec{\phi}_{pi} \cdot \frac{\partial K_p}{\partial x_i} \, dv \quad (4.53)$$

and represents the heat flow into the phase p across phase p interfaces in v .

If heat transfer by radiation is negligible the heat flux vector can be written as :

$$\frac{\partial^2 \phi_{Fi}}{\partial x_i^2} = -\lambda \frac{\partial^2 T_i}{\partial x_i^2} \quad (4.54)$$

If the heat transfer between particles in collision is neglected as a secondary effect the only interfacial heat transfer which takes place will be between the fluid and the particle phases. With this assumption and Equation 4.54 the expression 4.52 can now be written as :

$$-\int_V \left[\frac{\partial}{\partial x_i} \left[\lambda \frac{\partial T_i}{\partial x_i} \right] \right] dv + \int_V \left[\frac{\partial^2 T_i}{\partial x_i^2} \right] \left[\frac{\partial^2 \phi_{Fi}}{\partial x_i^2} \right] dv \quad (4.55)$$

Defining C_{Fi} as :

$$C_{Fi} = -\lambda \frac{\partial^2 T_i}{\partial x_i^2} \frac{\partial^2 \phi_{Fi}}{\partial x_i^2} \quad (4.56)$$

the probabilistic mean expression 4.55 can be written as :

$$-\int_V \left[\frac{\partial}{\partial x_i} \left[\lambda \frac{\partial T_i}{\partial x_i} \right] \right] dv - \int_V \left[\frac{\partial^2 T_i}{\partial x_i^2} \right] \left[\frac{\partial^2 \phi_{Fi}}{\partial x_i^2} \right] dv + \int_V C_{Fi} dv \quad (4.57)$$

The second term in the above expression arises from jump discontinuities along the curve formed from the intersection of the control volume surface and the outer surface of particles, straddling the control volume surface. It can be expressed in terms of the interfacial mean temperature T_p^a defined as :

$$\frac{1}{V} \frac{dx_i}{dt} = \frac{1}{V} \frac{dx_i}{dt}$$

Expression 4.56 can thus be written as :

$$-\int_V \left[\frac{1}{V} \frac{dx_i}{dt} \right] \left[\frac{1}{V} \frac{dx_i}{dt} \right] - \frac{1}{V} \frac{dx_i}{dt} \left[\frac{1}{V} \frac{dx_i}{dt} \right] = \dots$$

The expression 4.59 is valid for a solids phase p. A similar expression can be written for the fluid phase provided the interfacial heat transfer terms are summed over all solids phases.

4.5.2 Work by external forces

Expressions for the work done by external forces which are continuous with respect to time are developed simply by calculating the scalar product of the external force and the phase velocity at each application point and then summing the individual contributions.

For the fluid phase in terms of random variables this results in :

$$= \dots + \dots + \dots$$

$$= \dots + \dots$$

All forces acting on the solid phases which are continuous with respect to time can be treated in a similar way. The development of corresponding expressions for forces arising from particle collisions is somewhat more complex since these forces act instantaneously and the particle velocities undergo discontinuities at the moment when the collisions take place. The mean velocity of a phase p particle at the instant the collision occurs for a given experiment is the arithmetic mean \bar{v}_{pi} of the before and after collision velocities since the two are equally probable. The work done by these collision forces has been shown by Molodtsov (91) to be equal to the scalar product of the collision force and the velocity \bar{v}_{pi} . In terms of random variables this is :

$$\int_V \sum_i \bar{v}_{pi} \cdot F_{pi} \, dV + \dots$$

4.5.3 Energy equations

The results from the preceding sections can now be used to develop general probabilistic energy equations. For the fluid phase the First Law expressed in terms of random variables is:

$$\rho_f \frac{\partial}{\partial x_i} \tau_{ij}^f \dot{U}_i + \rho_f \tau_{ij}^f \dot{\epsilon}_i + \frac{\partial}{\partial x_i} \left[\rho_f \lambda_f \frac{\partial T_f}{\partial x_i} \right] + \dot{q}_{sf}$$

Rate of work by external forces
Rate of external heat transfer

$$= \frac{\partial}{\partial t} \rho_f c_f T_f + \frac{\partial}{\partial x_i} \rho_f c_f T_f \dot{U}_i$$

Rate of change of internal energy

$$+ \frac{\partial}{\partial t} \rho_f c_f (\dot{U}^2/2) + \frac{\partial}{\partial x_i} \rho_f c_f (\dot{U}^2/2) \dot{U}_i \quad (4.62)$$

Rate of change of kinetic energy =

The difference between the kinetic energy variation and the rate of work done by external forces can be expressed as a single term, the work done by internal forces via the kinetic energy theorem. The above equation can also be further simplified by expressing internal energy in terms of enthalpy:

and the fluid stress tensor in terms of its pressure and viscous components :

With these substitutions Equation 4.62 becomes :

$$\begin{aligned}
 & \frac{\partial}{\partial t} \left(\rho \frac{\partial \psi}{\partial x_i} \right) + \frac{\partial}{\partial x_j} \left(\rho \frac{\partial \psi}{\partial x_j} \frac{\partial \psi}{\partial x_i} \right) \\
 & = \frac{\partial}{\partial x_i} \left[\rho \frac{\partial \psi}{\partial x_j} \frac{\partial \psi}{\partial x_j} \right] + \frac{\partial}{\partial x_i} \left(\rho \frac{\partial \psi}{\partial x_j} \right) \frac{\partial \psi}{\partial x_j} \\
 & + \frac{\partial}{\partial x_j} \left(\rho \frac{\partial \psi}{\partial x_i} \right) \frac{\partial \psi}{\partial x_j} - \frac{\partial}{\partial t} \left(\rho \frac{\partial \psi}{\partial x_i} \right) - \frac{\partial}{\partial x_j} \left(\rho \frac{\partial \psi}{\partial x_j} \right) \frac{\partial \psi}{\partial x_i} \quad (4.65)
 \end{aligned}$$

The third term on the right hand side of Equation 4.65 represents viscous dissipation ; the fourth and fifth terms are work done by compression forces. These terms are generally negligible compared to

heat transfer terms. Neglecting these terms Equation 4.65 can be now written in terms of probabilistic mean variables as :

$$\frac{1}{\rho} \frac{\partial}{\partial t} \rho c_p \bar{T} + \frac{1}{\rho} \frac{\partial}{\partial x_i} \rho c_p \bar{T} U_i + \frac{1}{\rho} \frac{\partial}{\partial x_i} \rho c_p \bar{T} \epsilon_i^f$$

$$= \frac{\partial}{\partial x_i} \lambda_f \left[\frac{\partial}{\partial x_i} \bar{T} - \frac{\bar{T}}{T_f} \frac{\partial T_f}{\partial x_i} \right] + \bar{q}_f \quad (4.66)$$

where analogous to the velocity cofluctuation tensor which appears in the momentum equations, ϵ_i^f is the velocity-temperature cofluctuation tensor expressing enthalpy diffusion :

$$\epsilon_i^f = (\bar{U}_i - U_i) (\bar{T}_f - T_f) \quad (4.67)$$

The First Law equation for a particle phase p, in terms of random variables, is :

$$\bar{K}_f \frac{\partial}{\partial x_i} \bar{v}_{ij}^p v_i + \bar{K}_{cp} \bar{v}_i g_i + \bar{F}_i^{sp} v_i + \frac{\partial}{\partial x_i} \bar{G}_{fij}^p v_i$$

Rate of work done by
continuous external forces

Rate of work done by
external collision forces

$$+ \frac{\partial}{\partial x_i} \lambda_p \frac{\partial T_p}{\partial x_i} + Q_{fp} = \frac{\partial}{\partial t} \rho_p \epsilon_p + \frac{\partial}{\partial x_i} \rho_p \epsilon_p v_{pi}$$

Rate of external
heat transfer

Rate of change of internal energy

$$+ \frac{\partial}{\partial t} \rho_p \frac{(\bar{V}^2/2)}{p} + \frac{\partial}{\partial x_i} \rho_p \frac{(\bar{V}^2/2)}{p} v_{pi} \quad (4.68)$$

Rate of change of kinetic energy

As in the case of the fluid phase the work done by internal forces will generally be small compared to heat transfer terms and can be neglected. In addition, if the particles are rigid their internal energy will be equal to their enthalpy. The final form of the energy equation in terms of probabilistic mean variables thus becomes :

$$\frac{\partial}{\partial t} \rho_p \alpha_p C_p T_p + \frac{\partial}{\partial x_i} \rho_p \alpha_p C_p T_p v_{pi} + \frac{\partial}{\partial x_i} \rho_p \alpha_p C_p \epsilon_{pi}$$

$$= \frac{\partial}{\partial x_i} \lambda_p \left[\frac{\partial}{\partial x_i} \alpha_p T_p - T_p \frac{\partial \alpha_p}{\partial x_i} \right] + Q_{fp} \quad (4.69)$$

4.6. Concluding remarks

Table 4.1 summarizes the final forms of the general probabilistic multiphase flow equations. These equations differ from the previous attempts at formulating rigorous multiphase flow equations which were

reviewed in Chapter 3. The most important differences include :

- the probabilistic approach allows mean variables to be defined which are independent of the choice of an averaging interval,
- stress tensors are of the form $(\rho \frac{p}{ij}) \delta_{ij}$ and not of the form $\rho \tau_{ij}^F / \delta x_j$, the latter of which results from neglecting particles at the control volume surface,
- two stress tensors are present in the particle phase equations rigorously accounting for the two fundamentally different types of contact forces exerted on these phases in suspension,
- velocity and temperature fluctuations are present reflecting the random nature of suspension flows where overall boundary conditions impose only mean flow conditions,
- surface exchanges are treated in a rigorous fashion. Mean values of derivatives are clearly shown to be equal to derivatives of mean values plus an additional term accounting for interfacial phenomena.

In Chapter 7 the probabilistic equations developed here will form the framework for analyzing the results obtained in the experimental part of this work.

TABLE 4.1

GENERAL PROPAGATIONISTIC MULTIPHASE FLOW EQUATIONS

1. CONTINUITY

Any phase p (fluid, particle phase, overall solids phase)

$$\frac{\partial}{\partial t} \alpha_p \rho_p + \frac{\partial}{\partial x_j} \alpha_p \rho_p V_{pj} = 0$$

2. MOMENTUM

Fluid phase

$$\frac{\partial}{\partial t} \rho_f \alpha_f U_i + \frac{\partial}{\partial x_j} \rho_f \alpha_f U_i U_j + \frac{\partial}{\partial x_j} \rho_f \alpha_f R_{ij} = \frac{\partial}{\partial x_j} \alpha_f \tau_{ij}^f + \Gamma_i^{sf} + \rho_f \alpha_f g_i$$

Particle phase p

$$\frac{\partial}{\partial t} \rho_p \alpha_p V_{pi} + \frac{\partial}{\partial x_j} \rho_p \alpha_p V_{pi} V_{pj} + \frac{\partial}{\partial x_j} \rho_p \alpha_p \beta_{ij} = \frac{\partial}{\partial x_j} \alpha_p \tau_{ij}^p + \Gamma_i^{fp} + \Gamma_i^{sp} + \frac{\partial}{\partial x_j} s_{ij}^p + \rho_p \alpha_p g_i$$

Overall solids phase

$$\frac{\partial}{\partial t} \rho_s \alpha_s V_{si} + \frac{\partial}{\partial x_j} \rho_s \alpha_s V_{si} V_{sj} + \frac{\partial}{\partial x_j} \rho_s \alpha_s \beta_{ij} = \frac{\partial}{\partial x_j} \alpha_s \tau_{ij}^s + \Gamma_i^{fs} + \frac{\partial}{\partial x_j} s_{ij}^s + \rho_s \alpha_s g_i$$

TABLE 4.1 (continued)

GENERAL PROBABILISTIC MULTIPHASE FLOW EQUATIONS:

3. ENERGY

Fluid phase

$$\frac{\partial}{\partial t} \rho_f^\alpha C_{ff} T_f + \frac{\partial}{\partial x_i} \rho_f^\alpha C_{ff} T_{fU_i} + \frac{\partial}{\partial x_i} \rho_f^\alpha C_{ff} \epsilon_i^f = \frac{\partial}{\partial x_i} \lambda_f \left[\frac{\partial}{\partial x_i} u_f^T T_f - T_f^T \frac{\partial u_f^T}{\partial x_i} \right] + Q_{sf}$$

Particle phase p or overall solids phase

$$\frac{\partial}{\partial t} \rho_p^\alpha C_{pp} T_p + \frac{\partial}{\partial x_i} \rho_p^\alpha C_{pp} T_{pU_i} + \frac{\partial}{\partial x_i} \rho_p^\alpha C_{pp} \epsilon_i^p = \frac{\partial}{\partial x_i} \lambda_p \left[\frac{\partial}{\partial x_i} \alpha_p^T T_p - T_p^T \frac{\partial \alpha_p^T}{\partial x_i} \right] + Q_{fp}$$

EXPERIMENTAL INSTALLATION :

CHARACTERISTICS, OPERATING PROCEDURE AND VERIFICATIONS

5.1 Introduction

The vertical pneumatic transport installation was designed and constructed to meet the following objectives :

- The installation was required to allow the establishment of hydrodynamically fully developed gas-solids suspension flows. The literature review showed numerous studies on suspension pressure drops to have been carried out with short test sections, with " fully developed " measurements made at only small distances downstream from elbows and with limited numbers of pressure taps. The present installation was designed to eliminate ambiguities caused by these factors by providing a long acceleration zone between the solids feed point and the test section. Many pressure taps were placed both along the length of the test section and the acceleration zone in order to clearly establish whether or not flows were fully developed.
- Analysis of vertical pneumatic transport based on the probabilistic multiphase flow equations (See Chapter 7) shows the mean solids concentration and wall effects to be of crucial importance in suspension pressure drops. The experimental study of the latter effect required that a relatively small pipe diameter be used. Once the choice of quick-closing slide valves had been made to measure

mean solids concentrations, given the small pipe diameter, it was necessary to have a relatively long test section to minimize possible end effects and improve the precision of concentration measurements (See Section 5.2.5). Finally, to minimize perturbations in the flow due to the presence of the slide valves, it was necessary that they be "full bore".

- Instabilities in gas-solids suspension flows arise from two sources: those inherent in the flow itself and those induced by solids feeders, many of which have fluctuating operational modes. In order to eliminate the latter type of instability a fluidized bed feeder which gave very stable solids feed over a wide capacity range was designed as part of the overall installation.

The heat transfer installation represented a modified version of the pneumatic transport apparatus. It had the same characteristics as the former unit from a hydrodynamic point of view but also met the following requirements which were specific to the heat transfer study:

- The study of wall-to-suspension heat transfer under constant heat flux conditions allows access to local heat transfer coefficients and to asymptotic coefficients under conditions of thermally fully developed flow. To achieve essentially uniform heat flux an electrically heated thin-walled stainless steel pipe was chosen.
- Previous heat transfer studies using similar techniques have often used pipes which, given the increased thermal entry lengths exhibited by gas-solids suspension flows, are too short to achieve fully developed flow conditions at high solids loadings. A long (4 m) pipe was therefore chosen in the present study.

This chapter will describe the installations used both in the hydrodynamic and heat transfer experimental parts of this study. In addition to the installation characteristics, operating procedures, measurements techniques and details on the various system verifications which were carried out will be described.

5.2 Pneumatic transport installation and procedure

5.2.1 General description

The vertical pneumatic conveying installation used in the hydrodynamic experiments is shown schematically in Figure 5.1. It consisted of a 20 mm I.D. stainless steel transport line approximately 10 m in overall height, a fluidized bed solids feeder, a solids disengaging chamber and cyclone, a solids return line and reservoir and complete instrumentation for gas and solids flow, solids concentration and pressure gradient measurements. The installation extended over three floors of the Université de Compiègne - Chemical Engineering Research Hall ; a command post was located on the second floor with only minor instrumentation located on the levels above and below.

Gas flow system. Compressed air from the university compressed air supply (7 bar) was used in all experiments. Air was introduced into the system at two points : as fluidizing gas for the fluidized bed feeder and to the main transport line. Before being fed into the system the compressed air was filtered to remove traces of oil and its pressure was regulated using two regulators placed in series in each of the two feedlines, just upstream from the flowrate control valves. The regulators were set at 4 and 2 bars respectively and thus assured

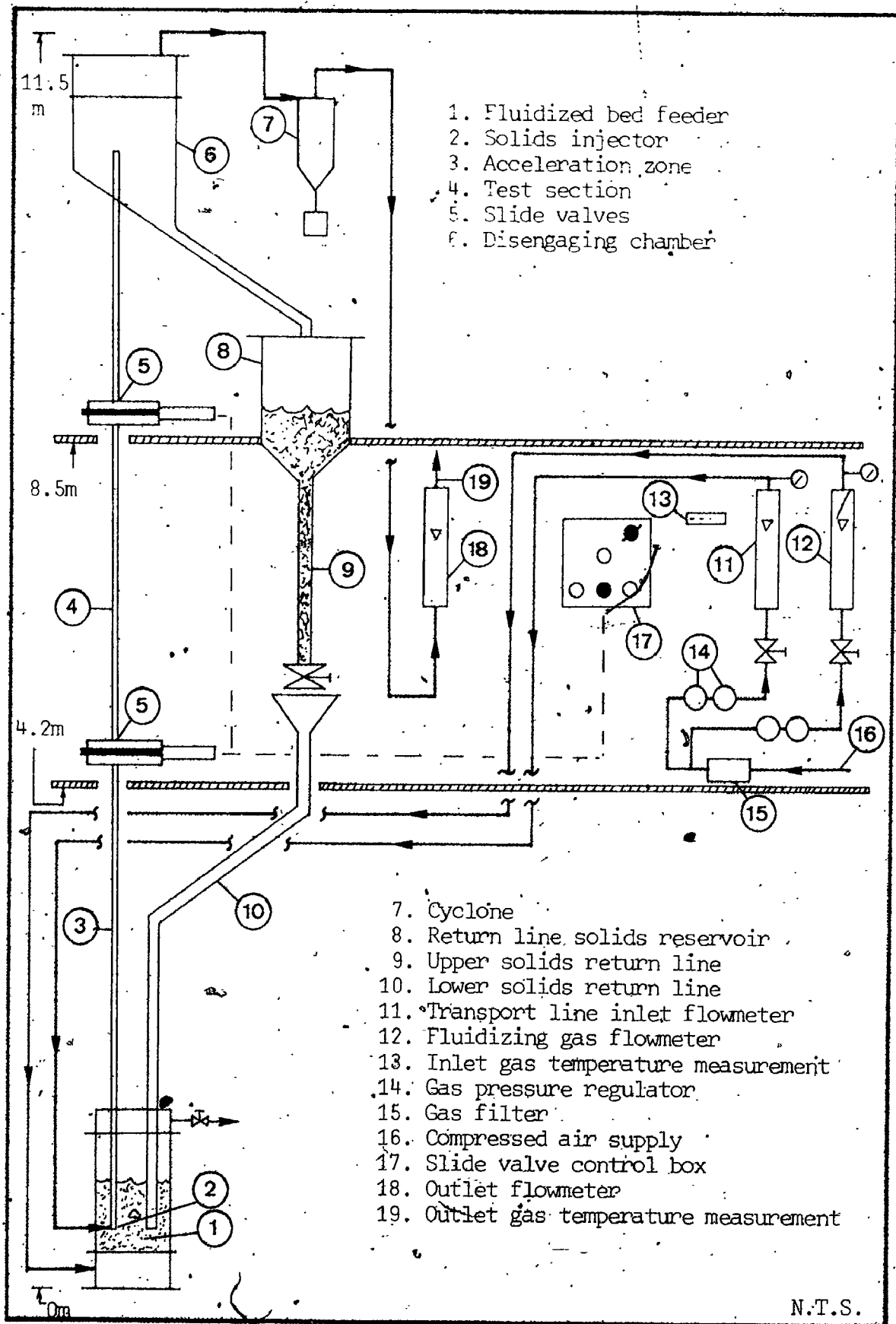


FIGURE 5.1 Vertical Pneumatic Conveying Installation

stable flows regardless of other users of the compressed air supply.

Inlet gas flowrates, as well as the flowrate of gas leaving the system downstream from the final cyclone were measured with calibrated rotameters equipped with Cu-Al thermocouples and Bourdon-tube pressure gauges. Details of the rotameter calibration, installation, methods and results are given in Appendix I.

Gas left the system in three places: at the outlet of the final cyclone, at the outlet of the fluidized bed feeder and, in small quantity, with the solids down the upper solids return line. As just mentioned, the first of these three flows was measured with a rotameter. The second was not measured but could be determined, if necessary, by a mass balance using the other flow measurements. In any case, knowledge of this gas flowrate was not required for the transport line results. The final flow mentioned above was important however as the gas flowing up the transport line was the sum of this final flow and that leaving the cyclone. Its experimental determination is considered in detail in Section 5.2.4.

The humidity of the transport line gas was varied in a number of runs in order to ensure that electrostatic forces had a negligible effect on the overall pressure drop measurements. The gas was humidified by passing it into a water-filled container, the temperature of which was varied by placing the container in an electrically heated water bath. Varying the bath temperature allowed variation of the quantity of water absorbed by the transport line gas, thus varying its relative humidity. This did not however lead to substantial

variations in the transport line gas temperature as the overall water uptake was still quite small. The method allowed the achievement of variations in the gas relative humidity of between 10 and 60% as measured by a wet and dry bulb thermometer placed at the line outlet flowmeter.

Solids flow system. Solids flowed in the installation in a closed circuit. They were introduced into the transport line using a fluidized bed feeder shown schematically in Figure 5.2. The solids feeder was specially designed to provide a fine solids feedrate control and to eliminate flowrate fluctuations which characterize rotary valve feeders and other mechanical devices with moving parts. The feeder consisted of 320 mm diameter, 500 mm high stainless steel fluidized bed supported on a porous plate grid under which several sheets of liquid chromatography paper were placed to increase its resistance. Fluidizing gas flowed into the bed via a 200 mm high windbox filled with plastic Pall ring packing. The combination of the high resistivity grid, the packing in the windbox and the inlet gas jet directed toward the bottom of the column (see Figure 5.2) led to an excellent distribution of gas across the column as evidenced by the uniform fluidization obtained at small bed heights.

The base of the transport line entered the bed from the side and was submerged in the fluidized solids to a height of about 200 mm. Small holes were drilled around the circumference of the submerged section allowing solids to flow from the bed into the line at a rate finely controlled by varying either the pressure above the bed or the

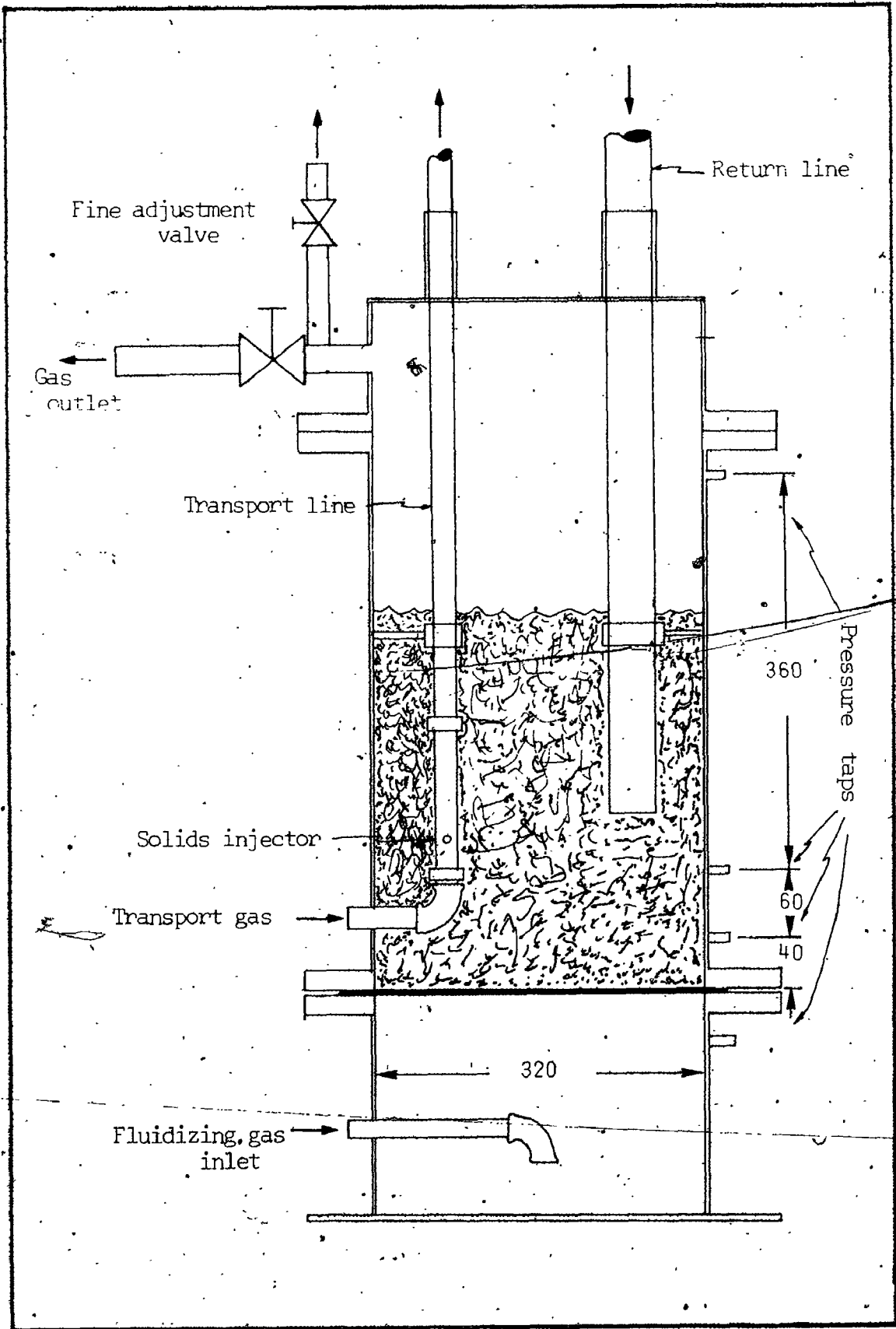


FIGURE 5.2 Fluidized Bed Feeder

bed height. The portion of the transport line in which the holes were drilled was detachable allowing its configuration (number of holes; hole diameter) to be varied according to the solids flowrate required. Most runs were carried out with the same injector configuration (two 2.5 mm holes located on the same plane directly opposite one another) as the bed pressure and bed height variations allowed solids flowrates varying over two orders of magnitude to be achieved with this single configuration.

The bed was equipped with a plexi-glass cover and gas outlet pipe through which most of the fluidizing gas flowed. This pipe was fitted with two valves mounted in parallel providing the possibility of finely controlling the pressure above the bed. Solids returned to the bed via a 42 mm standpipe immersed in the fluidized solids.

The bed was also fitted with 4 pressure taps: one in the windbox, two submerged in the solids and one above the bed. These pressure taps provided simple measurements of the pressure in the bed at the solids injection point and of the overall bed height.

Solids leaving the transport line were separated from the gas in a 500 mm diameter, 1.5 m high disengaging chamber. This unit consisted of a mild steel column into which the top of the transport line was inserted approximately 100 mm. A deflector was placed 150 mm above the end of the transport line to break the gas-solids jet. Solids left the bottom of the chamber which was sloped at 60° from the horizontal to facilitate flow to the return line solids reservoir. Gas left the top of the chamber and flowed to a 150 mm diameter (Zenz design) cyclone. The solids recovered at the cyclone were not recycled as they

represented a negligible quantity (about 5 g over a month of runs) compared to that circulating in the system.

The solids return line reservoir consisted of a plexi-glass column 290 mm in diameter and 500 mm high with a funnel-shaped bottom connected to the upper part of the solids return line. This line was a 42 mm ID, 1.5 m long mild steel pipe fitted with a 100 mm x 10 mm window which allowed solids movement to be observed. At the base of the upper solids return line a ball valve was placed to control the solids flowrate out of the upper section of the installation. This line was also fitted with two pressure taps which were used to determine the flowrate of gas down the return line with the solids (see Section 5.2.4).

The lower solids return line consisted of a 42 mm diameter stainless steel pipe approximately 5 m in total length including a 2 m long sloped section which re-aligned it with the axis of the fluidized bed feeder.

Transport line. The transport line consisted of a 20 mm ID, 23 mm OD pipe, 9 m in total height divided into a 4 m acceleration zone, a 4.4 m test section and 1.6 m upper section. Pressure taps (10 mm OD) were welded along its length at locations shown in Figure 5.3. Two millimeter diameter holes were drilled in the transport line at the centre of the pressure tap tube (See Figure 5.3). Low resistance cigarette filters were placed in the pressure tap tubes to prevent solids from entering the manometer lines. All line pressures were measured with either water or mercury U-tube manometers.

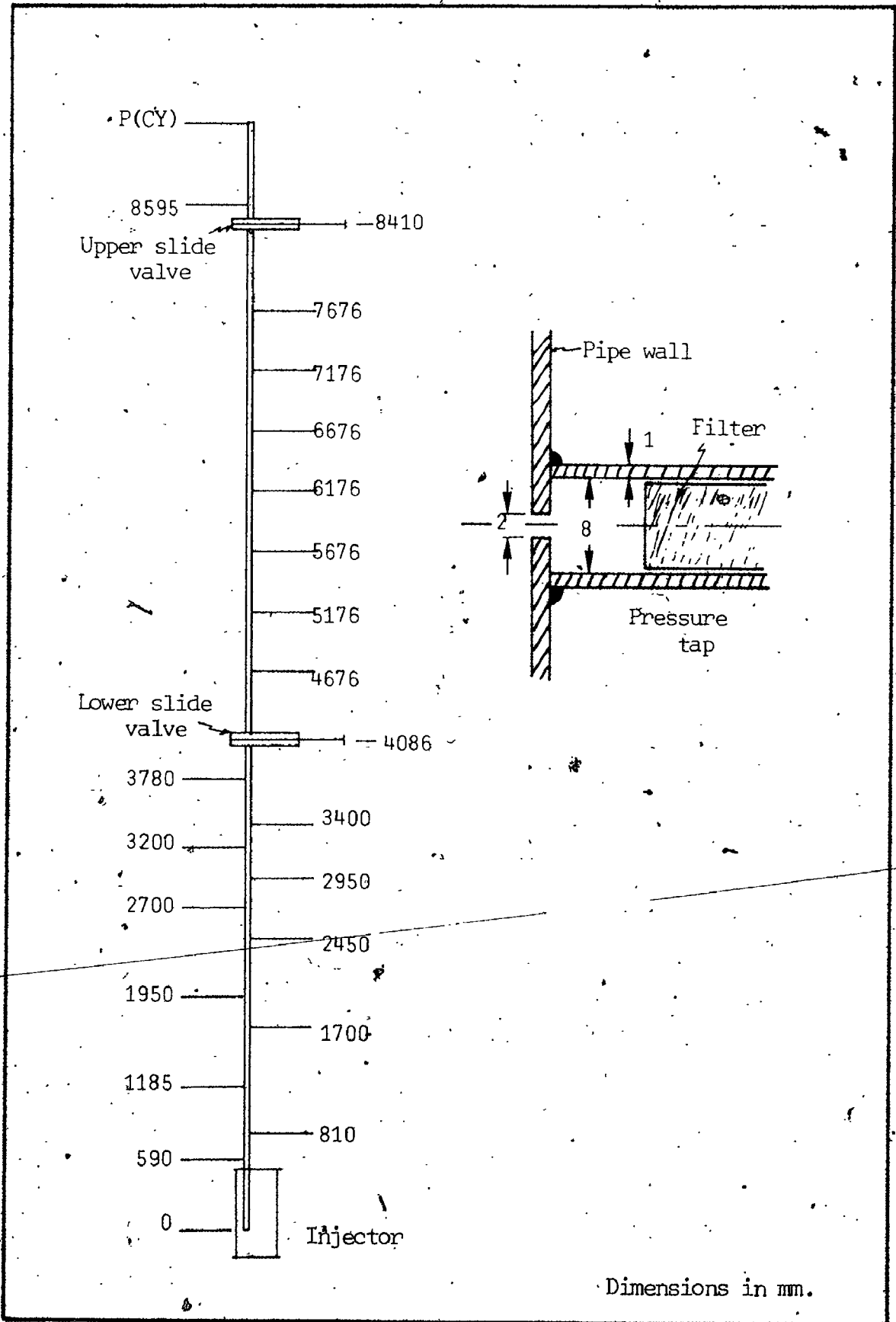


FIGURE 5.3 Pressure tap configuration and locations

Slide valves. Two pneumatically actuated slide valves, manufactured by Vraco-Systèmes, were placed in the transport line at locations of 4086 mm and 8410 mm respectively above the solids feed point (See Figure 5.3). The valves consisted of 5 mm thick stainless steel plates connected to pneumatically operated pistons and sandwiched between a heavy cast iron housing (Figure 5.4). The plates and the housings were drilled to the inside pipe diameter (20 mm). In the open position the valves were therefore "full bore" so as not to affect solids and gas flow patterns as would have been evidenced by disruptions in the transport line pressure profile. Airtightness was ensured by inflatable rubber gaskets held at 3 bar pressure in the valve housing.

The valve closing sequence involved opening an electrically controlled valve which deflated the gaskets. The drop in pressure in the gaskets actuated the pneumatic pistons. Once closed, contactors at the end of the piston displacement acted to re-inflate the gaskets. The entire operation, between pushing the button to deflate the gaskets and their re-inflation took about 3 seconds. The actual time required for the plate to block the pipe cross-section however only took about 0.01 second. During the remaining time the flow in the transport line was unaffected. Indeed, the gaskets provided almost perfect airtightness even when deflated.

Considerable care was taken to ensure simultaneous closing of the two valves as significant errors would have been introduced in the concentration measurements had the closings not been at least quasi-

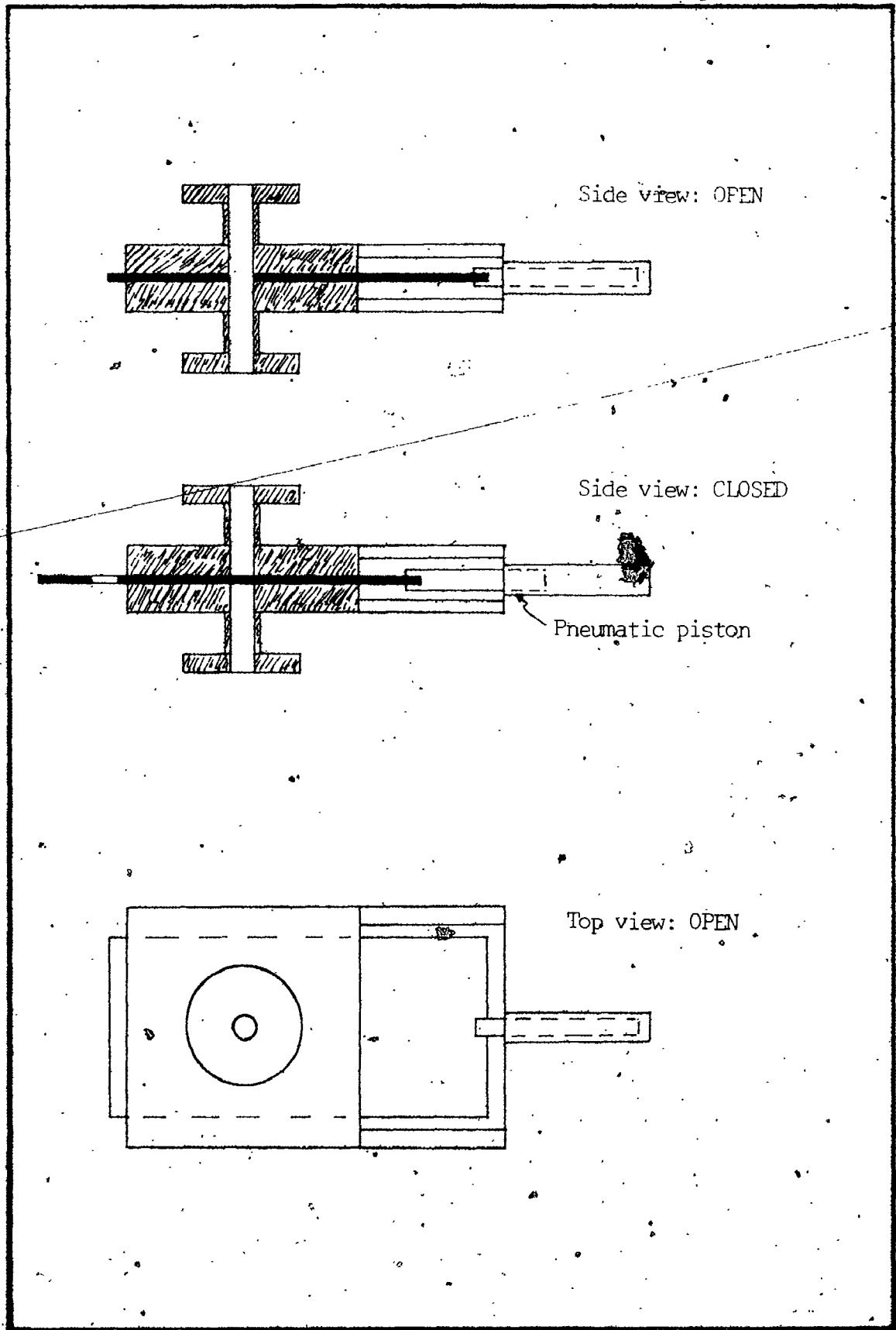


FIGURE 5. Pneumatic slide valves

simultaneous. The end of course contactors supplied by the manufacturer originally were to be used only to signal the re-inflation of the gaskets. In order to ensure simultaneous closing however, a timer circuit was mounted in parallel using these contactors. The actuation of either of the contactors started the timer; the actuation of the contactor of the other valve stopped it. In this way it was possible to measure non-synchronized closings and intervene in the pneumatic circuits if the difference became sizeable. As the resistance in the pneumatic circuits was somewhat variable it was not often possible to reduce the difference to zero (less than 0.01 second) but as indicated in the data tables in Appendices IV and V, in all cases, the difference was held to less than 0.1 s. The timer was also equipped to indicate which valve closed first. The effect of non-simultaneous closings on solids concentration measurements is taken up in Section 5.2.5.

5.2.2 Operating procedure

Before beginning a hydrodynamic experiment the slide valves were opened and closed several times and the pneumatic time delays on the respective control circuits were adjusted to ensure almost simultaneous closing. Granular solids were added to the fluidized bed feeder, if necessary, in order to bring the bed level up to at least 100 mm above the injector holes. Both feeder outlet valves were generally opened, although if the run in question was to be carried out under conditions similar to those of the preceding experiment only the "fine adjustment" valve located on the second level was fully opened.

A small gas flow was started to the transport line. Fluidizing air was then introduced to the feeder and the gas velocity was set to about three times the minimum fluidization velocity of the solids being used. This rate of gas flow to the fluidized bed ensured smooth solids feeding to the transport line and smooth dipleg operation. It also ensured good solids mixing in the fluidized bed. It was initially thought that, at low fluidization velocities segregation in the vertical direction in the bed might take place thereby leading to a feed to the transport line with a significantly different particle size distribution than was present in the bed. Verification that the same particle size distribution was circulating in the system compared to that in the bed was carried out by sieving solids samples taken periodically at the return line valve. The results of these tests showed there to be no significant difference between the two.

The gas velocity was then set to about the desired value in the transport line and the solids circulation rate was fixed.

Two different methods were used to control solids circulation rate depending on the flowrate required. The first method, which was particularly convenient at higher solids flowrates ($W_S > 15$ g/s), was based on the self-stabilizing feature of the fluidized bed feeder. At the beginning of a run using this method, a relatively large quantity (about 20 kg) of solids was loaded into the return line solids reservoir. The desired solids flowrate was then fixed at the valve at the base of the upper part of the return line. The pressure above the fluidized bed feeder was then adjusted to the "appropriate" (see below) level using the feeder outlet valves. The

system then stabilized itself : if the flowrate of solids into the bed as fixed by the return line valve was greater than the solids flowrate into the transport line, as fixed by the difference in pressure between the transport line and the fluidized bed at the injector hole level, the bed height tended to increase. This led to a corresponding increase in the pressure in the bed at the injector hole level and, thus, to an increase in the solids flowrate to the line. The bed height continued to rise until the two flowrates were equal. If the flowrate of solids fixed at the return line valve was less than the flowrate to the transport line the reverse process took place ; the bed height dropped until the two flowrates equilibrated. Provided the pressure above the bed was initially fixed at a value within the range which allowed these two processes to occur within the physical limits of the system (i.e. before the bed height dropped to the injector holes or rose to the top of the column) the system arrived at steady state after about 10 minutes as evidenced by a constant bed height measured using the feeder wall pressure taps.

As the gas flowrate from the bed into the transport line with the solids depended, in a very small way, on the solids feedrate, once the solids circulation was at steady state the desired transport line gas velocity was re-adjusted if necessary. This final adjustment was generally only very minor and the system was fully restabilized at the desired gas and solids flowrates only two or three minutes later.

As mentioned, the above method of setting the solids flowrates was particularly convenient at higher solids flowrates. The strong dependence of bed to transport line feedrate on pressure at the

injector holes led to wide operating ranges with bed height as the only variable. Once a certain experience was obtained in setting above bed pressures, practically no further intervention was necessary and the operator had only to watch a single U-tube manometer to follow the self-stabilization process.

The method was less convenient at low solids flowrates however due to the relatively large bed cross-section. Indeed, when the solids flowrate was less than about 20 g/s a relatively long time was necessary for the difference in the input and output solids flows to and from the bed to manifest itself as a bed height increase or decrease sufficient for the flows to equilibrate. Another method was therefore developed to deal with these situations.

At low solids flowrates only a small solids inventory was maintained in the return line system. As before, the solids flowrate was first fixed with the solids return line ball valve. The pressure above the bed was then adjusted using the fine adjustment bed outlet valve to increase or decrease the solids flow to the transport line in order to bring the solids level in the return line window up or down to a reference mark. This level was maintained by above bed pressure adjustments: if the level in the return line window dropped, the above bed pressure was increased slightly; if it rose the pressure was decreased. Generally, about 10 minutes required to stabilize the level such that no further pressure adjustments were required.

It should be noted that the principle behind this second method is essentially the same as in the first case: the solids flowrate is

3



1.0



1.1



1.25



1.4



1.6

1.8
2.0
2.2
2.5
2.8
3.2
3.6
4.0



2.8



3.2



3.6



4.0



2.5



2.2



2.0



1.8

fixed at the solids return line and the flowrate from the bed to the transport line is adjusted as a consequence. In the first case the flowrates are equilibrated as a function of bed height; in the second case as a function of above bed pressure. In the first case, non-steady state is indicated by bed height changes; in the second by level changes in the solids return line. As the cross-section of the return line is much smaller than that of the bed, the second method was much more sensitive to deviations from steady state at low solids flowrates. An additional check that the system was at steady state before measurements were taken involved use of the transport line pressure profile. Transport line pressures, being very sensitive to solids flowrate, were constantly monitored to determine drifts or upsets from the steady state which had been achieved. Only after 30 minutes of steady state operation were measurements taken. These measurements were:

- . inlet and outlet gas flowrates given by rotameter readings, pressures and temperatures,
- . pressure readings in fluidized bed feeder,
- . transport line pressure profiles,
- . return line pressure drop and absolute pressure to determine the gas flowrate down the return line,
- . solids flowrates determined by weighing samples taken over a given time period at the return line outlet valve.

Once all steady state measurements were taken the slide valves were closed to allow measurement of the solids hold-up in the line. Immediately afterwards, the inlet gas flows were halted in order to


prevent pressure buildup in the system and flooding of the manometers. A section of the transport line below the lower slide valve was then dismantled and the lower slide valve was opened to allow recovery of the solids hold-up between the two valves. These solids were then weighed and, in some cases, their particle size distribution was determined by sieving.

Care was taken to ensure that all the solids hold-up were collected in this way. In the first few runs, the slide valve and test section were completely dismantled to see if any solids were trapped in the valve housing. None were observed.

Regular maintenance and checks were carried out on the installation to ensure the precision of measurements and the overall integrity of the system. In addition to the gas flowrate and pressure measurement verifications to be described in the following section, gas leak checks were carried out on a weekly basis. This involved closing all outlet valves and applying a pressure of about 500 mm Hg to the system. Soapy water was then applied at all locations susceptible to wear producing gas leaks. The slide valves were dismantled about once every three months to verify alignments. Filters in the manometer lines were changed whenever a slow response was observed.

5.2.3 Overall gas flow measurements and pressure drop verification : Moody diagram

Pressure profiles as a function of gas flowrates were measured at regular intervals during the experimental programme without solids flow. These experiments had the following objectives :



a) Pressure profiles allowed an indirect verification that all the manometers were functioning correctly. A leaking manometer line showed up quickly as a discontinuity in the pressure profile. A plugged manometer line showed a slow response and, in some cases, an offset (discontinuity in the profile). Pressure profiles also indicated that the presence of the slide valves did not lead to perturbations in the flow which would have manifested themselves as additional pressure drops.

b) Comparison of gas friction factors as a function of Reynolds number (the Moody diagram) with accepted correlations for smooth pipes provided an important verification of the correct operation of all hydrodynamic measurement systems functioning as a unit.

These experiments consisted simply of measuring the pressure profile along the transport line as a function of gas flowrate using the same techniques as during the hydrodynamic runs with the following exceptions :

- the return line valve (solids feed) was tightly closed since there was no solids feed,
- the fluidized bed feeder was by-passed ; that is, the injector air feed line was disconnected and reconnected directly to the feed line (See Figure 5.5). This particular procedure was used because of the fact that the fluidized bed feeder was not airtight. Connecting the injector feed flowmeter in airtight series with the outlet flowmeters allowed a verification of all flowmeters (both feed and outlet) simultaneously.

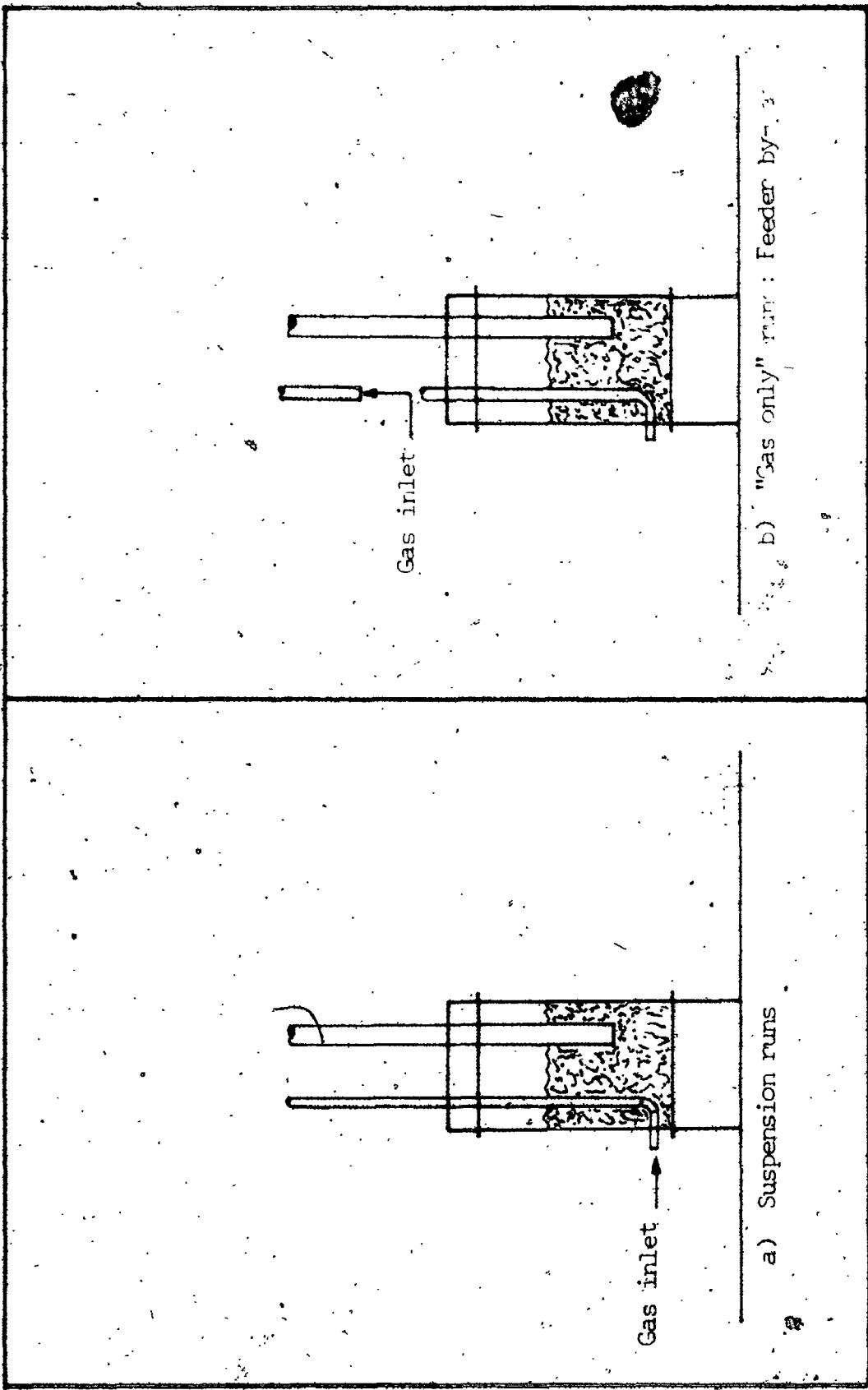


FIGURE 5.5 Gas inlet positions for Suspension runs and "Gas only" verifications

J

A typical pressure profile for the "gas only" runs is shown in Figure 5.6. The curve shows no discontinuities, in particular, in the region near the slide valves.

The Moody diagram obtained in this way is shown in Figure 5.7. The gas friction factor was calculated from the following definition:

$$f_g = \frac{\Delta P}{\Delta L} \left[\frac{D}{U^2} \right] \quad (5.1)$$

The curve shows results over the entire range of gas flowrates used during runs with solids flow. The different symbols indicate different outlet flowmeters. For Reynolds numbers less than 2000 the relationship between the friction factor and the Reynolds number corresponds to the laminar flow equation:

$$f_g = 64/Re \quad (5.2)$$

Between $Re = 3000$ and $Re = 30\,000$ the experimental results correspond well with the empirical Blasius correlation for smooth pipes:

$$f_g = \frac{0.3164}{Re^{0.25}} \quad (5.3)$$

It will be noted that the f_g versus Re curves are extremely sensitive to experimental error as they depend on combinations of flow, pressure, temperature, and distance measurements. Any upset (leak, malfunctioning flowmeter) resulted in values which deviated substantially from those given in Figure 5.7. Periodic verification of the Moody diagram thus provided an excellent check of the operation of the overall system.

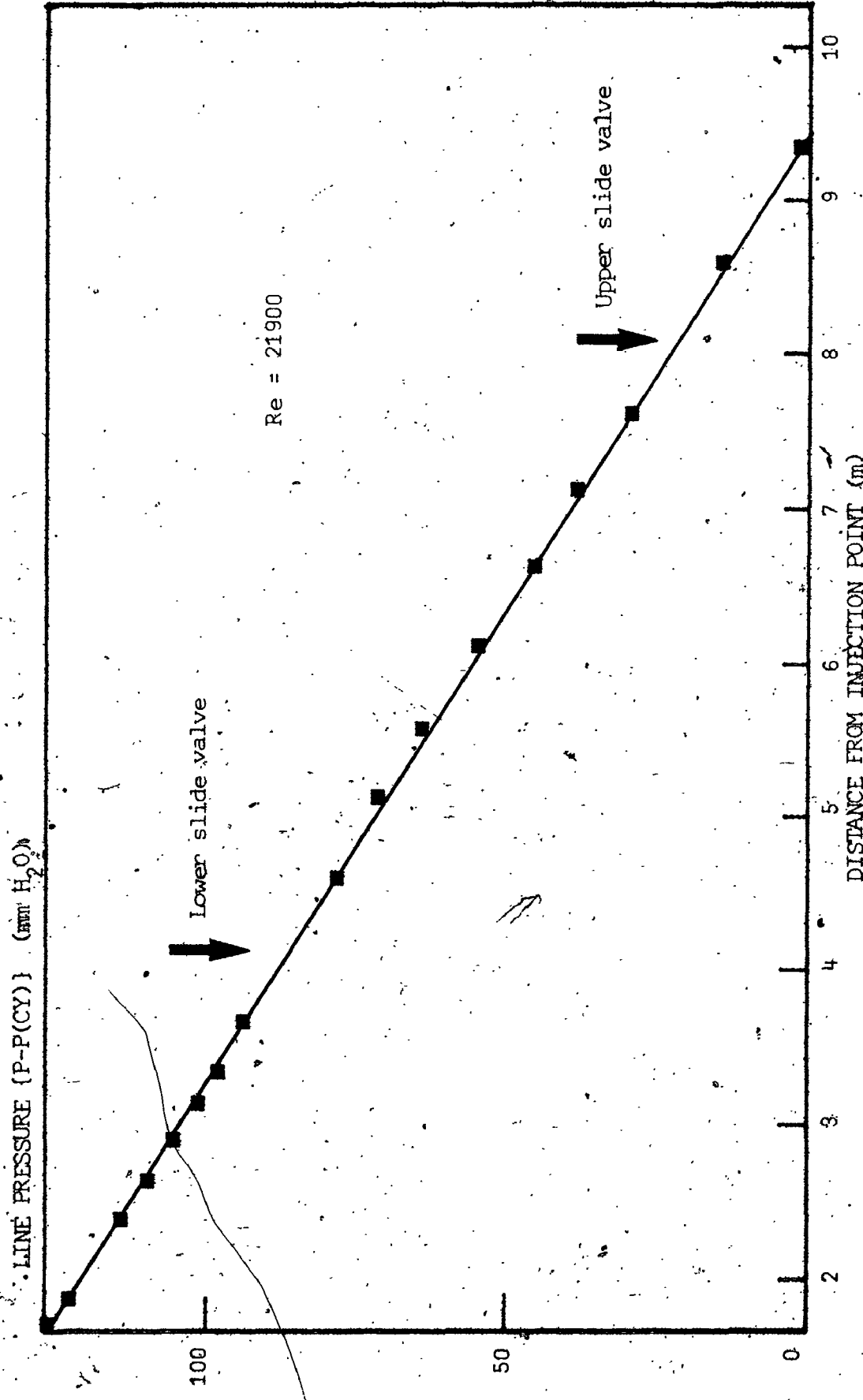


FIGURE 5.6 Typical transport line pressure profile: "Gas only" runs

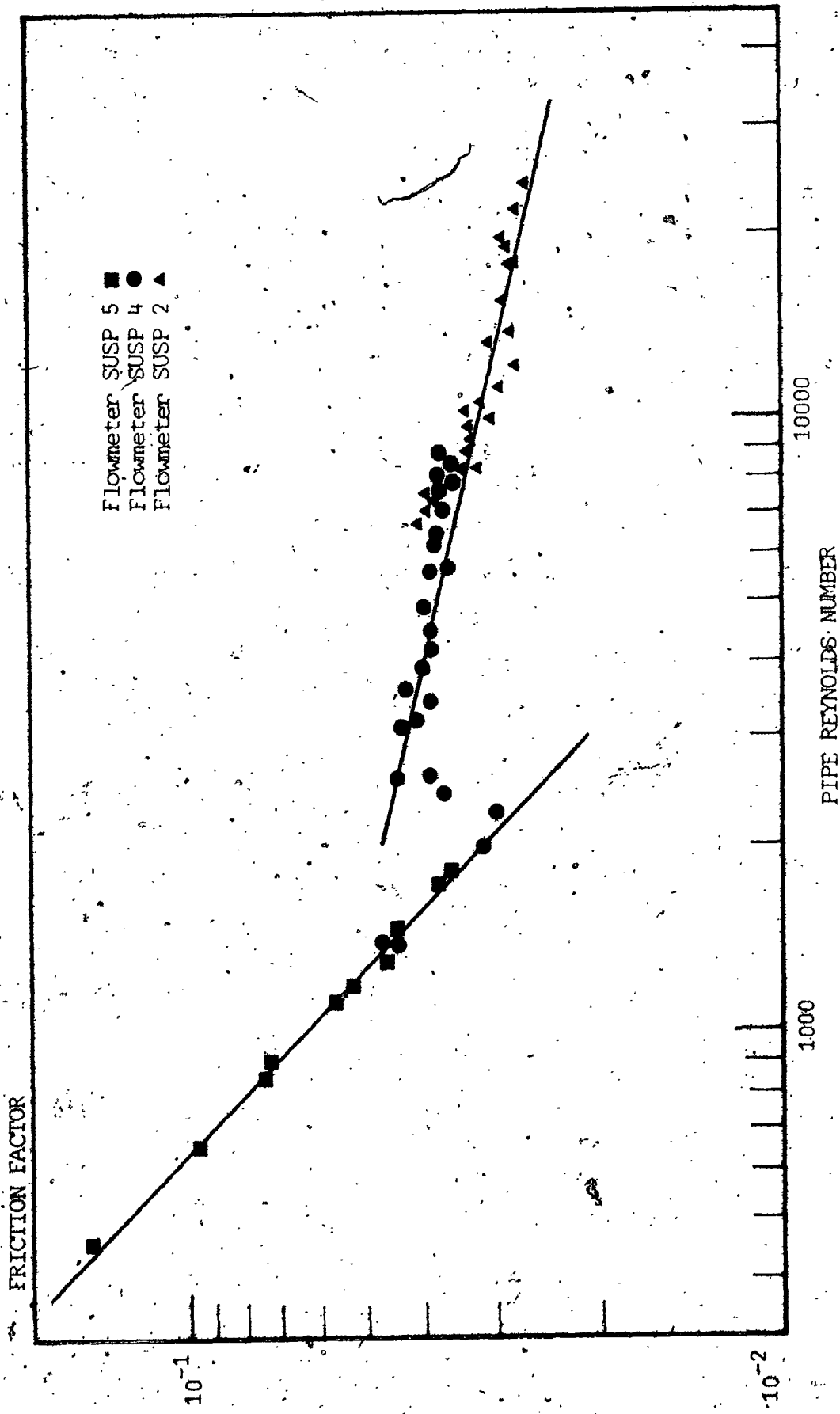


FIGURE 5.7 Experimental Moody diagram

5.2.4. Return line gas flowrate determination

Two possibilities existed for the determinations of the mass flowrate of gas up the transport line. The first would have involved a mass balance on the fluidized bed feeder. The transport line flowrate would, in this case, have been given by the main transport line inlet flow measured by rotameter plus the gas entering the line with the solids from the fluidized bed. The latter flow could have been determined by the difference between the feeder gas inlet flow and the flow at the feeder gas outlet, both of which would have been measured by rotameters.

The disadvantage with this method is the fact that it involves determination of a small flowrate (gas injected with the solids) via the difference between two large flowrates. Experimental error would therefore have been substantial.

The second possibility involved a mass balance on the disengaging chamber. In this case, the transport line flowrate would be taken as the sum of the gas flowrate measured at the cyclone outlet by rotameter plus the gas flowrate down the solids return line. The presence of a fixed bed of solids above the return line solids control valve kept the second flowrate almost negligible with respect to the first. Thus, provided this flowrate could be estimated and proved to be almost negligible, the overall precision of the transport line gas flowrate depended only on the precision of one rotameter. This second method was therefore used to determine the transport line gas flowrate. The present section describes the procedure used to estimate

the flowrate down the solids return line and the independent experimental verification of the estimation method.

The pressure drop of a gas across a fixed bed of granular solids can generally be calculated using the Ergun equation. For small particles the Ergun equation reduces to the Kozeny-Carmen equation (81) :

$$\frac{\Delta P}{\Delta L} = \frac{150 \mu (1-\epsilon)^2 U_g}{\epsilon^3 (\phi_s d_p)^2} \tag{5.4}$$

where U_g is the superficial gas velocity. Assuming that this relation applies for a bed of moving solids provided this superficial gas velocity is replaced in the above equation by the relative velocity between the solids and the gas, Eq. 5.4 can be re-written as :

$$\frac{\Delta P}{\Delta L} = \frac{150 \mu (1-\epsilon)^2}{\epsilon^2 (\phi_s d_p)^2} \left[\frac{U_g}{\epsilon} - \frac{W_s}{\rho_s (1-\epsilon) A} \right] \tag{5.5}$$

where : W_s = solids mass flowrate
 A = bed cross-section

Re-arranging the above equation gives :

$$Q_g = \frac{\epsilon W_s}{\rho_s (1-\epsilon)} + \left[\frac{\Delta P}{\Delta L} \right] \left[\frac{(\phi_s d_p)^2 A}{150 \mu} \right] \left[\frac{\epsilon^3}{(1-\epsilon)^2} \right] \tag{5.6}$$

where $Q_g = U_g A$ = volumetric gas flowrate.

The gas flowrate down the return line should therefore vary linearly as a function of the solids flowrate and its absolute value should be fully determined by the system geometry, the particle system, the pressure drop between two points along the return line axis and the solids flowrate. The slope of the Q_g versus W_s curve will give the porosity of the moving bed.

In order to verify Equation 5.6, and thus justify its subsequent use in determining the gas flowrates down the disengaging section solids return line, experiments were carried out in an installation fitted with an identical return line to the one used on the main pneumatic transport installation (it was, in fact, the same return line temporarily detached from the main installation).

This second installation (Figure 5.8) was composed of a cylindrical 290 mm dia. hopper with a conical base fitted with the above-mentioned return line: a section of pipe 1.5 m in length and 42 mm inside diameter. The return line was fitted with a ball valve at its bottom end to control solids flowrates and two pressure taps along its length. The hopper had a removable cover fitted with a small tube through which gas could be fed into the system at a controlled and measured rate (Rotameter SUSP. 6).

As shown in Eq. 5.6, once the system geometry and solids are fixed, it is possible to vary two of Q_g , W_s and ΔP in order to determine the third. As the main objective of these experiments was to verify Eq. 5.6 over the operating range of the pneumatic transport installation it was decided to fix the solids flowrate W_s and the pressure drop between the two points on the return line since the

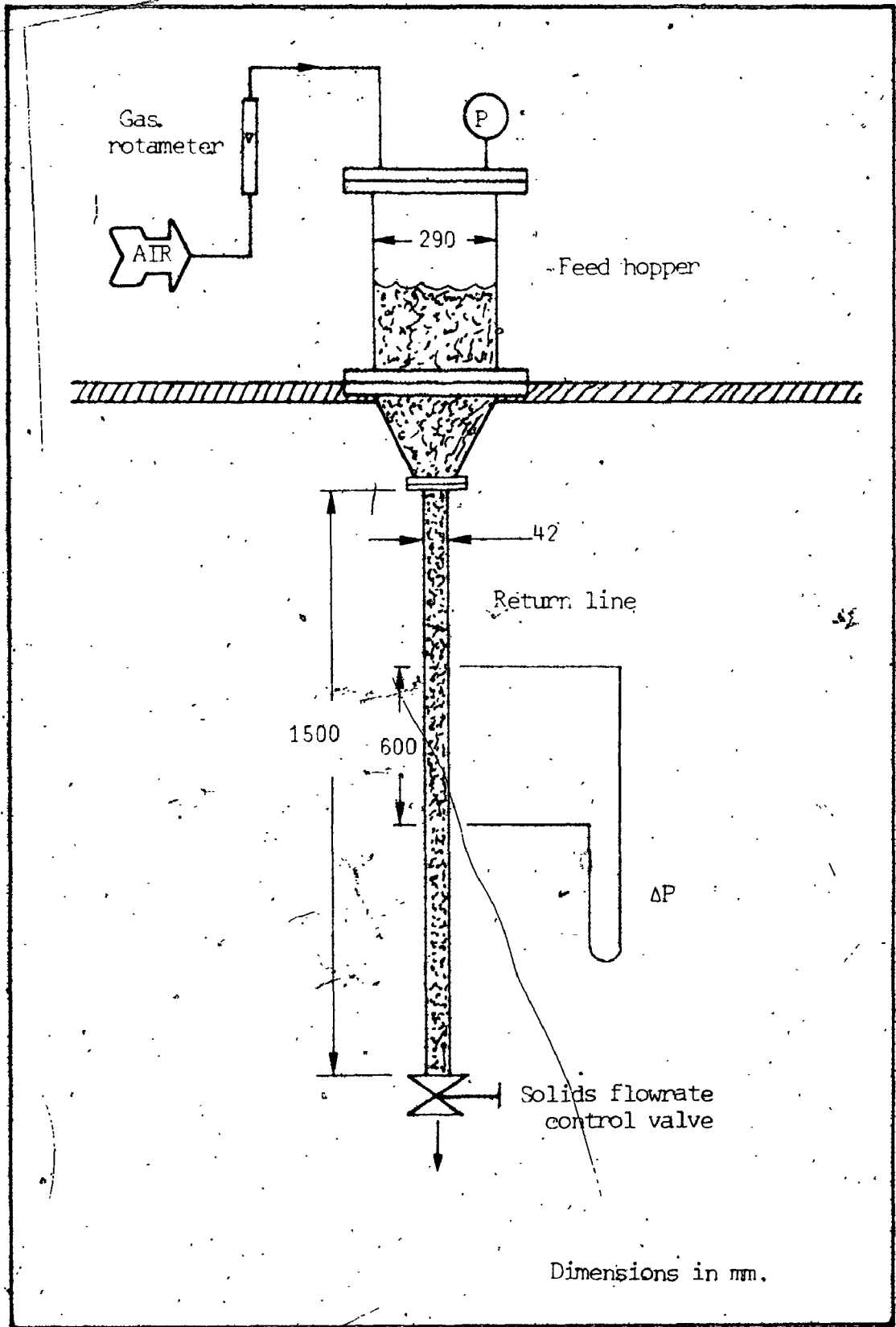


FIGURE 5.8 Return line gas flowrate verification installation

range of values of these parameters was known from the early pneumatic transport experiments. The experiments consisted then of filling the hopper with solids and closing the cover. The solids flowrate was set and the gas flowrate entering into the hopper was adjusted to keep a fixed pressure drop between the two points in the return line. Solids used in the experiments were the 250 μm mean diameter sand (P.S.D. 1). In addition to runs for various solids flowrates up to 200 g/s and three different pressure drops, a fixed bed run (i.e with zero solids flow) was undertaken to verify the measurement techniques.

It should be noted that the moving bed experiments were not carried out under perfect steady state conditions. Indeed, as the solids level went down in the hopper the resistance to the gas flow decreases. The pressure above the solids in the hopper necessary to maintain the same gas flow down the leg declines and this in turn changes the mass flowrate of gas into the hopper which is required to replace the solids leaving (the total volumetric gas flow into the hopper is the sum of that leaving down the return line and that which flows in to replace the solids flowing out). Nevertheless, the hopper cross-section was sufficiently large to allow near steady state conditions to be attained for all the solids flowrates tested here.

Figure 5.9 shows the results of the fixed bed run plotting pressure drop as a function of gas flowrate. The slope of this curve allows the determination of the bed porosity via Equation 5.4. The value found in this way is 0.392 which compares favorably with a value of 0.390 found by weighing the solids in the pipe (the shape factor ϕ_s used was 0.65 for sharp sand (81)).

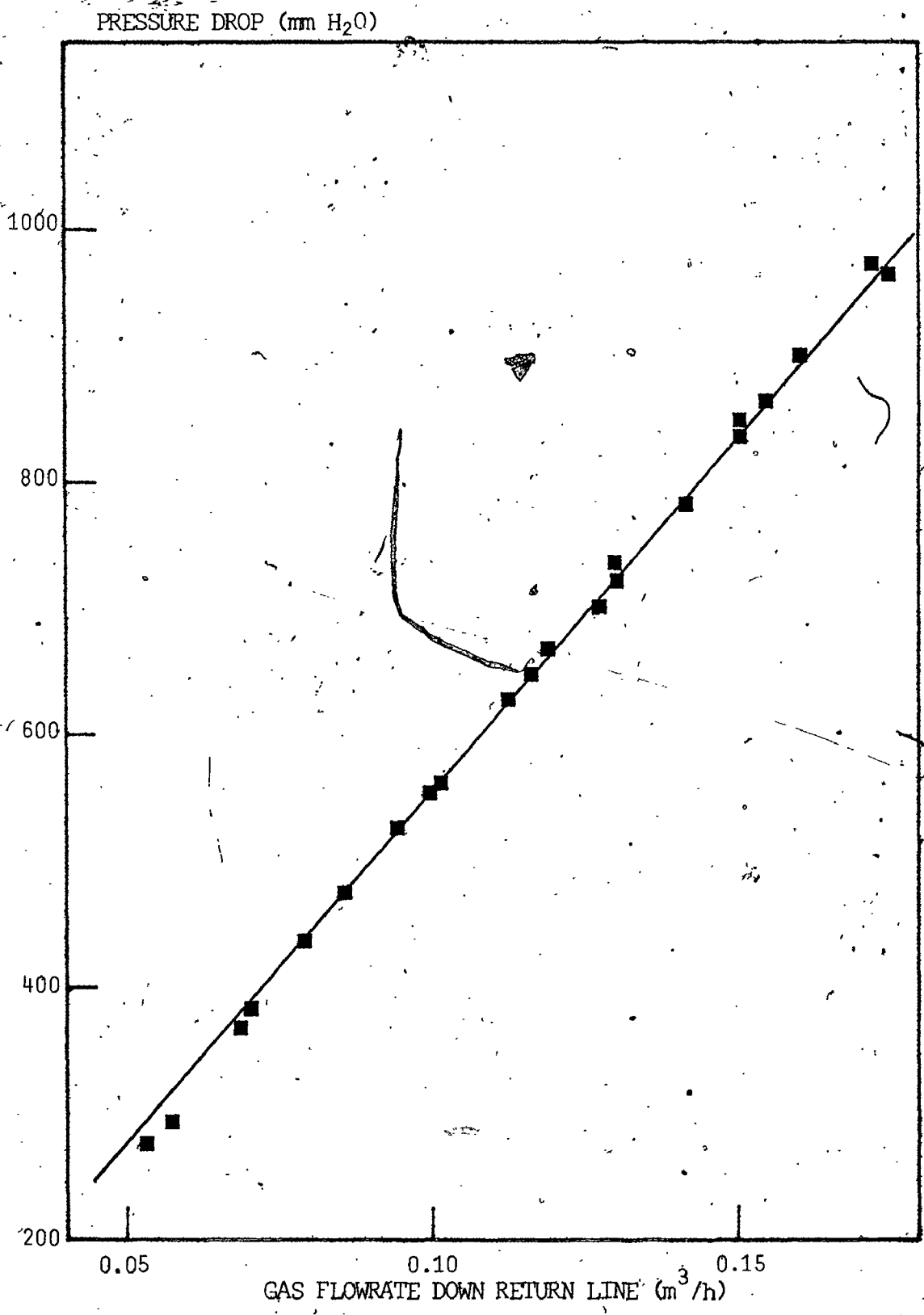


FIGURE 5.9 Pressure drop versus gas flowrate down return line: Fixed bed of sand (P.S.D 2)

Figure 5.10 shows the results for the moving bed runs. The three different curves show linear variations of gas flowrate as a function of the solids flowrate as predicted by Eq. 5.6. The slopes of the curves define the porosity of the moving bed in the return line. Porosity values calculated in this way varied from 0.37 to 0.39. A value of 0.38 was used in subsequent calculations of gas flow down the return line in the main transport line installation for runs using sand. The same method was used in the glass bead runs using a porosity value of 0.43.

The good correspondence between the experimental results and those predicted by Equation 5.6 justified the use of this method in determining the gas flowrate down the return line in subsequent experiments. All that was required for its use were simple measurements of return line pressure drop and solids flowrates. Finally, it will be noted that, under typical operating conditions, this gas flow represented only about 2 % of the total gas flow in the line.

5.2.5. Calculations

Pressure gradients. Fully developed pressure drops per unit pipe length were determined by linear regression of the test section pressure measurements. The gauge pressure in the transport line was measured at a single point (Position 2450 ; cf. Figure 5.3). Atmospheric pressure was measured with a mercury barometer. Absolute pressures in the line were thus determined by interpolating the pressure gradient data from the above-mentioned reference point.

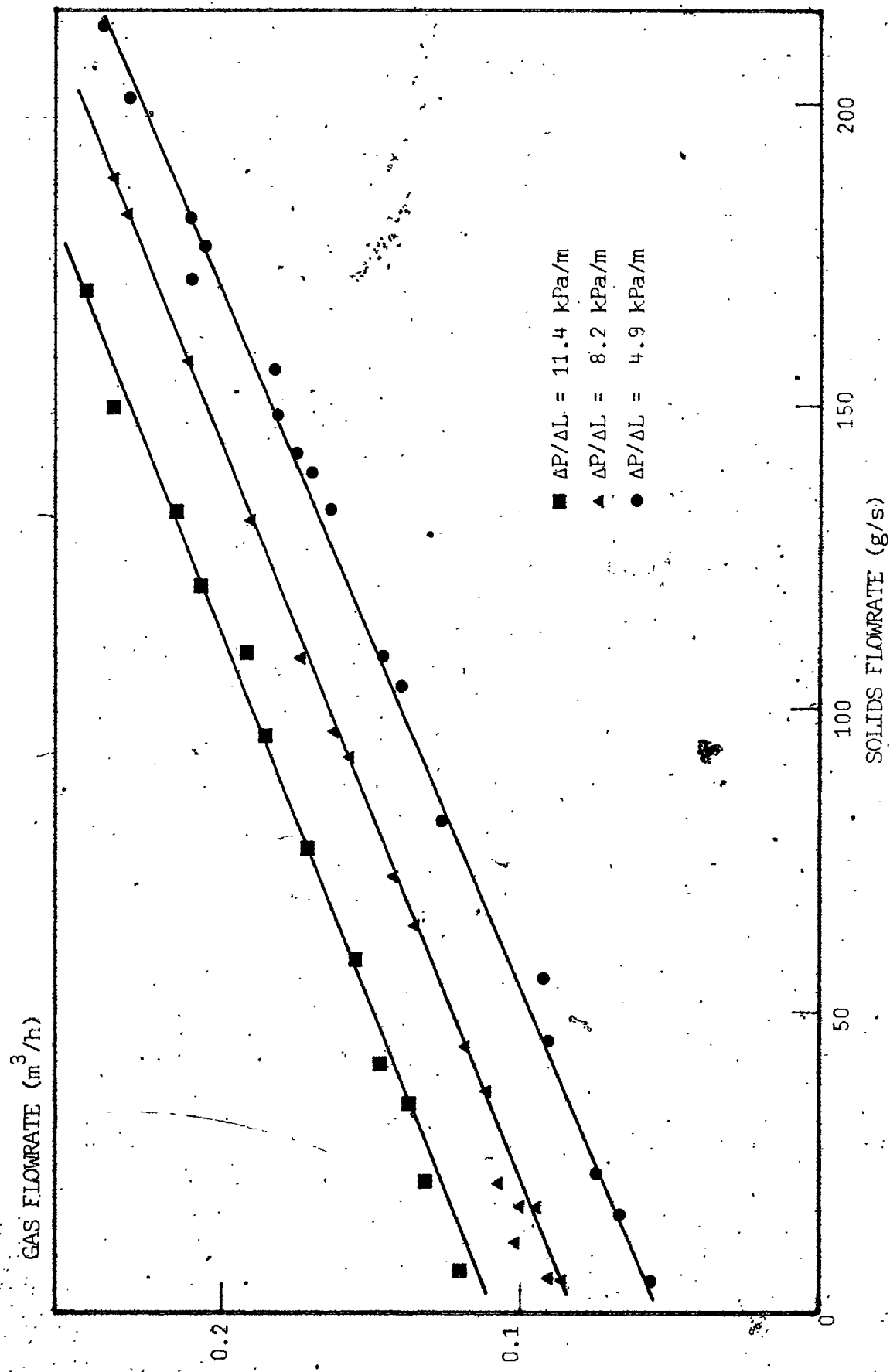


FIGURE 5.10. Gas flowrate down return line as a function of solids flowrate: Moving bed of sand (P.S.D. 2)

Temperatures. The hydrodynamic experiments were carried out under nearly isothermal conditions as evidenced by the nearly equal temperatures at the gas inlet and outlet. For calculation purposes the gas temperature in the line was taken to be the arithmetic mean of these two temperatures.

Transport line gas velocity. The mass flowrate of gas up the transport line was taken to be the sum of the gas flowrate measured by rotameter at the cyclone outlet and the gas escaping down the solids return line as calculated from the return line pressure readings and the solids flowrate using Eq. 5.6. The mean gas velocity at points in the line could then be calculated using the pressure and temperature data described above. As the absolute pressure along the line varied little, all velocities presented in the following chapters are given for pressure and temperature conditions at the lower slide valve level (Position 4086 ; cf. Figure 5.3).

Mean solids concentration. The mean solids concentration by volume was determined using the weight of solids recovered following the slide valve closings. The distance between the two slide valves was 4324 mm ; the inside pipe diameter was 20 mm. The mean solids concentration was then given by :

$$\bar{\alpha}_s = \frac{4 m_{sv}}{\rho_s \pi (20 \times 10^{-3})^2 (4.324)} \quad (5.7)$$

The maximum error involved in the mean solids concentration was estimated based on the following hypotheses: when the lower slide valve closed first, the solids continued to leave the test section at

176

a rate W_s during the time Δt_{sv} , the time elapsed before the upper valve closing. Similarly, when the upper slide valve was first to close, solids continued to flow into the test section at the rate W_s during Δt_{sv} . The difference between the measured and real value of the solids concentration would then be given by :

$$\Delta \bar{\alpha}_s = \frac{4W_s \Delta t_{sv}}{\rho_s \pi D^2 L_{sv}} \quad (5.8)$$

The mean solids concentration is related to the mean solids velocity by the equation :

$$\bar{\alpha}_s = \frac{W_s}{\rho_s \bar{V}_s A} \quad (5.9)$$

The percentage error is given by combining the above two equations :

$$\frac{\Delta \bar{\alpha}_s}{\bar{\alpha}_s} = \frac{100 \bar{V}_s \Delta t_{sv}}{L_{sv}} \quad (5.10)$$

Figure 5.11 shows a plot of the above equation using the range of valves found in the experiments. In general Δt_{sv} was less than 0.05 s. The maximum errors were thus generally less than 5 %.

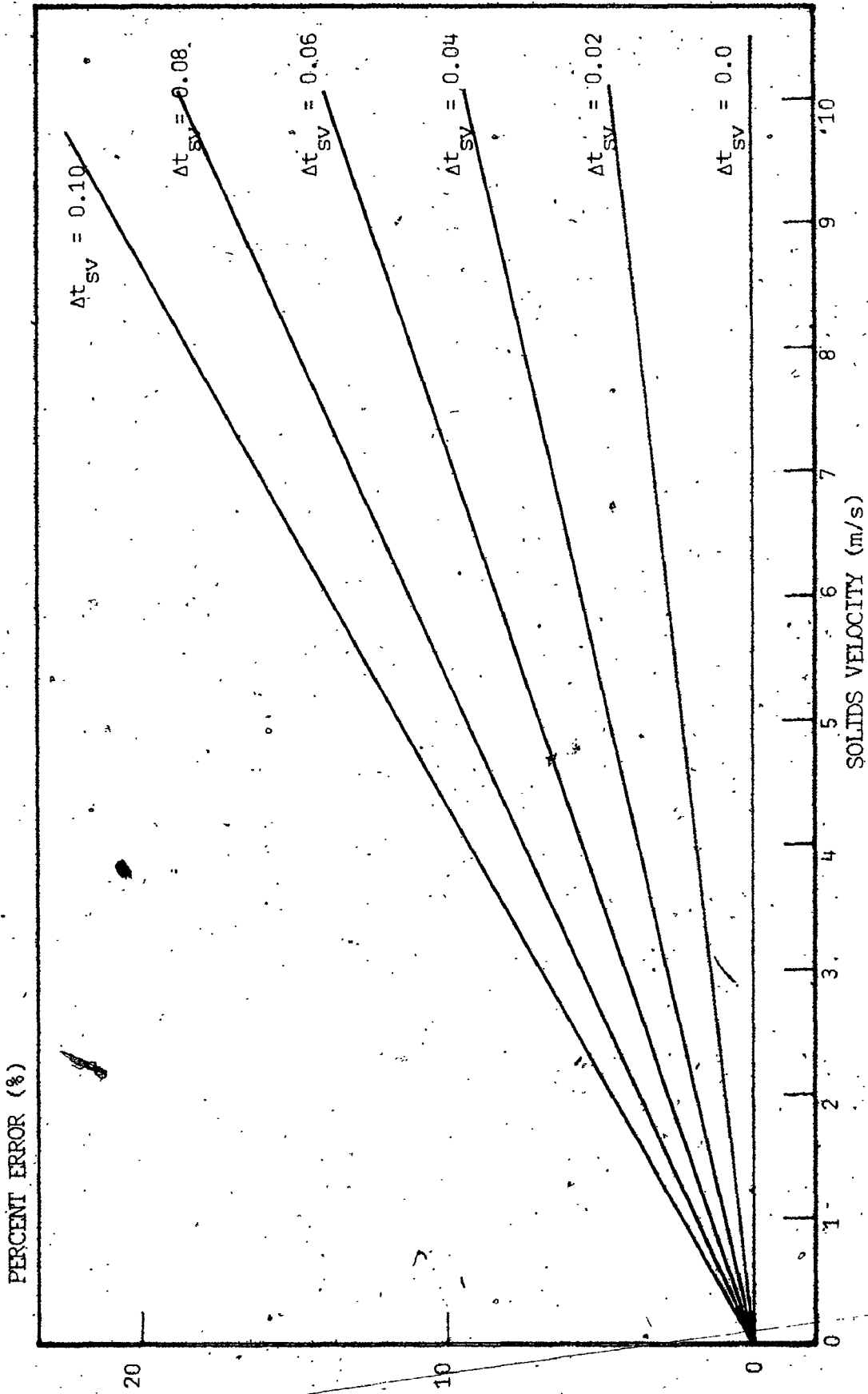


FIGURE 5.11 Maximum errors in mean solids concentration measurements as a function of non-simultaneous slide valve closing times

5.3 Heat transfer installation and procedure.

5.3.1 Description

The installation used in the heat transfer experiments was essentially the same as that used in the hydrodynamic experiments with the one major change being the replacement of the test section pipe by an electrically heated pipe instrumented to measure power input and outer pipe wall temperatures.

The solids circulation system was unchanged; the slide valves remained in place separating the test section from the acceleration zone below and the disengaging zone above. Additional Ch-Al thermocouples were placed in the fluidized solids in the feeder and in the acceleration zone just upstream from the test section. These thermocouples were used as one indication that the overall heat losses from the system (outside of the test section) corresponded to the heat input into the system: Had the system not been at steady state thermally, changes in these two temperatures with respect to time would have been observed. Identical temperatures at these two points also indicated that the gas and solids were at the same temperature entering the heat transfer section.

Pressure gradients in the line were still available, despite the fact that the test section itself was not equipped with pressure taps. Earlier hydrodynamic experiments showed that the pressure gradients obtained by regressing the test section pressure readings were essentially the same as those obtained by regressing the readings from the five pressure taps immediately upstream from the test section. These

latter taps were therefore used as the source of pressure gradient data for hydrodynamically fully developed flow in the heat transfer runs.

The heat transfer section, power supply and instrumentation are shown schematically in Figure 5.12. The test section consisted of a 20 mm ID, 21 mm OD drawn stainless steel (AISI 316 L) pipe 4 m in length to which 99 % pure copper flanges, 5 mm in thickness were silver-soldered. The pipe material was chosen for its high electrical resistivity (7.34×10^{-2} ohms-m); the pipe was specially manufactured to ensure even wall thickness in order to provide a uniform heat flux when electrically heated. Had the wall thickness varied, either around the circumference or along the length of the pipe local resistances would have varied leading to variations in local heat fluxes.

Even wall thickness was verified using a simple test: a known voltage was applied between the ends of the heat transfer pipe. A voltmeter was then used to measure voltage as a function of position along the pipe axis and around the circumference. The circumferential voltage measurements were identical within the four significant figure precision of the voltmeter at each axial position; identical voltage drops per unit length were also found from the axial measurements.

The test section pipe, when electrically heated, expanded along its axis. In order to prevent warping between the two fixed slide valves an expansion joint was placed between the heat transfer section and the upper slide valve. This joint consisted of a rubber expandable tube which, in the relaxed position, had the same inner diameter as

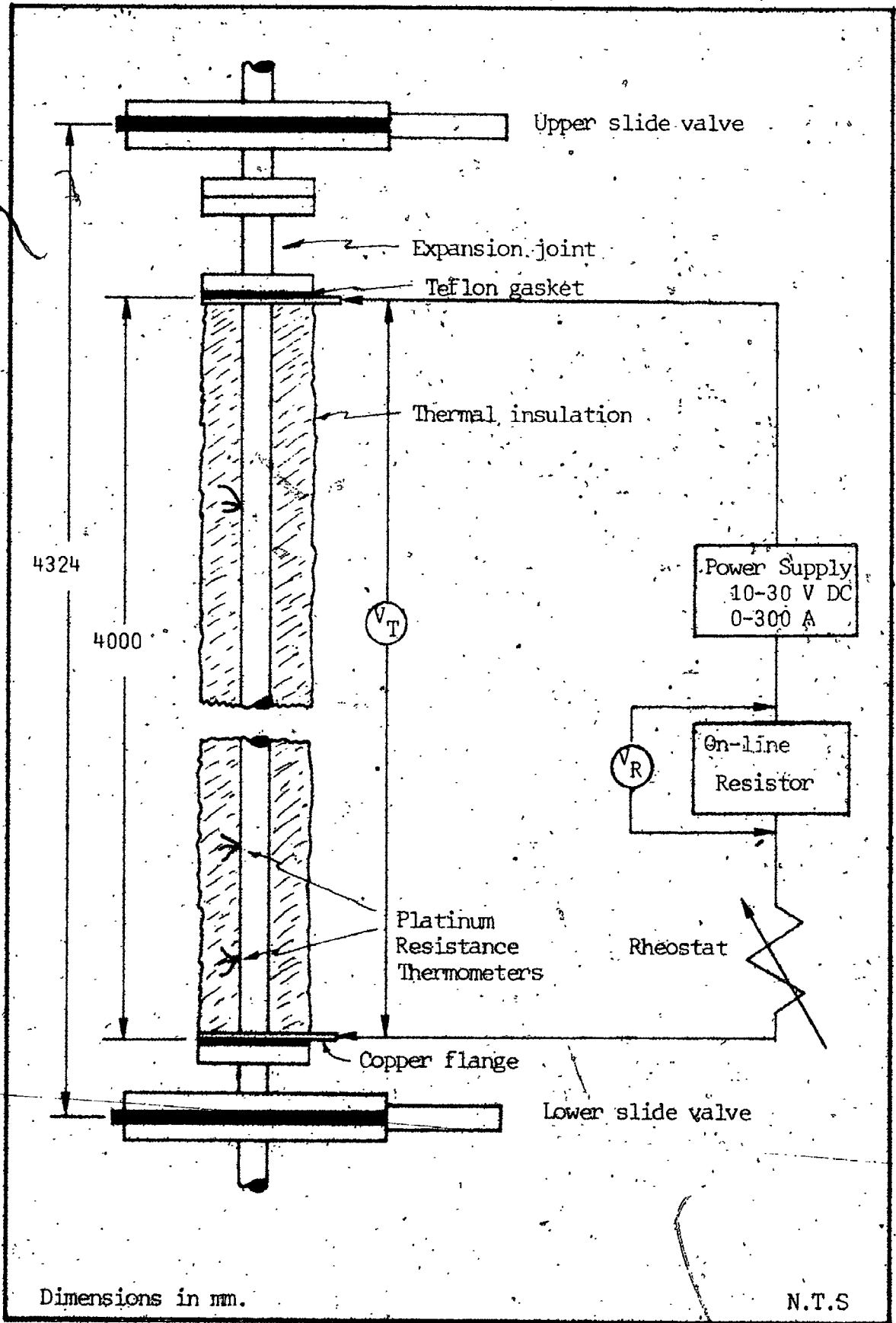


FIGURE 5.12 Heat Transfer Test Section

the test section (20 mm). When the test section was heated, the rubber tube contracted slightly (about 1 mm). The corresponding diameter change was not enough to disturb the flow as would have been evidenced by disruptions in the pressure profile however. In order to further ensure that all thermal pipe expansion did not lead to pipe warping, guides consisting of U-clamps were placed at two positions along the test section axis. These guides were fixed to the rigid support structure around the test section, and were insulated, electrically and thermally from the pipe wall using asbestos cloth..

The test section pipe was insulated electrically from the two slide valves by placing 5 mm thick Teflon gaskets between the flanges. Bolts between the flanges were insulated using Teflon tube inserts and washers.

Outside pipe wall temperatures were measured using 2 x 2 x 1 mm, 3-wire platinum resistance thermometers (RTD's) (Degussa, type F2105). The flat surface of the RTD's were fixed tightly on the outside wall surface at various positions along the pipe axis using hose clamps. The hose clamps were insulated from the RTD's and from the pipe wall by placing styrofoam inserts formed cylindrically in such a way as to neatly fit between the clamp and the pipe. The inserts also made it possible to exert a sufficient pressure on the RTD's to ensure good wall-thermometer contact without creating mechanical stresses which would have broken the fragile resistor heads.

The three-wire RTD's operate according to the following principle: the finely-wound platinum wire in the probe head has a

resistance which varies as a function of temperature. The temperature measurement involves passing a small fixed electrical current through the winding and measuring the corresponding voltage drop. As the voltage drop is measured between the ends of the extension wires, it is really a measurement of overall circuit resistance (platinum winding plus the extension wires). The presence of the third wire allows the separate measurement of the extension wire resistance; the winding resistance is thus obtained by subtracting the extension wire resistance - which is assumed to be the same for all three wires of a given probe - from the overall circuit resistances.

The RTD probes supplied by the manufacturer were equipped with 500 mm long silver extension wires. The large number of probes, together with their spatial separation necessitated the addition of further extension wires. Copper cables were therefore added to the silver wires to extend them to jacks located in the central control box. The copper cables were all cut at precisely the same length in order to ensure that all extension wire had all the same resistance. Temperatures were then read by plugging the lead wires from a digital thermometer (CHAUVIN-ARNOUX Model, NUTA LSI 144 G 2000) into the probe jacks.

The RTD's and corresponding circuit were calibrated over the ranges of temperature studied in a water bath. Details and results of the calibrations are given in Appendix II.

Power was supplied to the test section pipe using a 8600 VA rectifier-transformer (BLEVIN, Model TFC) which supplied direct

current between 0 and 300 amperes at between 10 and 30 volts. The electrical connection between the power supply and the pipe flanges was made using large (185 mm² cross-section) insulated copper cable which were fixed to the test section copper flanges using brass bolts.

Partial regulation of the power input was possible by varying to transformer output voltage between 10 and 30 volts DC. Additional regulation was obtained using a 2500 W rheostat (COUDOINT Model SQV-1) inserted in the power supply circuit. These two adjustments allowed power into the system to be varied between 0 and 8500 W.

Measurement of the power input into the system required measurements of the voltage drop across the test section pipe and of the electrical current in the heating circuit. Two copper wires were silver-soldered on the copper flanges and extended to jacks in the central control box for the former measurement. A 0.33 mΩ on-line resistor mounted in the heating circuit was used for the latter measurement. As before copper wires were extended between the shunt and jacks mounted in the control box. All voltages were then measured at the jacks using a Metrix multimeter (Model MX 590).

Once the fully equipped heat transfer pipe had been mounted between the two slide valves, thermal rock wool insulation (Kerlane) was carefully wrapped around the pipe and was held in place using reflective tape.

5.3.2 Operating procedure

The heat transfer experiments were carried out with the installation operating at steady state both hydrodynamically and thermally.

In order to attain steady state hydrodynamically, with known gas and solids flowrates, the procedure described in Section 5.2.2. was followed.

Before a heat transfer experiment was run, a calculation of the approximate power input required to heat the suspension to between 20 and 40°C above its inlet temperature for the selected gas and solids flowrates was carried out. This allowed transformer and rheostat settings to be made before the power supply was turned on.

The above-mentioned temperature difference represented a compromise between the need to attain sufficiently large temperature gradients along the wall to have good precision in the heat transfer coefficient measurements and the desire to maintain essentially constant gas and solids physical properties along the length of the pipe.

Once the electrical input was set and hydrodynamic steady state had been achieved, no further adjustments were made and the system operator had only to survey the key indicators (line pressure gradient, fluid bed feeder pressures and wall temperatures) while waiting for thermal steady state to be attained. The critical factor in the achievement of this latter steady state was the heating of the pipe thermal insulation. The time required for this was independently determined to be about 2 hours as described in detail in the following section.

Once the system had reached steady state, all hydrodynamic data (flowrates, pressure gradients) were taken as described in Section 5.2.2. The pipe wall temperature profile was recorded along with the

voltage drops across the test section and the on-line resistor. Thermocouple readings were also recorded. Finally, the slide valves were closed and the solids held-up in the test section were recovered and weighed.

5.3.3 Test section heat losses and time required to reach thermal steady state:

The heat input into the system during the heat transfer experiments was divided into three separate fluxes: heat transferred to the flowing suspension; radial heat losses to the surrounding atmosphere and axial heat losses at the flanges of the heat transfer section. In order to approach constant heat flux conditions to the suspension it was necessary to minimize heat losses in all directions; in order to compute the actual local heat fluxes to the suspension it was necessary to independently measure and correlate the heat losses as functions of known variables. Finally it was necessary to determine the time required for the thermal insulation to reach their steady state temperatures in order to apply the correlations.

A series of experiments was undertaken to achieve these objectives. The first, to be outlined in this section, allowed the effective radial heat transfer coefficient from the outside pipe wall to the surrounding atmosphere to be determined as a function of the pipe wall surface temperature and of time. It also allowed verification that axial conduction along the pipe was negligible and affected only pipe wall temperatures in the first few centimeters from the test section flanges. An ultimate verification of the heat loss model,

consisting of using the above results as well as further experimental results on heat transfer to a flowing gas to confirm a well-known equation relating the Nusselt number to the Reynolds number, will be described in the following section.

The first series of experiments consisted of closing the slide valves and applying an electrical input into the system via the flange connections. The heat transfer section was heated in this way and, as the slide valves were tightly closed, all heat input into the system was eventually lost toward the surrounding atmosphere either in the radial direction or axially through the flanges connecting the heat transfer section to the rest of the system. Temperature profiles along the length of the heat transfer pipe were noted as a function of time until they stabilized at their steady state values. These experiments were carried out at several different values of the electrical input into the system; in this way, the final mean temperature of the pipe surface was varied between 40°C and 95°C.

As a check, in particular concerning the correct functioning of the platinum resistance thermometers, these experiments were repeated several times during the course of the experimental program.

Heat loss model. Heat losses in the above-described experiments as well as in the suspension heat transfer were represented mathematically as follows:

- radial heat losses were taken to be proportional to the difference between the wall surface temperature and the temperature of the surrounding atmosphere:

$$dq_{tr} = \pi D_o U_o (T_w - T_\infty) dz \quad (5.11)$$

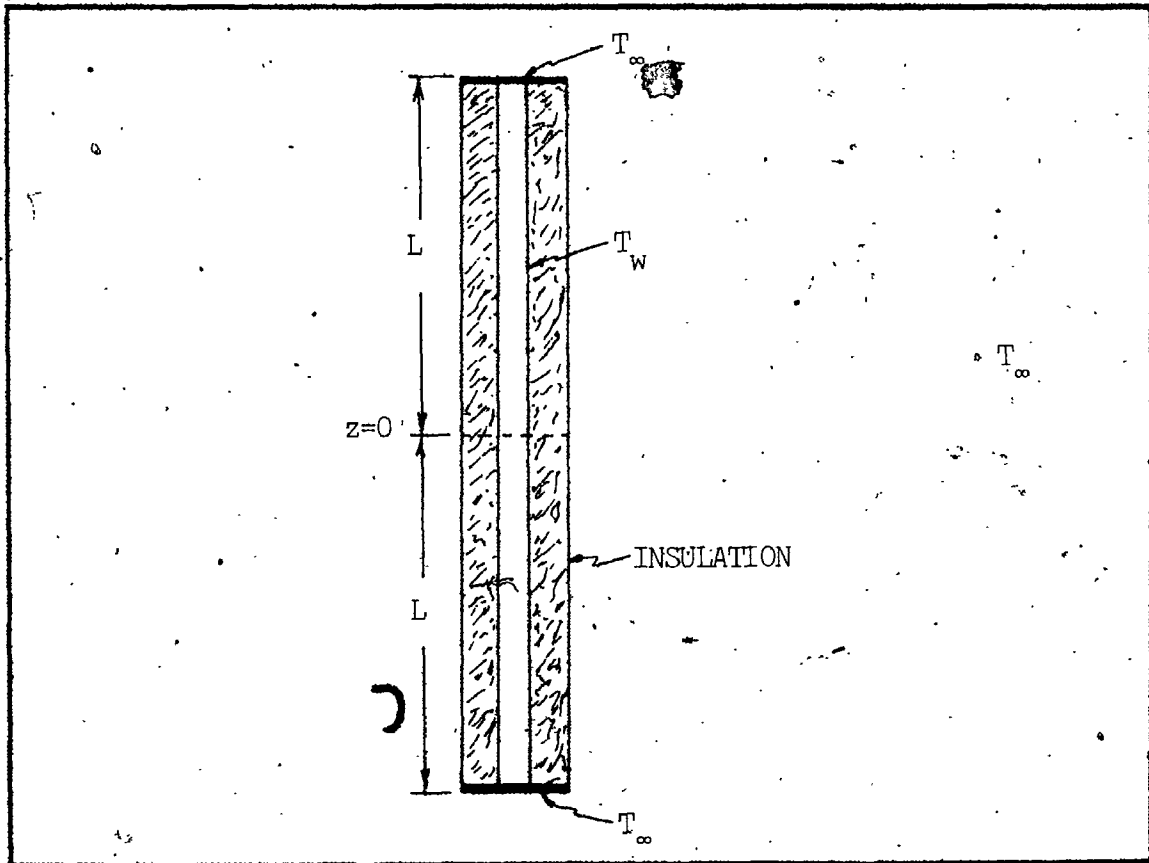
- end losses, and axial conduction in general, were taken to be given by the standard Fourier heat conduction :

$$dq_A = (\pi/4) (D_o^2 - D_i^2) \lambda_T \frac{dT_w}{dz} \quad (5.12)$$

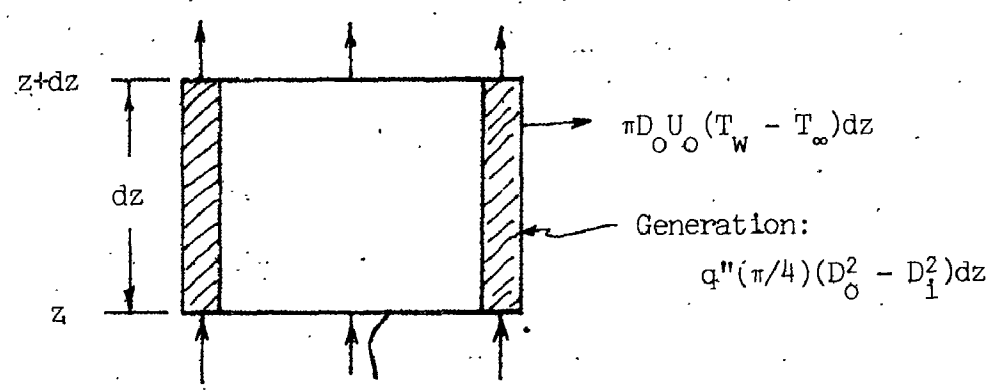
In order to derive values of the effective radial heat transfer coefficient from the above-described experiments, three additional assumptions were made :

- radial temperature gradients in the pipe are negligible. The mean temperature across the pipe is thus given by the pipe wall temperature,
- heat is transferred in the gas enclosed between the two slide valves by conduction only when the slide valves are closed,
- the slide valves act as perfect heat sinks. This was assumed in order to determine the maximum ratio of end losses versus radial losses. The validity of this assumption was tested by measuring the slide valve flange temperatures while the test section was being heated. The flange and ambient temperatures were found to be the same within 1°C.

A heat balance on a pipe section dz at steady state during the closed slide valve experiments is given by (See Figure 5.13) :



$$\left[\frac{\lambda_g \pi D_1^2}{4} + \frac{\lambda_T \pi (D_0^2 - D_1^2)}{4} \right] \frac{dT_w}{dz} \Big|_{z=z+dz}$$



$$\left[\frac{\lambda_g \pi D_1^2}{4} + \frac{\lambda_T \pi (D_0^2 - D_1^2)}{4} \right] \frac{dT_w}{dz} \Big|_{z=z}$$

FIGURE 5.13 Heat loss model

$$\begin{aligned}
 & (\pi D_1^2/4)\lambda_g + \{\pi(D_0^2 - D_1^2)/4\} \frac{d^2 T_w}{dz^2} \\
 & - U_0 \pi D_0 (T_w - T_\infty) = q'' \{\pi(D_0^2 - D_1^2)/4\} \quad (5.13)
 \end{aligned}$$

Re-arranging gives :

$$\begin{aligned}
 \frac{d^2 T_w}{dz^2} & - \frac{U_0 \pi D_0 T_w}{\{(\pi/4)D_1^2 \lambda_g + (\pi/4)(D_0^2 - D_1^2)\lambda_T\}} \\
 & = \left[\frac{-q''(\pi/4)(D_0^2 - D_1^2) - U_0 \pi D_0 T_\infty}{(\pi/4)D_1^2 \lambda_g + (\pi/4)(D_0^2 - D_1^2)\lambda_T} \right] \quad (5.14)
 \end{aligned}$$

which is an ordinary differential equation of the form :

$$\frac{d^2 T_w}{dz^2} + b T_w = R \quad (5.15)$$

The solution of the above equation is :

$$T_w = C_1 \exp(z\sqrt{b}) + C_2 \exp(-z\sqrt{b}) - R/b \quad (5.16)$$

where the constants C_1 and C_2 are given by :

$$C_1 = \frac{\{T_\infty + R/b\} \{\exp(L\sqrt{b}) - \exp(-L\sqrt{b})\}}{\exp(2L\sqrt{b}) - \exp(-2L\sqrt{b})} = C_2 \quad (5.17)$$

in the case where the slide valves act as perfect heat sinks, both of which are held at the ambient temperature T_∞ .

The radial heat transfer coefficient can be calculated from the measured temperature profile via :

$$U_o = \frac{q'' \{ \pi(D_o^2 - D_1^2)/4 \}}{T_w - T_\infty \Big|_{z=0}} \quad (5.18)$$

since at $z = 0$, $dT_w/dz = 0$ in the case where the two slide valves are held at the same temperature.

The radial heat losses can be calculated from :

$$q_r = U_o \pi D_o \int_{-L}^L (T_w - T_\infty) dz \quad (5.19)$$

or in terms of the mean surface temperature from :

$$q_r = 2\pi D_o U_o L (\bar{T}_w - T_\infty) \quad (5.20)$$

where \bar{T}_w is defined by :

$$\bar{T}_w = \frac{1}{2L} \int_{-L}^L T_w dz \quad (5.21)$$

The axial heat losses can be determined from the temperature profile via :

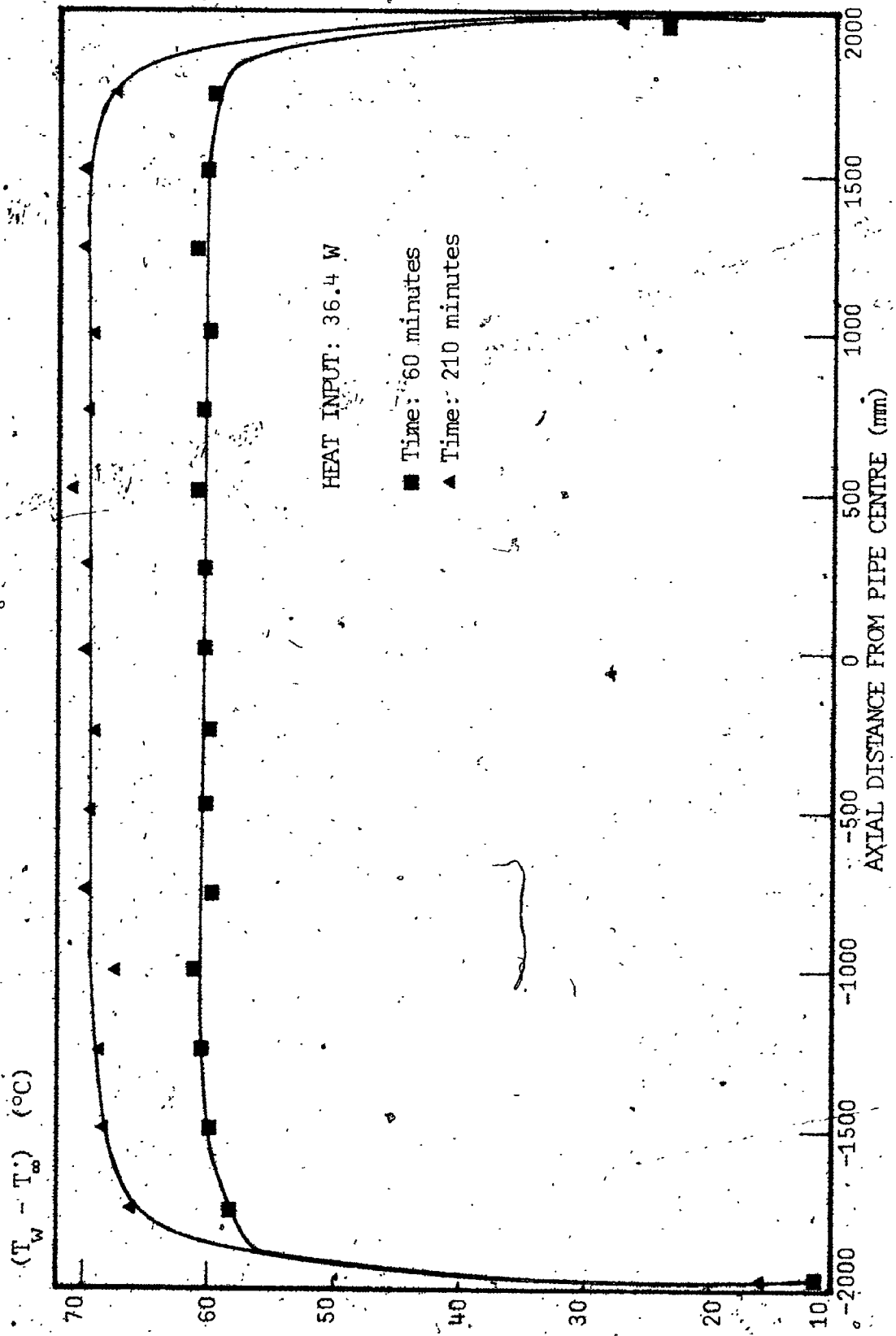
$$q_A = -2 \left\{ \lambda_T \pi (D_0^2 - D_1^2)/4 - \lambda_g \pi D_1^2/4 \right\} \left. \frac{dT_w}{dz} \right|_{z=L} \quad (5.22)$$

or in terms of the mean surface temperature from :

$$q_A = -2L \left\{ \lambda_T \pi (D_0^2 - D_1^2)/4 - \lambda_g \pi D_1^2/4 \right\} (\bar{T}_w + R) \quad (5.23)$$

Results. Two typical temperature profiles obtained in the closed valve experiments are shown in Figure 5.14. These profiles are characterized by a flat portion which extends nearly the length of the pipe and by sharp gradients as the slide valves are approached. This signifies the relative importance of the radial losses with respect to the end losses. Indeed as Equation 5.14 shows, if axial conduction had been zero the profile would have been completely flat with singular points at each end. End losses determined from the experimental profiles were less than 3.5 % of the radial losses. As the overall losses (end plus radial) in most heat transfer runs were less than 10 % of the total heat input, end losses played an insignificant role in the overall heat balance on the system. They did however affect temperature measurements in the first few centimeters close to the slide valves.

The effective local radial heat transfer coefficient U_o was determined from the experimental temperature profile using Eq. 5.18. The curves superimposed on the experimental results in Figure 5.14



HEAT INPUT: 36.4 W

■ Time: 60 minutes
▲ Time: 210 minutes

AXIAL DISTANCE FROM PIPE CENTRE (mm)

FIGURE 5.14 Typical axial temperature profiles obtained during heat loss calibrations

represent Eq. 5.16 using the measured local radial heat transfer coefficient and the physical parameters of the system. The good correspondance between the curves and the experimental data justifies the hypotheses made in developing the mathematical representation of the heat losses.

The variation of the effective radial heat transfer coefficient with time, for several final surface temperatures, is shown in Figure 5.15. This curve shows an exponential decay typical of unsteady state heat conduction problems. The time required for the system to reach steady state was shown to be relatively long ; in excess of 2 hours was required for the insulation to heat up to its final temperature. The system was therefore allowed to stabilize for at least two hours in all subsequent heat transfer runs before any data were taken..

Figure 5.15 also shows small variations in the final effective radial heat transfer coefficient as a function of the mean surface temperature. This was to be expected, firstly since the thermal conductivity of the pipe insulation is temperature dependent and secondly because the film coefficient due to natural convection between the outside surface of the insulation and the surrounding atmosphere is also temperature dependent. The overall variation as a function of surface temperature (between 1.8 and 2.0 W/m²C) was not sufficiently large however for it to be necessary to account for this variation in calculating the heat flux into the suspension during later heat transfer runs. This was due to the fact that given the large coefficients between the pipe wall and the suspension, the ratio of the radial losses to the heat flux to the suspension was small (as

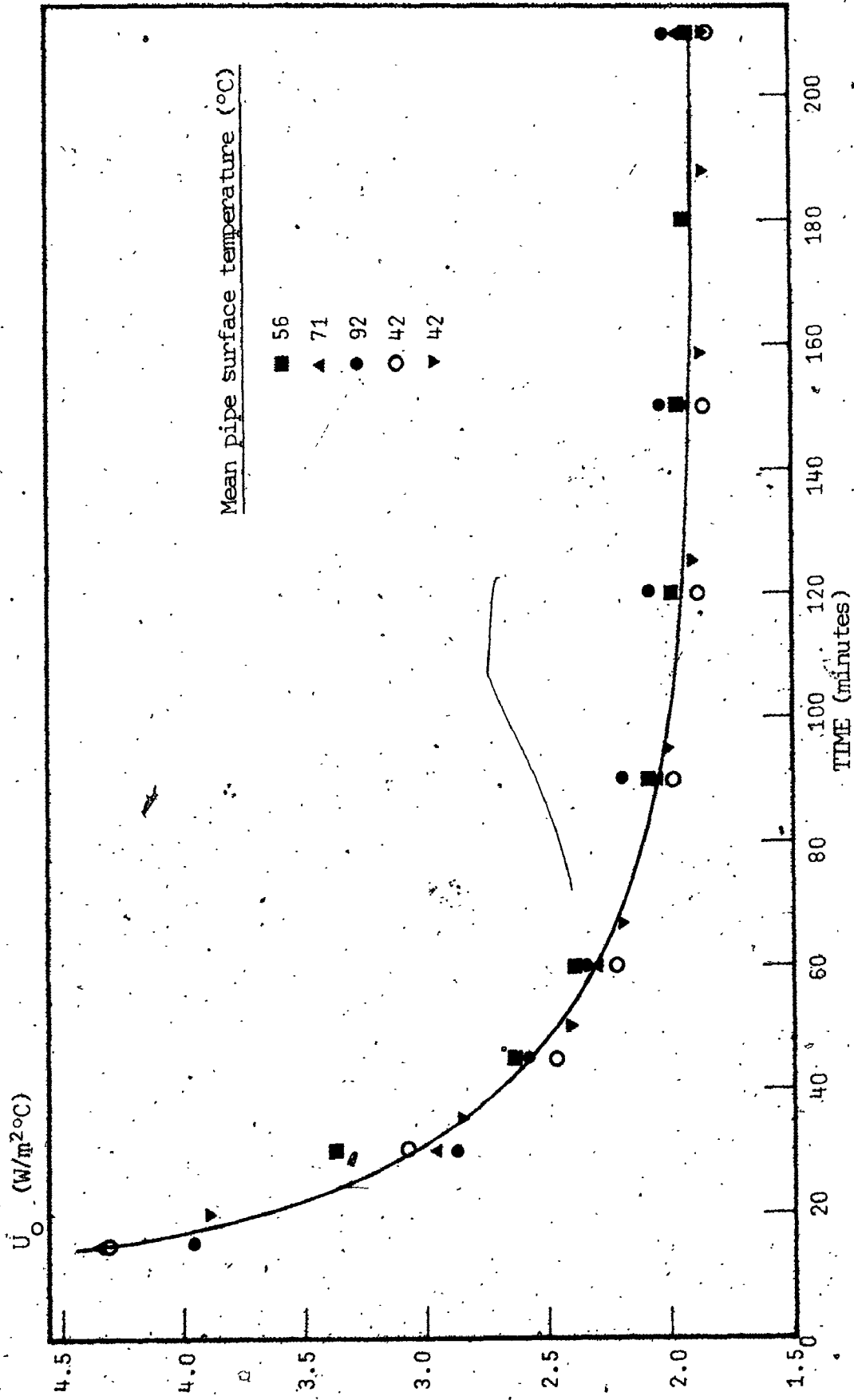


FIGURE 5.15 Variation of the effective radial heat transfer coefficient during heat loss correlation experiments

mentioned, less than 10 %):

The value of $U_o = 1.9 \text{ W/m}^2\text{C}$ was therefore used for all subsequent calculations. It can be noted finally that the value obtained in this way corresponded well with that calculated from the thermal conductivity of the insulation and known correlations for natural convective coefficients from insulated pipes. Using a pipe diameter of 21 mm, an insulation thermal conductivity of $4.33 \times 10^{-2} \text{ W/mC}$ and an outside natural convective coefficient of $10 \text{ W/m}^2\text{C}$ (See Ref. 100 page 10-11) the calculated result, again based on the outer pipe diameter, is $2.04 \text{ W/m}^2\text{C}$.

5.3.4. Overall heat transfer system verification :
Seider Tate Equation

In the same way as the Moody diagram was used to verify the instrumentation of the hydrodynamic installation operating as a unit, the heat transfer installation was verified by measuring heat transfer coefficients between the pipe wall and gas flowing without solids as a function of gas flowrate and comparing the results with those given by the Seider-Tate Equation for single phase flow. As in the case of the hydrodynamic experiments, these latter measurements were carried out periodically during the course of the heat transfer programme. All measurements, except those dealing with the solids phase, intervene in the determination of the heat transfer coefficient, in these experiments ; any malfunctions such as a gas leak, improperly operating flowmeter or poorly fixed RTD showed up immediately as deviations between the measured coefficients and those predicted by the correlation. These relatively simple experiments also provided an ad-

ditional check on the validity of the heat loss model described in the previous section.

The procedure for those experiments followed closely that described in Section 5.2.3 for the hydrodynamic system verification. The feeder was short-circuited as shown in Figure 5.5 and the upper return line valve was fully closed. The power supply was then turned on and the system was allowed to reach steady state. During the first verification runs (before the first experiments with solids) the power input was regulated to obtain three different gas inlet and outlet temperature differences : 20°C, 40°C and 60°C. As these three temperature differences gave similar heat transfer coefficient results only the 20°C difference series was used later in the periodic verifications.

A typical wall temperature profile found in these experiments is shown in Figure 5.16. The profile is characterized by a steep initial rise near the test section entry point, followed by a constant gradient thereafter. The initial rise corresponds to the establishment of the thermal boundary layer.

Local heat transfer coefficients as a function of distance from the test section entry point for a number of different gas flowrates are shown in Figure 5.17 (The calculation of these coefficients from temperature profiles and flowrates, accounting for heat losses was carried out using the same relations given in the following section for suspension flows : the only difference involves setting $W_s = 0$). The curves show constant coefficients beyond the thermal entry region.

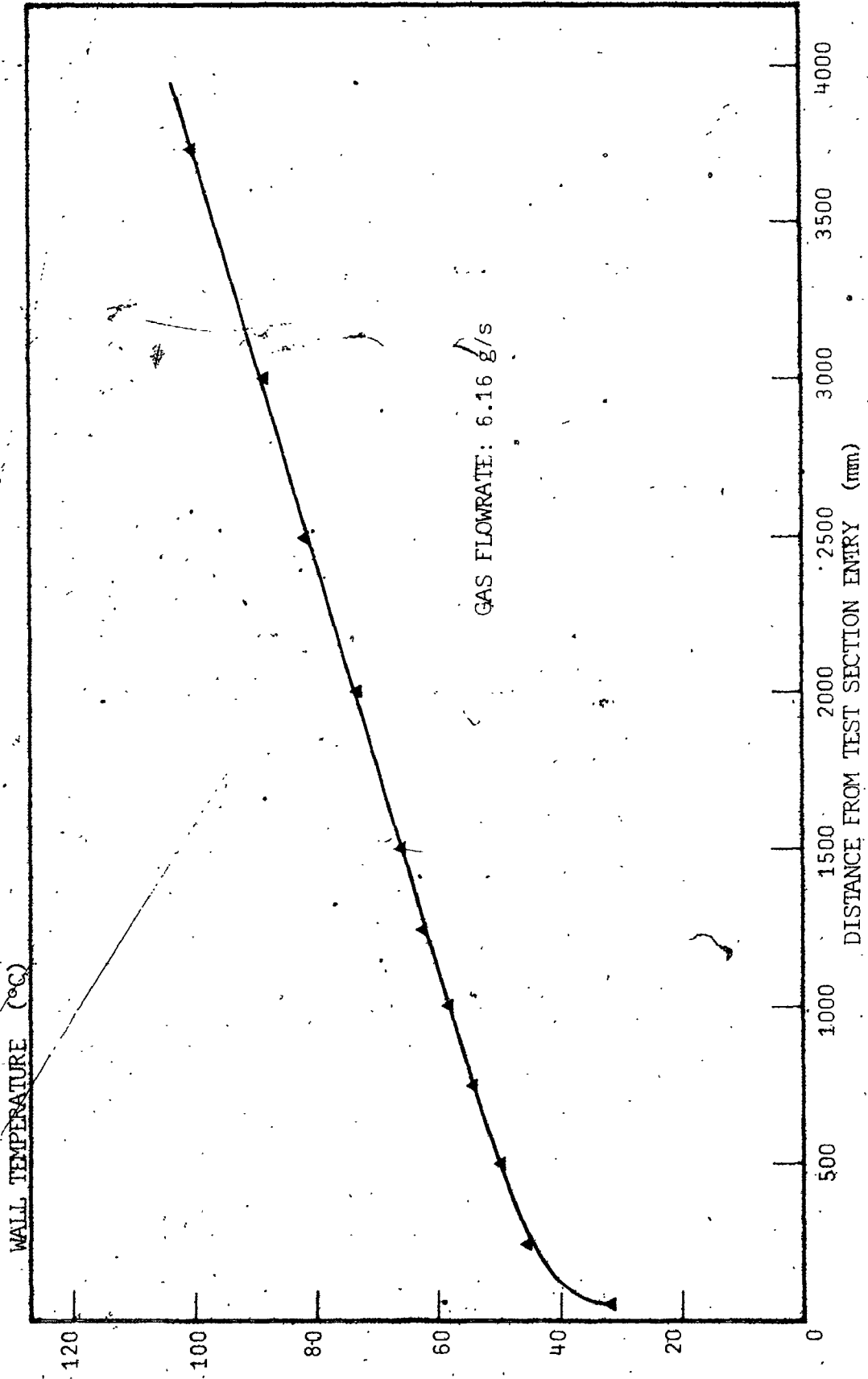


FIGURE 5.16. Typical pipe wall temperature profile - Gas only run

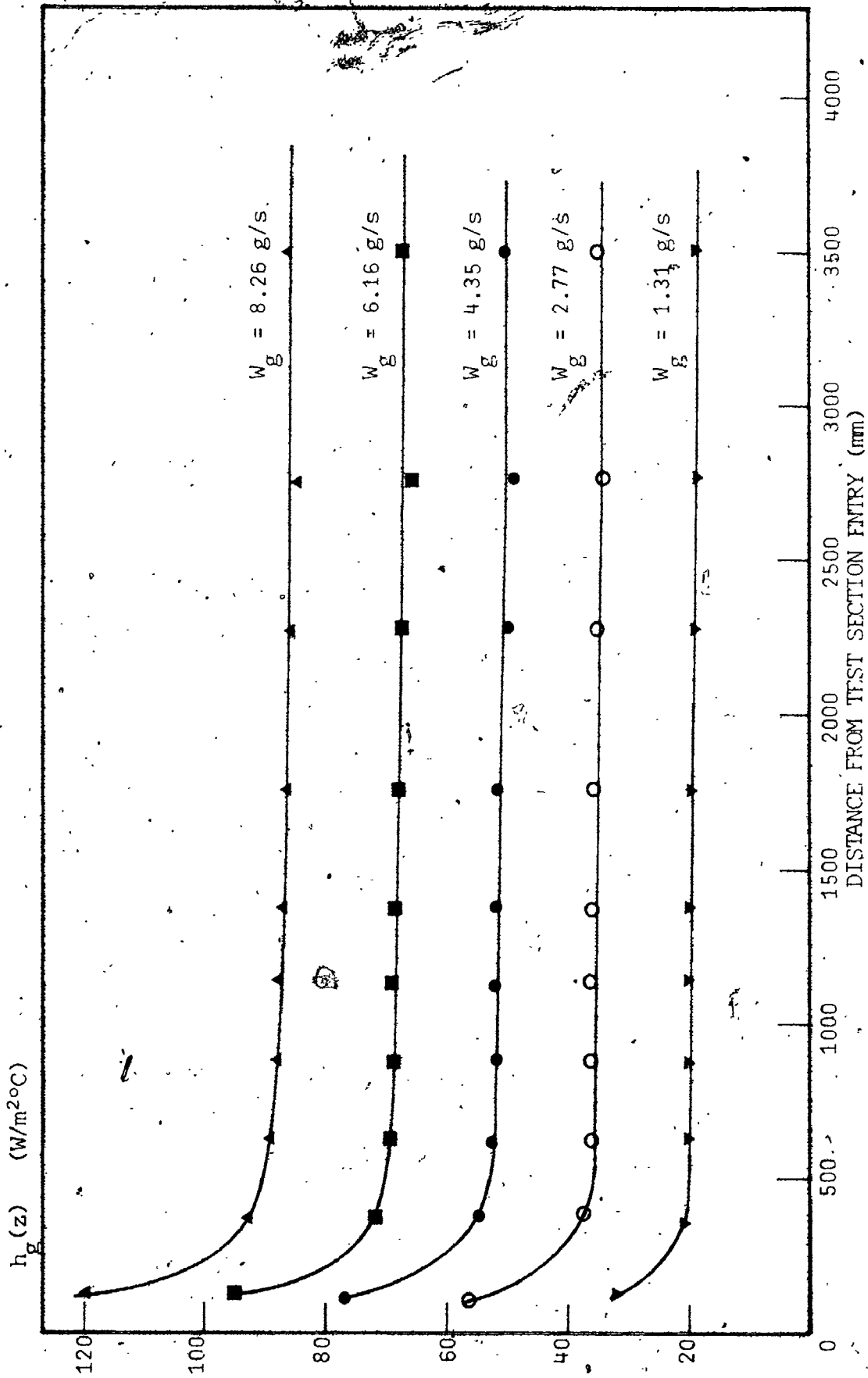


FIGURE 5.17 Local heat transfer coefficients for gas-only runs.

The asymptotic coefficients (beyond the thermal entry region) are plotted as a function of gas flowrate in Figure 5.18 for the three different inlet and outlet temperature differences. The data show no substantial change due to temperature difference. The curve drawn through the data is the correlation given for single phase fluid flow under constant heat flux conditions in Reference 71 :

$$Nu_E = 0.022 Re^{0.8} Pr^{0.6} \quad (5.24)$$

The agreement is excellent.

5.3.5. Calculations

All relevant hydrodynamic calculations necessary to analyze data from the heat transfer experiments were carried out as already described in Section 5.2.5. This section will deal only with the treatment of temperature and power measurements to determine local heat transfer coefficients.

For calculation purposes the heat transfer test section was considered to be divided into discrete lengths the boundaries of which were given by RTD temperature probe positions (See Figure 5.19). The calculation of the local coefficients within each of these intervals involved the following steps :

- 1) Individual radial losses (within each interval) were calculated from wall surface temperatures, the ambient temperature and the overall radial heat transfer coefficient determined from the experiments described in Section 5.3.3.

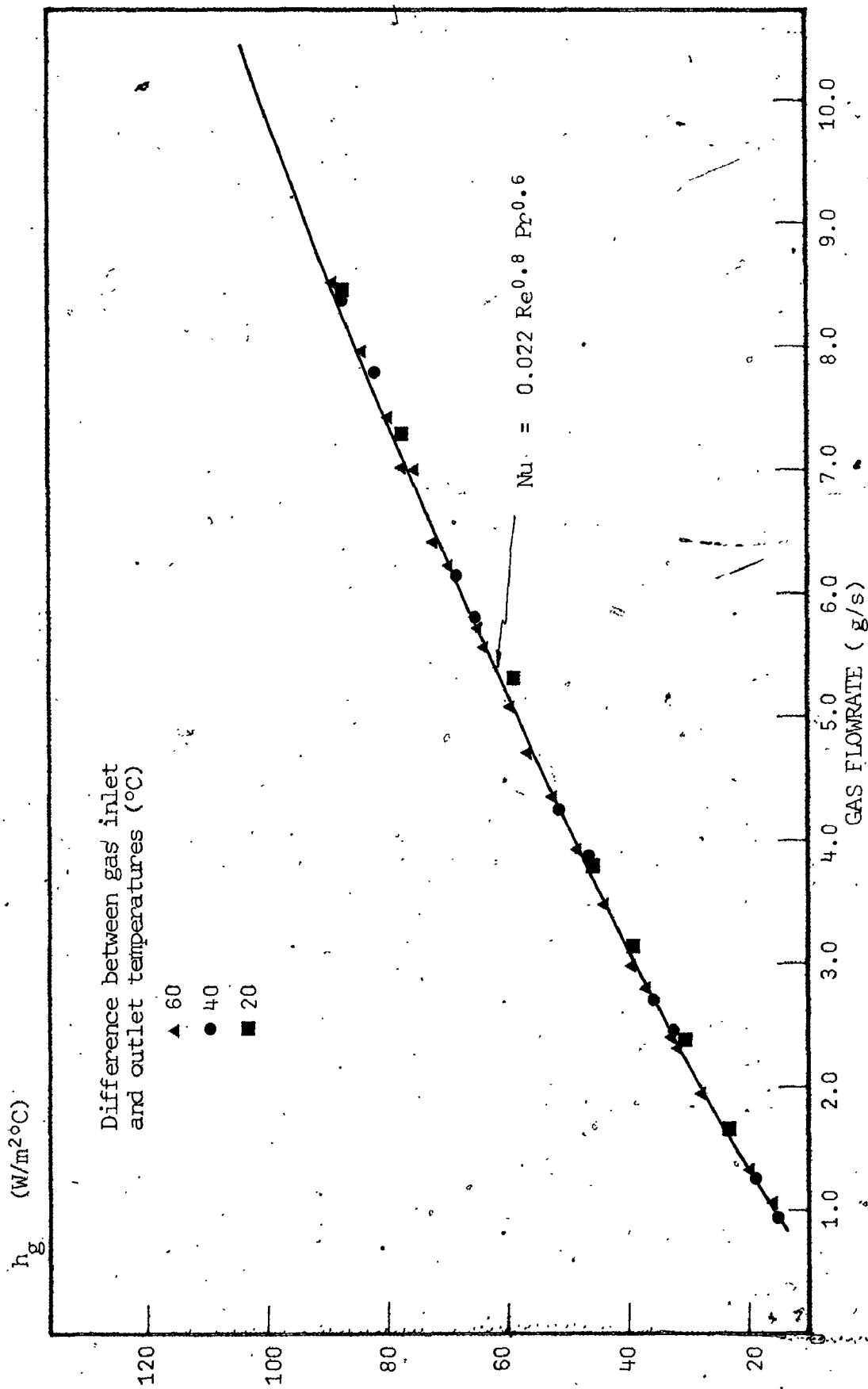


FIGURE 5.18 Gas-only asymptotic coefficients versus Gas flowrate

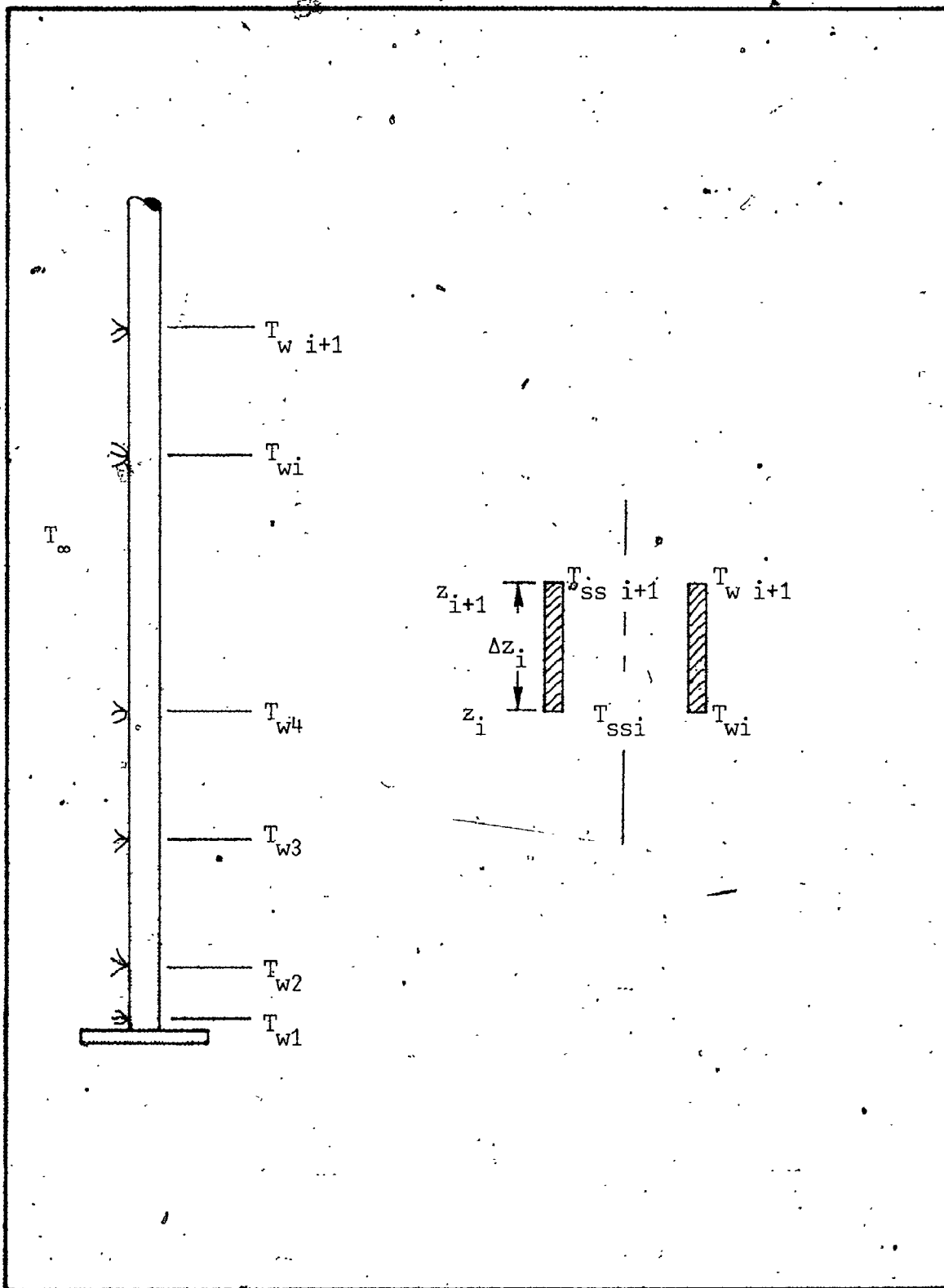


FIGURE 5.19 Basis for heat transfer coefficient calculation

- 2) Individual heat inputs were calculated from the difference between the power input for a given interval and the radial losses.
- 3) The suspension mixed mean temperature at the outlet of an interval was determined by a heat balance.
- 4) Local heat transfer coefficients were determined from the difference between the wall temperature and mixed mean suspension temperature.

The last calculation involved the assumption that the outside pipe wall temperature, as measured by the RTD's was identical to the inside pipe wall temperature upon which the heat transfer coefficient was based. The validity of this assumption is examined with the temperature probe calibrations in Appendix III where it is shown, that under the operating conditions used here, the difference is never more than $6.0 \times 10^{-2} \text{ } ^\circ\text{C}$. Hence this assumption is the source of little or no error.

Individual losses. The heat losses in the interval between z_i and z_{i+1} are given by :

$$q_{p \ i,i+1} = U_o \pi D_o \int_{z_i}^{z_{i+1}} (T_w - T_\infty) dz \quad (5.25)$$

which can be approximated by :

$$q_{p \ i,i+1} = U_o \pi D_o \Delta z_i \{ (T_{wi} - T_\infty) + (T_{wi+1} - T_{wi})/2 \} \quad (5.26)$$

Individual heat generation. The overall heat input was determined from the voltage measurements between the test section flanges and across the on-line resistor :

$$Q_T = \frac{V_T V_R}{R_R} \quad (5.27)$$

which, given the fact that the on-line resistance had a value of $0.333 \text{ m}\Omega$ gives :

$$Q_T = 3000 V_T V_R \quad (5.28)$$

where the voltages are given in volts, the power in watts.

This heat was dissipated uniformly over the entire 4 m length of the test section. The heat input to an interval of length Δz_i is therefore given by :

$$q_{T \text{ } i, i+1} = \frac{3000 V_T V_R \Delta z_i}{4} \quad (5.29)$$

The heat input into the suspension is given simply by the difference between the above term and the heat losses :

$$q_{ss \text{ } i, i+1} = q_{T \text{ } i, i+1} - q_{r \text{ } i, i+1} \quad (5.30)$$

Heat transfer coefficients. The suspension mixed mean temperature was determined by a heat balance on each interval :

$$T_{ss\ i+1} = T_{ssi} + \frac{q_{ss\ i,i+1}}{W_g C_g + W_s C_s} \quad (5.31)$$

The wall-suspension heat transfer coefficient is given by :

$$q_{ss\ i,i+1} = \pi D_i \int_{z_i}^{z_{i+1}} h_{ss} (T_w - T_{ss}) dz \quad (5.32)$$

which can be approximated by :

$$q_{ss\ i,i+1} = \pi D_i h_{ssi} \Delta z_i \left\{ (T_{w\ i+1} + T_{w_i})/2 - (T_{ss\ i+1} + T_{ssi})/2 \right\} \quad (5.33)$$

The initial value T_{ssi} in the equation above was the measured suspension inlet temperature.

5.4 Gas and solids physical properties

5.4.1. Gas properties

The physical properties of the compressed air used in all experiments were determined from local measurements of pressure and

205
temperature and from data in standard reference works.

The gas heat capacity was determined as a function of temperature from the following expression derived from data in Ref. 58 :

$$C_g = 0.028 T_g + 1007.7 \quad (5.34)$$

$$0 < T_g < 140^\circ\text{C}$$

where T_g is in ($^\circ\text{C}$) and C_g in ($\text{J}/\text{kg}^\circ\text{C}$).

The gas thermal conductivity as a function of temperature was determined by the following expression derived from data in Ref. 100 :

$$\lambda_g = 7.225 \times 10^{-5} T_g + 2.406 \times 10^{-2} \quad (5.35)$$

$$0 < T_g < 140^\circ\text{C}$$

where T_g is in ($^\circ\text{C}$) and λ_g in ($\text{W}/\text{m}^\circ\text{C}$).

The gas viscosity was determined using the following expression derived from data in Ref. 7 :

$$\mu = 1.711 \times 10^{-5} \left[\frac{T_g + 273}{273} \right]^{0.718} \quad (5.36)$$

where T_g is in ($^{\circ}\text{C}$) and μ in $\text{kg/m}\cdot\text{s}$.

5.4.2 Solids properties

The particle size distribution of the sand used in both the hydrodynamic and heat transfer experiments was determined by sieving. Care was taken in these determinations to select appropriate sample sizes and sieving times and a series of experiments were carried out to ensure that the selections had been correctly made. All sieve samples were obtained by splitting the entire solids in the system using a rifler.

The two sand particle size distributions used in the experiments (P.S.D. 1 and P.S.D. 2) are shown graphically in Figures 5.20 and 5.21 respectively.

The particle size distribution of the glass beads was determined using a sedimentation balance and verified by examining the beads under a microscope. The glass beads particle size distribution curve is given in Figure 5.22.

Care was taken throughout the experimental program to ensure that the particle size distribution of the solids under study did not evolve either by generation or loss of fines. At regular intervals the entire system was emptied, the solids split using a rifler and the

PERCENT SMALLER THAN (%)

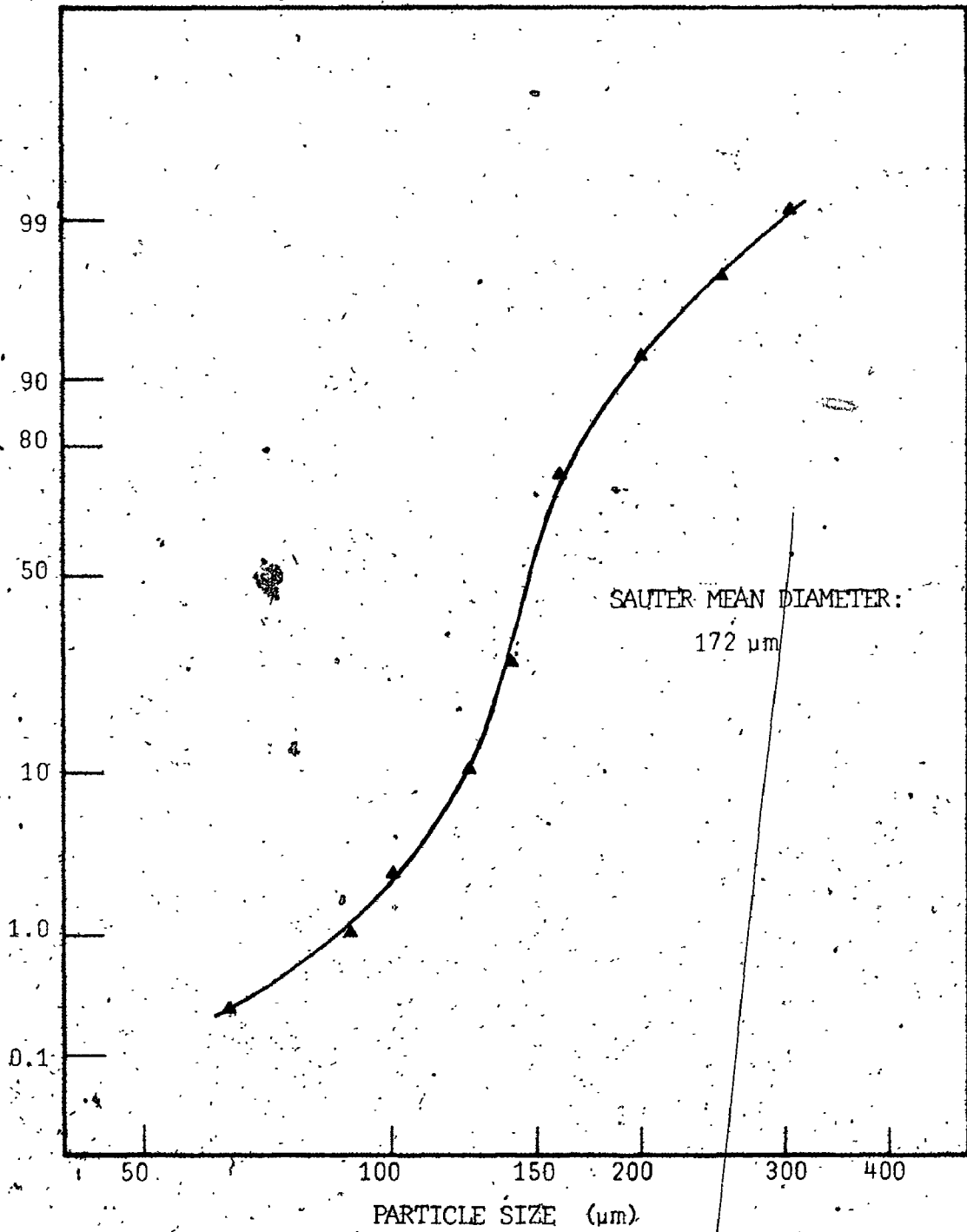


FIGURE 5:20 P.S.D 1 Sand particle size distribution

PERCENT SMALLER THAN (%)

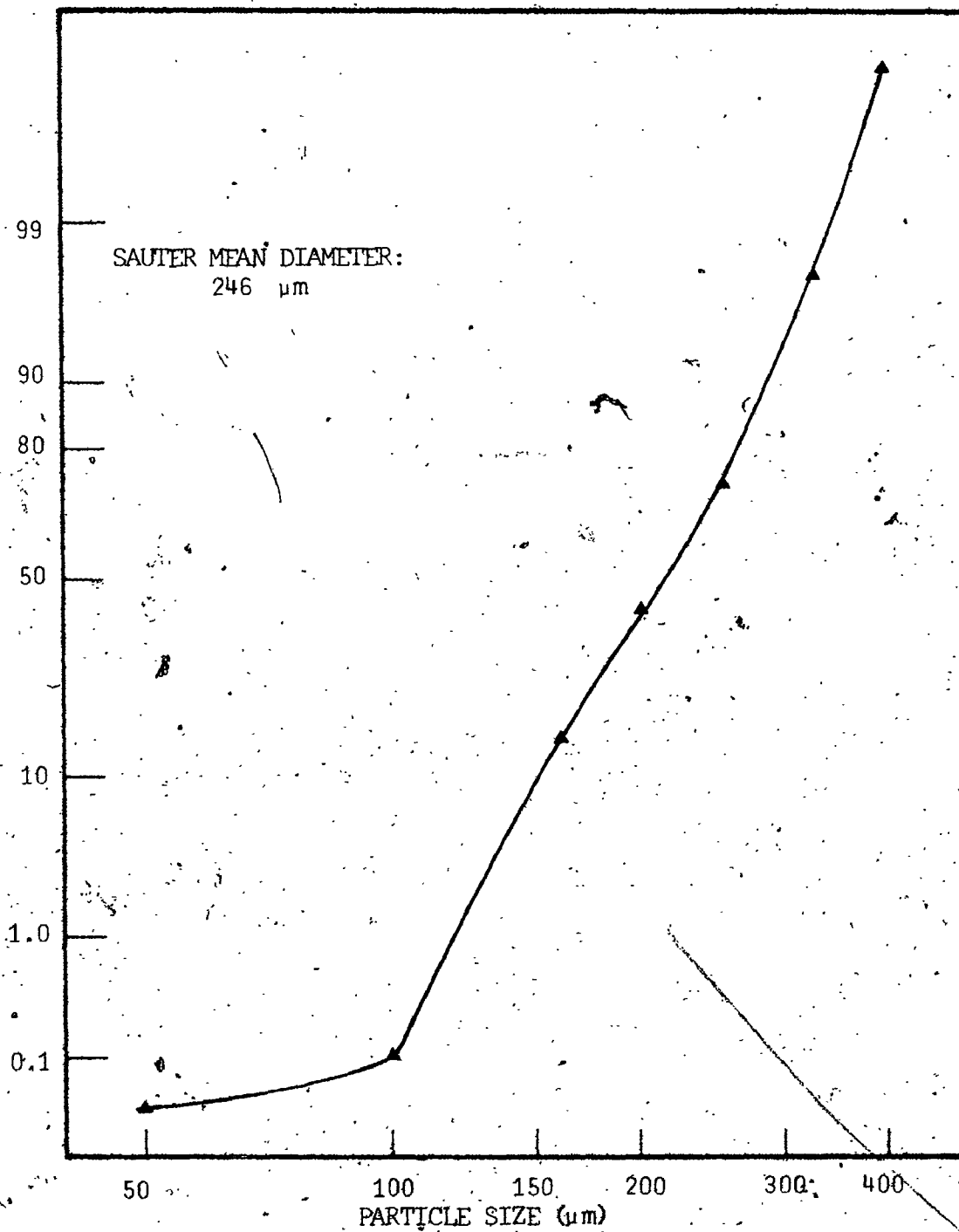


FIGURE 5.21 P.S.D. 2 Sand particle size distribution

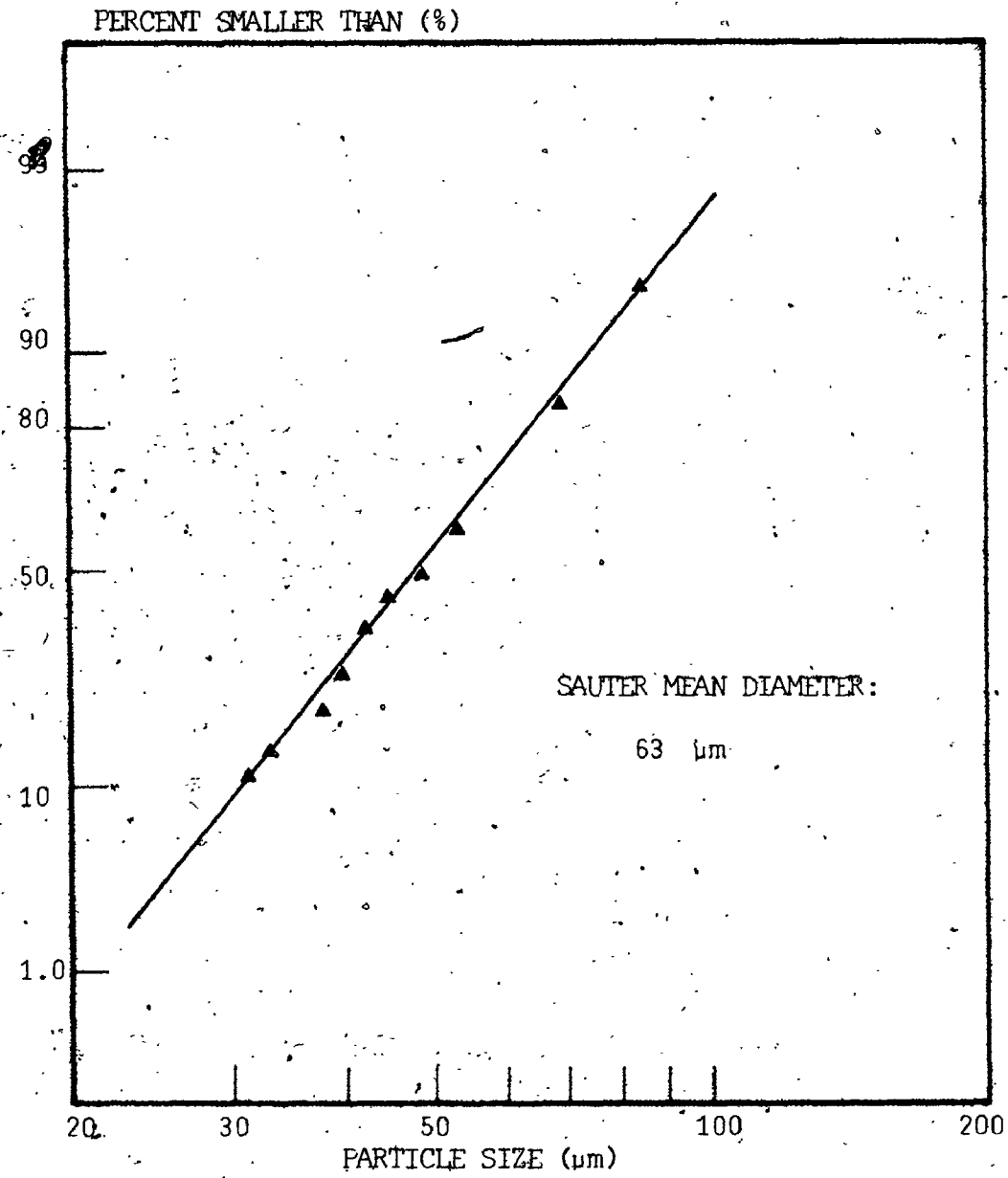


FIGURE 5.22 Glass beads particle size distribution

particle size distribution was checked. No change in either the sand or the glass beads was observed.

Particle density was measured using a picnometer. The values found were $2\,620\text{ kg/m}^3$ and $2\,420\text{ kg/m}^3$ for the sand and glass beads respectively.

The heat capacity of the sand was measured by the sand supplier in a calorimeter. The heat capacity used for calculation purposes was obtained from the following expression derived from the supplier's data :

$$(C_s)_{\text{sand}} = 1.65 T_s + 695.0 \quad (5.37)$$

$$0 < T_s < 200^\circ\text{C}$$

where T_s is in $^\circ\text{C}$ and C_s in $(\text{J/kg } ^\circ\text{C})$.

EXPERIMENTAL RESULTS AND DISCUSSION

6.1 Experimental programme

The experimental programme was divided into four distinct phases. The initial phase consisted of hydrodynamic and heat transfer experiments carried out on the installation without solids flow. Well established pressure drop and heat transfer coefficient correlations for single phase flow were used to verify the operation of the newly-constructed experimental installation. The results from these experiments were presented and discussed in Chapter 5.

The second experimental phase consisted of preliminary pneumatic transport runs (Series A). These experiments had the objectives of verifying the overall installation with solids flow and examining the qualitative behavior of vertical pneumatic transport. In order to compare results with similar data available in the literature, the entire series consisted of fixing a particular solids flowrate and varying the gas velocity over the range 0-30 m/s. These experiments resulted in curves of the Zenz type (cf. Section 2.2.1) which have been traditionally used to present pneumatic transport data.

The first three sub-series in this group included only gas and solids flowrate and pressure profile measurements. The final two sub-series (A-4, A-5) represented the first runs with mean solids concentration measurements using the pneumatic slide valves. As other

workers have frequently made reference to unknown influences of electrostatic effects on pneumatic transport behavior, the humidity of the transport line. air was varied during the latter of these two series as described in Section 5.2.1:

The third phase of the experimental programme represented the main series suspension hydrodynamic results. The general equation analysis having shown the solids concentration to be of essential importance in the determination of transport line pressure drop (see Chapter 7), these experiments consisted of varying solids flowrates at a number of different gas velocities. The analysis also showed that the additional pressure drop due to the solids could be less than that given by the solids hold-up when mean solids velocities at the wall were directed downwards. For this reason a number of gas velocities only slightly in excess of the terminal velocities of the solids were examined.

Data of this type were obtained for P.S.D.1 sand (Series B). Additional data for a slightly larger sand (P.S.D.2 : Series C) were obtained during the heat transfer experiments. Finally the general hydrodynamic behavior exhibited during the sand runs was checked for another solid, (glass beads) having a substantially smaller mean particle size (Series D).

The complete hydrodynamic measurement system was in place for all of these experiments. In addition, the particle size distribution of the solids held-up between the two slide valves was determined for most of the Series B runs.

The final phase of the experimental programme consisted of measuring suspension-pipe wall heat transfer coefficients at varying solids flowrates for a number of different gas velocities. The choice of varying the solids concentration at constant gas velocity resulted from two factors: Firstly, pressure drop data from the pneumatic transport runs were found to be explainable by assuming the radial solids concentration and velocity profiles to be independent of the mean solids concentration. Secondly, this hypothesis when used in the energy equation analysis predicted a unique relation, independent of α_s between heat transfer coefficient ratios and loading ratios for a given gas velocity. The heat transfer runs, carried out in the above-mentioned way, thus provided the possibility to confirm this theoretical result.

Table 6.1 summarizes the operating parameters for all the suspension experimental data obtained. Complete lists of raw data are given in Appendices IV and V.

The present chapter will be concerned with the presentation and discussion of these experimental results making reference to comparable results in the literature. The following chapter will analyse the results more fully in light of the Probabilistic Multiphase Flow Equations developed in Chapter 4.

6.2 Preliminary pneumatic transport runs

Typical pressure profiles obtained during the preliminary Series A pneumatic transport runs are shown in Figure 6.1. The two profiles in the figure are linear both before the lower slide valve

TABLE 6.1.

SUMMARY OF EXPERIMENTAL PROGRAMME

Series	W_s (g/s)	U_g (m/s)	P.S.D.	Measurements
A-1	1	$0 < U_g < 10$	2	$W_s, W_g, \Delta P_{ss}$
A-2	2	$0 < U_g < 10$	2	$W_s, W_g, \Delta P_{ss}$
A-3	3	$0 < U_g < 10$	2	$W_s, W_g, \Delta P_{ss}$
A-4	50	$0 < U_g < 25$	2	$W_s, W_g, \Delta P_{ss}, \alpha_s$
A-5	25	$0 < U_g < 25$	2	$W_s, W_g, \Delta P_{ss}, \alpha_s$
B-1	$0 < W_s < 1.2$	1.48	1	$W_s, W_g, \Delta P_{ss}, \alpha_s, P.S.D.$
B-2	$0 < W_s < 3.1$	1.72	1	$W_s, W_g, \Delta P_{ss}, \alpha_s, P.S.D.$
B-3	$0 < W_s < 4.8$	2.00	1	$W_s, W_g, \Delta P_{ss}, \alpha_s, P.S.D.$
B-4	$0 < W_s < 25$	4.30	1	$W_s, W_g, \Delta P_{ss}, \alpha_s, P.S.D.$
B-5	$0 < W_s < 30$	5.22	1	$W_s, W_g, \Delta P_{ss}, \alpha_s, P.S.D.$
B-6	$0 < W_s < 30$	6.16	1	$W_s, W_g, \Delta P_{ss}, \alpha_s, P.S.D.$
B-7	$0 < W_s < 30$	10.2	1	$W_s, W_g, \Delta P_{ss}, \alpha_s, P.S.D.$
C-1	$0 < W_s < 10$	4.63	2	$W_s, W_g, \Delta P_{ss}, \alpha_s, h_{ss}$
C-2	$0 < W_s < 25$	5.23	2	$W_s, W_g, \Delta P_{ss}, \alpha_s, h_{ss}$
C-3	$0 < W_s < 10$	3.37	2	$W_s, W_g, \Delta P_{ss}, \alpha_s, h_{ss}$
C-4	$0 < W_s < 25$	6.19	2	$W_s, W_g, \Delta P_{ss}, \alpha_s, h_{ss}$
C-5	$0 < W_s < 35$	10.2	2	$W_s, W_g, \Delta P_{ss}, \alpha_s, h_{ss}$
D-1	$0 < W_s < 10$	4.61	glass beads	$W_s, W_g, \Delta P_{ss}, \alpha_s$
D-2	$0 < W_s < 10$	3.40	glass beads	$W_s, W_g, \Delta P_{ss}, \alpha_s$
D-3	$0 < W_s < 5$	2.00	glass beads	$W_s, W_g, \Delta P_{ss}, \alpha_s$

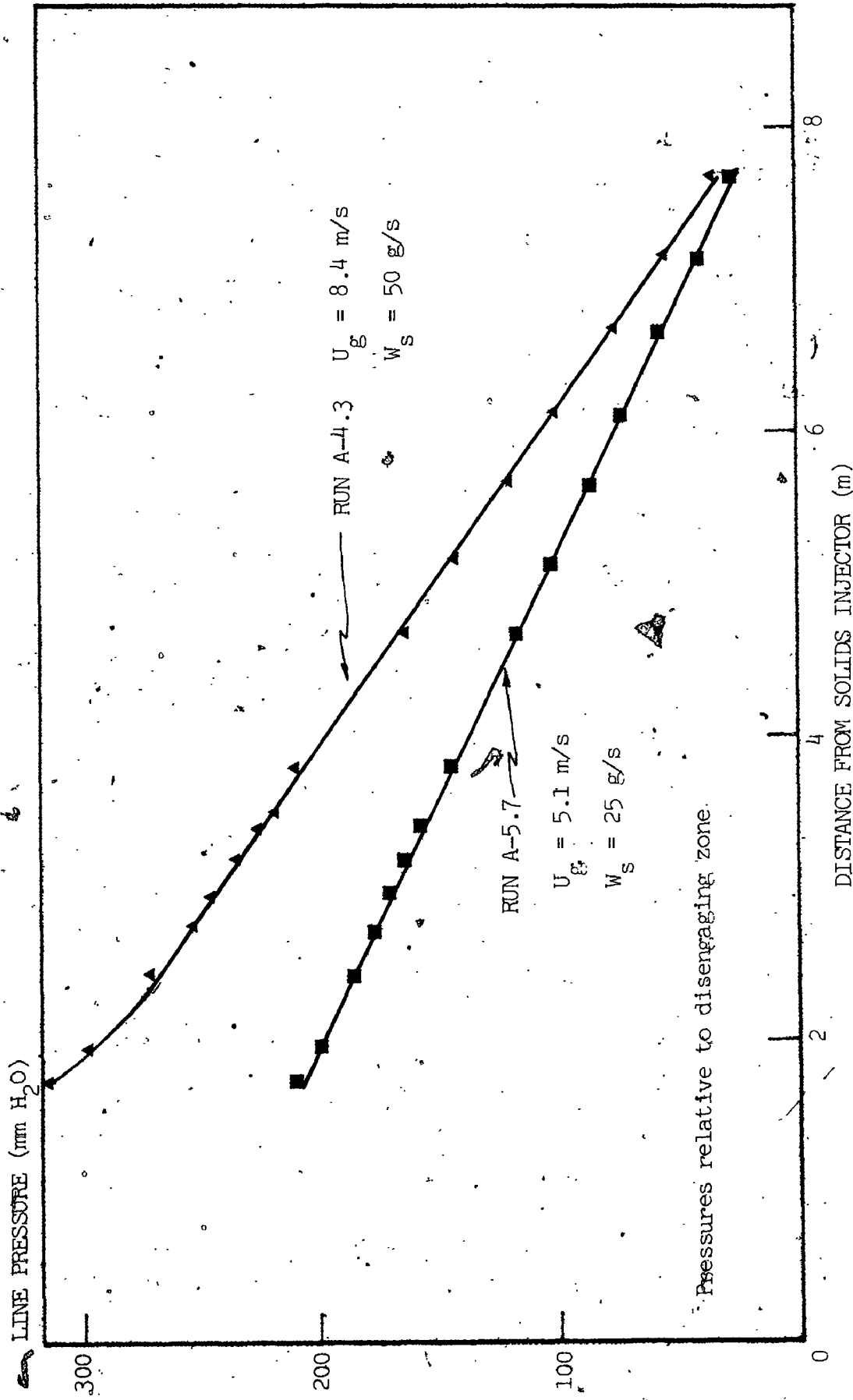


FIGURE 6.1 Typical line pressure profiles : Preliminary suspension runs

and in the test section itself. These constant pressure gradients indicate that the solids had been fully accelerated before they had reached the test section; subsequent hold-up measurements were thus made under fully developed flow conditions.

Little or no disruption in the pressure profile was observed across the bottom slide valve. As mentioned in Section 5.2.3 this signified that the valves were indeed "full bore" and that their presence in the line led to a negligible modification of the flow. The significance of this test was evidenced on a number of occasions when the slide valves became mis-aligned. Even the overlapping of the slide valve plate by 1 to 2 mm in the transport line resulted in large discontinuities in the pressure profile at the slide valve locations and in non-linear profiles in the test section as solids were re-accelerated following collisions with the plate. The pressure profiles were, as a result, closely monitored at the beginning of each run and the observation of anomalies led to the dismantling of the valves to check their alignment.

During the Series A runs, pressure taps were located only starting from a distance of 1950 mm above the solids injection point (hence, the first point at position 1950 in Figure 6.1). Additional taps were later added to cover the entire transport line as shown by the two profiles given in Figure 6.2 from the main hydrodynamic runs Series B. The additional information shown on these curves is that, while the flow was fully developed before the test section, the acceleration zone, where the profile was non-linear, nevertheless extended to over two meters. This is of the same order of magnitude as

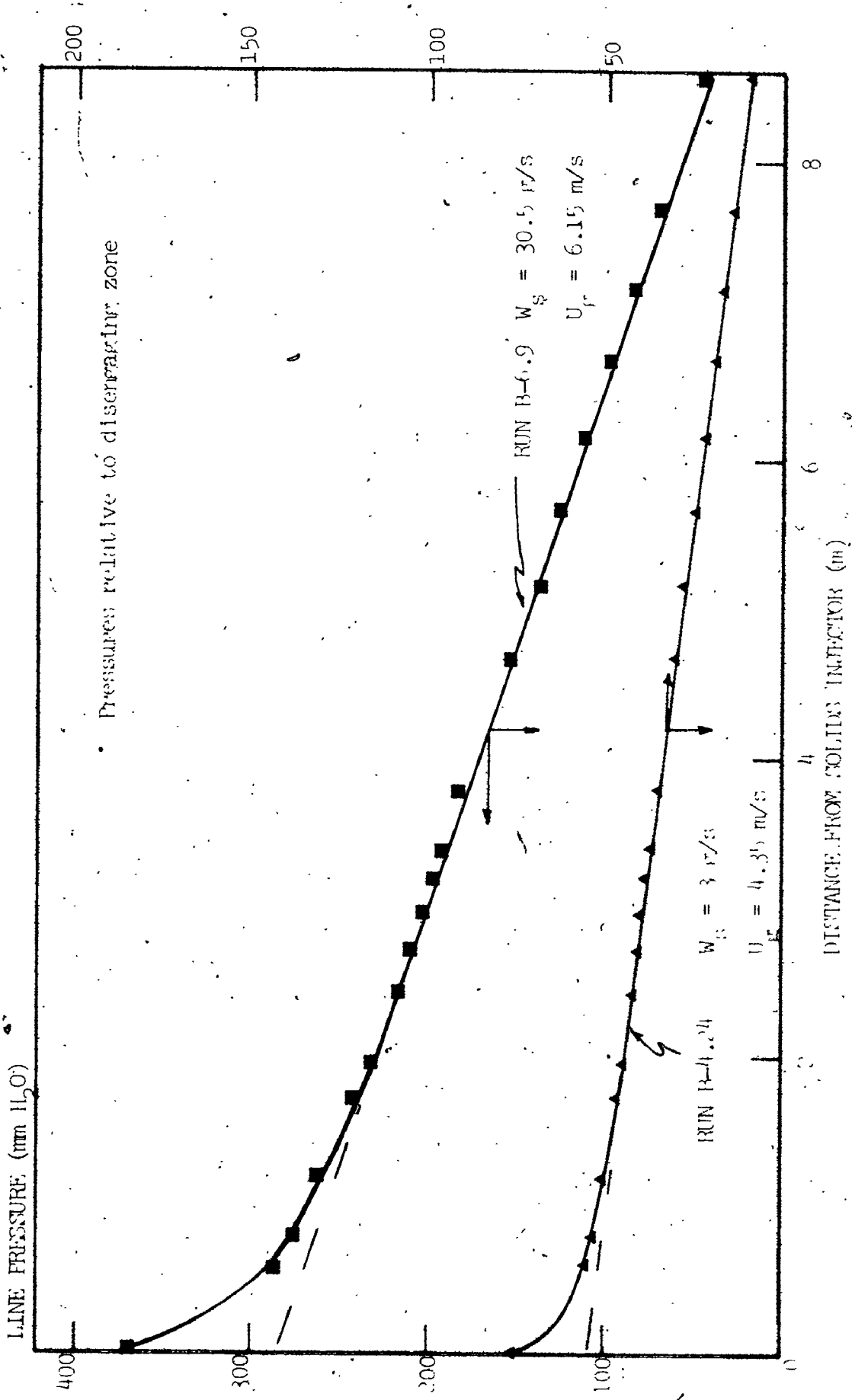


FIGURE 6. Typical line pressure profiles: Multi hydrodynamic series

what was found under variable operating conditions by Capes and Nakamura (20), Konno and Saito (29) and Stermerding (126). This observation is interesting to compare with the overall pipe lengths used in previous studies on supposedly "fully developed" suspension flows as given in Table 2.1 : four of the 18 studies listed used pipes which were less than 3 m in length.

It will finally be noted that the pressure profile between Positions 3450 and 3780, that is, upstream from the bottom slide valve showed the same gradients as that in the test section. This justified the use of the former profile in extracting pressure drop data during the heat transfer Series 7 runs.

Figures 6.3 and 6.4 show plots of transport line fully developed flow unit pressure drop as a function of gas velocity for the five different solids flowrates examined in the preliminary Series A experiments. These curves show the same typical behavior as the Zenz graphical representation of pneumatic transport given in Figure 2.1 : minimum pressure drops are exhibited at gas velocities which increase with increasing solids flowrates. Below and above the gas velocity at which the minimum occurs there are steep pressure drop rises.

Two types of points are shown for the Series A-8 runs in Figure 6.4, those obtained with a transport line gas relative humidity of less than 25% and those obtained at greater than 25% relative humidity. All points fall on the same curve leading to the conclusion that electrostatic forces had a negligible effect on the pressure drop measurements.

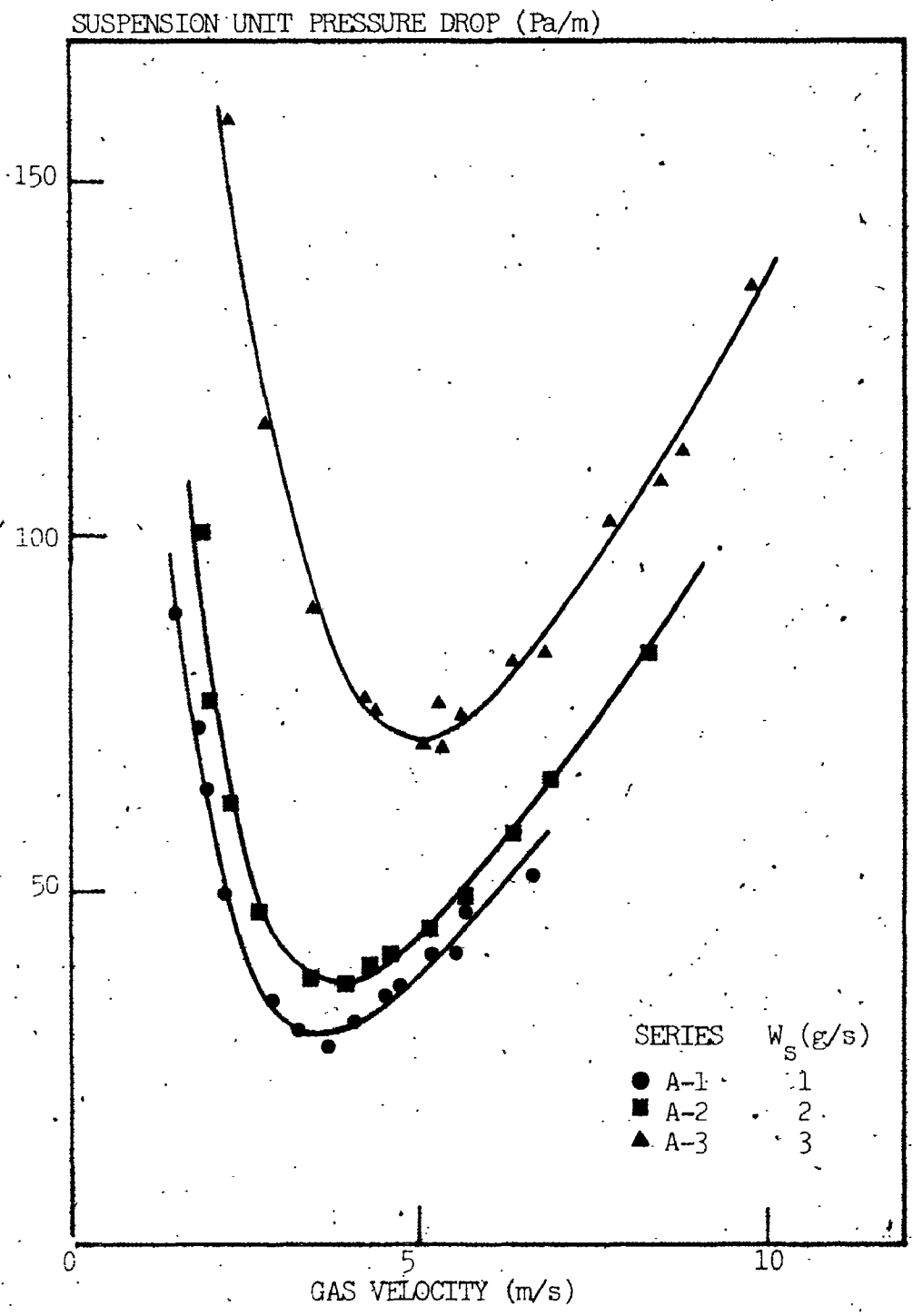


FIGURE 6.3 Suspension pressure drop as a function of gas velocity: Low solids flowrates

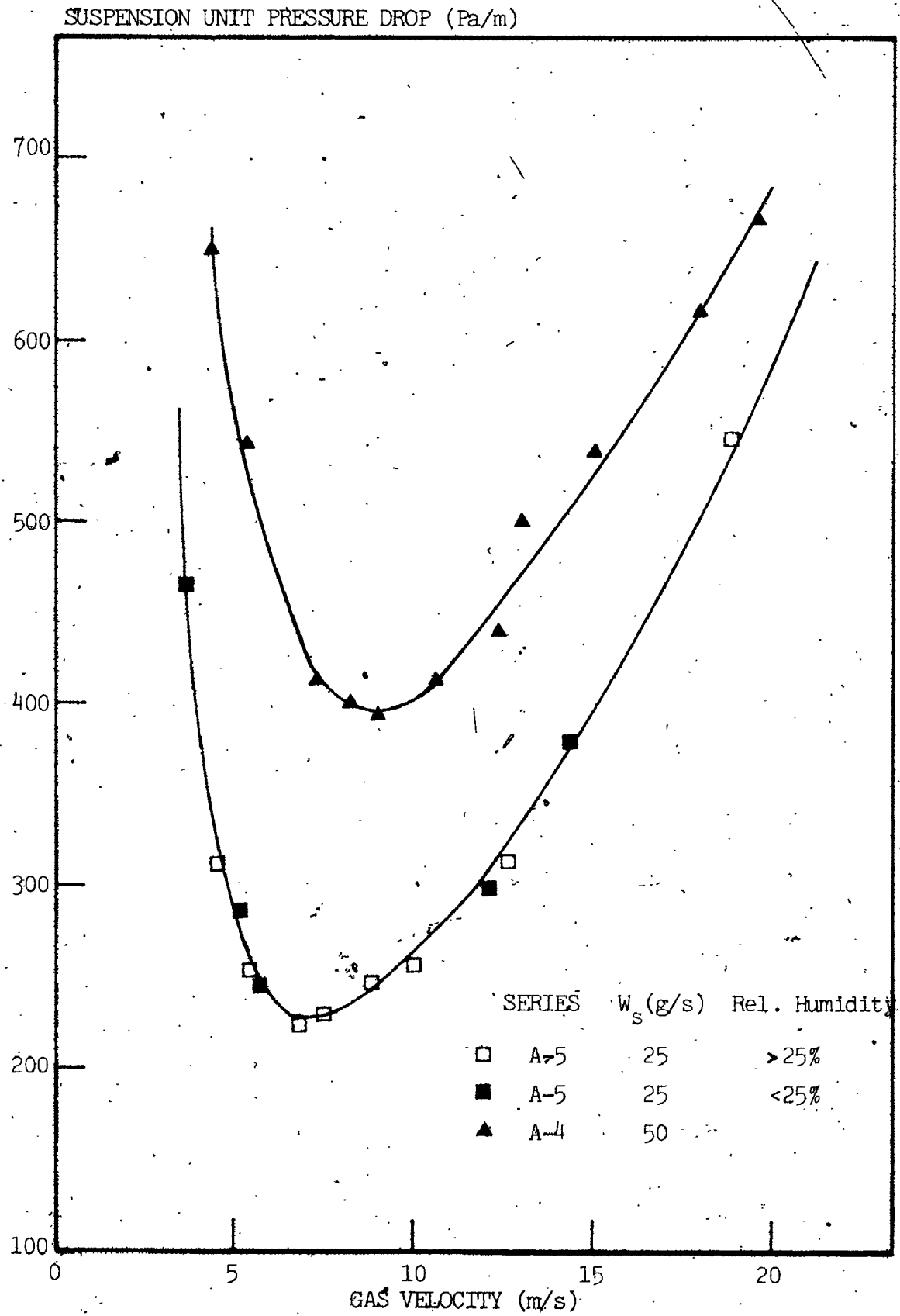


FIGURE 6.4 Suspension pressure drop as a function of gas velocity: High solids flowrates

Figures 6.5 and 6.6 show the mean solids concentration measured in the test section as a function of gas velocity for Series A-4 and A-5 respectively. The latter figure again show little difference between the humidified transport gas results as opposed to those obtained without humidification.

The curves show a steep decline in the mean solids concentration as the gas velocity was increased. This is an expected result since the mean solids concentration, at a given solids flowrate, is inversely proportional to the solids velocity with the latter factor logically increasing with gas velocity. The same data are plotted as mean solids velocity as a function of gas velocity in Figure 6.7. These results show a linear increase in the solids velocity as gas velocity is increased with little difference between the 25 g/s (Series A-5) and 50 g/s (Series A-4) results. The slope of the curve obtained by regressing the mean solids velocity values is approximately equal to 1 (0.96) indicating a relatively constant slip velocity as gas velocity is increased. The intercept at zero mean solids velocity is 1.7 m/s which is approximately equal to the terminal settling velocity of the P.S.D. 2 sand used in these series. The variations in mean solids velocity with gas velocity were examined more systematically in Series B, C and D to be discussed in the following sections.

Overall the results of these preliminary experiments served to verify the operation of the pneumatic conveying installation: hydrodynamically fully developed flow was seen to have been achieved before the suspension had reached the test section; solids flowrate measurement techniques were found to give good precision even at very low

MEAN SOLIDS CONCENTRATION ($\alpha_s \times 10^3$)

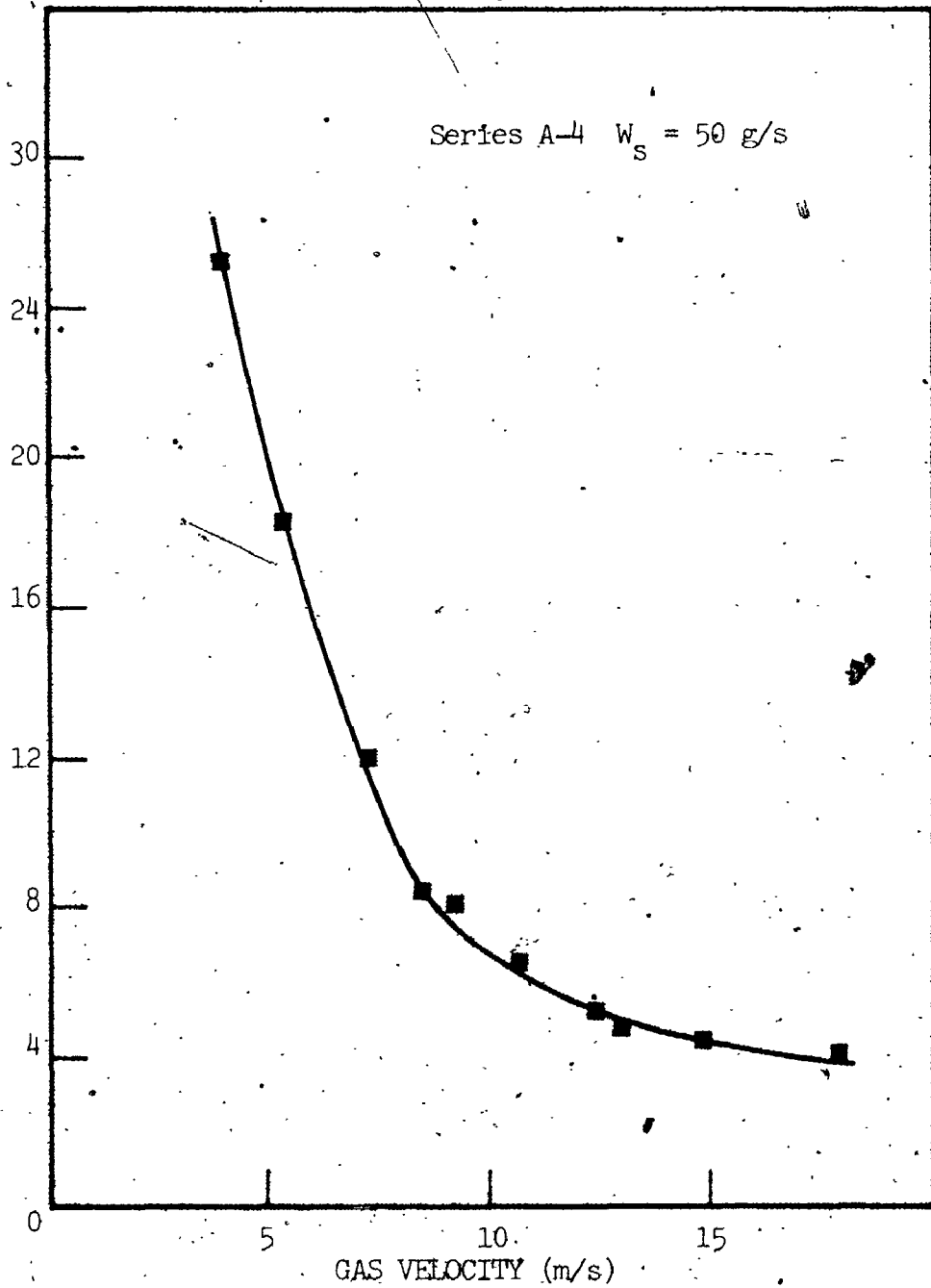


FIGURE 6.5 Mean solids concentration as a function of gas velocity (Series A-4)

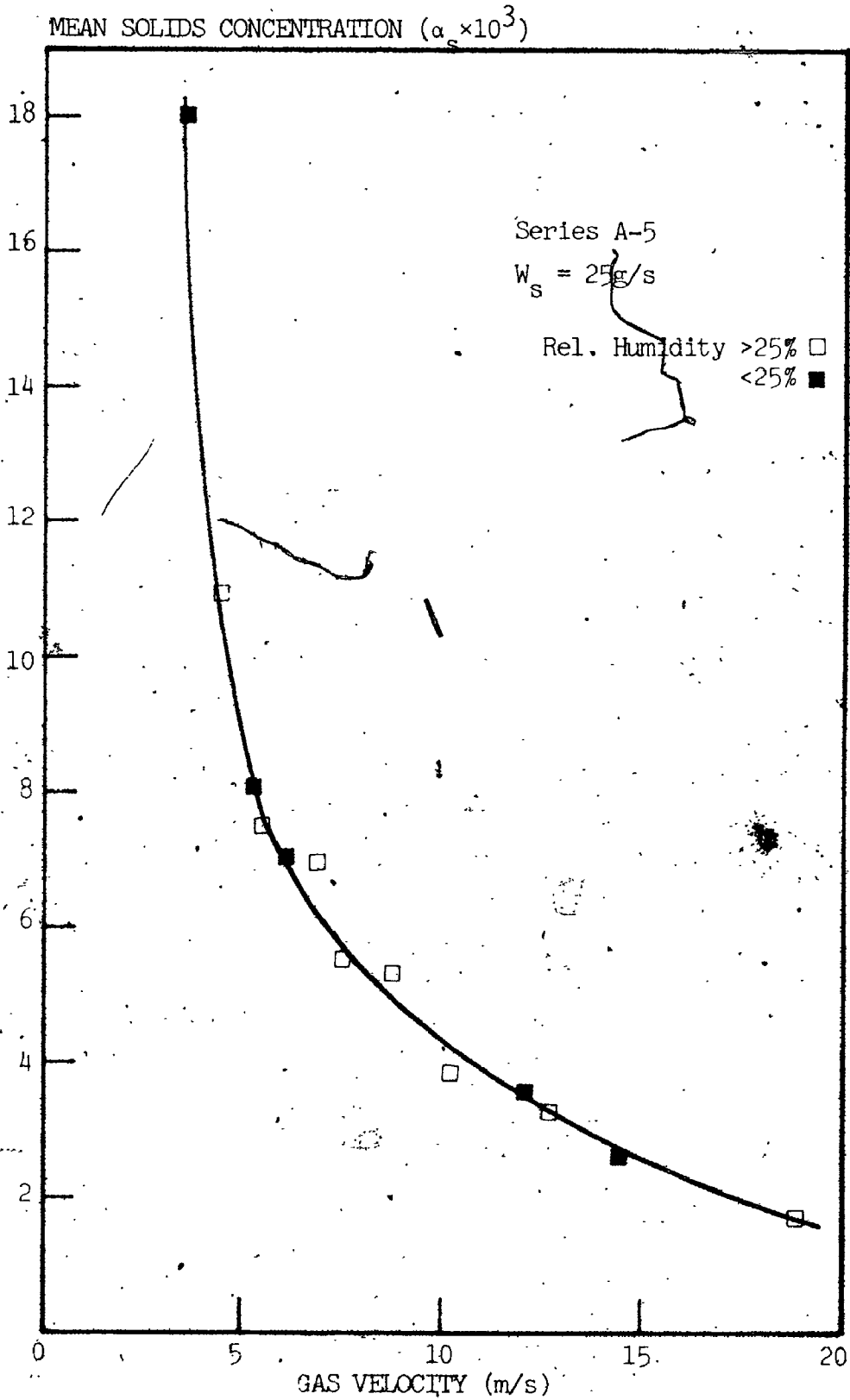


FIGURE 6.6 Mean solids concentration as a function of gas velocity (Series A-5)

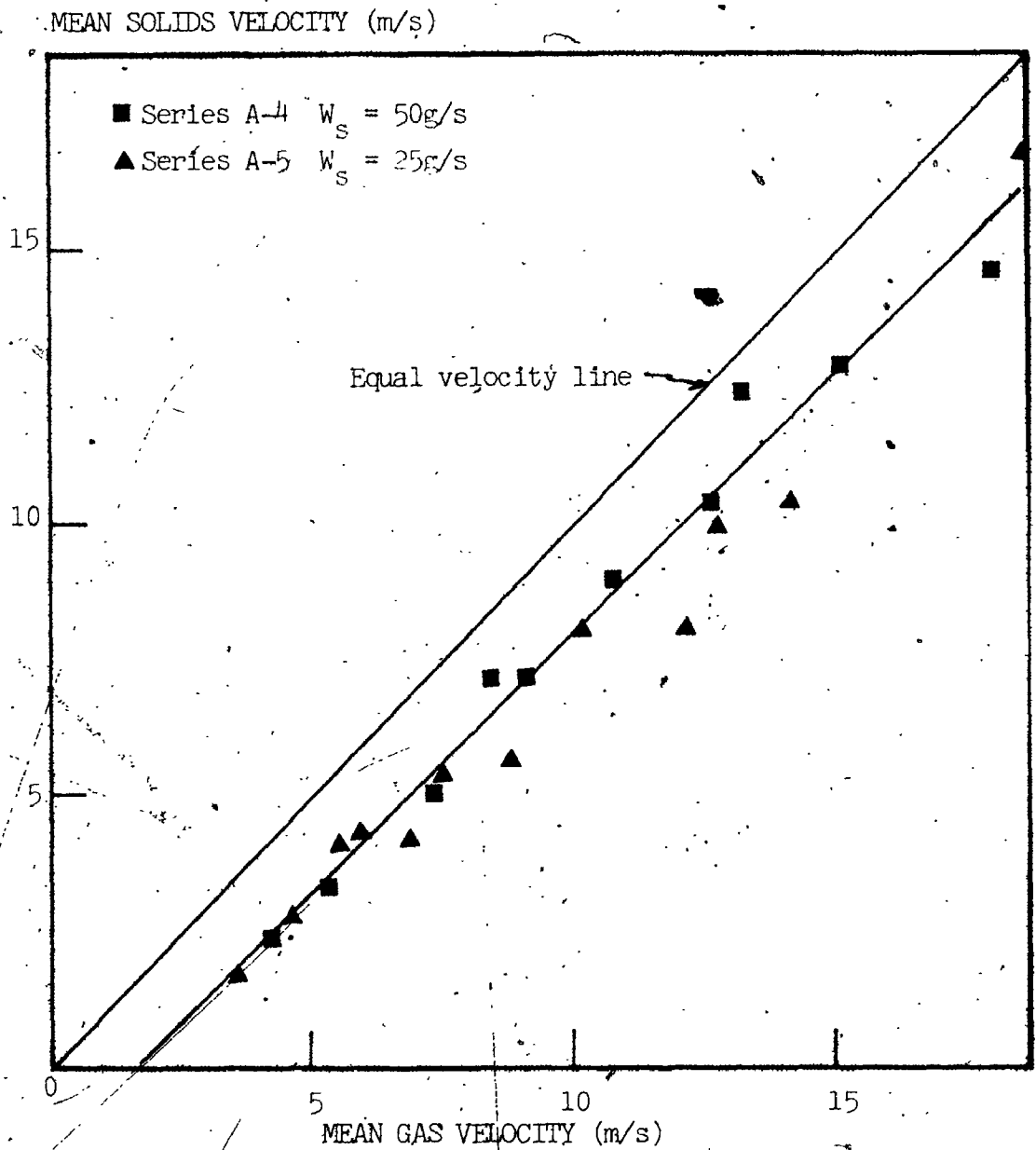


FIGURE 6.7 Variation of mean solids velocity with mean gas velocity: Series A-4, A-5

solids flowrates as shown in Figure 6.3 where distinct pressure drop curves were obtained at solids flowrates of 1 and 2 g/s. Finally, the general qualitative behavior of the vertical suspension flows corresponded well with that evidenced in similar studies. These results prepared the way for the more systematic investigations to be presented in the following sections.

6.3 Main series suspension hydrodynamic results

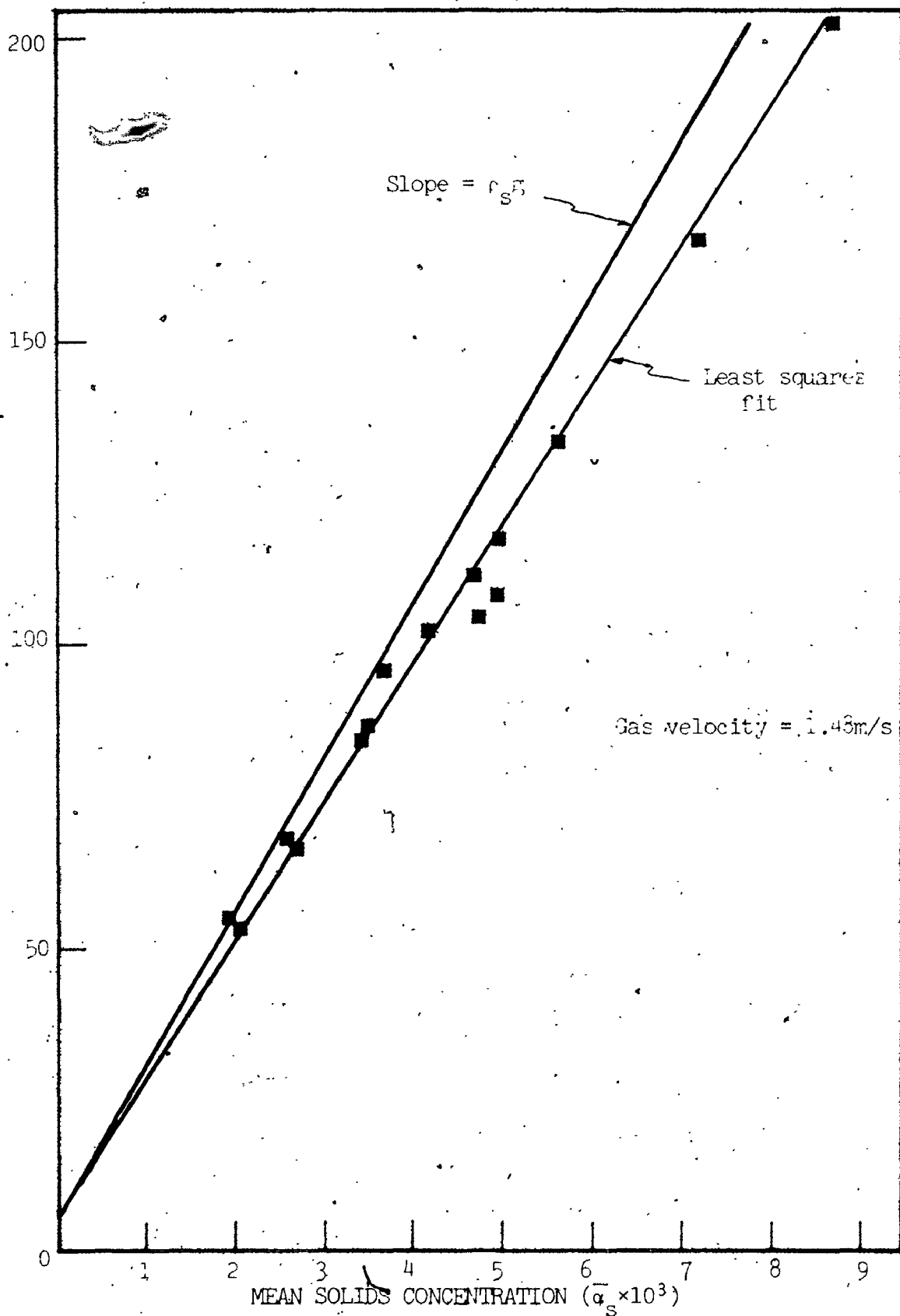
6.3.1 Pressure drop as a function of mean solids concentration

Figures 6.8 through 6.14 summarize fully developed flow suspension pressure drops as a function of mean solids concentration for the different gas flowrates examined in Series B, C and E.

The curves in the figures all have similar characteristics: pressure drops show linear increases with mean solids concentration over the entire range of 0 to 1% mean solids concentration by volume which corresponds to loading ratios of up to 18. All the curves have positive intercepts which in all cases correspond well with the pressure drop of the gas flowing at the same superficial velocity in the absence of solids particles as determined by the experimental Moody diagram given in Figure 5.7.

The slopes of all the curves in Figures 6.8 to 6.14 increase with increasing gas velocity. This signifies that the overall pressure drop in the suspension is generally different from that given by the sum of the pressure drops due to the gas flowing alone and that due solids hold-up in qualitative accordance with results obtained by numerous

SUSPENSION UNIT PRESSURE DROP (Pa/m)

FIGURE 6.8 Pressure drop versus $\bar{\alpha}_S$: Series B-1

ly dependent on the gas velocity but not in a unique way; the slope of the curve in Figure 6.15 is less than that of the linear portion of the curve for the larger P.S.D. 2 sand given in Figure 6.16; the glass bead curve (Figure 6.17) increases more rapidly than the other two however. Some reasons for this will be suggested by the analysis carried out in Chapter 7.

6.3.2 Mean solids concentrations as a function of solids flowrates

Typical variations in the mean solids concentrations as functions of solids flowrates for the different gas velocities examined in Series B, C and D are summarized in Figures 6.18 to 6.21. These curves exhibit linear relationships between the two variables at fixed gas velocities over the entire range examined; that is, as in the previous section, up to loading ratios of 18 and mean solids concentrations of up to 1%. Note that the data presented in Figure 6.21 for the glass beads are indicated by bars due to the solids sticking problem described previously.

The mean solids velocity across the pipe cross-section is directly proportional to the quotient W_s / \bar{n}_s as follows:

$$W_s = \rho_s \bar{a}_s \bar{V}_s A \quad (6.11)$$

The linear relationship between the solids flowrate and the mean solids concentration thus implies that the mean solids velocity was constant, that is, independent of the solids loading for a given gas flowrate.

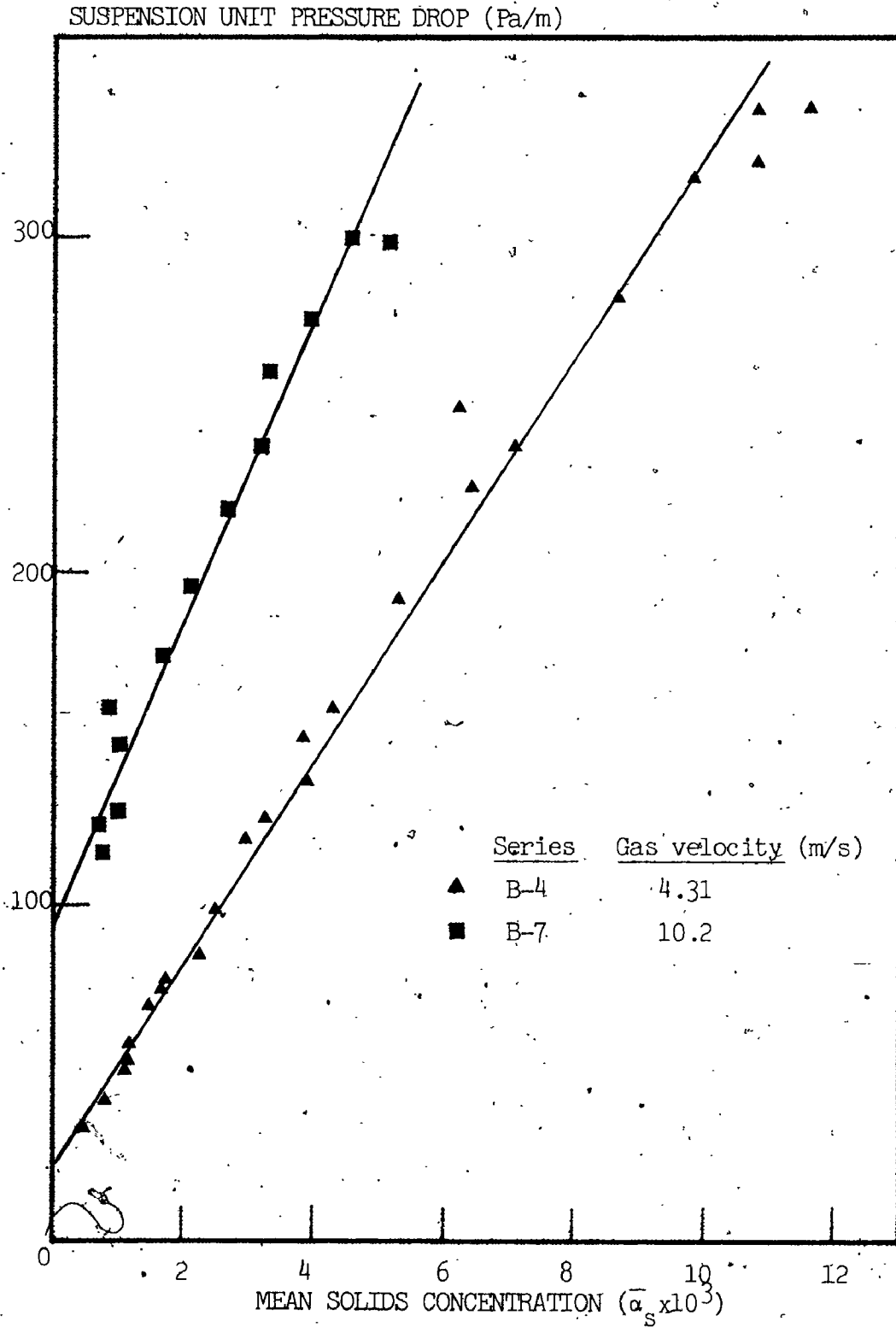


FIGURE 6.10 Pressure drop versus $\bar{\alpha}_s$: Series B-4, B-7

SUSPENSION UNIT PRESSURE DROP (Pa/m)

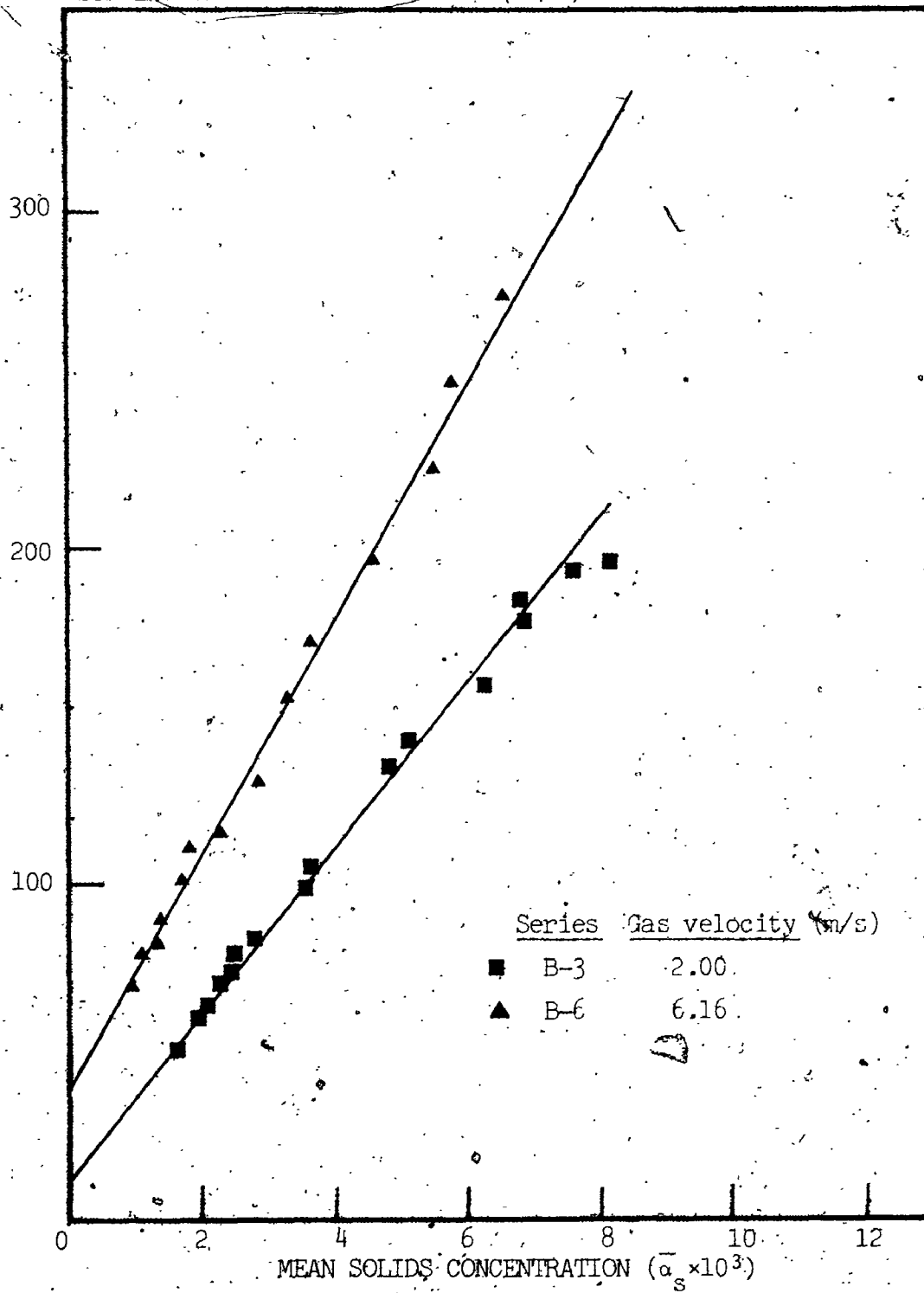


FIGURE 6.11 Pressure drop versus $\bar{\alpha}_s$; Series B-3, B-6

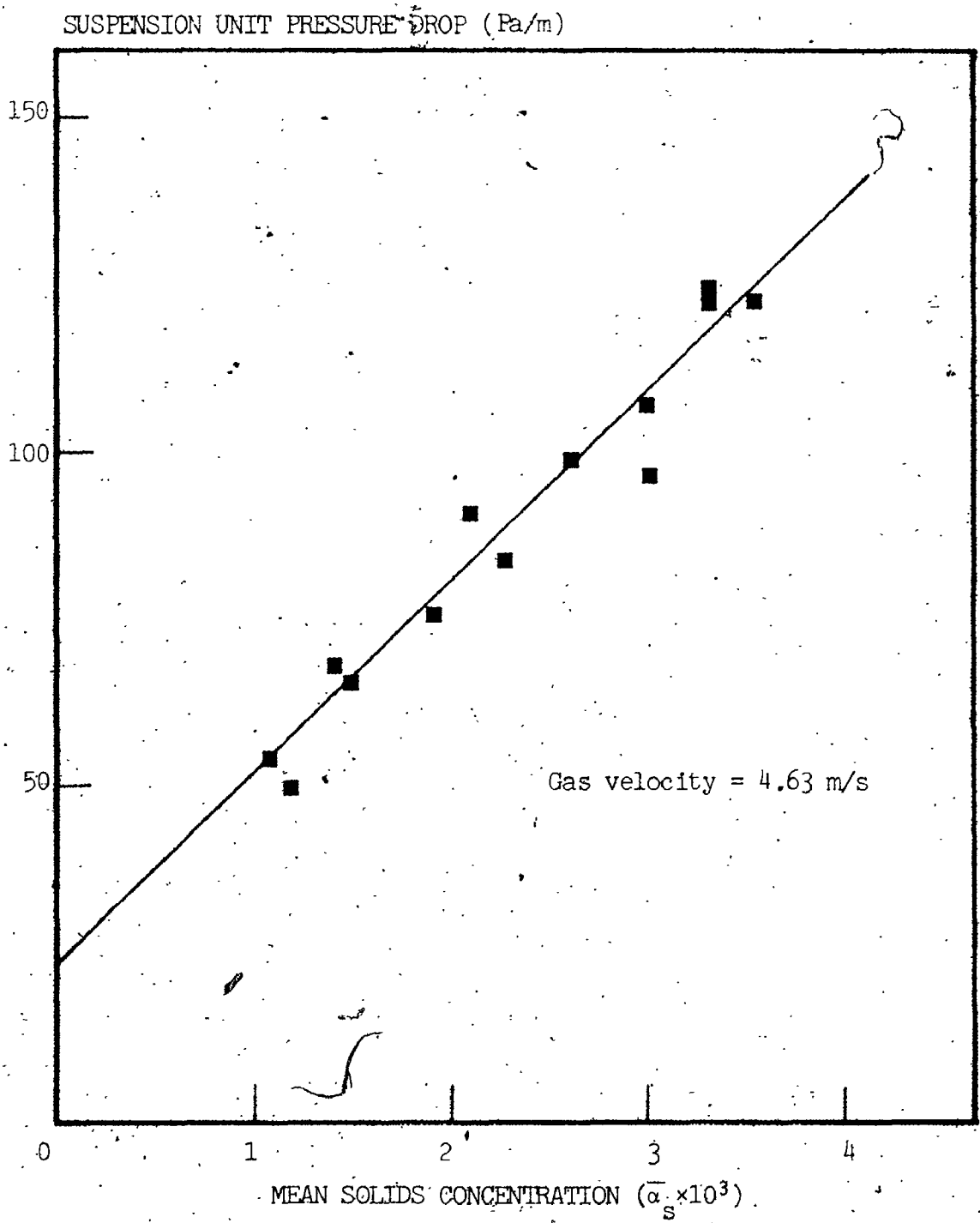


FIGURE 6.12 Pressure drop versus $\bar{\alpha}_s$; Series C-1

SUSPENSION UNIT PRESSURE DROP (Pa, m)

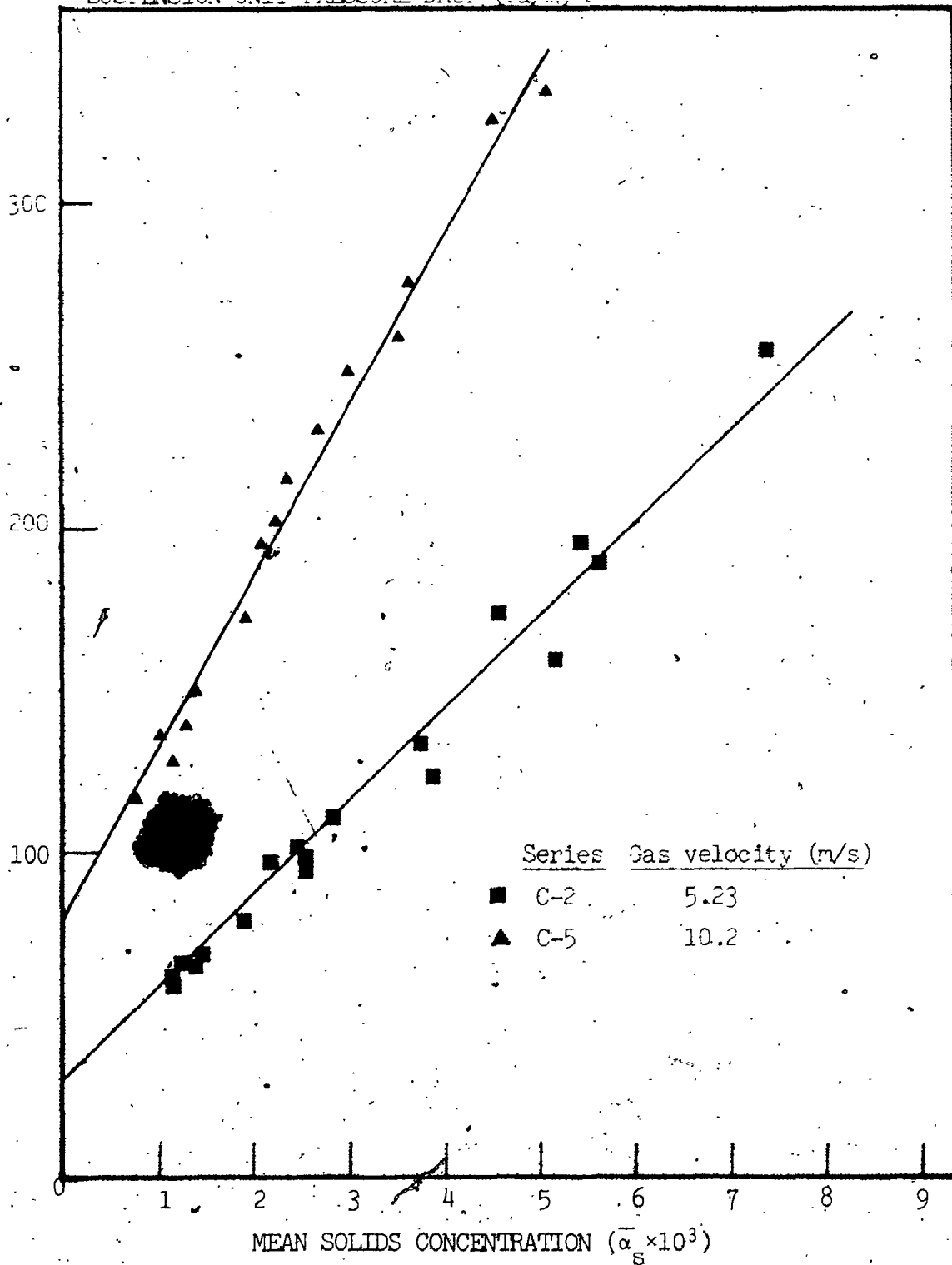
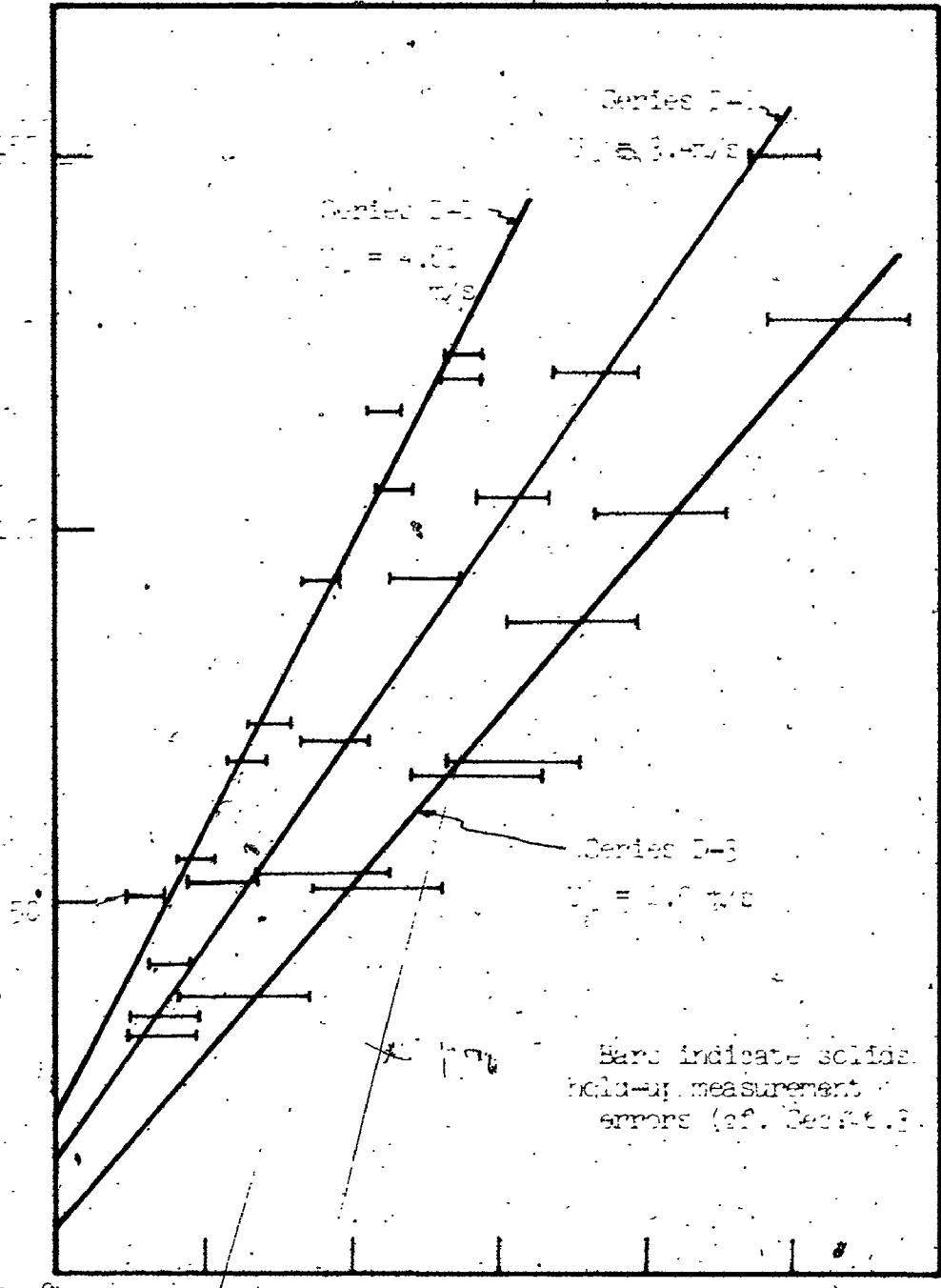


FIGURE 6.13 Pressure drop versus $\bar{\alpha}_s$: Series C-2, C-5

SUSPENSION UNIT PRESSURE DROP (Pa/m)



MEAN SOLIDS CONCENTRATION ($\bar{c} \times 10^3$)

FIGURE 6.14. Pressure drop versus \bar{c} : Glass beads.

other workers' discussed in Chapter 2. Nevertheless, since the overall pressure drop minus that due to the gas flowing alone remained proportional to the mean solids concentration and the pressure drop attributable to the solids hold-up is strictly proportional to $\bar{\alpha}_s$, the additional pressure drop due to the solids was, as a consequence, also found to be proportional to $\bar{\alpha}_s$.

A remarkable aspect of the data in these figures however is the fact that the slopes of the curves at low velocities ($U_g = 1.48$ m/s, 1.72 m/s, 2.00 m/s in Series B-1, B-2 and B-3 respectively and $U_g = 2.7$ m/s in Series D-3) are less than $\bar{\alpha}_s g$ which would have been the case had the solids hold-up been solely responsible for the difference in suspension pressure drop from that due to the gas flowing alone. In the Harju and Molstad three component pressure drop expression this finding signifies that the frictional pressure drop due to the presence of the solids would be negative. Recalling that all the friction factor correlations presented in Chapter 2 predict positive solids frictional losses, it is obvious that these methods would be inapplicable in this type of situation.

The observation that total suspension pressure drop can be less than that given by the sum of the gas only and solids hold-up pressure drops has, as was mentioned in Chapter 2, been observed on at least two other occasions (Capes and Nakamura (20) ; Van Swaaij et al. 134), although in larger diameter pipes. Both of the above authors suggested that this occurred under conditions where particle recirculation at the pipe wall was present, the former at low gas velocities, the latter at high solids concentrations and "low to medium gas

velocities". The results here agree with the Capes and Nakamura observation in so far as gas velocity is of major importance. They cited 1.33 times the terminal velocity of the mean particle as the critical velocity at which this occurred. The series B results show the suspension pressure drop to be less than the sum of the gas only and solids hold-up pressure drop at velocities below 2.4 m/s. which is 1.8 times the terminal settling velocity of P.S.D.1 sand ($V_t = 1.35$ m/s based on the Sauter mean diameter and the calculation method given in Ref. 81). The present results disagree with the Van Swaij et al. results obtained in a 250 mm dia. riser on the concentration effect in so far as the curves remain proportional to the mean solids concentration over the range tested even when the slope was less than $\frac{1}{a_s g}$.

As mentioned, both Capes and Nakamura and Van Swaij et al. observed particle recirculation at the pipe wall accompanying this effect. This was also true in the present study. Interpretation of this via the probabilistic multiphase flow equations will be undertaken in Chapter 7.

Additional comments are necessary concerning the glass bead results shown in Figure 6.14. The results, when initially obtained, showed similar variations compared to the sand runs; that is, pressure drops varied as linear functions of the mean solids concentration. Two additional observations were made however: Firstly, the pressure drops were always lower than that given by the sum of the gas only and solids hold-up pressure drops by up to 60%. Secondly, when

the lines were extrapolated to zero solids concentration, the intercepts were substantially lower than the pressure drop given by the gas flowing alone.

It was subsequently discovered that the glass beads were sticking to the inside wall of the test section pipe. The closing of the slide valves jarred the pipe and these solids were therefore recovered with the solids actually held-up by the gas and included in the values obtained for the mean solids concentrations.

As humidification of the transport line gas failed to solve this problem it was postulated that the quantity of solids sticking to the wall was dependent only on the gas velocity and not on the solids concentration, the idea being that, once a layer of solids built up, the "scouring" action of the suspension held the quantity to a more or less steady state value. In order to verify this hypothesis a series of runs were carried out at variable solids flowrates for a given gas flowrate. The system was operated during a length of time equal to a typical pneumatic transport run (approx. 1 hr). The solids flow was then stopped and the slide valves were closed. The test section pipe was then vibrated and all solids sticking to the wall were recovered. This was repeated several times for varying solids flowrates at the three gas velocities tested in the Series D runs. The results of these tests confirmed the initial hypothesis made showing constant quantities of solids sticking to the pipe wall for a given gas velocity and variable solids flowrates and increasing quantities as gas velocity decreased. The Series D data were then re-treated, subtracting the quantities of solids attributable to wall sticking.

For these reasons, the data are presented in Figure 6.13 as bars : the right hand limit represents the uncorrected solids concentration value ; the left hand limit is the new value based on the above-described correction.

The uncertainties associated with this method obviously renders the Series D hold-up results as only of qualitative interest. They nevertheless show the same trends as with the sand data : pressure drops increase linearly with mean solids concentrations. In addition, since the solids sticking to the wall were found to be independent of solids concentration, the slopes of the curves are the same for the corrected and uncorrected values.

The slopes of the pressure drop vs. mean solids concentration curves increase with increasing gas velocity for both the sand experiments and the glass bead experiments. These slopes are plotted in Figures 6.15, 6.16 and 6.17 for the Series B, C and D results respectively. The horizontal lines plotted on the figures represent the pressure drop due to the solids hold-up. As mentioned earlier, the series B and D results show several points below the horizontal line indicating lower than solids hold-up overall pressure drops.

The increases in slope as a function of gas velocity are linear for the three hydrodynamic series, with the exception of Series C-3 results which do not fall in line with the other Series C results. These increases with U_g suggest that in addition to the solids concentration dependence evidenced in Figures 6.8 through 6.14 the difference between the suspension and gas pressure drops is strong-

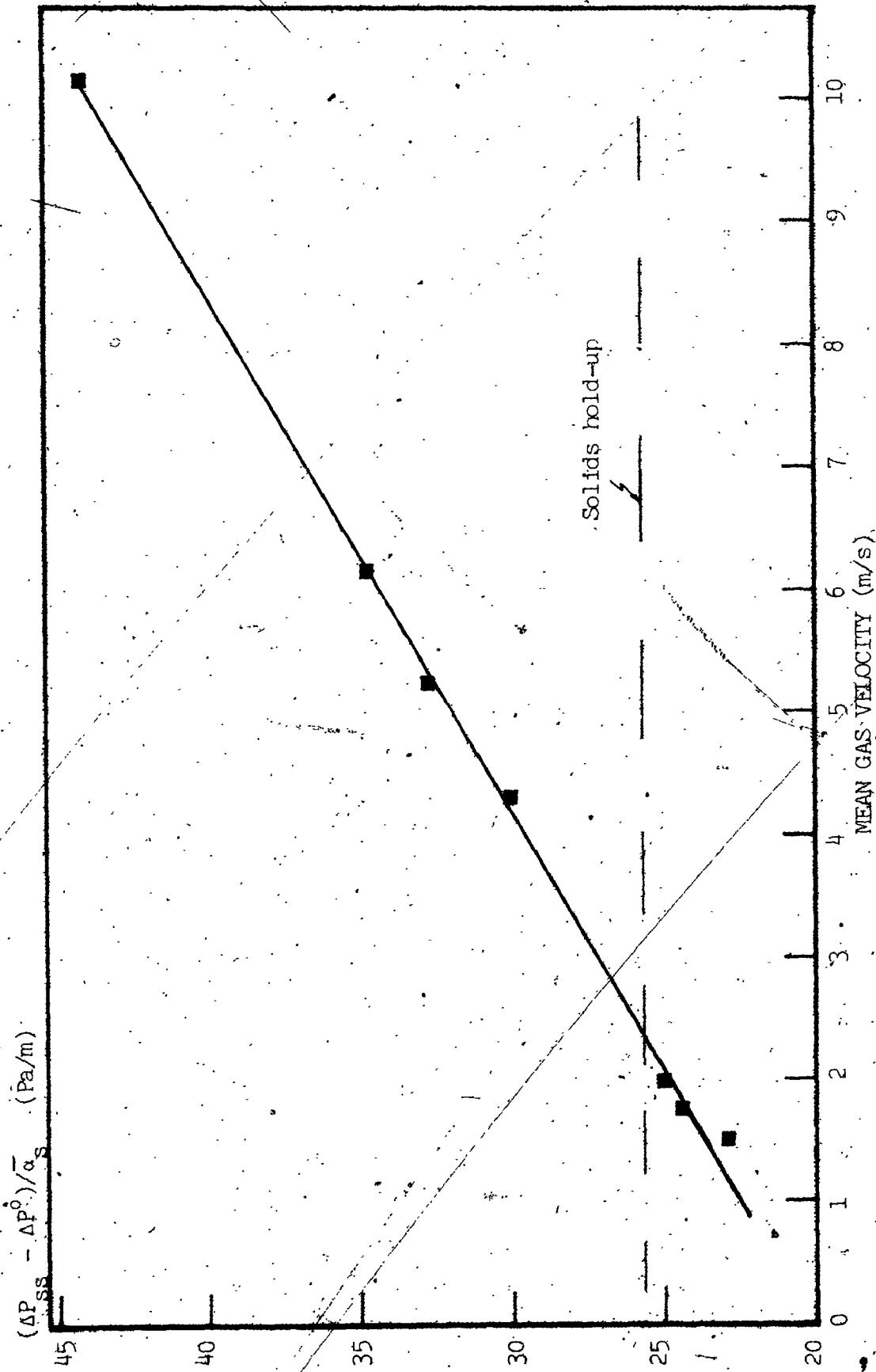


FIGURE 6.15. Slopes of Pressure drop vs. Mean solids concentration curves as a function of gas velocity: SERIES B

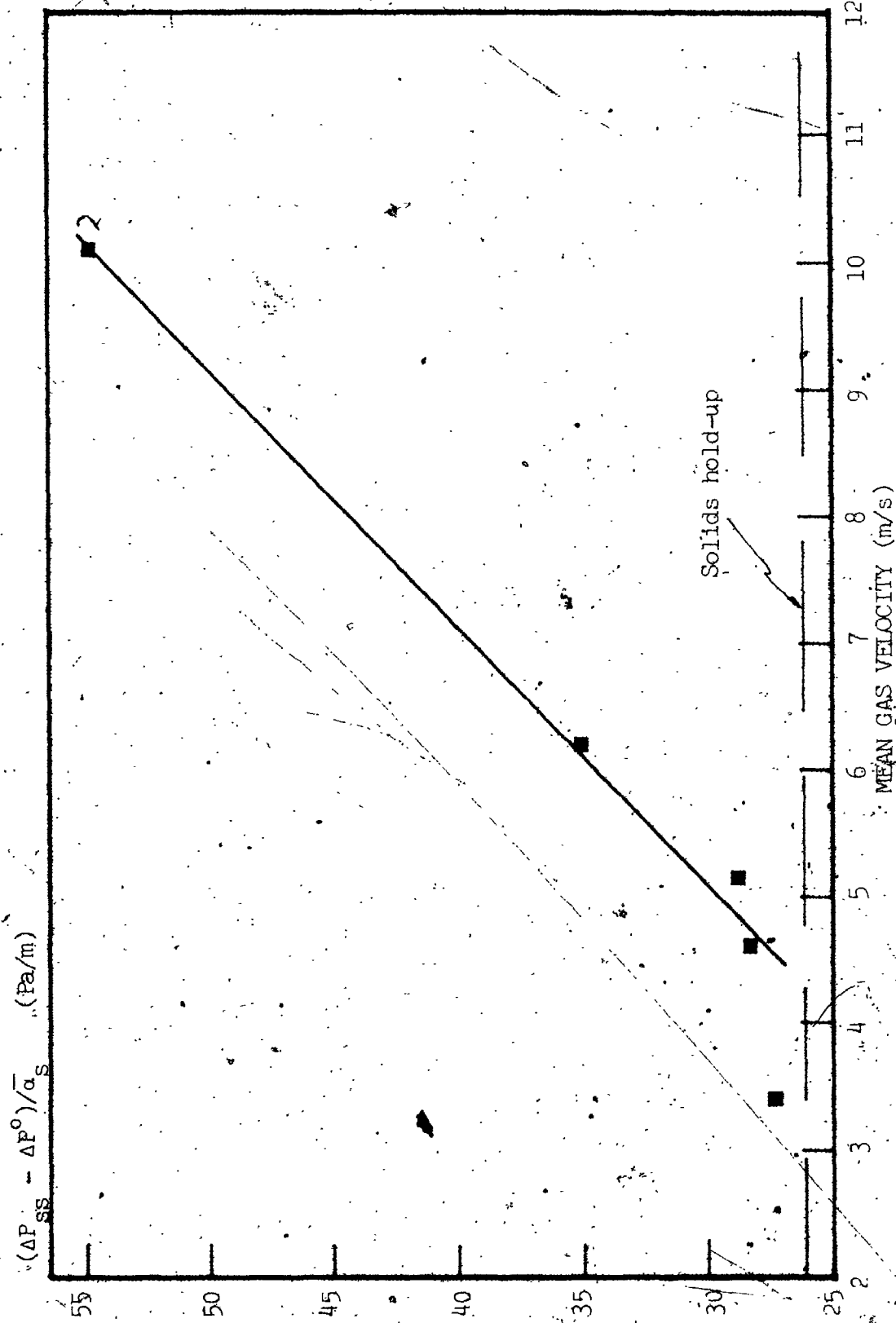


FIGURE 6.16 Slopes of Pressure drop vs. Mean solids concentration curves as a function of gas velocity: SERIES C

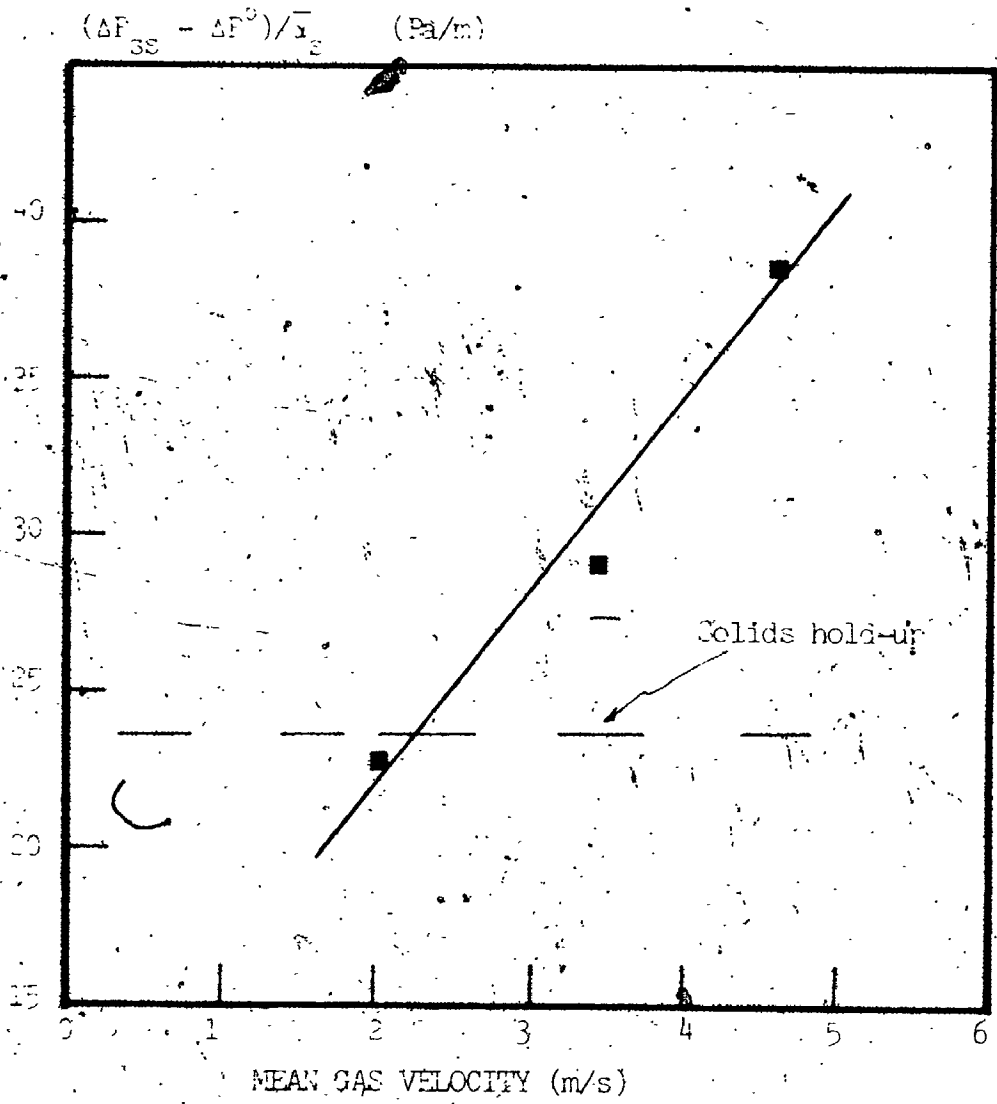


FIGURE 6.17 Slopes of Pressure drop vs. Mean solids concentration curves as a function of gas velocity: SERIES D (Glass beads)

ly dependent on the gas velocity but not in a unique way; the slope of the curve in Figure 6.15 is less than that of the linear portion of the curve for the larger P.S.D. 2 sand given in Figure 6.16; the glass bead curve (Figure 6.17) increases more rapidly than the other two however. Some reasons for this will be suggested by the analysis carried out in Chapter 7.

6.3.2 Mean solids concentrations as a function of solids flowrates

Typical variations in the mean solids concentrations as functions of solids flowrates for the different gas velocities examined in Series B, C and D are summarized in Figures 6.18 to 6.21. These curves exhibit linear relationships between the two variables at fixed gas velocities over the entire range examined; that is, as in the previous section, up to loading ratios of 18 and mean solids concentrations of up to 1%. Note that the data presented in Figure 6.21 for the glass beads are indicated by bars due to the solids sticking problem described previously.

The mean solids velocity across the pipe cross-section is directly proportional to the quotient w_s/\bar{n}_s as follows:

$$w_s = \rho_s \bar{\alpha}_s \bar{V}_s A \quad (6.1)$$

The linear relationship between the solids flowrate and the mean solids concentration thus implies that the mean solids velocity was constant, that is, independent of the solids loading for a given gas flowrate.

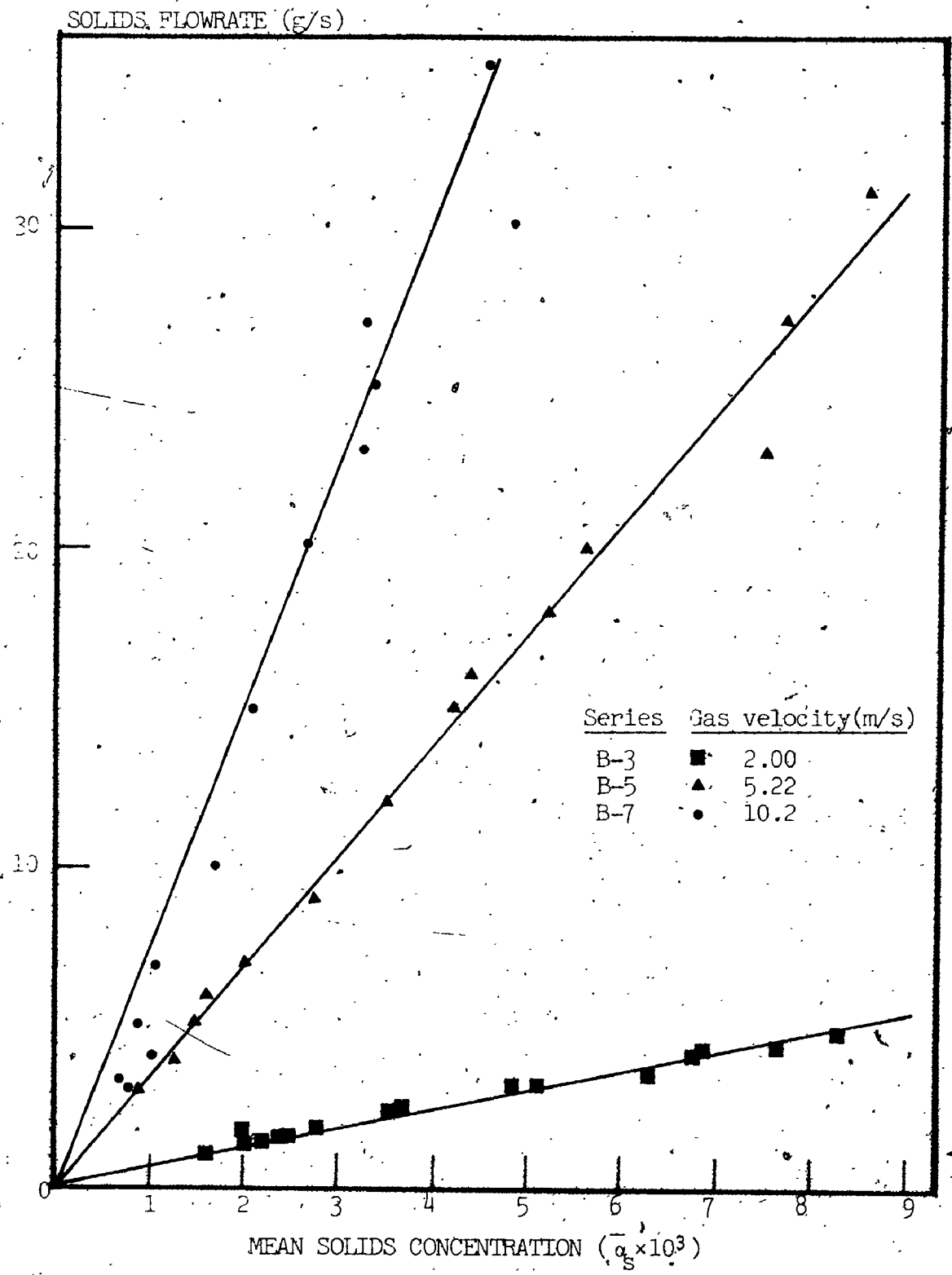


FIGURE 6.13 Solids flowrate versus Mean solids concentrations:
SERIES B-3,B-5,B-7

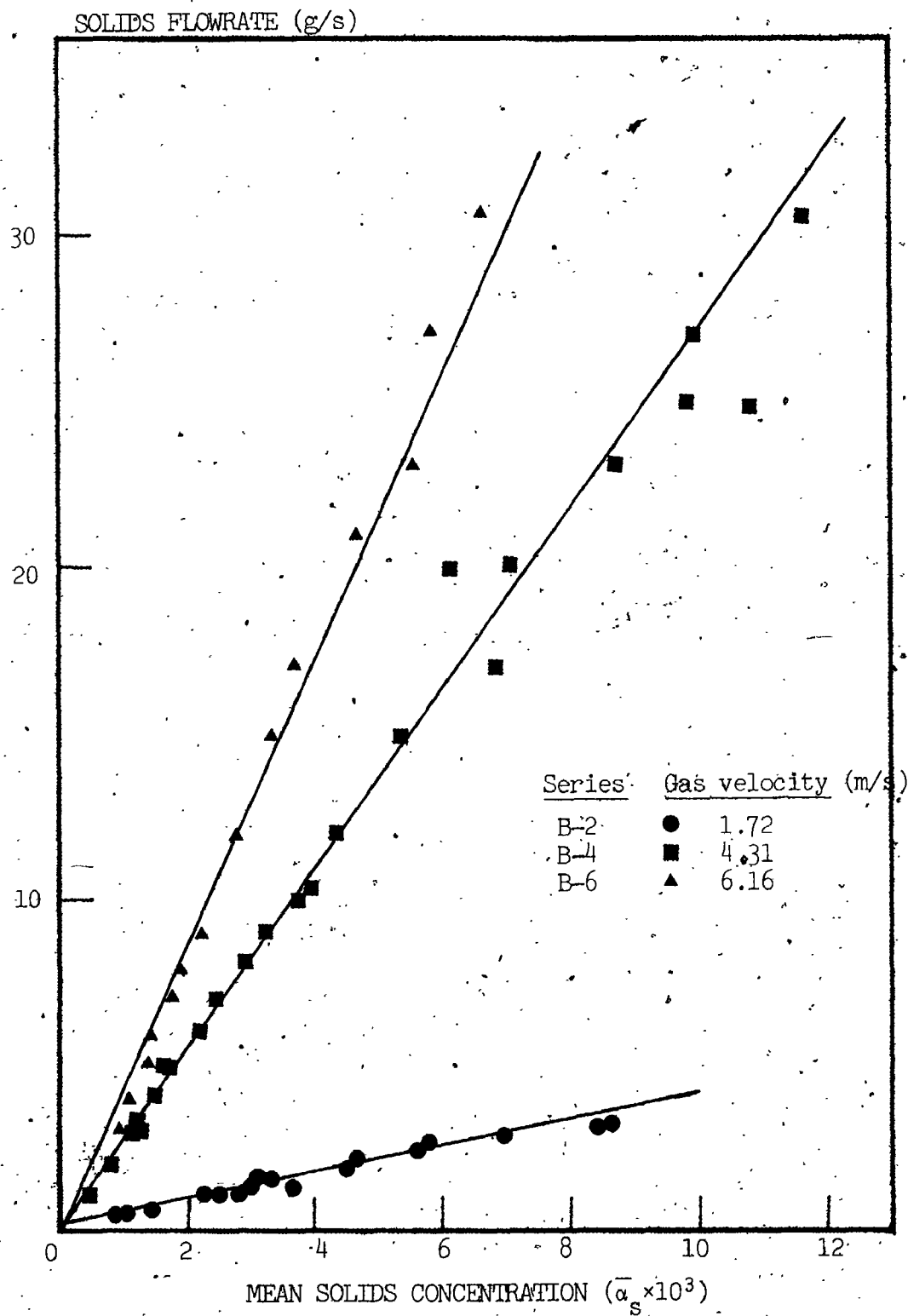


FIGURE 6.19 Solids flowrate versus Mean solids concentration:
SERIES B-2, B-4, B-6

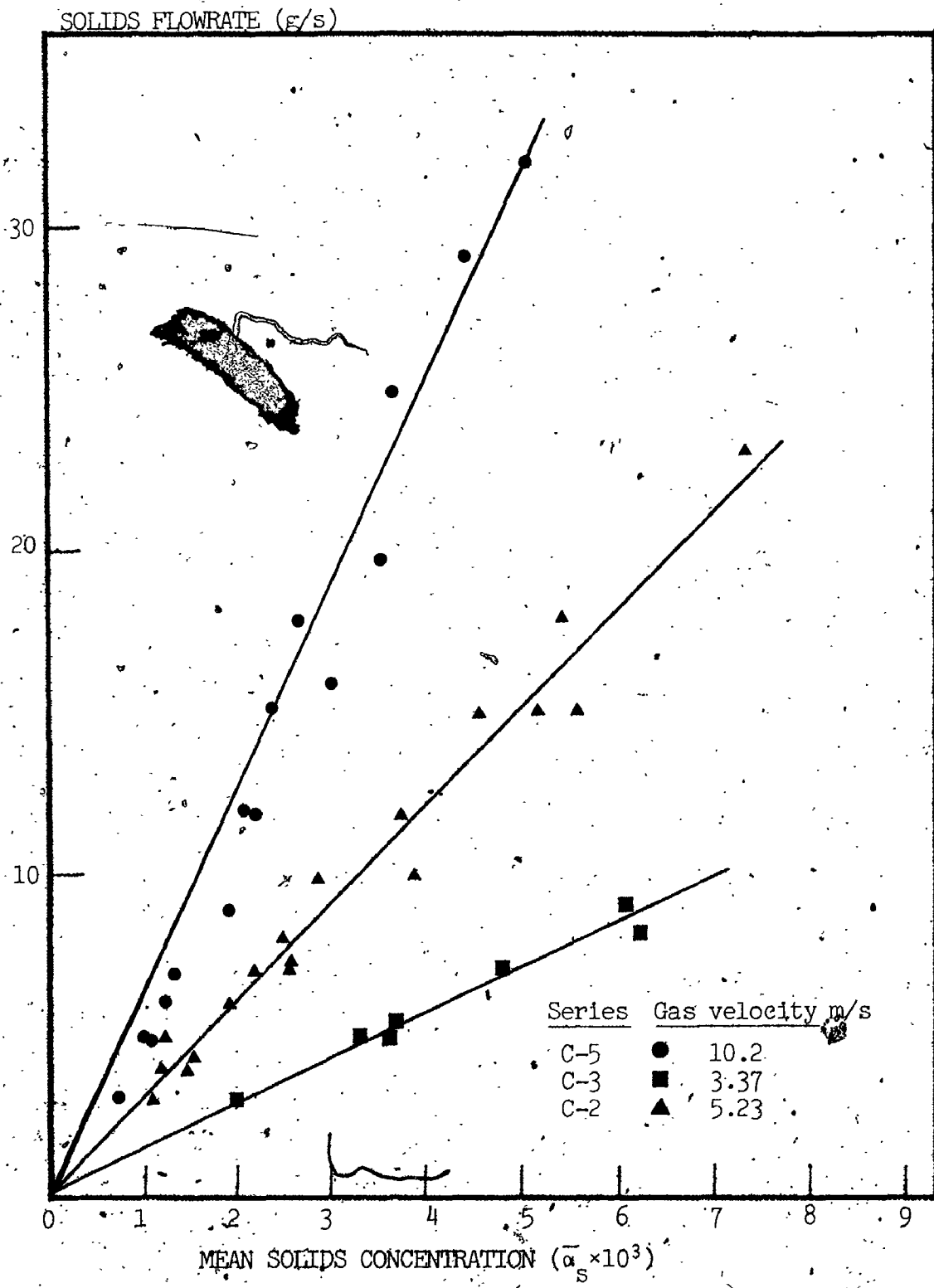


FIGURE 6.20 Solids flowrate versus Mean solids concentration
 SERIES C-2, C-3, C-5

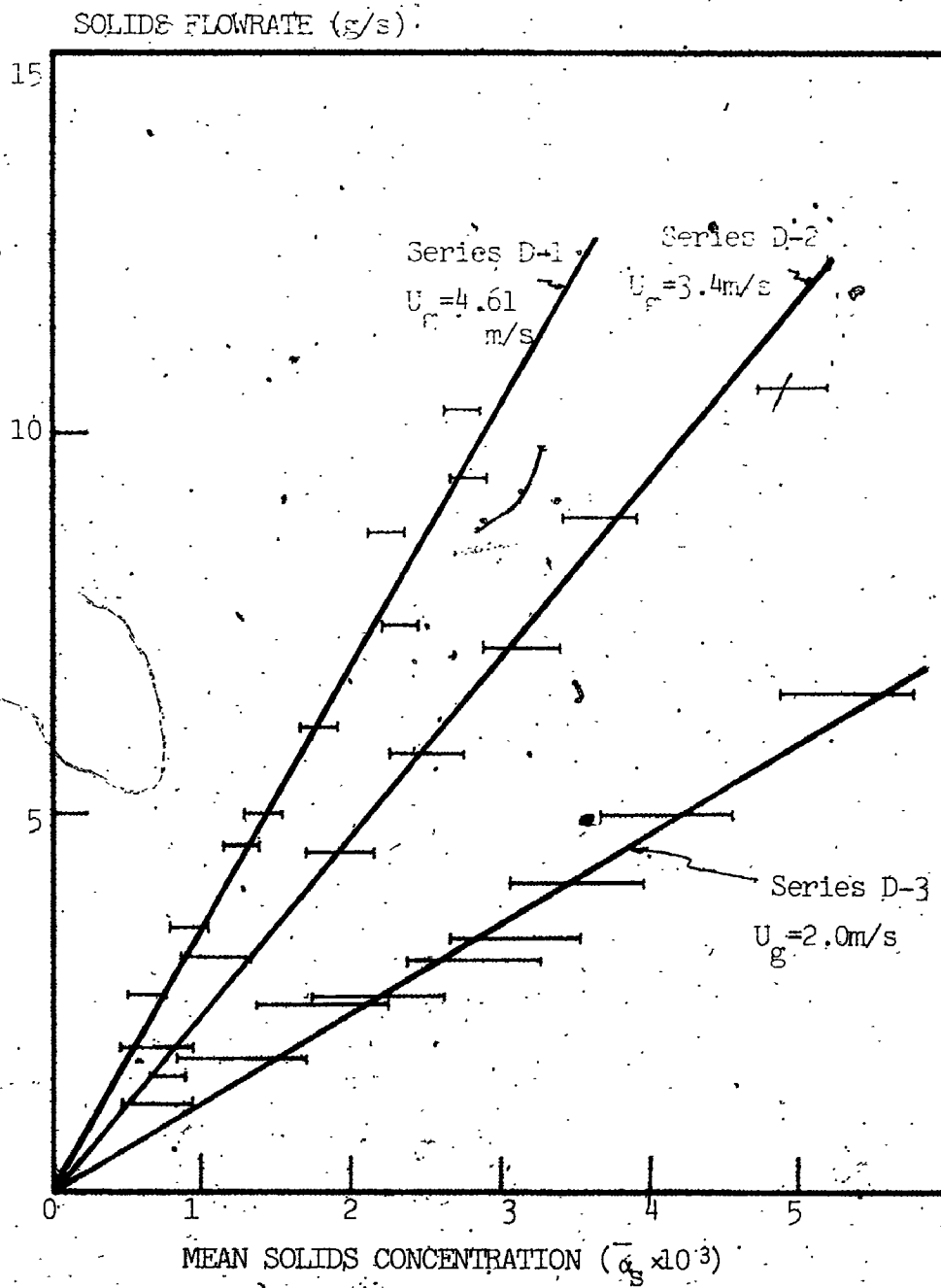


FIGURE 6.21 Solids flowrates versus Mean solids concentration: Glass bead runs

The slopes of the W_s versus \bar{a}_s curves in Figures 6.18 to 6.21, as well as those of the other results not shown in the figures, systematically increase as a function of gas velocity. In other words, the mean solids velocity increases with the gas velocity. The variations of mean solids velocity with gas velocity are given for the three hydrodynamic series in Figures 6.22 and 6.23. As in the case of the preliminary experiments, a linear relationship is shown. The dispersion in the data is much lower in the latter two figures compared to Figure 6.7 since each point in Figures 6.22 and 6.23 are derived from the slopes of the W_s versus \bar{a}_s curves which amounts to averaging over at least a dozen different experiments; each point in Figure 6.7, on the other hand, represents a single experiment.

In all three series the slope of the solids velocity versus gas velocity curves was equal to unity; slip velocities were therefore found to remain constant as a function of gas velocity. The slip velocities increase with increasing particle size and correspond well with the terminal settling velocities of the mean particle size in each of Series B, C and D.

Similar findings were reported by Mehta et al. (88) for 36 μm particles in a 12.7 mm diameter pipe using hand-operated slide valves. They nevertheless found that slip velocity increases with increasing gas velocity for 97 μm particles in the same pipe although there is considerable dispersion in their results and extrapolation of their data to zero gas velocity shows a positive intercept; that is, a positive mean solids velocity. Konno and Saito (78) using a photographic technique found slip velocities to be essentially equal to the

MEAN SOLIDS VELOCITY (m/s)

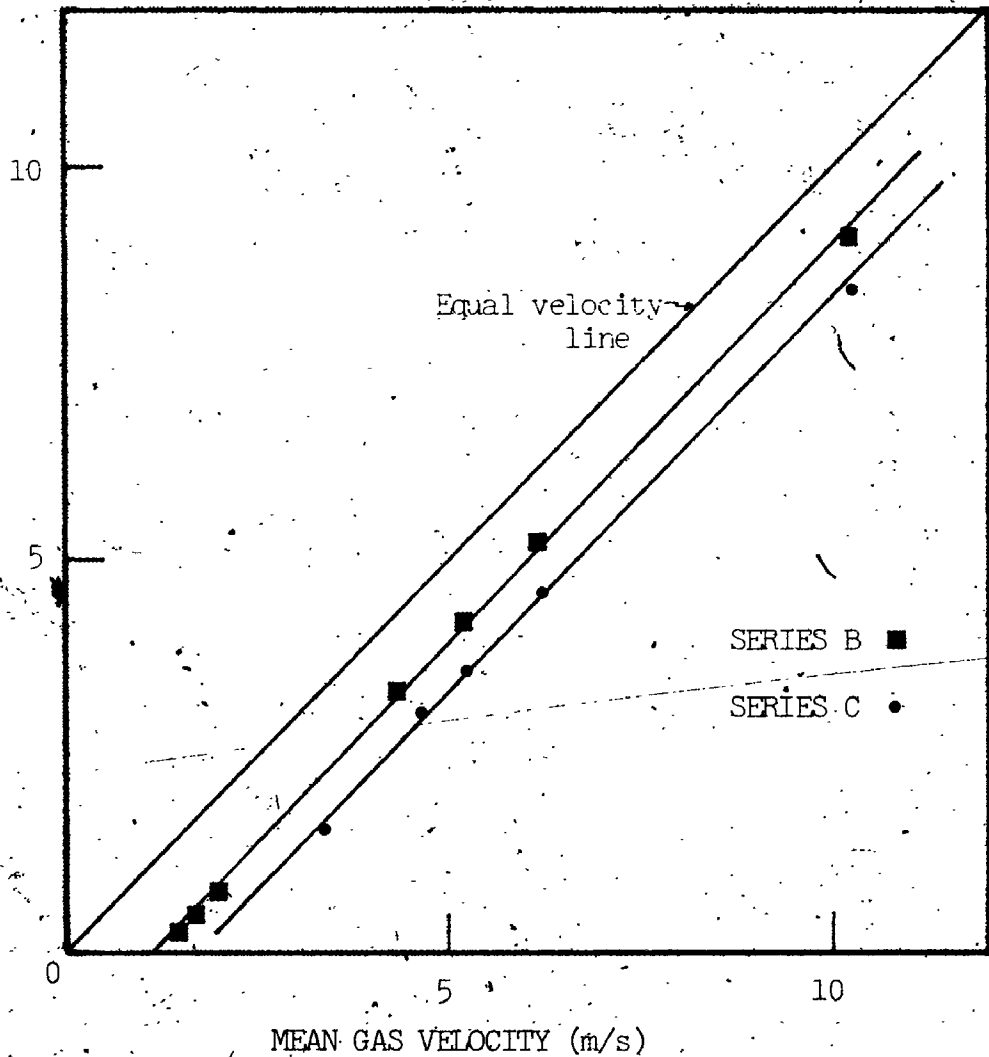


FIGURE 6.22 Mean solids velocity versus Mean gas velocity: Series B and C

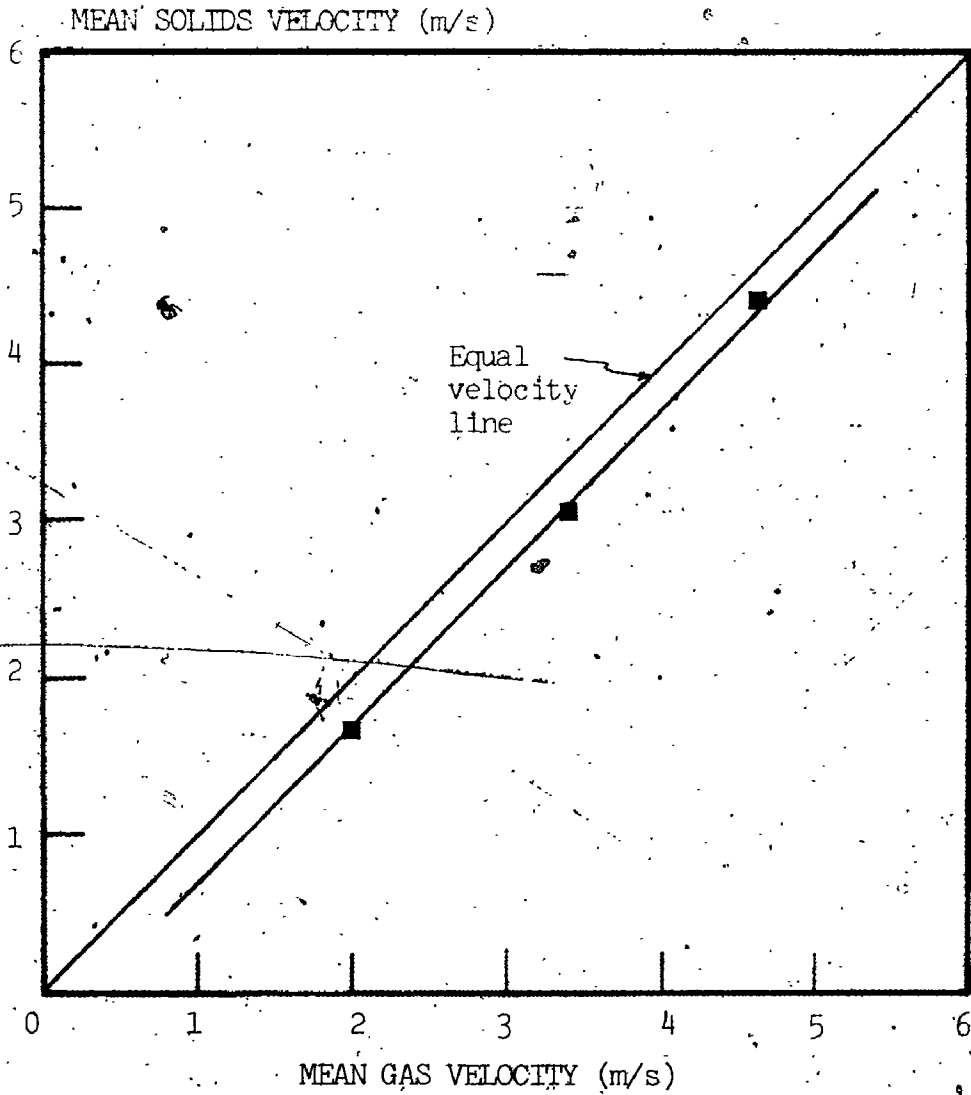


FIGURE 6.23 Mean solids velocity versus Mean gas velocity: SERIES D (Glass beads)

particle terminal settling velocity at gas velocities up to 20 m/s for large (3.25 mm) and small (120 μm) particles. Capes and Nakamura (20) using a similar solids velocity measurement technique as in the present study observed the same variation for particles having a terminal settling velocity of less than 6.10 m/s. Increasing slip velocities with gas velocity were observed for larger particles. Explanations for the present findings as well as those of others having made similar measurements will be advanced in Chapter 7.

Recalling from the previous section that overall suspension pressure drop was found, in some cases, to be lower than that given by the sum of the pressure drop of the gas alone and the solids hold-up it can be noted by comparing Figures 6.15 and 6.22 and Figures 6.17 and 6.23 that this occurred when mean solids velocities were quite low (i.e. less than 1 m/s for the Series B sand runs and less than 2 m/s for the glass bead runs).

The variations of the slopes of the pressure drop curves (Figures 6.8 to 6.14) as a function of solids velocity parallel those given in 6.15 to 6.17 as a function of gas velocity. In other words, the slopes of pressure drop versus \bar{u}_s curves increased with mean solids velocity. This is consistent with observations made under different experimental conditions by Reddy and Pei (106), Konno and Saito (78) and Capes and Nakamura (20).

6.3.3 Pressure drop as a function of loading ratio

The data presented in the preceding two sections can also be represented as pressure drops as a function of loading ratio and a

typical sampling of such results are presented in Figures 6.24 to 6.26.

The hydrodynamic results are presented in this way for two reasons: Firstly, few investigators studying pneumatic transport measure either solids velocities or solids concentrations and thus generally present data from experiments carried out at constant gas velocity in this way. The second reason will become more evident in Section 6.4 when heat transfer results are presented: several investigators (12, 30) have suggested that minima in heat transfer coefficients plotted as a function of loading ratio are accompanied by analogous pressure drop curves.

The curves presented in Figure 6.24 to 6.26 show linear variations in pressure drop as a function of loading ratio which is obviously consistent with the results of the previous two sections. It will be noted that the glass bead data (Figure 6.26) is presented as points, not as bars in this case since the sticking problem had no effect on either the solids flowrate nor the pressure drop measurements.

6.3.4 Solids hold-up particle size distributions

As mentioned in the introduction of this chapter the particle size distribution of the solids held-up between the two slide valves was measured during the Series B hydrodynamic experiments.

Typical results of this kind as a function of the mean solids concentration are shown in Figure 6.27. Despite some scatter in the data due to the relatively small quantities of solids being retained

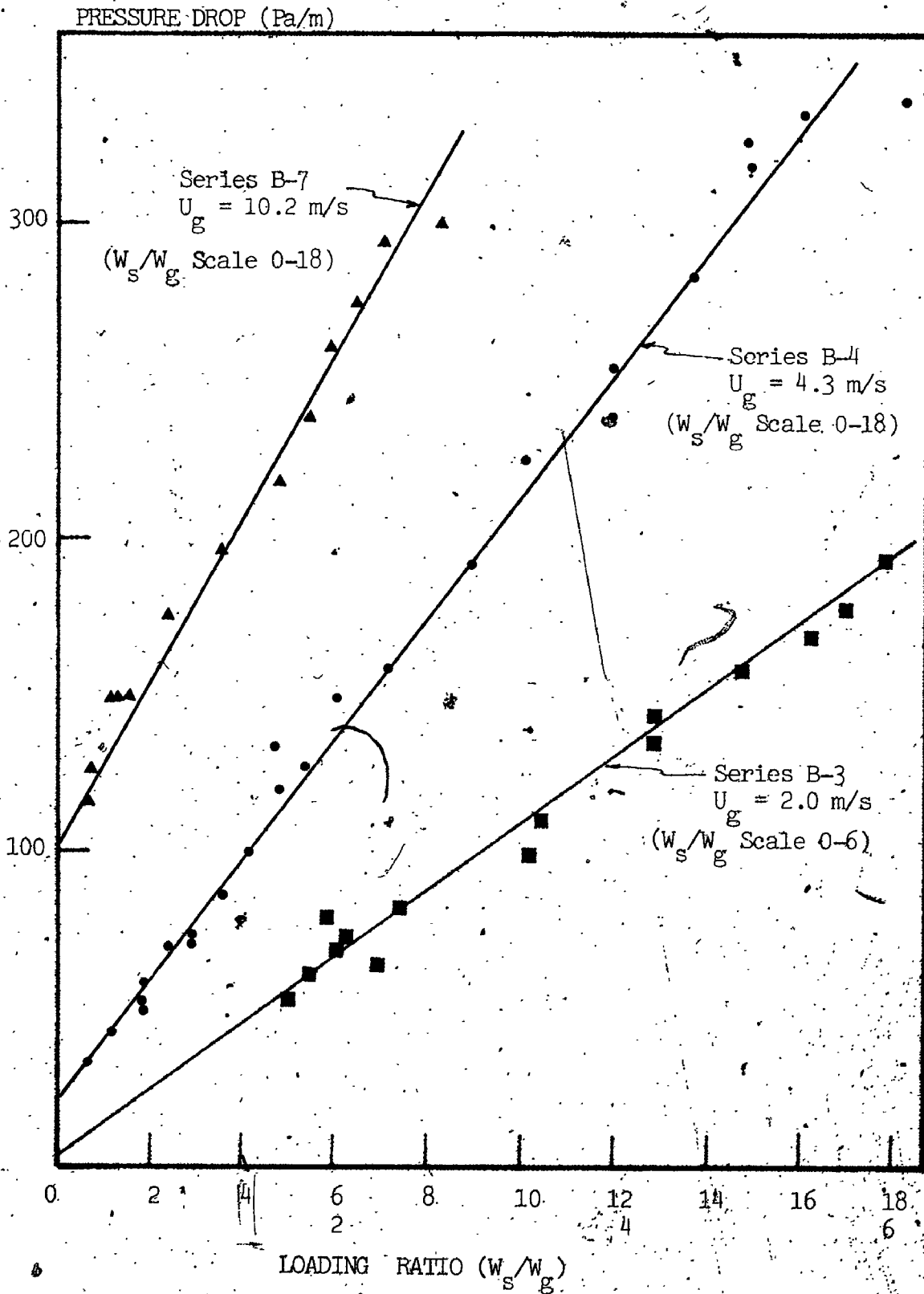


FIGURE 6.24 Suspension-pressure drop as a function of Loading ratio: Typical SERIES B results

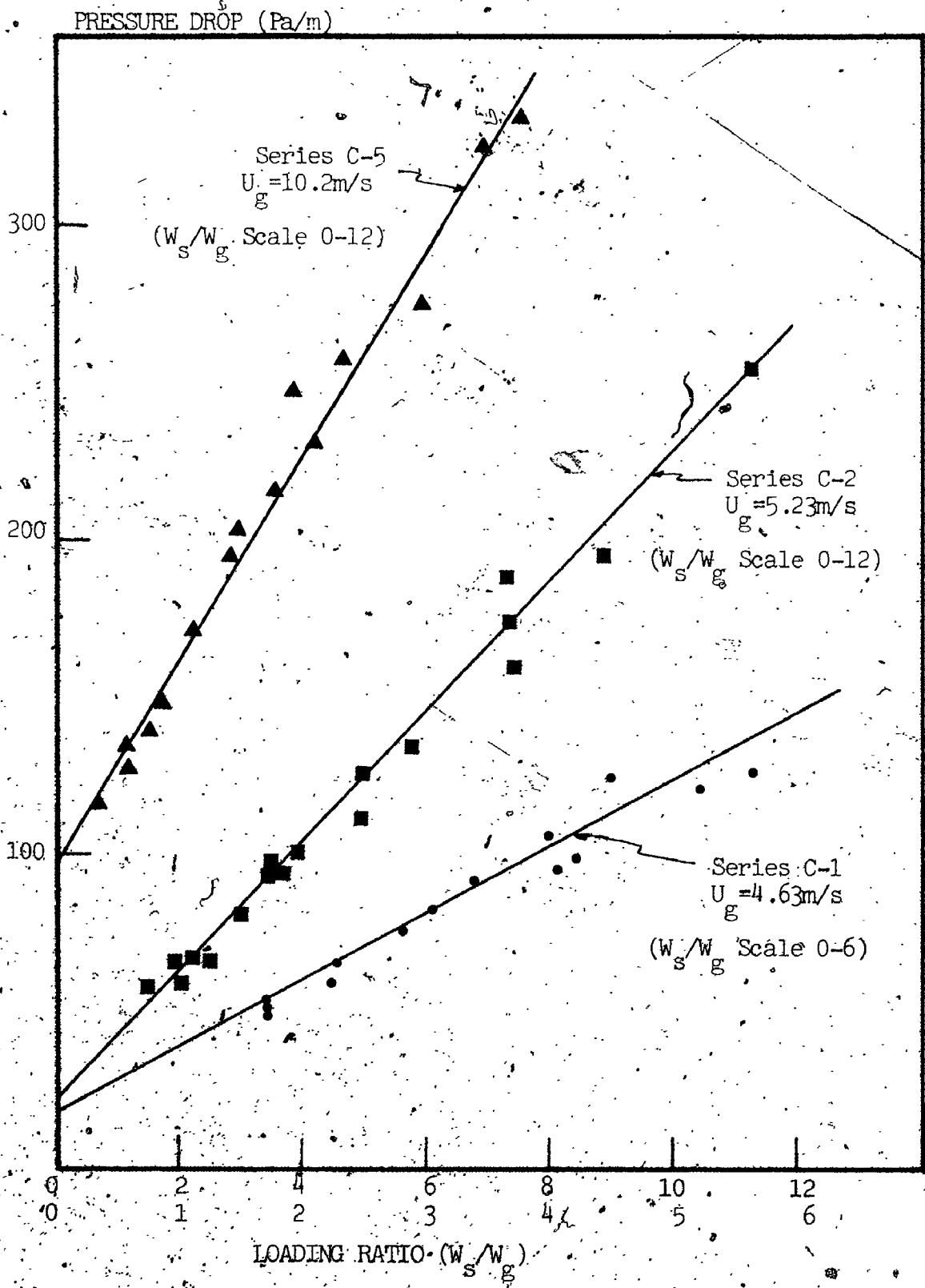


FIGURE 6.25 Suspension pressure drop as a function of Loading ratio: Typical SERIES C results

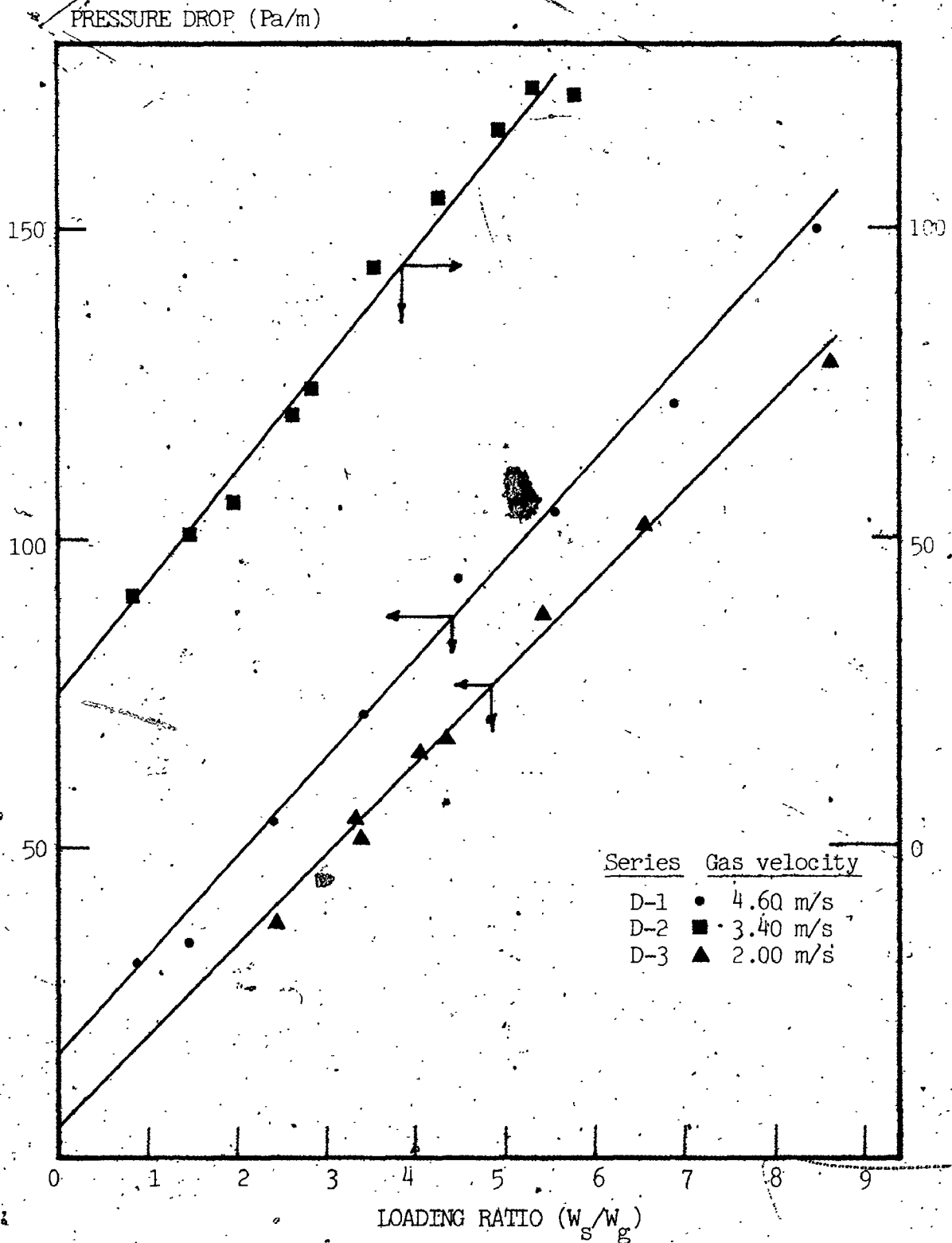


FIGURE 6.26 Suspension pressure drop as a function of Loading ratio : SERIES D (Glass beads)

generally less than 20 g the results showed the hold-up mean particle diameter to be essentially constant with respect to the mean solids concentration for a given gas velocity ; it was nevertheless found to vary as gas velocity varied (See Figure 6.28).

The latter figure shows that the mean diameter of the solids hold-up decreases as gas velocity increases approaching the mean diameter of the solids circulating in the system (172 μm for Series B) at high gas velocities. If direct particle-particle interaction played an important role in the hydrodynamics of dilute suspension flows, one would expect a more or less constant solids hold-up mean particle diameter as a function of gas velocity. This would be due to small particles colliding with large particles with the net result being deceleration of the small and acceleration of the large. The type of variation shown in Figure 6.28 on the other hand would naturally arise if each particle species attained its own slip velocity independent of the other species present. Small particles would have a mean velocity greater than that of the larger particles leading to a hold-up which was lower in proportion to their presence in the feed. This effect would be more pronounced at low gas velocities where the ratio of the small particle to large particle velocities was greatest. The single point at the lowest gas velocity which deviates from this behavior could be explained by the fact that the largest fraction of sand was not conveyed upwards at this particular velocity.

Little or no data of this type exist in the literature. Hair and Smith (55) studied the differences in pressure drops obtained with uniform and non-uniform sized particles but made no hold-up or

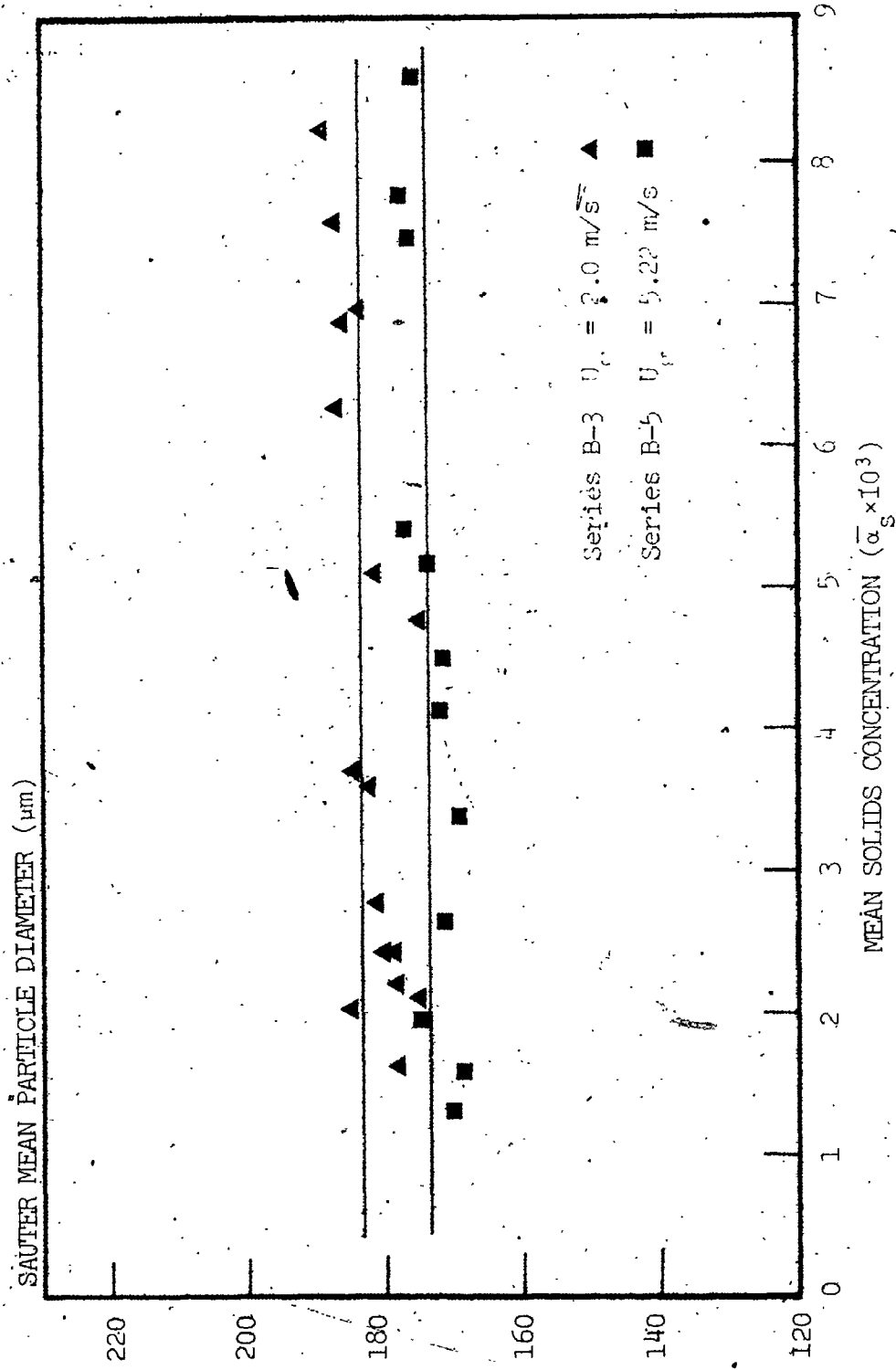


FIGURE 6.27. Variation of the mean particle diameter of the solids hold-up as a function of mean solids concentration

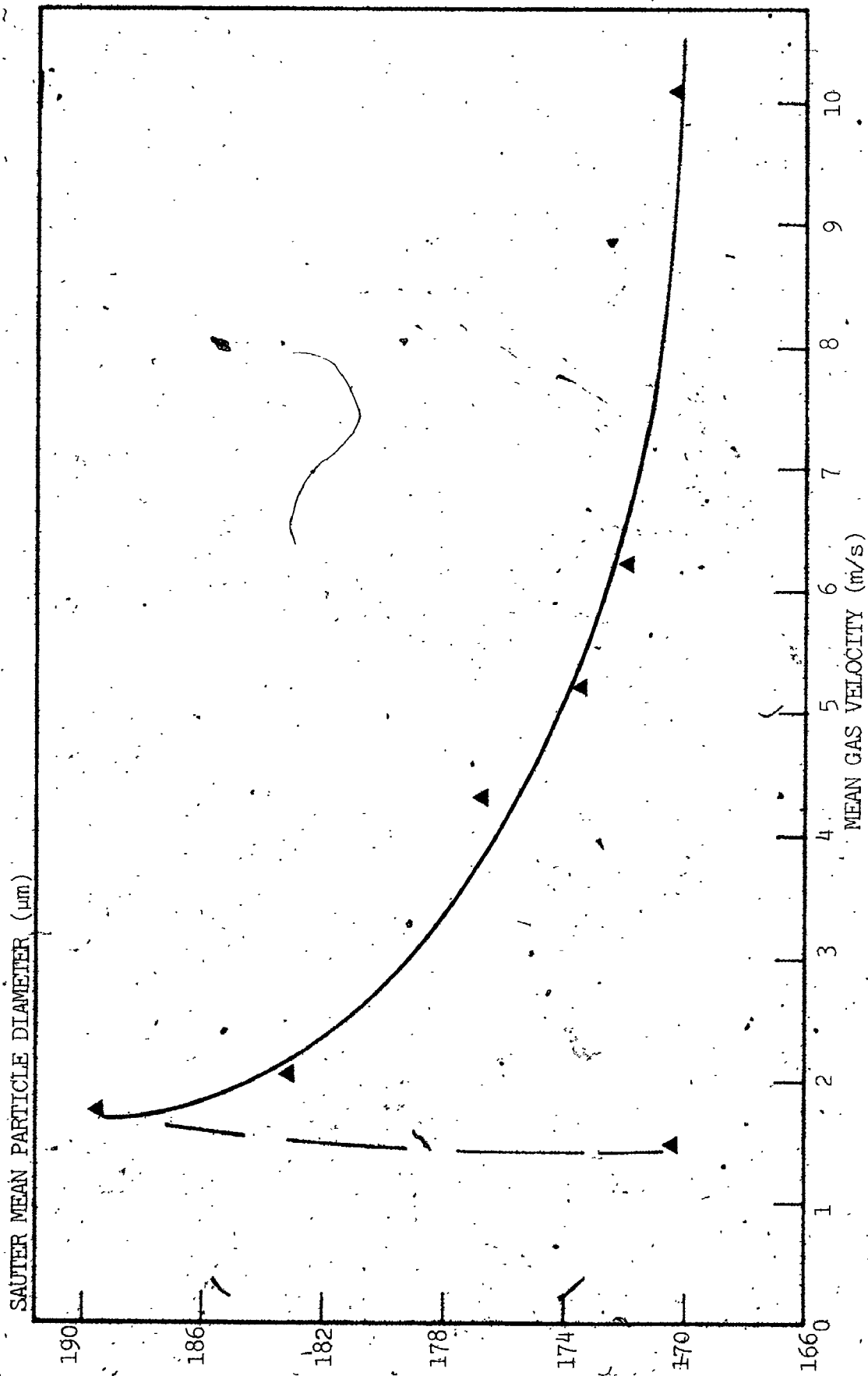


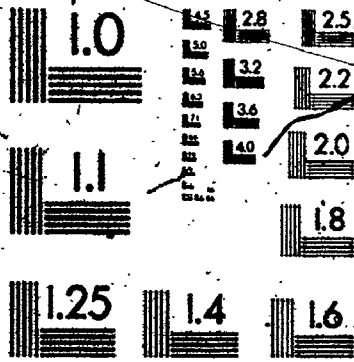
FIGURE 6.28 Variation of mean particle diameter of solids hold-up as a function of gas velocity (SERIES B)

particle velocity measurements. Nakamura and Capes (97) studied conveying of mixtures of glass beads and steel shot and found segregation effects to occur; that is, a proportionally greater number of heavy particles were found to be held-up compared to light ones. No measurements on a continuous particle size distribution solid appear to have been made before however.

The results in Figures 6.27 and 6.28 add to the evidence presented in the previous sections suggesting that, for relatively dilute suspension, the laws governing overall suspension behaviour are independent of the mean solids concentration: pressure drops remained proportional to $\bar{\alpha}_s$ over the entire ranges studied in the three series; mean solids velocities were found to be independent of $\bar{\alpha}_s$; the mean particle diameter of the solids held-up were independent of $\bar{\alpha}_s$ and finally the variation in the hold-up mean particle diameter as a function of gas velocity was consistent with the particles establishing their own mean velocities independent of the other particles present in the mixture.

These observations will play a central role in the analysis of both the hydrodynamic and heat transfer analysis using the probabilistic multiphase flow equations to be carried out in Chapter 7.

4



6.4 Suspension to pipe wall heat transfer results

6.4.1. Temperature and heat transfer coefficient profiles

Figure 6.29 shows typical pipe wall temperature, suspension mixed mean temperature and resulting heat transfer coefficient axial profiles obtained during the heat transfer runs. As in the case of the experiments carried out on the gas flowing alone, the wall temperature profile is characterized by a steep rise in the first meter of the heat transfer section followed by a linear variation thereafter. The rise corresponds to the establishment of the thermal boundary layer; there is an accompanying drop in the local suspension-wall heat transfer coefficients after which they remain constant.

It will be recalled from Chapter 5 that the experimental determination of heat transfer coefficients integrates independent measurements of the gas and solids flowrates, the power input into the system and the radial wall heat losses in order to calculate the local suspension mixed-mean temperature via a heat balance. Measurement errors in any of the above factors would falsify the heat balance and lead to suspension mixed mean temperature profiles, which, beyond the thermal entry region, would not parallel the wall temperature profile. This, in turn, would lead to local coefficients continuing to vary along the entire length of the pipe. The fact that the coefficients were constant beyond the thermal entry region is therefore an indirect verification of the overall measurement system and heat balance calculation with solids flow as well as of the physical properties of the gas and solids (the slope of the mixed mean

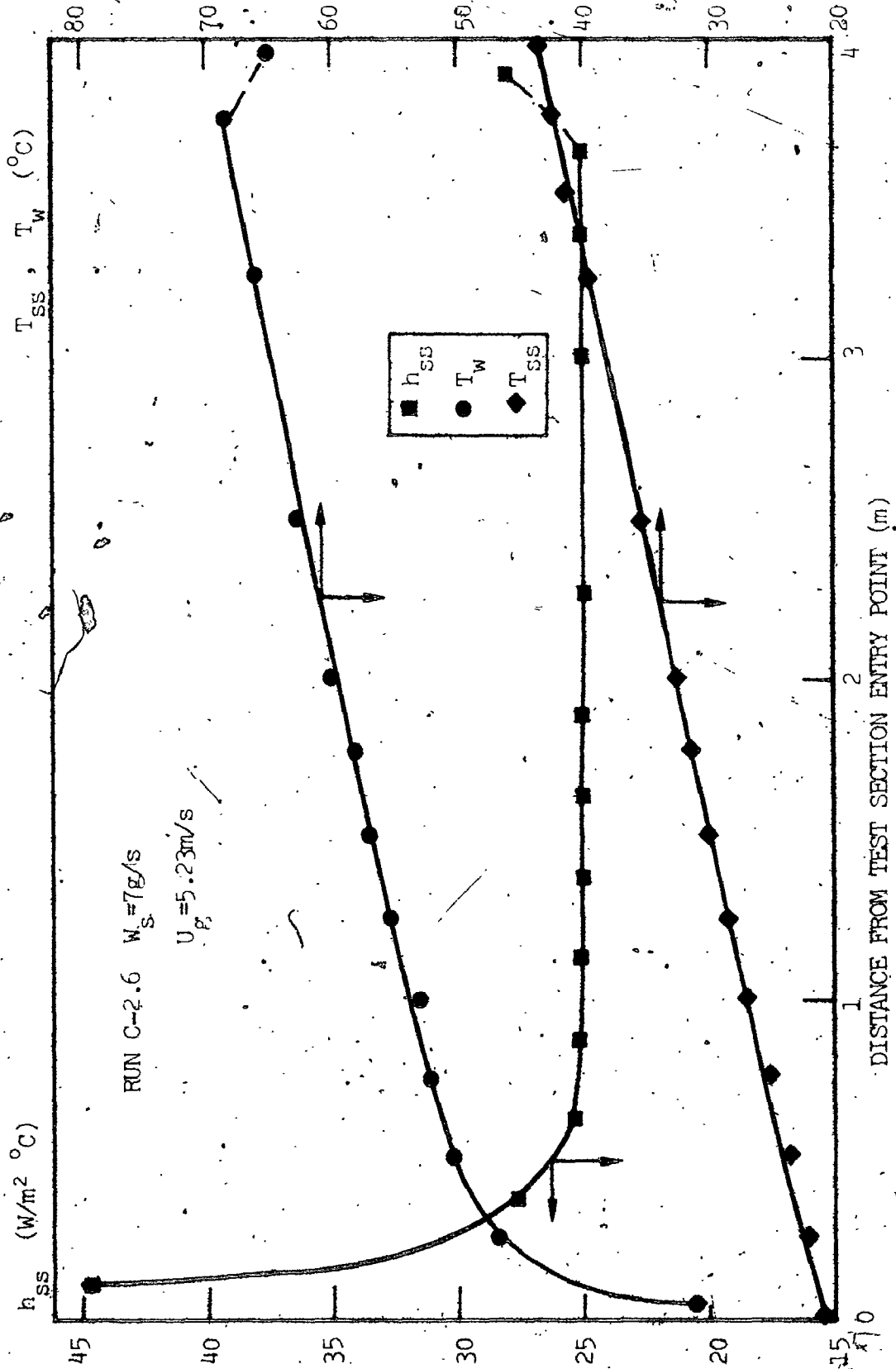


FIGURE 6.29 Typical wall temperature, suspension mixed near temperature, and heat transfer coefficient profile for suspension runs

temperature profile is $q_{ss} / (W_s C_s + W_g C_g)$; cf. Equation 5.31).

An exception to these linear behaviours as shown in Figure 6.29 is the last point at the upper extremity of the test section where the pipe wall temperature was almost systematically lower than the temperature at the preceding point; the local coefficient at this point was consequently found to rise. This is an end effect caused by the fact that the slide valve at the heat transfer section outlet represented an almost perfect heat sink as described in Section 5.3.3. The last point (and to a lesser extent the first point immediately above the lower slide valve) was thus affected by axial conduction toward the slide valve. This end effect, again, as demonstrated in Section 5.3.3 had a negligible influence on the overall heat balance. The asymptotic coefficients, beyond the thermal entry length were therefore taken to be the average of the experimental values between the local coefficients between 2000 and 3500 mm beyond the heat transfer section entry point; that is, the last value which was subject to axial heat losses was neglected in this determination.

Figures 6.30 to 6.33 show a sampling of the variations of the local heat transfer coefficients as functions of solids flowrate for several of the different gas flowrates examined in Series C. These curves show the same general variations as that given in Figure 6.29 and are presented essentially to show that, over the entire ranges of gas and solids flowrates studied in Series C, the flow was thermally fully developed over a significant portion of the heat transfer section thus providing access to fully developed coefficients for comparison with those of the gas flowing alone. Some of the problems

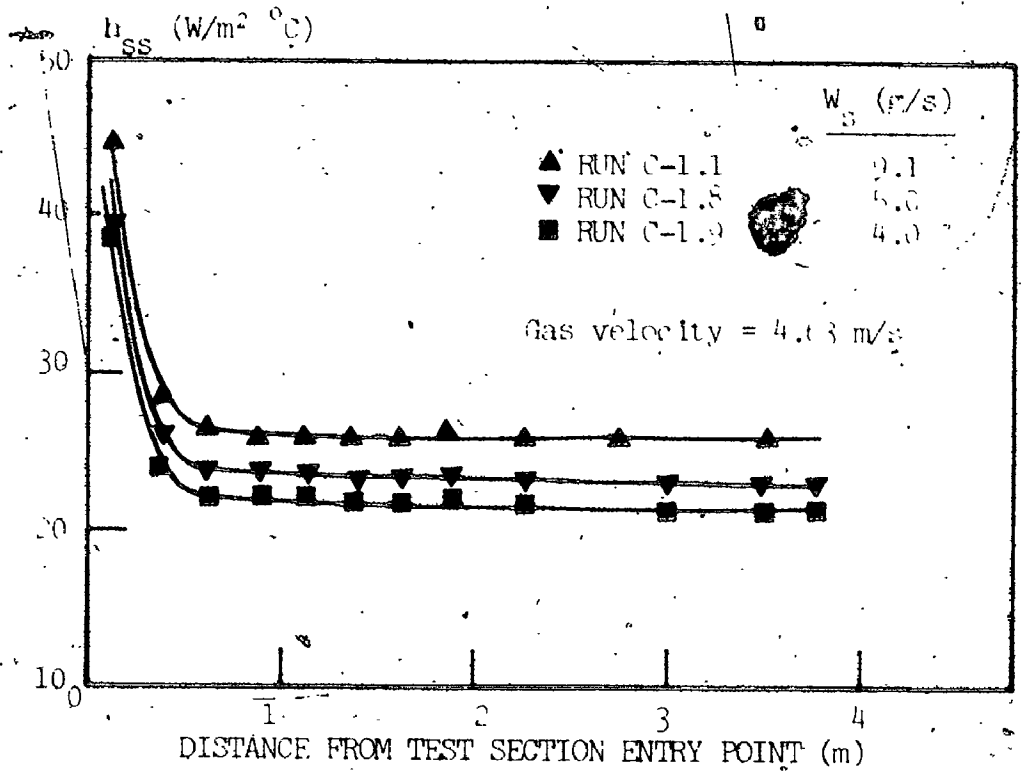


FIGURE 6.30 Heat transfer coefficient axial profiles (SERIES C-1)

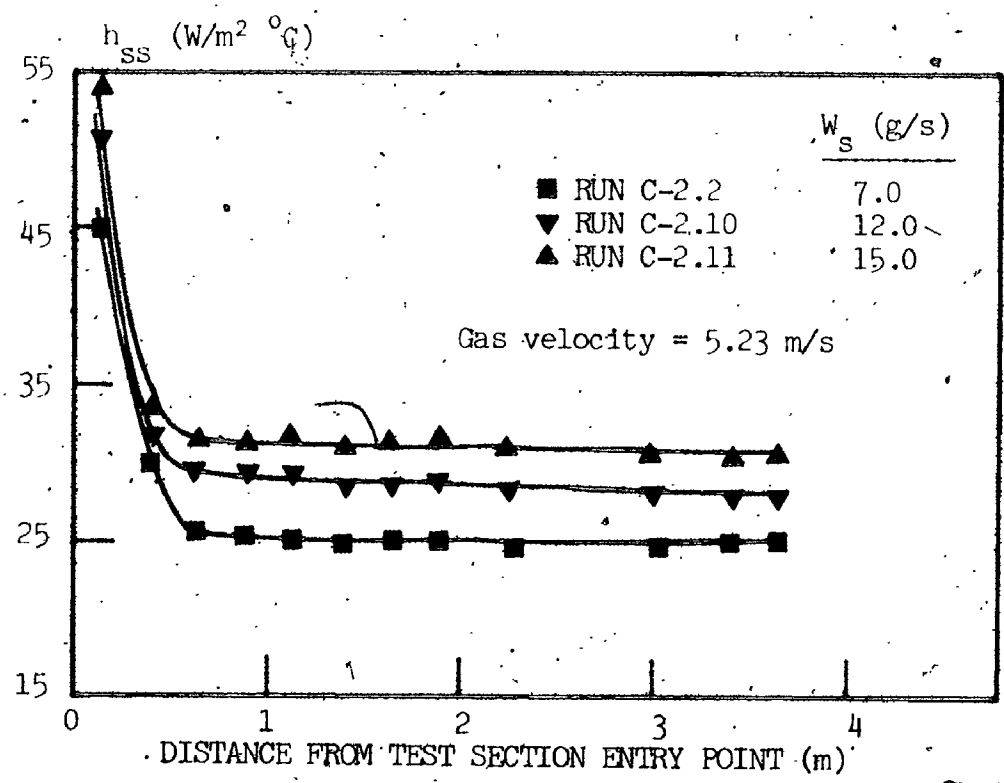


FIGURE 6.31 Heat transfer coefficient axial profiles (SERIES C-2)

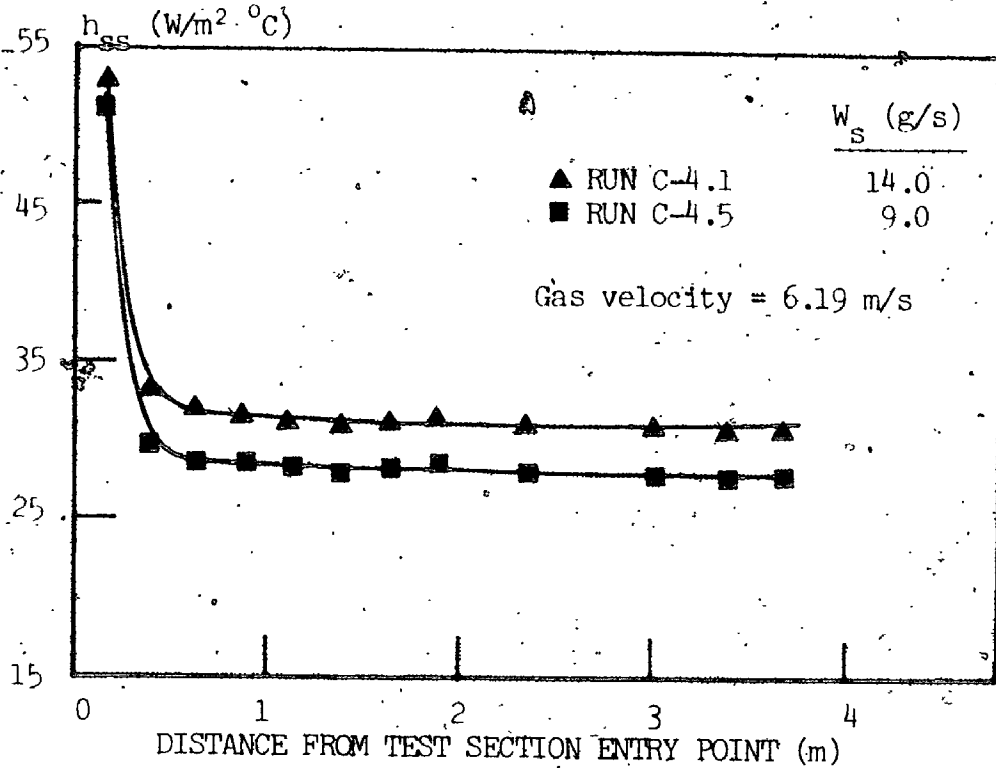


FIGURE 6.32 Heat transfer coefficient axial profile (SERIES C-4)

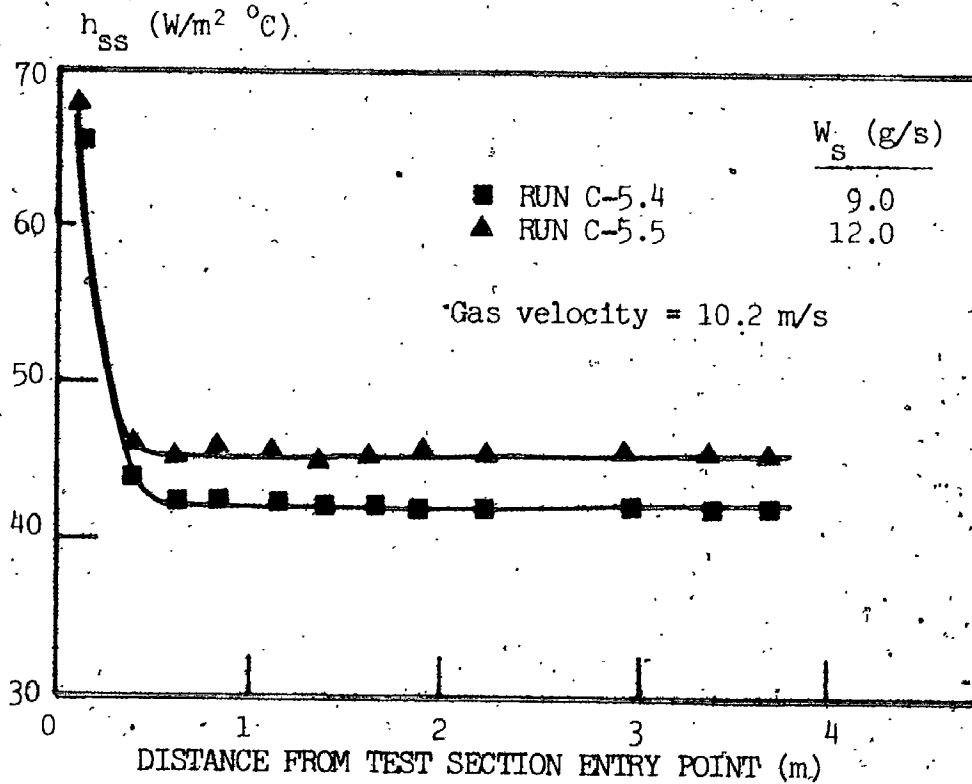


FIGURE 6.33 Heat transfer coefficient axial profiles (SERIES C-5)

discussed in Chapter 2 with the experimental determination of these coefficients using short pipes were thus avoided in the present study.

The curves in Figures 6.30 to 6.33 show that the heat transfer coefficients became constant at between 750 mm and 1 m beyond the test section entry point regardless of the solids flowrate or the gas velocity being examined. This independence of the thermal entry length with respect to these two factors contradicts results of some previous workers in so far as thermal entry length has generally been found to increase as a function of solids loading and, to a lesser extent, as a function of Reynolds number. Studying similar sized particles however, Farbar and Depew (45) and Tien and Quan (130) found these increases to be the order of 250 mm although over a range of loading ratios which were much smaller than those studied here. The wall temperature measurements in the present study were made at 250 mm intervals, mainly in order to have a large number of points in the fully developed flow zone; hence it is possible that variations in the thermal entry length as a function of loading ratio and gas velocity were not picked up. The extension of the present work to the study of non-fully developed flow would therefore require additional measurements to be made in the first meter of the heat transfer test section.

6.4.2. Variation of heat transfer coefficients as a function of solids loading

Figures 6.34 through 6.38 summarize the variations of the thermally fully developed suspension-wall heat transfer coefficients for the five series of heat transfer experiments. The curves are plotted as

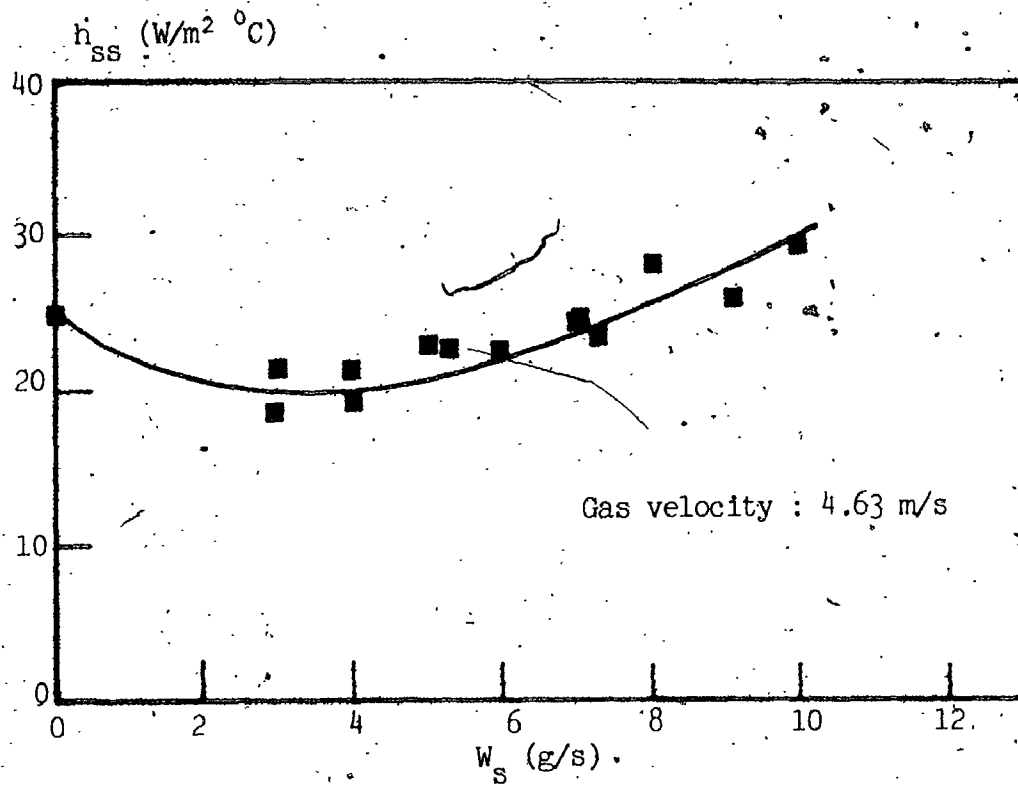


FIGURE 6.34 Variation of fully developed heat transfer coefficients as a function of solids flowrate (SERIES C-1)

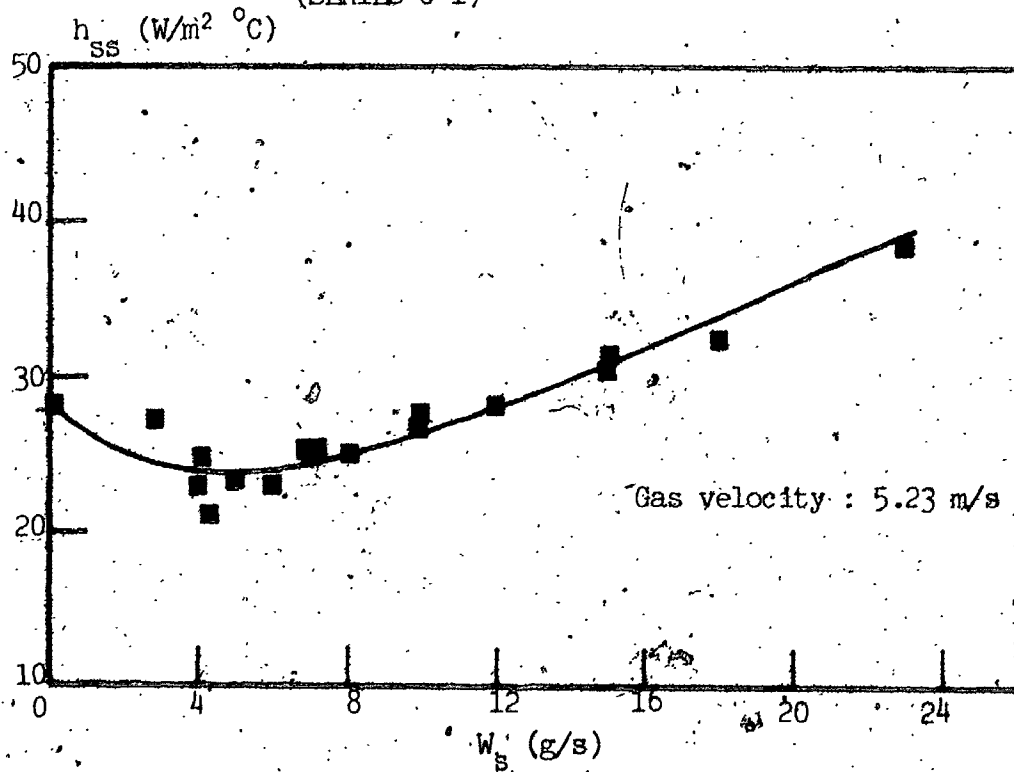


FIGURE 6.35 Variation of fully developed heat transfer coefficients as a function of solids flowrate (SERIES C-2)

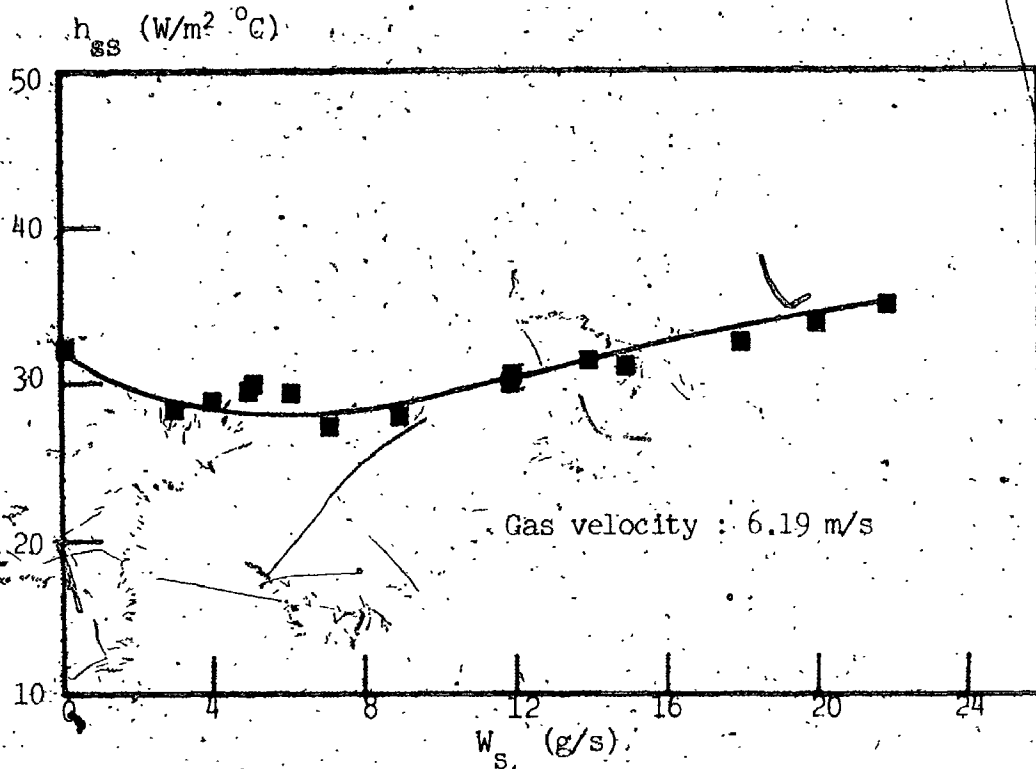


FIGURE 6.36 Variation of fully developed heat transfer coefficients as a function of solids flowrate (SERIES C-4)

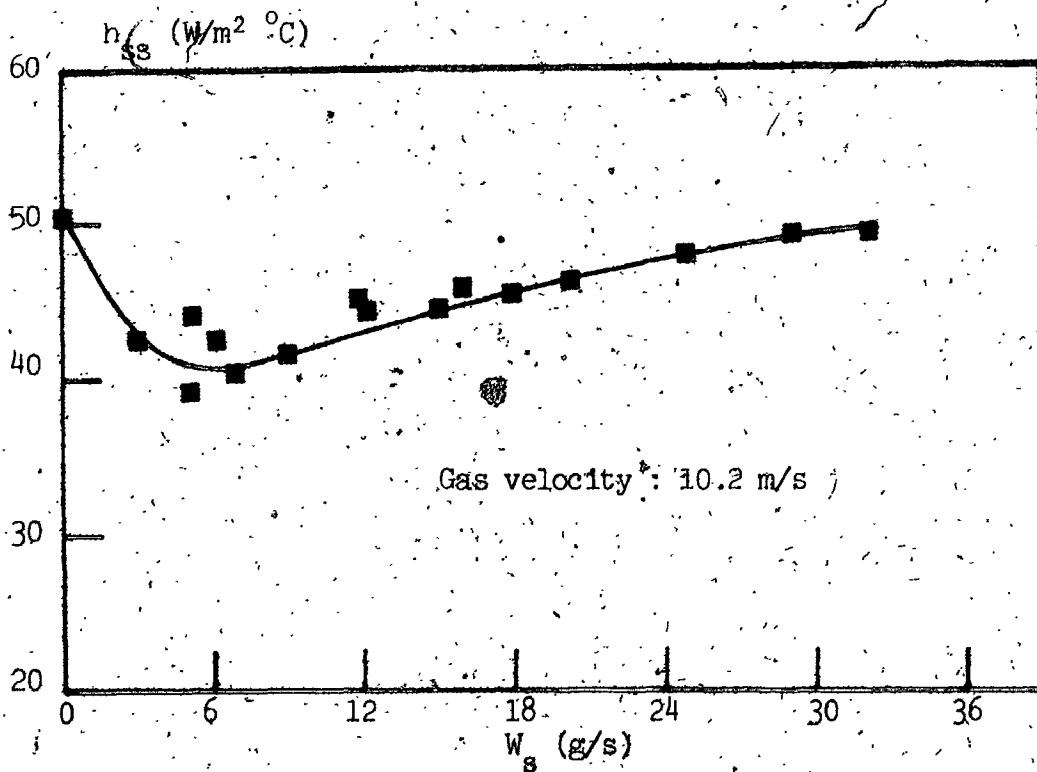


FIGURE 6.37 Variation of fully developed heat transfer coefficients as a function of solids flowrate (SERIES C-5)

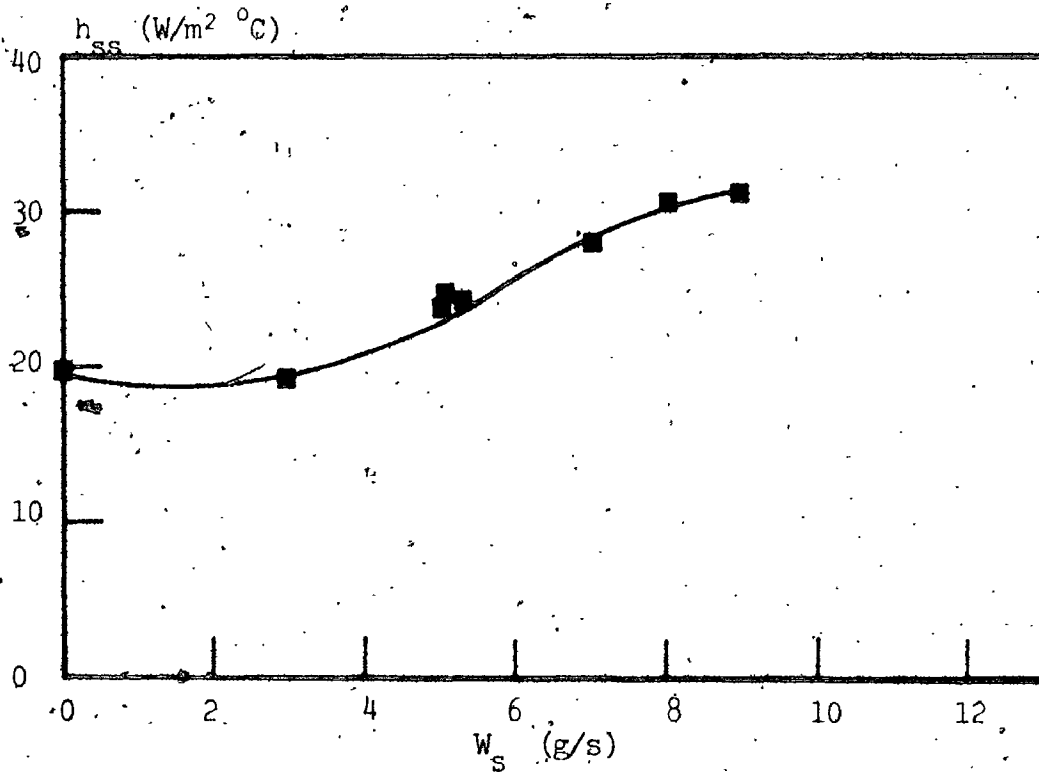


FIGURE 6.38 Variation of fully developed heat transfer coefficients as a function of solids flowrate (SERIES C-3)

h_{ss} as a function of solids flowrate for each of the five different gas flowrates examined. Reynolds number varied between 4500 and 15000 ; loading ratios varied between 0 and 12.

The general behavior exhibited by the curves in Figures 6.34 to 6.38 is a tendency toward an initial decline in the heat transfer coefficient compared to that of the gas flowing alone at the same superficial velocity followed by a passage through a minimum at low solids loading. The ratio of the minimum heat transfer coefficient to that of the gas flowing alone was found to be about 0.75 in all series with the exception of the lowest gas velocity (Series C-3 ; $Re = 4500$) which exhibited a somewhat different behavior compared to the other series ; the heat transfer coefficient was found to be relatively constant at low loading ratio and increased as loading ratio increased.

The variations of fully developed heat transfer coefficients as a function of the mean solids concentration are similar to those given by the curves in Figures 6.34 to 6.38 as a function of solids flowrate. This results from the fact that, as was shown in Section 6.3.2, the solids concentration was found to vary in direct proportion to the solids flowrate over the entire range studied in all hydrodynamic series.

The observation of a minimum heat transfer coefficient, as mentioned in Chapter 2 has been made before (27, 64, 95, 130, 138) although not at Reynolds numbers as low as the ones studied here. The data most closely resembling those obtained here are those of Farbar and Depew (45) and Tien and Quan (130) who both studied 200 μm

glass beads at Reynolds numbers of 15000 and 30000. Both of these two pairs of investigators also found decreases in the fully developed heat transfer coefficient as a function of solids loading ; in both cases however the experimental heat transfer sections were too short to provide fully developed coefficients for loading ratios above 3. No increases were therefore observed following the initial declines.

Chapter 2 discussed some of the reasons previously put forth to explain this type of behavior. It will be recalled that declines were held to be provoked by turbulence inhibition and increases by boundary layer thinning and enhanced radial transport by the solids phase. It will also be recalled that the quantitative effects of these factors have yet to be integrated into either a model or a correlation for suspension heat transfer coefficients.

This type of speculation will be dispensed with here as the major reasons for this type of behavior will become apparent based on the analysis to be carried out in Chapter 7.

It can nevertheless be noted that previous workers (eg. Ref. 130) evoking this kind of argument have suggested that, since these are hydrodynamic effects, similar curves for pressure drop as a function of solids flowrate should accompany such heat transfer results. It was shown however, in Section 6.2.3 that pressure drops as a function of loading ratio for all the hydrodynamic runs, including those of Series C showed linear variations without any minimum occurring.

6.5. Summary of major experimental findings

- a) Fully developed pressure drops at constant gas velocity were found to vary linearly with mean solids concentration for all three solids examined at loading ratios up to 18 and gas velocities which varied between 1.5 and 10 m/s.
- b) Fully developed pressure drops were found to be lower than the sum of the pressure drop of the gas flowing alone at the same superficial velocity and the solids hold-up at low gas velocities.
- c) Pressure drops were found to increase as a function of both gas and solids velocities.
- d) Mean solids velocities at a fixed gas velocity were found to remain constant as a function of mean solids concentration (and solids flowrate) over the entire range of variables tested.
- e) Slip velocities remained constant as gas velocity varied between 1.5 and 10 m/s.
- f) The mean particle size of the solids held-up in the line remained constant as a function of solids concentration but varied as a function of gas velocity, decreasing as gas velocity increased.
- g) Suspension to pipe wall heat transfer coefficients at fixed gas velocity initially decreased as solids flowrate (or solids concentration) increased, passed through a minimum and then increased in all heat transfer series except at the lowest gas velocity ($U_g = 3.37$ m/s) where they remained constant at low solids loading and increased thereafter.

CHAPTER 7

ANALYSIS OF EXPERIMENTAL RESULTS

USING PROBABILISTIC MULTIPHASE FLOW EQUATIONS

7.1 Introduction

Full resolution of the general probabilistic multiphase flow equations derived in Chapter 4 would provide complete details of the concentration, velocity and temperature fields for a given problem. Full resolution however confronts the problem of closure : the number of unknowns in the final continuity, momentum and energy equations clearly exceeds the number of equations.

The full set of equations for each phase consists of :

- one continuity equation
- three projections of the momentum equation
- one energy equation.

In the case where there are only two phases present (fluid and the solids taken as a whole) the total number of equations is ten. The unknowns for the solids phase are :

- the phase presence probability α_s
- three velocity components V_i
- six velocity fluctuations β_{ij}
- six stress terms due to hydrodynamic interaction τ_{ij}^s
- six stress terms due to particle collisions s_{ij}
- three fluid-solids interaction terms F_i^{fs}

- the solids phase temperature T_s
- three temperature cofluctuations ϵ_i^s .

Additional unknowns for the fluid phase are :

- three velocity components U_i
- six velocity cofluctuations B_{ij}
- pressure P
- the fluid phase temperature T_f
- three temperature cofluctuations ϵ_i^f

assuming the relationship between fluid stress and velocity is known (in the case of a Newtonian fluid for example).

Full resolution can only be achieved therefore if all the secondary variables (cofluctuations, stresses and interactions) can be expressed in terms of the primary variables (α_s , velocities, temperature and pressure) and this would require models to be developed for each of the former terms. In cases where full resolution is required the general equations would nevertheless be invaluable as a guide to what indeed must be modelled to fully describe the system; given the large number of terms to be modelled however this would generally constitute a fastidious task.

Full resolution is fortunately not required to draw benefit from the equations. Even in partially solved form they provide important indications concerning the relative importance of the various phenomena involved in multiphase flows, thereby identifying the essential terms which must be modelled in order to relate factors

of practical interest to overall boundary conditions in specific cases.

This chapter will be concerned with using the multiphase flow equations in this latter way. Firstly the form of the momentum equations required for the analysis of fully developed gas-solids pipe flow will be examined to identify the determinant phenomena controlling pressure drop in suspension flows. A model for particle-wall collisions will then be proposed to interpret the results of the preceding chapter. The hydrodynamic analysis, in addition to its use in treating the hydrodynamic data, will lead to some important conclusions which will play a key role in the heat transfer analysis. While no full solutions for the energy equations will be offered the analysis will nevertheless provide the general form of the variation of fully developed heat transfer coefficients with loading ratio. The heat transfer data will be shown to be consistent with the predicted variation and numerical values for the hydrodynamic parameters correlating these and comparable existing data will be determined.

7.2 Analysis of Hydrodynamic Results

7.2.1 Fully developed flow

Fully developed flow in single phase fluid mechanics is characterized by the velocity field which is independent of time and position along the axis in the direction of the mean flow. In the probabilistic treatment of multiphase flow the definition is analogous: the flow is fully developed when the phase presence

probabilities and the laws of probability governing the phase velocities are independent of time and position along the axis in the direction of flow. In axisymmetrical pipe flow then, the phase presence probabilities, mean velocities and velocity fluctuation tensors in each phase will thus depend only on radial position. It results from this that the viscous shear tensor in the fluid phase and particle phase stress tensor due to particle collisions are also independent of time and axial position.

Under these conditions the axial projections of the momentum equations (Equations 4.42 and 4.49), written in cylindrical coordinates, become :

$$\frac{1}{r} \frac{\partial}{\partial r} (r \rho_f \alpha_f B_{rz}) = - \alpha_f \frac{\partial P}{\partial z} + \frac{1}{r} \frac{\partial}{\partial r} (r \alpha_f \sigma_{rz}) + F_z^{sf} - \rho_f \alpha_f g \quad (7.1)$$

and

$$\frac{1}{r} \frac{\partial}{\partial r} (r \rho_s \alpha_s \beta_{rz}) = \alpha_s \frac{\partial}{\partial z} \tau_{zz}^s + \frac{1}{r} \frac{\partial}{\partial r} (r \alpha_s \tau_{rz}^s) + F_z^{fs} - \rho_s \alpha_s g + \frac{1}{r} \frac{\partial}{\partial r} (r s_{rz}) \quad (7.2)$$

The stress tensor τ_{ij}^s , as will be recalled from Chapter 4, results from the hydrodynamic interaction between the solids phase

and the medium external to it. Molodtsov (93) has shown that, under fully developed flow conditions, the axial gradient of this term is equal in magnitude and opposite in sign to the axial pressure gradient in the gas phase and that these two gradients are constant. Analysis of the hydrodynamic results under fully developed flow conditions, that is, where the axial pressure profile is linear, will therefore be based on :

$$\frac{1}{r} \frac{d}{dr} (r \alpha_f \rho_f \beta_{rz}) = - \alpha_f \frac{\partial P}{\partial z} + \frac{1}{r} \frac{d}{dr} (r \alpha_f \rho_f r_z) + F_z^{sf} - \rho_f \alpha_f g \quad (7.3)$$

and

$$\frac{1}{r} \frac{d}{dr} (r \alpha_s \rho_s \beta_{rz}) = - \alpha_s \frac{\partial P}{\partial z} + \frac{1}{r} \frac{d}{dr} (r \alpha_s \rho_s r_z) + F_z^{fs} - \rho_s \alpha_s g + \frac{1}{r} (r s_{rz}) \quad (7.4)$$

7.2.2 Pressure drop : model for s_{ij} at the pipe wall

Examination of the phenomena affecting the pressure drop in vertical fully developed pipe flow of gas-solids suspensions can be carried out by adding the above two equations and integrating them across the pipe cross-section. This leads to :

$$\begin{aligned}
& \int_0^R d(r\alpha_f^B)_{rz} + \int_0^R d(r\alpha_s^{\rho_s \beta_s})_{rz} = \int_0^R -\frac{\partial P}{\partial z} r dr + \int_0^R d(r\alpha_f^\sigma)_{rz} \\
& + \int_0^R d(r\alpha_s^\tau)_{rz} + \int_0^R d(rs)_{rz} - \int_0^R \rho_s \alpha_s g r dr - \int_0^R \rho_f \alpha_f g r dr
\end{aligned}
\tag{7.5}$$

The above equation can be simplified by introducing overall boundary conditions at the pipe wall. Note that local boundary conditions already appear in Equations 7.3 and 7.4 in the form of interaction terms as a result of the probabilistic averaging process carried out in their derivations in Chapter 4.

The first boundary condition is the wall no-slip condition for the fluid phase which applies in the case of multiphase mixtures in the same way as in the case of single phase fluids. This condition leads to the result :

$$(r\alpha_f^B)_{r=R} = 0 \tag{7.6}$$

The second major boundary condition concerns the presence of the solids phase at the wall. When particles are spherical the particles and the wall will be in contact only at a finite number of points. Thus :

$$(\alpha_s)_{r=R} = 0 \tag{7.7}$$

The same condition holds for angular particles and indeed for all types of particles which do not have planar surfaces. The above condition will thus be assumed to hold generally. This results in :

$$\left(r \alpha_s \rho_s \bar{s}_{rz} \right)_{r=R} = \left(r \alpha_s \tau_{rz}^s \right)_{r=R} = 0 \quad (7.8)$$

and

$$\left(\alpha_s \sigma_{rz} \right)_{r=R} = R \left(\sigma_{rz} \right)_{r=R} \quad (7.9)$$

With these relations, the integrated form of the suspension overall momentum equation becomes :

$$-\frac{\partial P}{\partial z} = -\frac{4}{D} \left(\sigma_{rz} \right)_{r=R} - \frac{4}{D} \left(s_{rz} \right)_{r=R} + \left(\rho_s - \rho_f \right) \bar{\alpha}_s g + \rho_f g \quad (7.10)$$

where the mean solids concentration across the pipe cross-section $\bar{\alpha}_s$ is defined as :

$$\bar{\alpha}_s = \frac{2}{R^2} \int_0^R \alpha_s r dr \quad (7.11)$$

It should be noted that the first term on the right hand side of Eq. 7.10 represents the shear stress at the pipe wall in the "real" gas, that is, in the gas the flow field of which is disturbed by the presence of the particles. The pressure drop in the gas flowing alone, undisturbed by the presence of the particles, is given by the Navier-Stokes equation integrated over the pipe cross-section :

$$-\frac{\partial P^0}{\partial z} = -\frac{4}{D} (\sigma_{rz}^0)_{r=R} + \rho_f g \quad (7.12)$$

The ⁰ superscripts refer to the gas flowing alone at the same superficial velocity in the absence of particles. Subtracting the above equation from Equation 7.10 gives :

$$-\frac{\partial P}{\partial z} = -\frac{\partial P^0}{\partial z} - \frac{4}{D} (\sigma_{rz} - \sigma_{rz}^0)_{r=R} - \frac{4}{D} (\tau_{rz})_{r=R} + (\rho_s - \rho_f) \alpha_s g \quad (7.13)$$

The second term on the right hand side of Equation 7.13 represents the difference between the shear stress of the "real" gas flow field, in the presence of particles, from that in the gas flowing at the same superficial velocity in the absence of particles.

In 1906 Einstein showed that the apparent viscosity of dilute suspensions could be written as

$$\mu = \mu^0 (1 + O(\alpha_s)) \quad (7.14)$$

that is, the apparent viscosity of suspensions was composed of two terms, the viscosity of the fluid in the absence of particles plus perturbation terms of the order of magnitude of the solids concentration. Molodtsov (93) generalized this result to show that

$$\sigma = \sigma^0 (1 + O(\alpha_s)) \quad (7.15)$$

which implies that for, dilute suspensions

$$\frac{4}{D} (\sigma_{rz} - \sigma_{rz}^0) = O \left[\alpha_s \frac{\partial P^0}{\partial z} \right] \quad (7.16)$$

that is, negligible compared to the other terms in Eq. 7.13. As a result, Eq. 7.13 can be written:

$$-\frac{\partial P}{\partial z} = -\frac{\partial P^0}{\partial z} - \frac{4}{D} (s_{rz})_{r=R} + (\rho_s - \rho_f) \alpha_s g \quad (7.17)$$

Equation 7.17 shows the pressure drop in vertical suspension flow to be equal to the sum of three components: the gas and solids hold-ups, the shear stress in the gas at the pipe wall and the stress in the particle phase due to particle-pipe wall collisions. This result gives a theoretical basis to the three-component pressure drop decomposition proposed on an intuitive basis as described in Chapter 2.

It also shows the importance of the rigorous analysis of external forces acting on the solids phase which was carried out in Chapter 4, where two types of solids phase stress tensors were elaborated. None of the previous general equation formulations discussed in Chapter 3 contained a term corresponding to s_{ij} . The absence of such a term would have led to a final pressure drop expression containing only fluid stress and hold-up terms which as will be shown below, does not account for the experimental findings in either the present study nor those of other workers carrying out similar experiments.

Only one term in Equation 7.17 now remains to be modelled, namely the particle collision stress tensor, in order to transform the pressure drop expression into a practically usable form. Recalling from Chapter 4 that this term arises from particles colliding with each other or with solid surfaces with the reference volume, in the case of pipe flow where the equation is integrated across the pipe cross-section this term represents particle-wall collisions.

Consider a particle moving in the vicinity of the wall as shown in Figure 7.1. The axial momentum loss of the particle colliding with the wall is proportional to the difference between the incident and reflecting velocities, that is,

$$\dot{M}_L = m_p (v_z^r - v_z^i) \quad (7.18)$$

The mean axial particle velocity at the wall is proportional to the time spent in the vicinity of the wall, or inversely proportional to the radial incident and reflecting velocities :

$$(v_z)_w = \left[\frac{v_r^i}{v_r^i - v_r^r} \right] v_z^r + \left[\frac{v_r^r}{v_r^i - v_r^r} \right] v_z^i \quad (7.19)$$

The reflecting velocities in the axial and radial directions are related to the incident velocities by the tangential and normal coefficients of restitution respectively :

$$v_z^r = x_t v_z^i \quad (7.20)$$

$$v_r^r = -x_n v_r^i \quad (7.21)$$

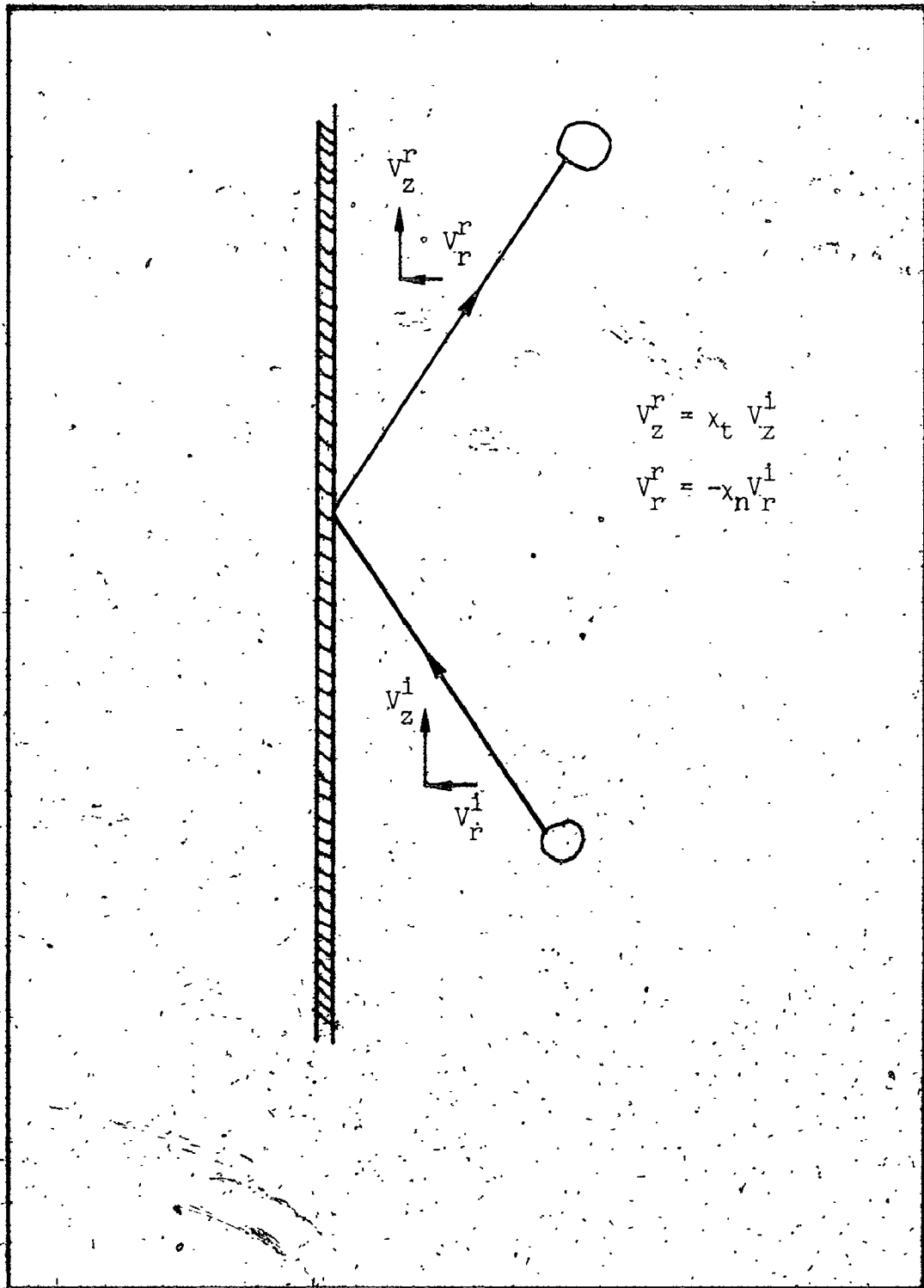


FIGURE 7.1 Particle-wall collisions

Combining the above two relations with Equation 7.19 results in :

$$(V_z)_w = \left[\frac{x_t + x_n}{1 + x_n} \right] v_z^i \quad (7.22)$$

The momentum loss expression, Equation 7.18, thus becomes :

$$m_p (v_z^r - v_z^i) = m_p (V_z)_w \left[\frac{(x_t - 1)}{(x_n + 1)} \right] (x_n + x_t) \quad (7.23)$$

The particle stress at the wall will be given by the momentum loss per collision multiplied by the collision frequency, which is, in turn, proportional to the mean solids concentration in the vicinity of the wall :

$$(s_{rz})_{r=R} = k_c (\alpha_s)_{vw} (V_z)_w \left[\frac{(x_t - 1)}{(x_n + 1)} \right] (x_n + x_t) \quad (7.24)$$

Note that the above dependence of s_{rz} on $(\alpha_s)_{vw}$ and the solids velocity at the wall holds even if the particles are not actually colliding with the wall but only sliding along it in continuous contact. The rate of momentum loss in the latter case will also

be proportional to the mean axial solids velocity at the wall and the number of contact points between the particles and the wall which in turn will be proportional to the mean solids concentration in the vicinity of the wall.

Substituting Equation 7.24 into Equation 7.17 gives :

$$\frac{\partial F}{\partial Z} = \frac{\partial P^0}{\partial Z} + k_c (\alpha_s)_{vw} (V_z)_w \left[\frac{(x_t - 1)}{(x_n + 1)} \right] (x_n + x_t) + (\rho_s - \rho_f) \bar{\alpha}_s g \quad (7.25)$$

7.2.3 Comparison with experimental results

Equation 7.25 shows the pressure drop in dilute vertically flowing gas-solids suspensions to be equal to the sum of the pressure drop given by the gas flowing alone at the same superficial velocity, the solids hold-up and a term which is dependent on the local motion of the solids phase in the vicinity of the wall. Even in the form given by Equation 7.25 which contains local variables (i.e. not measured directly in the present study) the expression provides important information on suspension pressure drops. All factors in the second term on the right hand side of Equation 7.25 are necessarily positive with the exception of $(V_z)_w$ which can be either positive (directed upwards) or negative (directed downwards). Hence Equation 7.25 allows for the possibility that the overall pressure drop is less than the sum of that due to the gas alone and the solids hold-up when the local mean solids velocity at the wall is directed

downwards. This agrees with the low gas velocity results for Series B and D presented in Chapter 6 and explains the Capes and Nakamura (20) and van Swaij et.al. (134) observations referred to earlier.

Equation 7.25 also shows the additional pressure drop to be dependent on the coefficients of restitution between the solids and the pipe wall. Indeed, elastic particle wall collisions would result in the second term on the right hand side of Eq. 7.25 being zero. This dependence may be one reason why attempts to empirically correlate pressure drops without accounting for the nature of the pipe-solids pair have been so unsuccessful (coefficients of restitution are conspicuously absent in all the correlations discussed in Chapter 2).

Another important result from Equation 7.25 is that the additional pressure drop due to the presence of the solids particles is not generally a simple function of gas and solids flowrates but depends on the nature of the solids concentration and velocity profiles across the pipe. The simplest hypothesis one could make in order to relate the local conditions present in Equation 7.25 to mean variables would be to assume that the solids concentration and velocity profiles were uniform across the pipe cross-section. Equation 7.25 would then become :

$$\frac{\partial P}{\partial z} = \frac{\partial P^0}{\partial z} + k_c (\bar{\alpha}_s) (\bar{V}_s) \left[\frac{(x_t - 1)}{(x_n + 1)} \right] (x_n + x_t) + (\rho_s - \rho_f) \bar{\alpha}_s g \quad (7.26)$$

This representation is consistent with the results presented in Chapter 6 in some respects and inconsistent in others. Firstly, the curves shown in Figures 6.8 to 6.14 for a given gas velocity (or as was later shown, a given mean solids velocity) exhibit systematic linear variations as a function of α_s . Furthermore the variations of the slopes of the curves in Figures 6.8 to 6.14 as a function of solids velocity (cf. Figures 6.15 to 6.17) were also linear over the entire range studied in Series B and D and in Series C except at the lowest gas velocity.

The assumption that concentration and velocity profiles are uniform is inconsistent with the results in Chapter 6 however in that it does not allow for additional pressure drops to be lower than the solids hold-up since all the terms in Equation 7.26 are necessarily positive; that is, the mean solids velocity averaged over the pipe cross-section is always directed upward. In addition the slopes of the curves in Figures 6.15, 6.16 and 6.17 are not consistent with this representation insofar as one would expect increasing slopes as a function of particle size since the factor k_c in Equation 7.26 is directly proportional to the particle mass. While this is true for the sand data (Series B and D) the slope of the curve in Figure 6.17 is greater than those of Figures 6.15 and 6.16 despite the fact that the glass beads had a smaller particle size.

Equation 7.25 and the above discussion show therefore that it is toward measurements of concentration and velocity profiles

where one must turn to find the necessary information required to explain suspension pressure drops.

Unfortunately such data are few and often conflicting: Konno and Saito (78) measured concentration profiles using an optical method and found glass particles to tend to concentrate near the pipe wall. The same investigators found polystyrene particles at the same gas velocity to be more concentrated near the centre of the pipe. Van Zoonen (135) in a large (500 mm) diameter pipe found 100 μm catalyst to concentrate near the pipe wall. The same observation was recorded by Matsumoto (86) with 181 μm glass particles, Doig and Roper (38) with 300-750 μm glass beads and Kramer (70) with 200 μm glass beads.

Contrary results (that is, particles concentrating near the centre of the pipe) were found by Matsumoto (86) with 1130 μm particles. Finally Reddy and Pei (106) found concentration profiles to be uniform with glass beads in a large diameter pipe at very low (0-0.6) loading ratios.

Similar ambiguous findings have been reported for particle velocity profiles: Konno and Saito (78) found them to be essentially uniform but only investigated radial locations well away from the critical area of the wall. Most other investigators found them either to be parabolic (van Zoonen (135)) or describable by power functions (Reddy and Pei (106), Kramer (79), Doig and Roper (38), Tsuji (132)) with a power index however which varied with gas velocity and particle size.

These observations and Equation 7.26 provide a further explanation concerning the lack of success in achieving pressure drop correlations based only on mean variables; clearly if, as Equation 7.27 states, the additional pressure drop is proportional to $(\alpha_s)_{vw}(V_z)_w$ the relation to $\alpha_s V_s$ of which depends on the concentration and velocity profiles which, in turn, vary with basic operating conditions, then no unique correlation would be anticipated.

Despite the ambiguities which exist in available data on solids concentration and velocity profiles, it is still possible to derive some useful information from the existing data which will help to further explain the pressure drop results and in the analysis of the heat transfer coefficient results in the next section. A common finding in all the studies cited above was a relative insensitivity of profiles, for a given solids system, to mean solids concentrations at low solids loadings. This is not to suggest that profiles are similar for similar solids systems and flow geometries when overall operating conditions are modified nor that profiles are similar once operating conditions are fixed and solids systems are changed (important variations have been found as a function of particle size for example); it is only to suggest that once operating conditions are fixed for a given solids system and flow geometry, profiles appear to be modified little by increases in solids loading provided the mean solids concentration is low.

The independence of solids concentration and velocity profiles with respect to α_s would logically result when individual particles

have little influence on the motion of neighbouring particles ; that is, when the addition of further particles has little influence on the laws governing the motion of those already present.

In addition to the profile measurements cited above, the results of Chapter 6 provided a preliminary indication of this possibility : it will be recalled that the mean particle size of the solids hold-up was found to be independent of mean solids concentration but variable as a function of gas velocity. It was argued that this could only result, under dilute conditions when particle motion was little affected by the addition of further particles.

These observations suggest that solids concentration and velocity profiles can be written in the form :

$$\alpha_s(r) = \bar{\alpha}_s f(r, U_g) \quad (7.27)$$

and

$$V_z(r) = h(r, U_g) \quad (7.28)$$

where the functions f and h are independent of the mean solids concentration, but vary, in general, as a function of gas velocity and of the solids system.

The above representations of the solids concentration and velocity profiles have been shown by Molodtsov (93) to provide asymptotic similar solutions to the probabilistic momentum equations for fully developed flow conditions. The elaborate mathematical demonstration of this will not be repeated here, although similar methods will be used in the heat transfer analysis in Section 7.3.2. What will be shown here however is that these profiles coupled with the earlier analysis leading up to Equation 7.25 is consistent with all of the hydrodynamic results presented in Chapter 6.

Firstly, the mean solids velocity averaged over the pipe cross-section defined by :

$$\bar{V}_s = \frac{1}{\alpha_s} \int_0^R \alpha_s(r) V_z(r) 2\pi r dr \quad (7.29)$$

can be written, after substituting Equations 7.27 and 7.28 into the integral as :

$$\bar{V}_s = \int_0^R f(r, U_g) h(r, U_g) 2\pi r dr \quad (7.30)$$

Since f and h are independent of the mean solids concentration, the mean solids velocity, at a given gas velocity, is also independent of α_s . This is consistent with the findings presented in Figures 6.18

through 6.21 where a linear relationship was found to exist between w_s and $\bar{\alpha}_s$; that is \bar{V}_s was found to be constant as a function of $\bar{\alpha}_s$.

It follows that Equation 7.28 can be written as :

$$V_z(r) = \bar{V}_s g(r, U_g) \quad (7.31)$$

Substituting Equations 7.27 and 7.31 into Equation 7.25 leads to the pressure drop expression of the form :

$$\frac{\partial P}{\partial Z} = \frac{\partial P^0}{\partial Z} + k_c (f)_{vw} (g)_w \left[\frac{(x_t - 1)}{(x_n + 1)} \right] (x_n + x_t) \bar{\alpha}_s \bar{V}_s + (\rho_s - \rho_f) \bar{\alpha}_s g \quad (7.32)$$

The independence of f and g with respect to solids concentration thus results in the additional pressure drop, at constant gas velocity, being strictly proportional to $\bar{\alpha}_s$, which as will be recalled from Chapter 6 (Figures 6.8 to 6.14) was found in all experiments. Despite the presence of the mean solids velocity in Equation 7.32, unlike the assumption that profiles were uniform, the above expression allows for additional pressure drops being less than the solids hold-ups since the function g can take on negative values at the pipe wall. Equation 7.32 also provides for increases in pressure drop as a function of mean solids velocity (Figures 6.14 to 6.16) although

not necessarily in a linear fashion since the dependence of f and g on gas velocity is not known.

Similar yet non-uniform profiles also provide an explanation for the observed variations in slip velocity. As mentioned earlier, most empirical approaches to the hydrodynamics of suspension flows implicitly assume that solids concentration and velocity profiles are uniform. It is generally further assumed (cf. Chapter 2) that interaction forces expressed in terms of the product of a drag coefficient and the slip velocity are balanced by gravitational and frictional forces at the wall; as frictional losses increase slip velocities show a corresponding increase.

Capes and Nakamura (20), proceeding with this type of analysis, found slip velocities for larger particles to be much greater than would have been expected from this type of reasoning.

Equation 7.30 as just mentioned predicts that mean solids velocities at a given gas velocity are constant with respect to solids loading. Mean slip velocities between the solids and the gas are, as a result, also independent of u_g . As gas velocity varies however, mean solids velocities and therefore slip velocities, will vary via variations in the functions f and h .

Thus, even if variations of frictional forces at the wall as a function of gas velocity are relatively small, large variations in mean slip velocity could easily occur if the profiles vary significantly with gas velocity: particles tending to concentrate in low gas velocity zones, near the wall for example, would lead

to higher mean slip velocities; particles concentrating near the centre of the pipe would lead to lower mean slip velocities.

The fact that Capes and Nakamura found different variations in mean slip velocities between large and small particles suggests different profiles in these two cases. The fact that slip velocities in the present study varied little as a function of gas velocity suggests that the reduced concentration profiles also varied little with gas velocity. The dependence of mean slip velocities on profiles, coupled with the lack of knowledge of the dependence of profiles on basic variables, nevertheless prevents generalization of this finding.

7.2.4. Conclusions of the hydrodynamic analysis

The analysis in the preceding sections has attempted to show the influence of system variables on the pressure drop in fully developed suspension flows. It was demonstrated that the additional pressure drop due to the presence of solids in a flowing gas stream was composed of a solids hold-up term and a term which depended on the local flow conditions of the solids phase at the pipe wall.

Relating the latter term to mean values of solids concentration and velocity averaged across the pipe cross-section requires a detailed knowledge of concentration and velocity profiles which is not, as yet, available. It was further shown that the assumption of uniform profiles is unfounded both based on direct measurements available in the literature and insofar as this assumption is inconsistent with the pressure drop results of the present and of similar studies

carried out previously.

The pressure drop and mean solids velocity data presented in Chapter 6 did however strongly suggest that reduced solids concentration and velocity profiles were independent of mean solids concentration for dilute suspensions; indeed all the hydrodynamic results were consistent with this representation.

This conclusion will play an important role in the analysis of fully developed heat transfer results to be carried out in the following section and will allow the nature of the variation of the heat transfer coefficient ratio to be determined as a function of loading ratio.

7.3 Analysis of Heat Transfer Results

7.3.1 Thermally fully developed flow

Hydrodynamically fully developed flow, as will be recalled from Section 7.2.1, is defined by the independence of the phase presence probabilities and laws of probability governing the phase velocities with respect to time and axial position. Thermally fully developed flow of gas-solids suspension in a pipe is defined in an analogous way: the temperature field is fully developed when the laws of probability governing the temperature difference of a given phase between two points in a cross-section normal to the direction of flow are independent of the choice of the cross-section. In other words, thermally fully developed flow occurs when the reduced radial temperature profiles are invariable along the pipe axis.

In this case

$$T_p(r_1, z) - T_p(r_2, z) = T_p(r) \quad (7.33)$$

which results in :

$$\left[\frac{\partial T_p}{\partial z} \right]_{r_1} = \left[\frac{\partial T_p}{\partial z} \right]_{r_2} = \text{constant} = b \quad (7.34)$$

That is, the axial temperature gradients are linear.

When the flow is thermally fully developed the energy equations in cylindrical coordinates thus simplify to :

$$\begin{aligned} \rho_f C_{p_f} U_z b + \frac{1}{r} \frac{d}{dr} (r \rho_f C_{p_f} \epsilon_r^f) \\ = \frac{\lambda_f}{r} \frac{d}{dr} r \left[\frac{d}{dr} (\alpha_f \theta_f) - \theta_a \frac{d}{dr} \alpha_f \right] - Q_{fs} \end{aligned} \quad (7.35)$$

and

$$\begin{aligned} \rho_s C_{p_s} V_z b + \frac{1}{r} \frac{d}{dr} (r \rho_s C_{p_s} \epsilon_r^s) \\ = \frac{\lambda_s}{r} \frac{d}{dr} r \left[\frac{d}{dr} (\alpha_s \theta_s) - \theta_a \frac{d}{dr} \alpha_s \right] + Q_{fs} \end{aligned} \quad (7.36)$$

for the gas and solids respectively and where θ is defined as the difference between T and the pipe wall temperature at the same axial position :

$$\theta = T - T_w \quad (7.37)$$

Summing Equations 7.35 and 7.36, integrating across the pipe cross-section and applying the same overall boundary conditions as in Section 7.2.2 amounts to writing a heat balance on a horizontal cross-section of the pipe :

$$(W_f C_f + W_s C_s) b = 2\pi R q_{ss} \quad (7.38)$$

where q_{ss} is the unit heat flux between the pipe wall and the suspension.

Equation 7.38 shows that the flow will be thermally fully developed (i.e. $b = \text{constant}$) only under constant wall heat flux conditions (hence, the choice of uniform heat flux for the experimental installation).

The first terms on the left hand sides of Equations 7.35 and 7.36 represent the enthalpy convected in the axial direction by the

gas and solids phases respectively ; the second terms are radial turbulent diffusion arising from the random velocities of each of the phases. The right hand sides of both equations are composed of radial heat conduction and interfacial heat transfer terms. It will be noted that all of these processes play a role in establishing the radial temperature profiles of each of the phases in suspension, not just that of the fluid phase, as is often assumed in treating this type of problem.

7.3.2 Asymptotic similar solutions to the energy equations

Solution to Equations 7.35 and 7.36 in order to obtain the gas and solids temperature profiles would first require knowledge of the radial variations in the hydrodynamic variables (velocity and concentration profiles) and detailed models for the interfacial transfer terms. These details, as was shown earlier in this chapter, are not yet accessible analytically nor are their variations generally known from experiment.

Since the factor of major practical interest is not the full details of the temperature profiles but the relationship between suspension heat transfer coefficients compared to those of the gas flowing alone, full solutions to the energy equations are not entirely necessary. What is necessary however is the determination of the nature of the modification in the radial temperature profiles which arises when solids are added to a flowing gas stream and the dependence of these modifications on basic flow variables.

Rather than attempt to solve the full energy equations then, the present section will be concerned with the less formidable task of examining their behavior in the case of dilute suspensions, such as the ones examined experimentally in Chapter 6. Solids and gas flow variables will be decomposed into reference and perturbation terms, the former applying to the temperature and flow fields which would be established as the mean solids concentration approaches zero, the latter applying to the modifications in these fields which arise due to the presence of solids. It will be shown that these variables provide asymptotic (as α_s approaches zero) similar solutions, independent of the mean solids concentration, to the energy equations. In the following section these variables will be substituted into the defining expression for the suspension mixed mean temperature. Reference and perturbation terms will be isolated in order to compare radial temperature profiles in the presence of solids with those in the absence of solids, thereby determining the effect of solids loading on heat transfer coefficients at constant gas velocity.

The first step in this analysis is to define reference flow and temperature fields such that the decomposed temperature and flow variables tend toward the reference fields when α_s tends toward zero. The reference flow field is defined simply as the flow field which would exist if the gas was flowing at the same superficial velocity as in the case where solids are present.

Two definitions are possible however for the temperature field. If it was required that the axial temperature field in the presence

of solids approach the reference field, this would be achieved by setting $b = b^{\circ}$ where the $^{\circ}$ superscript represents the reference field; as comparison of heat transfer coefficients requires comparison of radial temperature profiles it is necessary that the radial temperature profile in the presence of solids tend toward the radial reference temperature profile. This can only be achieved, not by setting $b = b^{\circ}$, but by setting $q_{SS} = q_g^{\circ}$, that is at equal heat fluxes. Following from Equation 7.38 the axial temperature profiles under these conditions are related to each other by :

$$\frac{b}{b^{\circ}} = \frac{W_f C_f}{W_f C_f + W_s C_s} \quad (7.39)$$

The gas and solids variables can now be expanded into Mac Laurin series about $\alpha_s = 0$:

$$\alpha_s \psi_f = \psi_f^{\circ} + \alpha_s \psi_f^1 \quad (7.40)$$

$$\psi_s = \psi_s^{\circ} + \alpha_s \psi_s^1 \quad (7.41)$$

where higher order terms are of the order α_s^2 , which in the case of dilute suspensions are negligible compared to other terms.

The above expansions as just mentioned, amount to considering the flow and temperature fields to be composed of two parts: the reference fields denoted by the $^{\circ}$ superscripts, toward which the real (i.e. in the presence of solids) fields tend as α_s approaches zero and the perturbation fields induced by the presence of solids. Both the reference and perturbation variables are independent of α_s and depend only on the superficial gas velocity and heat flux defining the reference flow and temperature fields.

Before these expansions can be introduced into the energy equations it is necessary to examine the interfacial heat transfer term Q_{fs} . As mentioned in Chapter 4, Q_{fs} represents the heat transfer per unit volume of suspension from the gas to the solids. Integrating the solids phase energy equation across the pipe cross-section, applying the same boundary conditions as in Section 7.2.2 leads to:

$$\bar{Q}_{fs} = \frac{1}{R^2} \int_0^R Q_{fs} 2r dr = \rho_s C_s \bar{\alpha}_s \bar{V}_s b \quad (7.42)$$

The term Q_{fs} thus represents a heat sink in the gas equation and a heat source in the solids equation. In most other theoretical treatments of suspension heat transfer behavior (eg. Refs. 34, 129) Q_{fs} has been taken to be equal to the internal energy increase in the solids phase in the direction of flow. Equation 7.36 however shows that only part of this heat is transferred axially at a given radial position, the rest being transferred radially by conduction

or by diffusion. Assuming that heat is transferred only axially in the solids phase amounts to neglecting these two processes.

It can be nevertheless noted that before heat can be transported either radially or axially by the solids it must first be absorbed by the gas since the solids phase presence probability is zero at the wall. The local heat flux from the gas to the solids must therefore be proportional to the local thermal heat capacity per unit volume of the particles in the neighbourhood surrounding a particular radial position. As the mean value of Q_{fs} , averaged over the pipe cross-section, is proportional to b , the local heat exchange between the gas and the solids will generally be of the form :

$$Q_{fs}(r) = \rho_s C_s \alpha_s b G(r) \quad (7.43)$$

where $G(r)$ has units corresponding to a velocity and depends only on the local hydrodynamic structure of the flow.

The Maclaurin series expansions can now be introduced into the energy equations 7.35 and 7.36 to give :

$$\begin{aligned} & \rho_f C_f (U_z^0 + \alpha_s U_z^1) b + \frac{1}{r} \frac{d}{dr} (r \rho_f C_f (\epsilon_r^{f0} + \alpha_s \epsilon_r^{f1})) \\ &= \frac{\lambda_f}{r} \frac{d}{dr} r \left[\frac{d}{dr} (\theta_f^0 + \alpha_s \theta_f^1) + (\theta_a^0 + \alpha_s \theta_a^1) \frac{d}{dr} \alpha_s \right] \\ & - \rho_s C_s \alpha_s b (G^0(r) + \alpha_s G^1(r)) \end{aligned} \quad (7.44)$$

for the gas and :

$$\begin{aligned}
 & \rho_s C_s \alpha_s (V_z^0 + \alpha_s V_z^1) b + \frac{1}{r} \frac{d}{dr} (r \rho_s C_s \alpha_s (\epsilon_r^{s0} + \alpha_s \epsilon_r^{s1})) \\
 & = \frac{\lambda_s}{r} \frac{d}{dr} r \left[\frac{d}{dr} (\theta_s^0 + \alpha_s \theta_s^1) - (\theta_a^0 + \alpha_s \theta_a^1) \frac{d}{dr} \alpha_s \right] \\
 & + \rho_s C_s \alpha_s b (G^0(r) + \alpha_s G^1(r)) \quad (7.45)
 \end{aligned}$$

for the solids.

Isolating and eliminating terms of the order α_s^2 leads to :

$$\begin{aligned}
 & \left[\frac{b^0}{1 + M\alpha_s} \right] \{ \rho_f C_f (\alpha_s U_z^1 - M\alpha_s U_z^0) + \rho_s C_s \alpha_s G^0(r) \} \\
 & = \frac{\lambda_f}{r} \frac{d}{dr} r \left[\frac{d}{dr} \alpha_s \theta_f^1 + \theta_a^0 \frac{d}{dr} \alpha_s \right] \quad (7.46)
 \end{aligned}$$

and

$$\begin{aligned}
 & \left[\frac{b^0}{1 + M\alpha_s} \right] \{ \rho_s C_s (V_z^0 - G^0(r)) \} \\
 & = \frac{\lambda_s}{r} \frac{d}{dr} r \left[\frac{d}{dr} \alpha_s \theta_s^0 - \theta_a^0 \frac{d}{dr} \alpha_s \right] \quad (7.47)
 \end{aligned}$$

for the gas and solids respectively, where

$$\bar{Ma}_s = \frac{W_s C_s}{W_f C_f} \quad (7.48)$$

It will now be recalled that the hydrodynamic analysis carried out in Section 7.2 led to the conclusion that the reduced mean solids concentration profile was independent of $\bar{\alpha}_s$. Introducing Equation 7.27 into the above two equations gives :

$$\left[\frac{\bar{\alpha}_s b^0}{1 + \bar{Ma}_s} \right] \{ \rho_f C_f (f U_Z^1 - M U_Z^0) + \rho_s C_s f G^0(r) \} \\ = \bar{\alpha}_s \frac{\lambda_f}{r} \frac{d}{dr} r \left[\frac{d}{dr} f \theta_f^1 + \theta_a^0 \frac{df}{dr} \right] \quad (7.49)$$

$$\left[\frac{\bar{\alpha}_s b^0 f}{1 + \bar{Ma}_s} \right] \{ \rho_s C_s (V_Z^0 - G^0(r)) \} \\ = \bar{\alpha}_s \frac{\lambda_s}{r} \frac{d}{dr} r \left[\frac{d}{dr} f \theta_s^0 - \theta_a^0 \frac{df}{dr} \right] \quad (7.50)$$

The mean solids concentration $\bar{\alpha}_s$ appears as a factor on both sides of the above two equations. Dividing both equations through by $\bar{\alpha}_s$ leaves only terms which are independent of solids concentration

except for the factor $1/(1+M\alpha_s)$. This signifies that the functions ψ_f^1 and ψ_s^0 represent asymptotic solutions to the energy equations which are independent of the mean solids concentration at low solids loadings provided $M\alpha_s$ is small compared to one. This condition can be lifted by reconsidering the Mac Laurin series expansions of the temperature field variables. The gas temperature field, it will be recalled, was written :

$$\alpha_f \theta_f = \theta_f^0 + \alpha_s \theta_f^1 \quad (7.51)$$

As was previously stated this expansion implies that the gas radial temperature field is composed of two parts : the reference temperature field θ_f^0 toward which the real temperature field tends as α_s approaches zero, and the perturbation field θ_f^1 . The latter term accounts for two types of perturbation : the difference between the reference and real gas temperature fields due to perturbation of a strictly hydrodynamic origin and the difference due to the fact that, at constant heat flux for the real and reference flows only part of the overall heat flux enters the gas phase. The proportion of the overall heat flux into the gas phase is given by

$$\frac{1}{1 + M\alpha_s}$$

Thus if the expansion is re-written as :

$$\alpha_f \theta_f^1 = \theta_f^0 + \frac{\alpha_s \theta_f^1}{1 + \overline{Ma}_s} \quad (7.52)$$

the new variable θ_f^1 represents only hydrodynamic perturbation. The term $(1 + \overline{Ma}_s)$ represents a similarity factor accounting for the added heat capacity of the suspension compared to that of the gas flowing alone.

Multiplying Equations 7.49 and 7.50 through by $(1 + \overline{Ma}_s)/\alpha_s$, the left hand sides become independent of α_s regardless of the value of \overline{Ma}_s . The equations thus allow for asymptotic similar solutions of the form :

$$\alpha_f \theta_f^1 = \theta_f^0 + \frac{\alpha_s \theta_f^1}{1 + \overline{Ma}_s} \quad (7.53)$$

$$\alpha_f \epsilon_r^1 = \epsilon_r^0 + \frac{\alpha_s \epsilon_r^1}{1 + \overline{Ma}_s} \quad (7.54)$$

$$\theta_a^0 = \frac{\theta_a^0}{1 + \overline{Ma}_s} \quad (7.55)$$

$$\theta_s^0 = \frac{\theta_s^0}{1 + \overline{Ma}_s} \quad (7.56)$$

$$\epsilon_r^0 = \frac{\epsilon_r^0}{1 + \overline{Ma}_s} \quad (7.57)$$

where $(1+M \bar{\alpha}_s)$ is a similarity factor.

7.3.3 Heat transfer coefficient variations

The conclusion of the preceding section, that the energy equations allow for asymptotic similar solutions, independent of the mean solids concentration when $\bar{\alpha}_s$ is small, is an extremely important result, since, as will be shown in this section, it allows the general variation of suspension heat transfer coefficient to be determined as a function of solids loading for a fixed gas velocity.

The difference between the pipe wall and suspension mixed mean temperature is defined by :

$$\begin{aligned} & (W_f C_f + W_s C_s) \theta_{mn} \\ &= \int_0^R (\rho_f C_f \alpha_f U_z \theta_f + \rho_s C_s \alpha_s V_z \theta_s) 2\pi r dr \end{aligned} \quad (7.58)$$

Substituting Equations 7.53 and 7.56 as well as the Mac'Laurin series expansion for the fluid velocity :

$$\alpha_f U_z = U_z^0 + \alpha_s U_z^1 \quad (7.59)$$

into Equation 7.58 yields :

$$\begin{aligned}
 & - (W_f C_f + W_s C_s) \theta_{mm} \\
 & = \int_0^R \rho_f C_f U_z \theta_f^0 2\pi r dr + \int_0^R \rho_f C_f \alpha_s (U_z^0 + U_z^1) \theta_f^0 2\pi r dr \\
 & \quad + \int_0^R \rho_f C_f U_z \alpha_s \frac{\theta_f^1}{1 + Ma_s} 2\pi r dr \\
 & \quad + \int_0^R \rho_s C_s \alpha_s V_z \frac{\theta_s^0}{1 + Ma_s} 2\pi r dr \tag{7.60}
 \end{aligned}$$

The first integral on the right hand side is equal to $-W_f C_f \theta_{mm}^0$, where θ_{mm}^0 is the mixed mean temperature of the gas reference field.

The other integrals on the right hand side can be written as :

$$\alpha_s \Lambda_f^0 \theta_{mm}^0 \tag{7.61}$$

$$\frac{\alpha_s}{1 + Ma_s} \Lambda_f^1 \theta_{mm}^0 \tag{7.62}$$

and :

$$\frac{\overline{Ma}_s}{1 + \overline{Ma}_s} \Lambda_s \theta_{mm}^0 \quad (7.63)$$

where the coefficients Λ_f^0 , Λ_f^1 and Λ_s are given by :

$$\Lambda_f^0 = \int_0^R f \frac{U_z^0 + U_z^1}{W_f} \frac{\theta_f^0}{\theta_{mm}^0} 2\pi r dr \quad (7.64)$$

$$\Lambda_f^1 = \int_0^R f \frac{U_z^0}{W_f} \frac{\theta_f^1}{\theta_{mm}^0} 2\pi r dr \quad (7.65)$$

$$\Lambda_s = \int_0^R f \frac{V_z}{\overline{V}_s} \frac{\theta_s^0}{\theta_{mm}^0} 2\pi r dr \quad (7.66)$$

The mixed mean temperature expression Equation 7.58 in terms of these variables becomes :

$$\begin{aligned} & (1 + \overline{Ma}_s) \theta_{mm}^0 \\ &= \theta_{mm}^0 \left[1 + \overline{\alpha}_s \Lambda_f^0 + \frac{\overline{\alpha}_s \Lambda_f^1}{1 + \overline{Ma}_s} + \frac{\overline{Ma}_s}{1 + \overline{Ma}_s} \Lambda_s \right] \end{aligned} \quad (7.67)$$

It will now be recalled that the reference temperature field was defined as that established when the reference and suspension flows were heated at constant heat flux. Comparison of heat transfer coefficients in the presence of solids to that of the reference gas flow thus amounts to comparing θ_{mm} and θ_{mm}^o since the coefficients are defined by :

$$h_g = \frac{q_g^o}{\theta_{mm}^o} \quad (7.68)$$

$$h_{ss} = \frac{q_{ss}}{\theta_{mm}} \quad (7.69)$$

Thus when $q_{ss} = q_g^o$ the following holds :

$$\frac{h_{ss}}{h_g} = \frac{\theta_{mm}^o}{\theta_{mm}} \quad (7.70)$$

Equations 7.67 and 7.70 thus yield :

$$\frac{h_{ss}}{h_g} = \frac{(1 + \overline{Ma}_s)^2}{1 + \overline{Ma}_s \left[1 + A_s + \frac{(\Lambda_f^o + A_f^1)}{M} \right] + \frac{\Lambda_f^o}{M} (\overline{Ma}_s)^2} \quad (7.71)$$

Equation 7.71 is the general expression for the variation of heat transfer coefficient ratios ~~as~~ a function of $W_s C_s / W_g C_g$ at constant gas velocity. The three coefficients which determine the functional relationship between h_{ss}/h_g and $W_s C_s / W_g C_g$ as shown in Equations 7.64, 7.65 and 7.66, represent gas flow field perturbation (Λ_f^0), the gas temperature field perturbation (Λ_f^1) and the effect of the solids temperature profile. As a result of the analysis in the preceding section and the conclusion from the hydrodynamic analysis that the reduced mean solids concentration profile and the solids velocity profile were independent of $\bar{\alpha}_s$ all three parameters are independent of the solids loading at a given gas velocity.

7.3.4 Comparison with experimental results

Equation 7.71 is a very important theoretical result since it shows that, depending on the relative magnitudes of Λ_s^0 , Λ_f^1 and Λ_s , the heat transfer coefficient ratio may either increase monotonically as a function of $W_s C_s / W_g C_g$, decrease monotonically, or decrease initially, pass through a minimum and increase thereafter. Indeed the general variations predicted by Eq. 7.71 allow for all of the behaviors exhibited by the experimental curves shown in Figure 2.4.

The general variation of h_{ss}/h_g at constant gas velocity can be seen by re-arranging Eq. 7.71 in the form :

$$\frac{(1 + M\bar{\alpha}_s)^2}{(h_{ss}/h_g)} = \left[1 + M\bar{\alpha}_s \left[1 + \Lambda_s + \frac{(\Lambda_f^0 + \Lambda_f^1)}{M} \right] + \frac{\Lambda_f^0}{M} (M\bar{\alpha}_s)^2 \right] \quad (7.72)$$

that is, in the general case, one should expect a parabolic relationship between $(1 + M \bar{\alpha}_s)^2 / (h_{ss}/h_g)$ as a function of $M \bar{\alpha}_s$ ((i.e.) $W_s C_s / W_g C_g$).

The fully developed heat transfer coefficient data from Chapter 6 is plotted in this way in Figure 7.2.

The first thing to note from in Figure 7.2 is that the data obtained at constant gas flowrate and variable solids loadings shows indeed the quadratic relationship predicted by Eq. 7.72 with the intercept at 1.

The second interesting aspect of Figure 7.2 is the fact that all the data from the four heat transfer series C-1, C-2, C-4, C-5 over Reynolds numbers varying from 6100 to 15000 falls on the same curve. This is something which was not predicted by the analysis leading up to Eq. 7.71. The three parameters Λ_f^0 , Λ_f^1 , and Λ_s were predicted to be constant at constant gas flowrate and variable solids loadings, but clearly vary as a function of gas velocity. The conclusion to be drawn from the unique curve in Figure 7.2 is that, while Λ_f^0 , Λ_f^1 and Λ_s vary with gas velocity, their variations are such that the overall result on the coefficients in Equation 7.69 is unchanged over the gas velocity range cited above.

Given the dependence of Λ_f^0 , Λ_f^1 and Λ_s on gas velocity the behavior exhibited by the series C-3 data (the lowest gas velocity examined) more closely resembles what would be expected from the analysis leading up to Eq. 7.71 : the general form of the variation

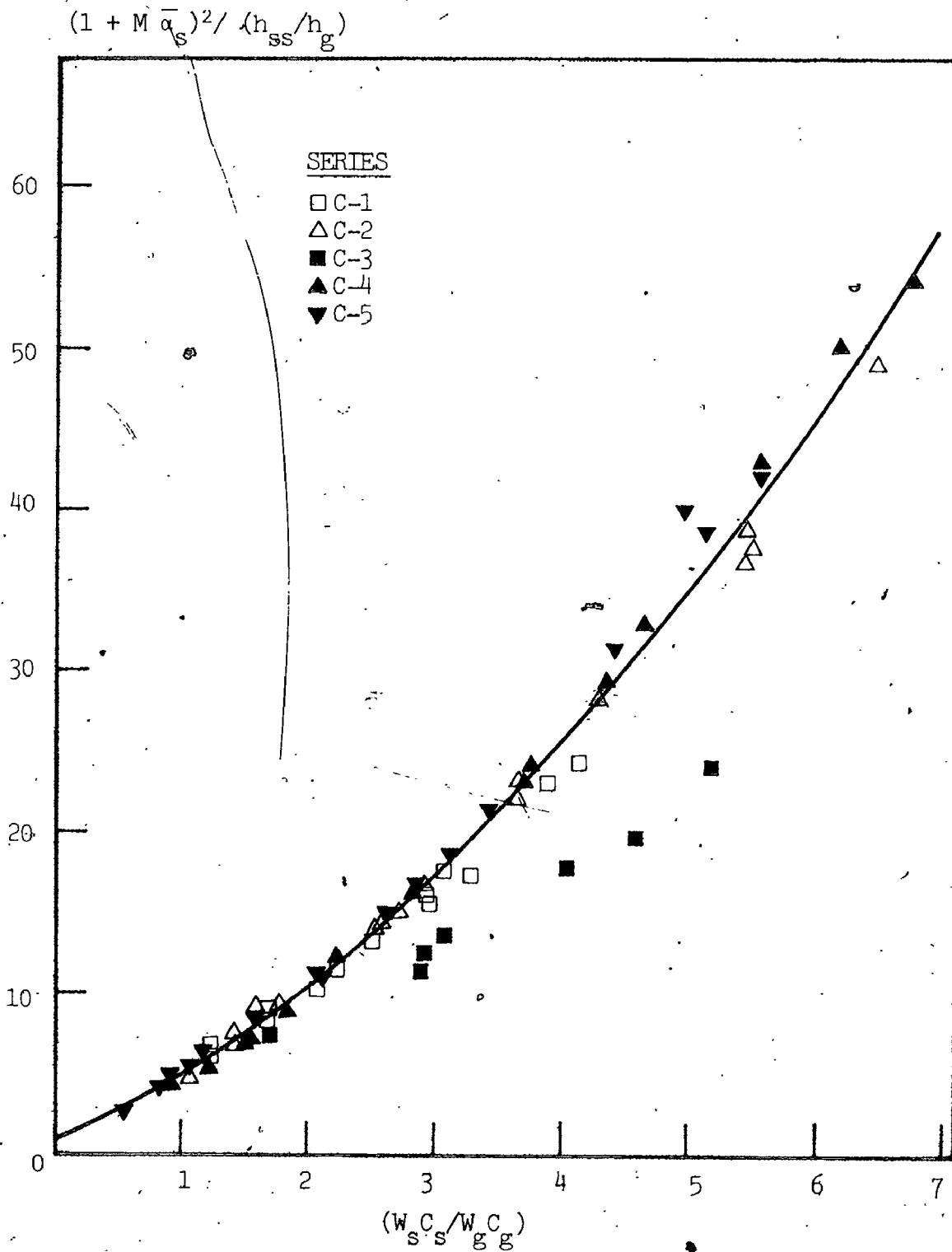


FIGURE 7.2 Variation of $(1 + M \bar{\alpha}_s)^2 / (h_{ss} / h_g)$ as a function of solids loading for the five heat transfer series

is quadratic as predicted however the coefficients have different values from those of the other four heat transfer series. It can be noted however that the series C-3 data correspond to a Reynolds number of 4500 which is not far from the laminar-turbulent transition. As the factors Λ_F^0 , Λ_F^1 and Λ_S are dependent on (indeed fully defined by) the flow structure more important variations in their values would seem reasonable near the transition.

Tien (129), as outlined in Chapter 2, attempted a theoretical approach to this same problem. Despite the numerous simplifying assumptions he was required to make (the most important of which concerned undisturbed gas flow field, uniform solids concentration profiles, and equal local solids and gas velocities) his analysis did show that heat transfer coefficients could pass through a minimum at low loading ratios. His analysis, hampered by the simplifying assumptions, did not however provide for the possibility of monotonic increases nor monotonic decreases, which as Figure 2.4 shows, have been observed experimentally. In the present analysis, the only simplifying assumptions concern the independence of the solids and concentration profiles with respect to mean solids concentration and these were substantiated by the hydrodynamic results discussed earlier.

The data in Figure 7.2 when regressed quadratically as a function of $W_S C_S / W_G C_G$ provide numerical values for the three coefficients in Eq. 7.72: (Figure 7.3 is a plot of heat transfer coefficient ratio for all data as a function of loading ratio)

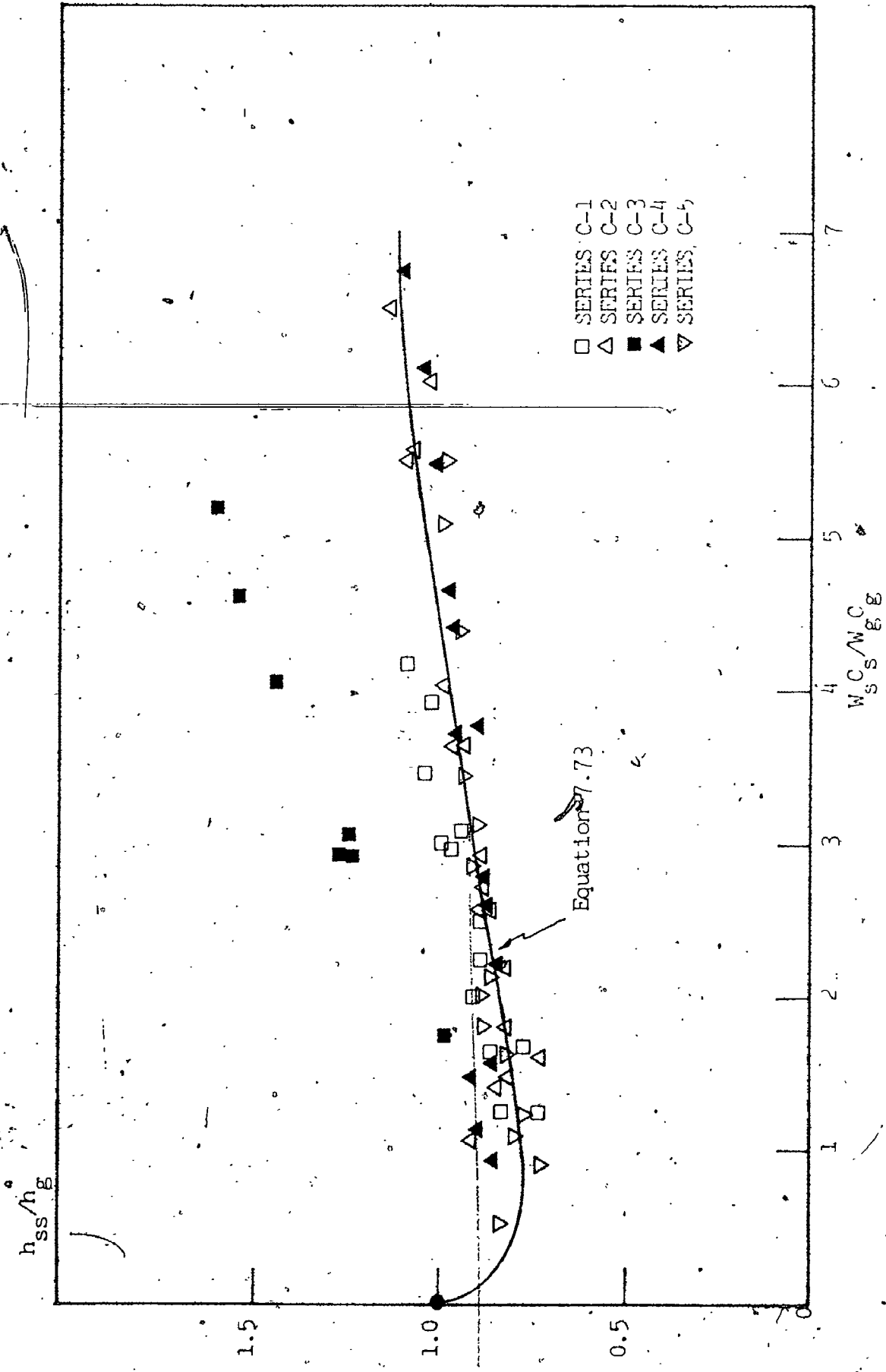


FIGURE 7.3 Variation of heat transfer coefficient as a function of solids loading for the five heat transfer series

$$\frac{(1 + \overline{Ma}_s)^2}{(h_{ss}/h_g)} = 1 + 3.426 \overline{Ma}_s + 0.681 (\overline{Ma}_s)^2 \quad (7.73)$$

(\overline{Ma} is essentially constant at constant gas velocity).

In addition to transforming Equation 7.72 into a practically usable form, the above expression adds further evidence to the invalidity of the assumptions upon which was based Tien's analysis: the terms involving gas flow and temperature field perturbations are clearly not zero as implied by Tien.

A further verification of the theoretical result given by Equation 7.71 can be obtained by re-examining similar heat transfer data existing in the literature. Figure 7.4 shows Equation 7.73 superimposed on the experimental data obtained by Depew and Farbar (34) and Tien and Quan (129) for 200 μm glass beads at four different Reynolds numbers. (Both the above pairs of authors carried out experiments in an 18 mm diameter pipe. Their data were obtained directly from the curves in their publications. The value for the glass bead heat capacity which was not available in their publications was taken to be 837 J/kg. $^{\circ}\text{C}$ based on data available in Reference 100.)

Figure 7.4 shows these data exhibiting the same quadratic variation as a function of $W_s C_s / W_g C_g$ as predicted by Equation 7.72, although over a reduced loading ratio range. The Depew and Farbar and Tien and Quan data are also shown to be well-described by the

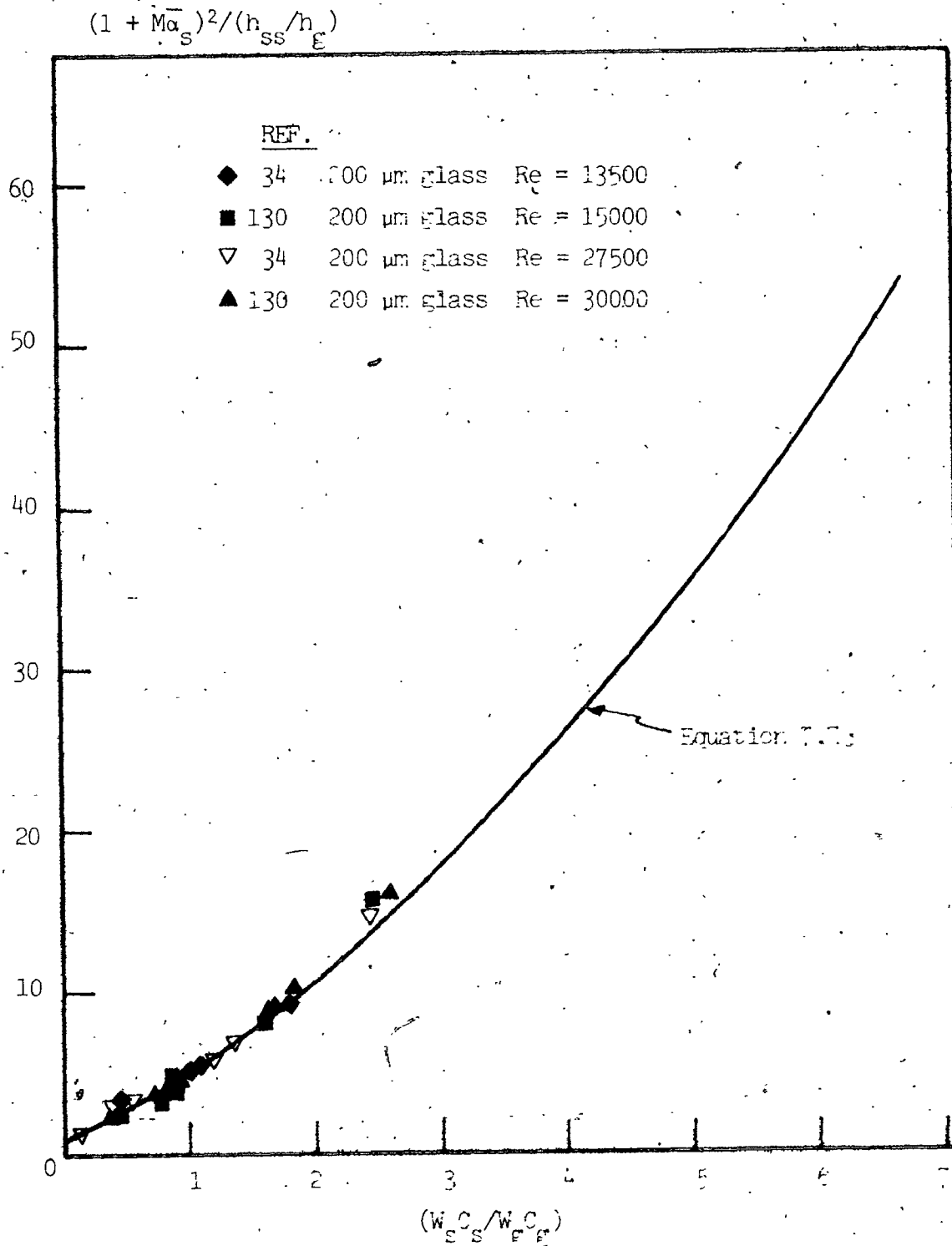


FIGURE 7.4 $(1 + Ma_s^2)^2 / (h_{ss} / h_e)$ as a function of loading:
Data of Depew and Farbar (34), and Tier and Quar (130)

same coefficients as the heat transfer data of the present study. Again little variation is shown as a function of gas velocity.

7.3.5 Conclusions of the heat transfer analysis

The analysis carried out in the preceding section has allowed the general form of the variations of heat transfer coefficient ratio as a function of loading ratio to be determined for dilute suspensions.

This result was made possible firstly, by showing the energy equations to have asymptotic similar solutions as α_s approaches zero and secondly, by introducing the major conclusion suggested from the hydrodynamic analysis, that the reduced mean solids concentration profile and solids velocity profiles were independent of the mean solids concentration.

The general variation predicted by this analysis was found to fully correspond with the variations in suspension heat transfer coefficients as a function of loading ratio presented in Chapter 6 as well as those of experiments carried out under similar conditions by others.

CHAPTER 8

CONCLUSIONS AND RECOMMENDATIONS FOR FURTHER STUDY

The introduction to this thesis referred to the need for a new line of attack in dealing with problems involving the hydrodynamic and heat transfer behaviour of gas-solids suspensions. It was suggested, based on arguments developed more fully in Chapter 2, that traditional empirical approaches to the analysis of gas-solids suspensions had failed, despite a truly astonishing number of attempts, both in providing an understanding of basic phenomena and in developing engineering design methods. It was further suggested that, given the intrinsic complexity of such flows, a more rigorous analysis was required in order to break from the sterile methodology which has characterized work in this area for the past 40 years.

The framework for a more rigorous approach, however, was found, following the detailed examination of existing general multiphase flow equation formulations presented in Chapter 3, to not have yet been developed in a fully satisfactory manner.

This thesis has therefore attempted to firstly develop the rigorous mathematical framework on which the analysis of suspension flows can be based. The probabilistic multiphase flow equations derived in Chapter 4, original in their rigorous definitions of basic flow variables and in their treatment of external forces acting on

individual phases in suspension, provide this framework.

The remainder of this thesis was concerned with the utilization of the probabilistic multiphase flow equations in the analysis of two simple yet important applications: the pressure drop and heat transfer behaviour of fully developed, dilute, vertically flowing gas-solids suspensions, the experimental study of which was made possible by the design and construction of the transport installation described in Chapter 5.

The probabilistic equations when simplified to treat the hydrodynamics of fully developed suspension flows were reduced to a form which left only one term to be modelled in order to fully determine suspension pressure drops: Pressure drops were shown to be dependent on three factors: coefficients of restitution between particles and the pipe wall and the local solids concentration and axial velocity in the vicinity of the pipe wall. The analysis showed that suspension pressure drops could be less than that given by the sum of the gas-only and solids hold-up pressure drops when solids velocities at the wall were directed downwards - a result which corresponded to what was found experimentally at low gas velocities.

The dependence of suspension drops on local conditions at the pipe wall signified that relating pressure drops to overall flow conditions required additional knowledge of concentration and velocity profiles across the pipe cross-section. It was shown that the assumption of uniform profiles was unfounded: direct experimental evidence in its favour is lacking and this assumption was shown to

not explain the overall pressure drop results from the present study.

The dependence of pressure drops on solids concentration and velocity profiles together with the lack of general experimental results on these profiles prevented the development of an overall expression for suspension pressure drops in terms of known quantities and mean flow conditions. The hydrodynamic data and observations made on profiles as reported in the literature nevertheless did strongly suggest that reduced concentration and solids velocity profiles, while not being uniform, could be considered to be independent of the mean solids concentration at low solids loadings. This result, suggested by the hydrodynamic analysis and experimental data formed the basis for the general equation analysis of the fully developed heat transfer coefficient results.

It was shown that the full gas and solids energy equations allowed for asymptotic similar solutions, independent of the mean solids concentration, when the above condition holds and the suspension is relatively dilute. These solutions were then used to develop a general expression for the variation of heat transfer coefficient ratios as a function of loading ratio. It was shown that heat transfer coefficient ratios could either increase monotonically, decrease monotonically or decrease, pass through a minimum and then increase as a function of loading ratio depending on the relative magnitudes of three parameters which are fully defined by the suspension hydrodynamics: the gas flow field perturbation, the gas temperature field perturbation, and the solids temperature field. The predicted form of the variation was confirmed experimentally using the data

of the present study and numerical values of the three coefficients cited above were determined. The resulting relation was also found to describe well similar data available in the literature.

It must be stressed that the final heat transfer coefficient expression is not a simply multi-parameter correlation. The form of the final expression was derived based on the asymptotic analysis of the full probabilistic energy equations and results suggested by the hydrodynamic analysis. The coefficients in the final expression have a clear physical significance: indeed, the heat transfer results could be used in order to determine indirectly the nature of these hydrodynamic variables.

The promising results of the more rigorous approach to gas-solids suspension initiated here and in the complementary work undertaken by Molodtsov (93) argue for the continuation in this methodological direction. The General Probabilistic Multiphase Flow Equations were elaborated to be used as a guide in the treatment of all problems involving multiphase mixtures. The experimental part of the present study, on the other hand, was limited to dilute vertically flowing gas-solids suspensions under fully developed flow conditions. Even in this specific area many questions within the general equation analysis framework remain to be answered: The pressure drop dependence on concentration and velocity profiles argues for more systematic experimental and analytic work on their determination. More heat transfer experiments will allow generalization of the findings of the present work under more diversified experimental conditions and provide further indications

on the variations of the three hydrodynamic coefficients appearing in the final heat transfer coefficient expression.

The asymptotic analysis was only strictly valid for mean solids concentrations which approach zero. Experimentally, this analysis was found to hold up to mean solids concentrations of 1% or loading ratios up to 18. The maximum value of the mean solids concentration for which this method holds must be determined experimentally in further work.

APPENDIX I

ROTAMETER CALIBRATIONS : METHODS AND RESULTS

I.1 STANDARDS

A standard orifice meter was designed and constructed in strict accordance with ASME-AFNOR specifications in order to calibrate all rotameters used in the experimental work (details of the ASME specifications are given in Ref. 7; the relevant AFNOR document is NF X 10-102).

The orifice meter installation consisted of a 58.3 mm ID drawn steel pipe, 6 m in length. At the centre of the pipe, 3 m from either end, two flanges which held the thin-plate square-edged orifice plates in place were welded. The flanges were specially designed to be interlocking so as to ensure that both the two pipe ends and the orifice plates were perfectly centered (Figure I.1). Flow straighteners were placed in the first meter of the inlet pipe 2 meters upstream from orifice-flange assembly. Pressure taps (D and $\frac{1}{2}$ D taps) were connected to water manometers allowing both the pressure drop and gauge pressure upstream to be measured. A thermocouple, placed downstream from orifice plate so as not to perturb the flow, was used to measure the gas temperature.

Various stainless-steel orifice plates ranging in diameter from 10 to 25 mm were used to cover a gas flowrate range between 8 and 80 kg/hr. For flowrates between 0 and 8 kg/hr a wet testmeter (Schlumberger: "Compteur hydraulique de précision pour laboratoires - 25 dm³") with a guaranteed precision of 0.5 % was used as a standard.

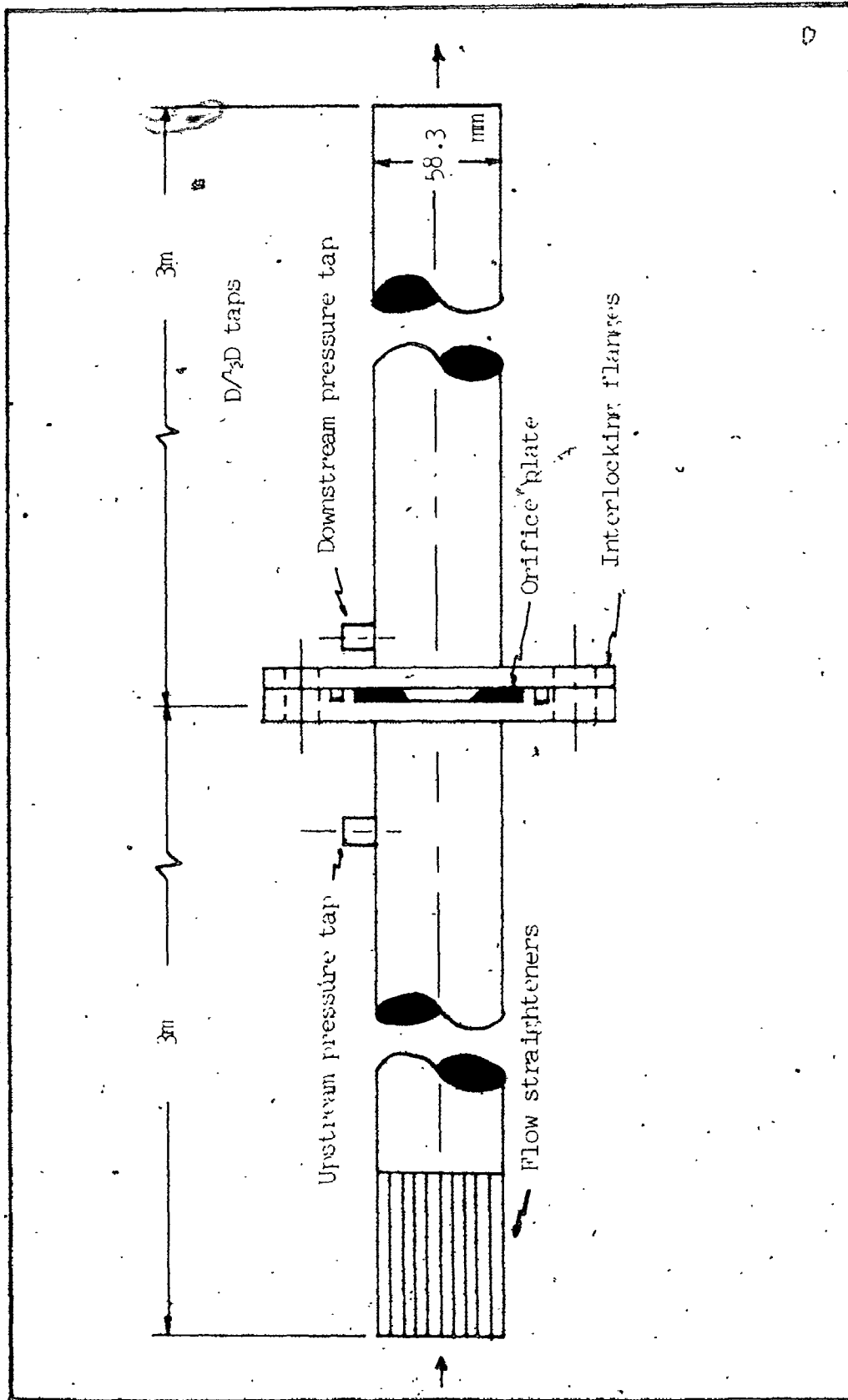


FIGURE I.1 Schematic diagram of standard orifice meter flowmeter calibration installation

I.2 METHODS, CALCULATIONS AND RESULTS

The rotameter equation describing the mass flowrate as a function of floater displacement and gas properties, as given by the rotameter supplier (Brooks, Division of Emerson Electric) is :

$$W_g = \rho_{st} k_{rm} \left[\frac{P_{ro}}{P_{st}} \right]^{0.5} \left[\frac{T_{st}}{T_{ro}} \right]^{0.5} S_c \quad (I.1)$$

where W_g = gas mass flowrate (kg/hr)

P_{ro} = pressure at rotameter outlet (kPa)

T_{ro} = temperature at rotameter outlet ($^{\circ}$ K)

S_c = scale reading

P_{st} = standard pressure = 100 kPa

T_{st} = standard temperature = 294 $^{\circ}$ K

ρ_{st} = standard air density = 1.18 kg/m³

k_{rm} = rotameter constant supplied by the manufacturer (m³/hr)

The calibrations were carried out to verify the rotameter constants as supplied by the manufacturer. In addition, it was considered possible that there be an error in the scale zero. Equation I.1 was therefore modified :

$$W_g = \rho_{st} k_r \left[\frac{P_{ro}}{P_{st}} \right]^{0.5} \left[\frac{T_{st}}{T_{ro}} \right]^{0.5} (S_c + D_s) \quad (I.2)$$

where : k_r = real rotameter constant (m³/hr)

D_s = zero scale displacement

Re-arranging Eq. I.2 gives :

$$W_g (T_{ro}/P_{ro})^{0.5} = \rho_{st} (T_{st}/P_{st})^{0.5} (k_r S_c + k_r D_s) \quad (I.3)$$

The unknowns k_r and D_s can therefore be determined by plotting $W_g (T_{ro}/P_{ro})^{0.5}$ versus S_c .

The rotameter calibrations were carried out by branching the rotameter in series with the orifice meter set-up. Temperatures, pressures, the rotameter floater displacement and the pressure drop across the orifice meter were measured for the entire flowrate range covered by the particular rotameter. The mass flowrate was determined by the standard orifice meter equation :

$$W_g = \left[\frac{\pi d_o^2}{4} \right] \left[\frac{C_d Y}{\{1 - (d_o/D)^4\}^{0.5}} \right] \sim (2\rho_g \Delta P_{orf})^{0.5} \quad (I.4)$$

where d_o = orifice diameter

ρ_g = gas density upstream from the orifice plates

ΔP_{orf} = pressure drop across the orifice

C_d = discharge coefficient

Y = gas expansion factor

The appropriate expressions for the discharge coefficient and the expansion factor are given in Ref. 7.

The various calibration curves for each of the rotameters used are shown in Figures I.2 through I.7. The corresponding formulae are given in Table I.1.

TABLE I.1

ROTAMETER FORMULAE

$$W_g = A_1 (P_{ro}/T_{ro})^{0.5} S_c + A_2 (P_{ro}/T_{ro})^{0.5}$$

$$W_g = \text{kg/s}, P_{ro} = \text{kPa}, T_{ro} = \text{°K}$$

Rotameter	A_1	A_2
SUSP 1	1.106×10^{-4}	0
SUSP 2 $30 < S_c < 57$	2.050×10^{-4}	$- 3.050 \times 10^{-3}$
SUSP 2 $57 < S_c < 100$	2.703×10^{-4}	$- 6.890 \times 10^{-3}$
SUSP 3	2.485×10^{-4}	0
SUSP 4	4.173×10^{-5}	1.222×10^{-4}
SUSP 5	8.830×10^{-6}	$- 3.744 \times 10^{-5}$
SUSP 6	1.257×10^{-5}	1.679×10^{-6}

$$W_g (T_{ro}/P_{ro})^{0.5} \times 10^3 \quad (\text{for } s^{-1} \text{ kPa}^{-1} \cdot K)$$

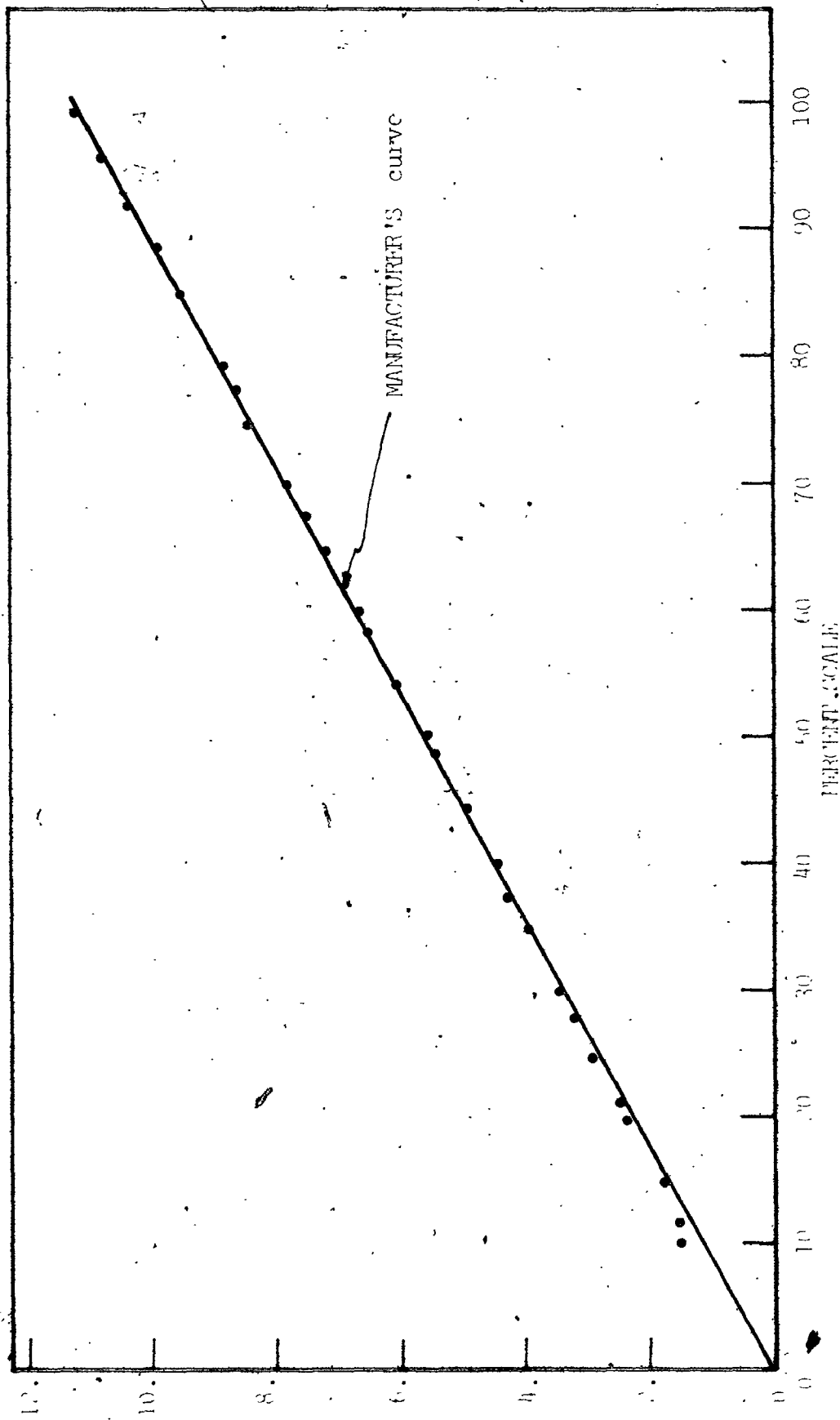


FIGURE 1.1 Calibration curve for Rotameter SUCP 4

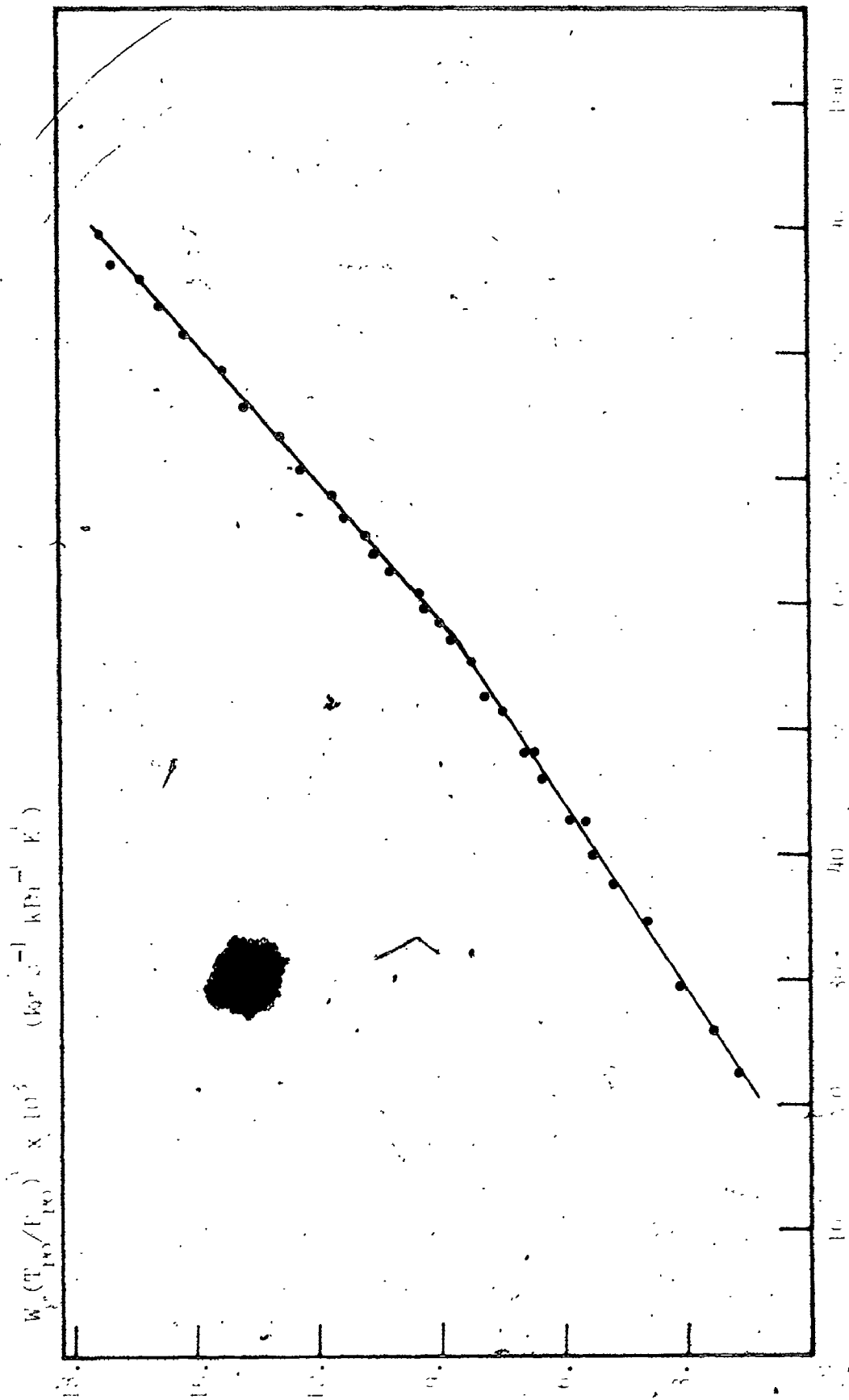


FIGURE 1. Calibration curve for detection of PCB

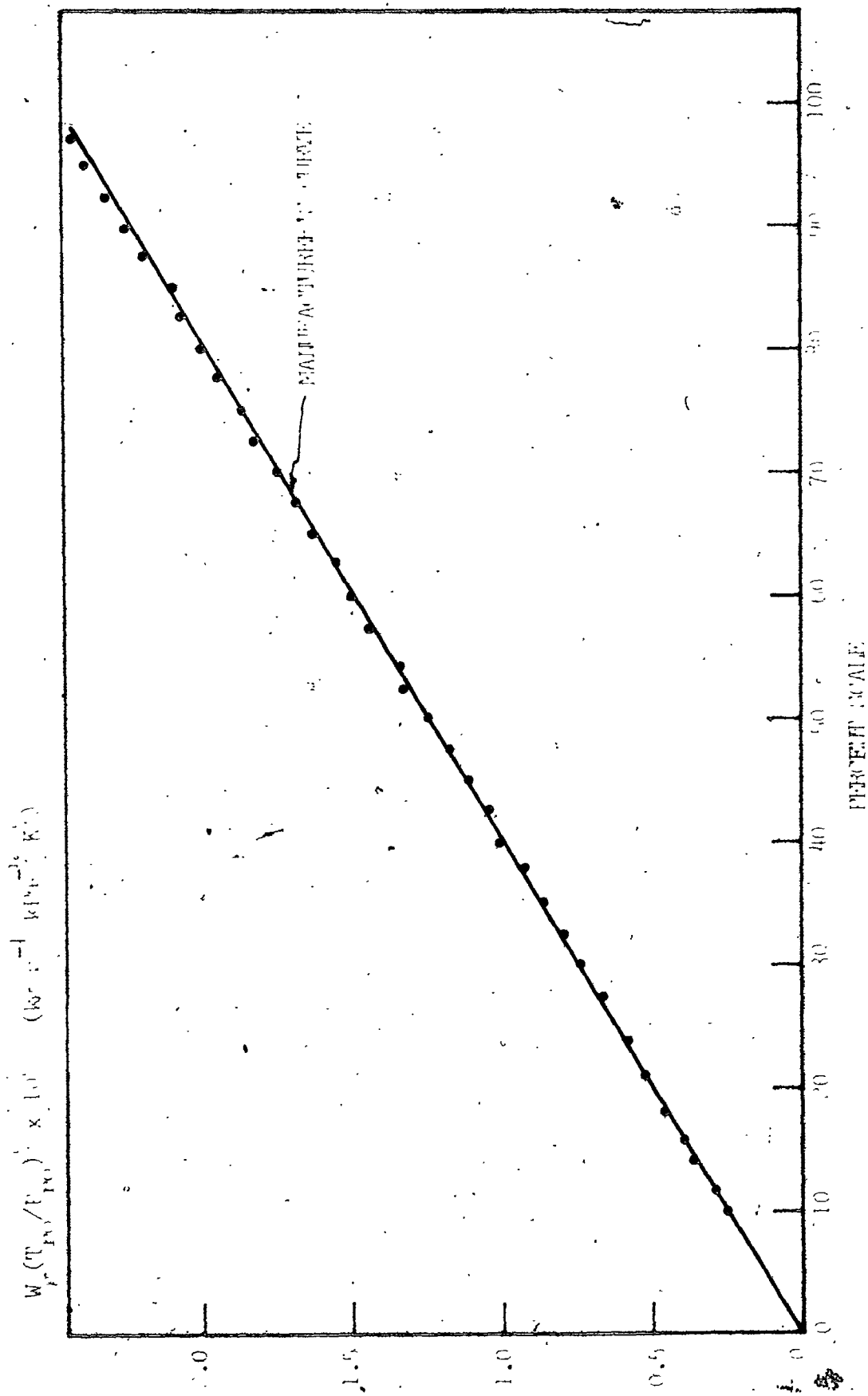


FIGURE 1.4 Calibrat. curve for Rotameter (Fig. 3)

$$W \left(\frac{T_{IV}}{T_{IV}^0} \right) \times 10^2 \quad (30^\circ \text{C}^{-1} \text{ MPa}^{-1} \text{ K}^{-1})$$

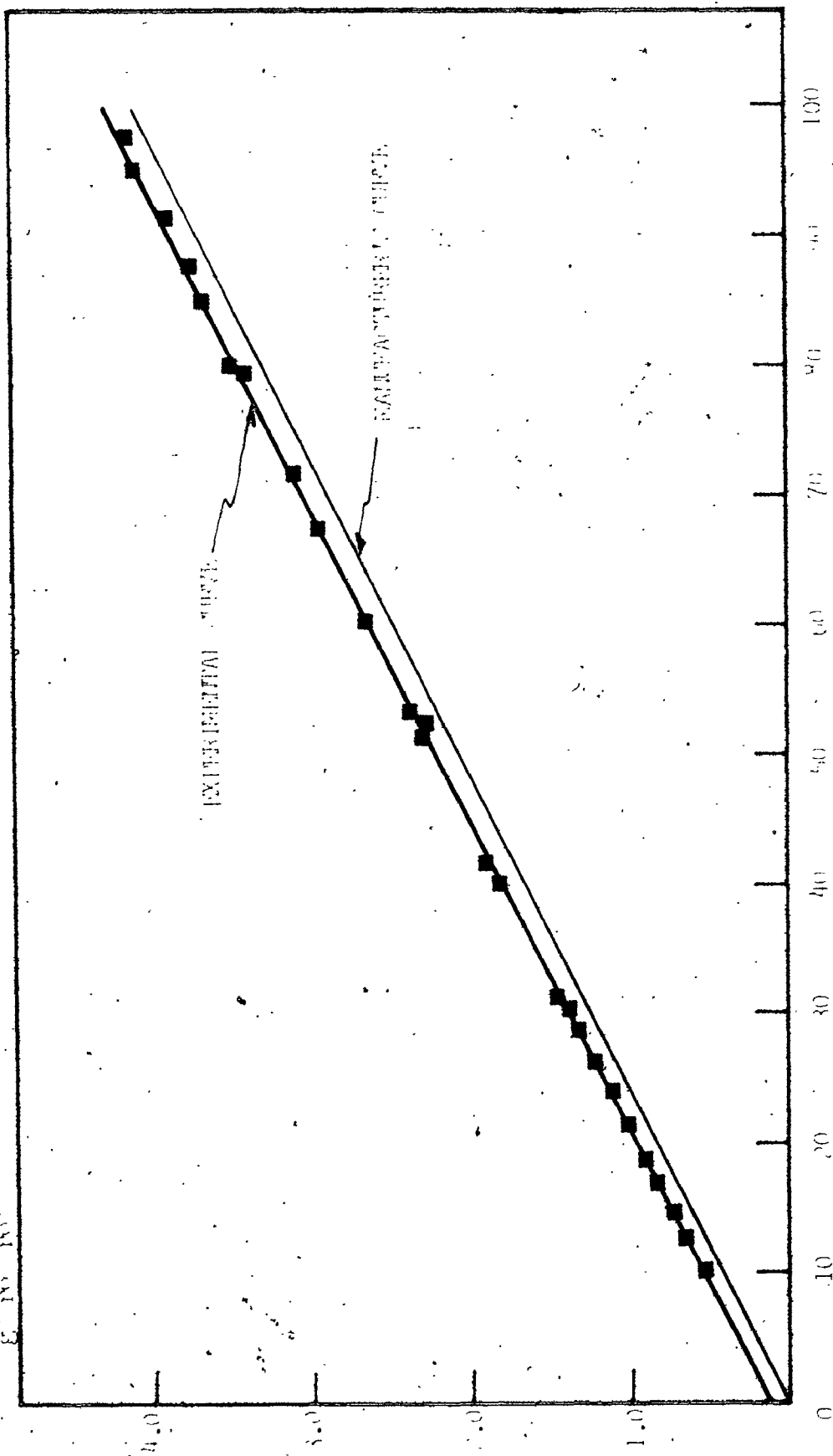


FIGURE 1.1 Calibration curve for Retanetop (MPT-4)

$$W_g (T_{ro}/P_{ro})^{1/2} \times 10^4 \quad (\text{kg s}^{-1} \text{ kPa}^{-1/2} \text{ K}^{1/2})$$

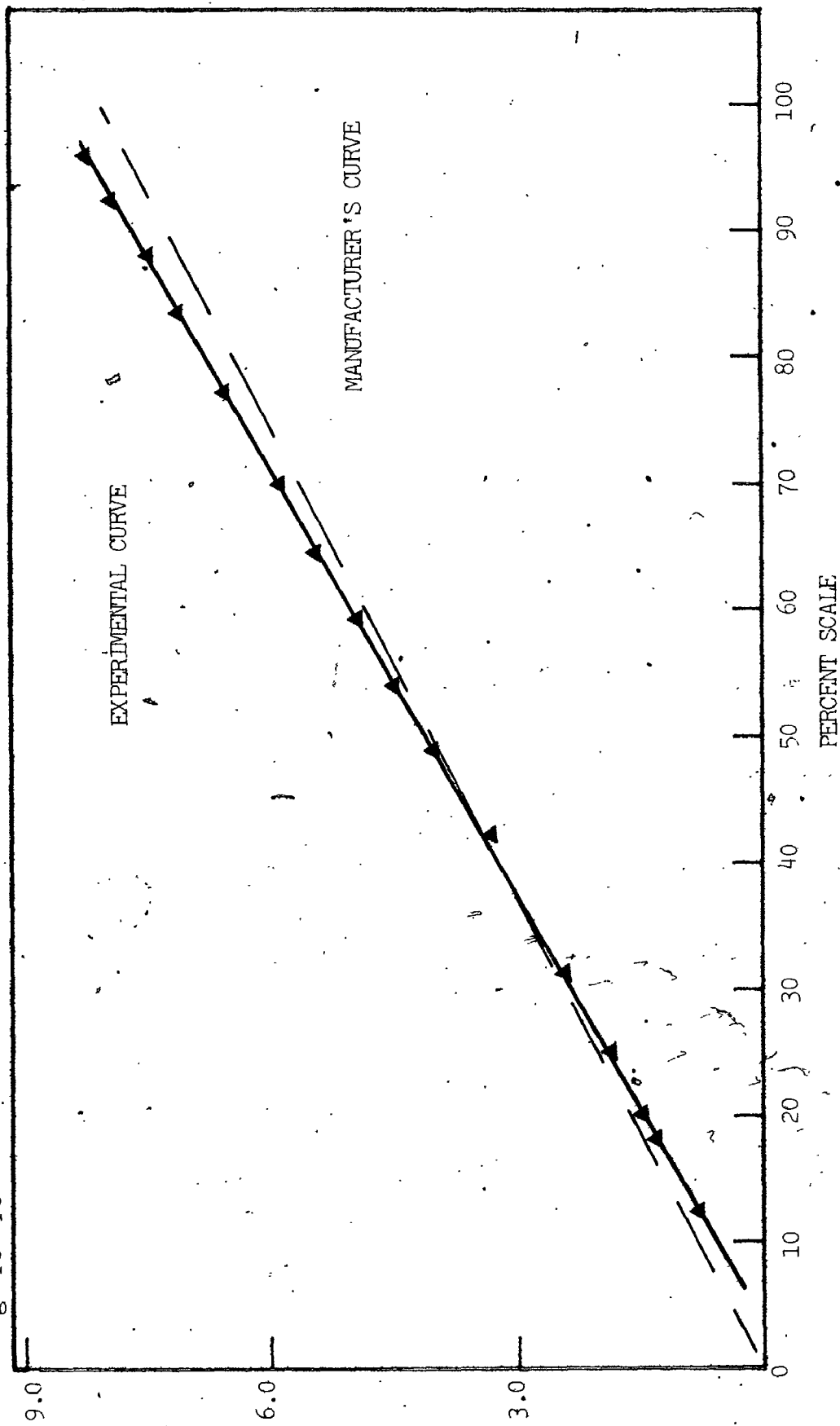


FIGURE I.6 Calibration curve for Rotameter SUSP 5

$$W_{g,ro,ro} (T/P_{ro})^{1/2} \times 10^4 \quad (\text{kg s}^{-1} \text{ kPa}^{-1/2} \text{ K}^{1/2})$$

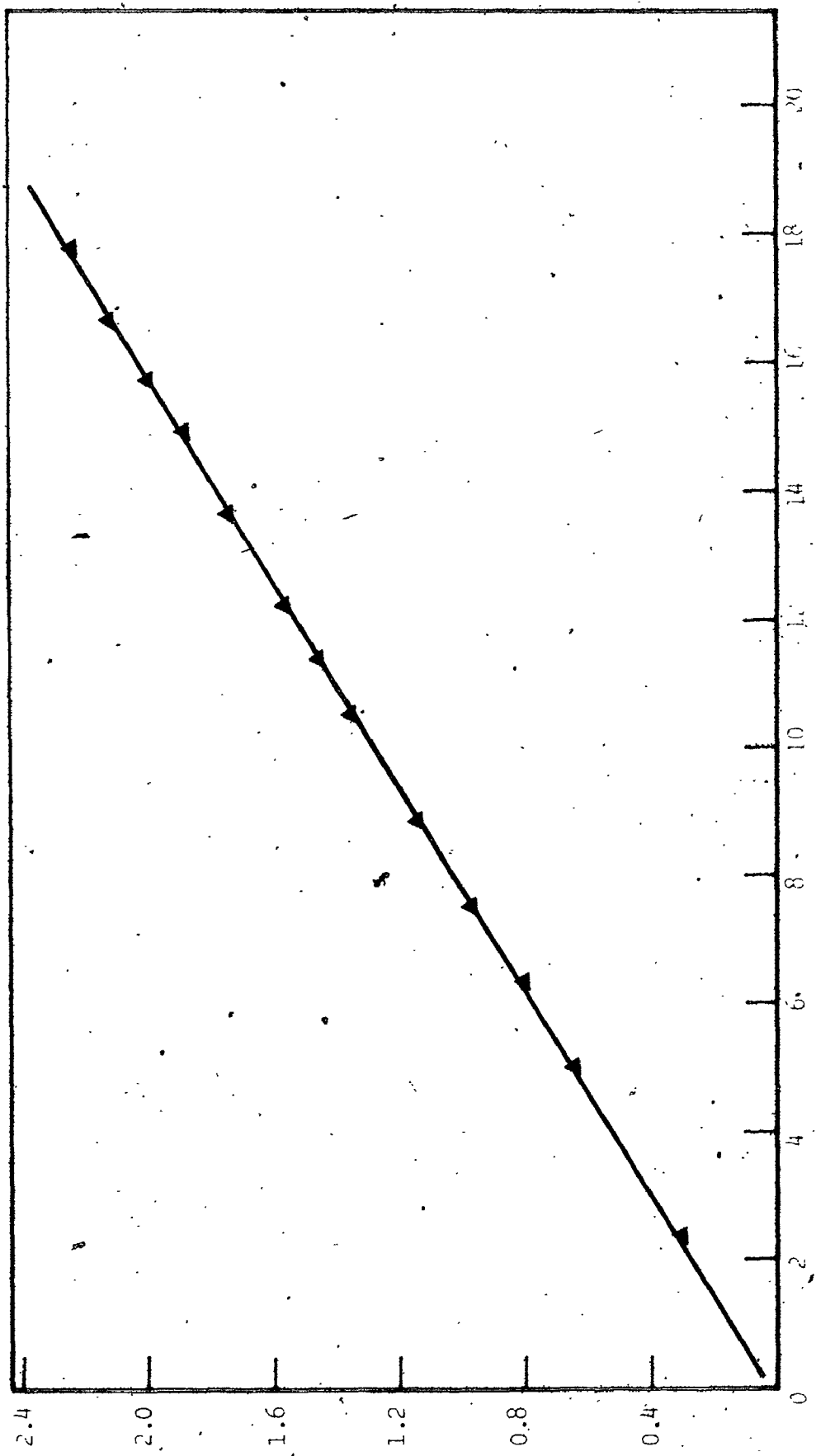


FIGURE 1.7 Calibration curve for Rotameter STCF 6



APPENDIX IV

HYDRODYNAMIC DATA

h

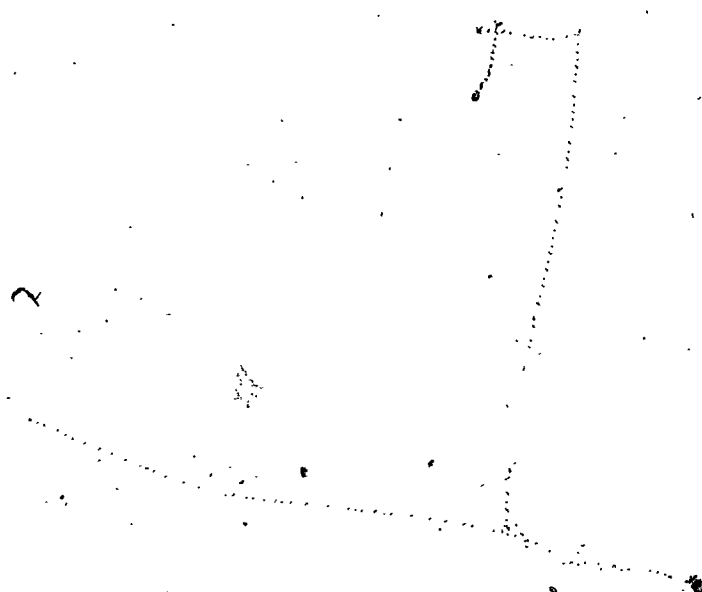
Methods and results

The calibrations of the platinum resistance thermometers were checked using a heated water bath. As the resistance heads were not immersible in water, they were first placed in a glass encapsulation which prevented them from getting wet. All the resistances were calibrated in the bath simultaneously with the full measurement circuit used in the heat transfer runs in place extension wires, etc. . . . A previously calibrated Ch. Al thermometer was used to independently measure the bath temperature. The results are presented in Table II.1.

TABLE II.1

PLATINUM RESISTANCE THERMOMETER CALIBRATIONS

Bath temperature (°C)	25.8	37.4	50.2	69.7	81.4
Resistance					
1	25.6	37.6	50.3	69.5	81.8
2	25.4	37.3	50.0	69.6	81.4
3	25.7	37.5	50.3	70.0	81.7
4	25.8	37.5	50.3	70.0	81.7
5	25.7	37.4	50.2	69.8	81.5
6	25.6	37.3	50.2	69.7	81.4
7	25.7	37.4	50.2	69.8	81.4
8	25.8	37.5	50.3	69.8	81.5
9	25.7	37.4	50.2	69.8	81.4
10	25.8	37.5	50.3	69.7	81.4
11	25.9	37.6	50.3	69.8	81.4
12	25.7	37.3	50.1	69.5	81.3
13	25.8	37.5	50.2	69.6	81.3
14	26.1	37.7	50.5	70.0	81.7
15	25.7	37.1	49.7	69.3	80.6
16	26.0	37.5	50.2	69.6	81.3



APPENDIX III

DIFFERENCE BETWEEN THE INSIDE
AND OUTSIDE PIPE WALL TEMPERATURES

III.1 INTRODUCTION

The heat transfer coefficient results between the pipe wall and the flowing gas solids suspension presented in this thesis were based on the following definition (cf. Eq. 5.32) :

$$q_{ss} = \pi D_1 h_{ss} (T_w - T_{ss}) \Delta z \quad (\text{III.1})$$

where T_w is the inside pipe wall temperature. In the experimental part of this work, the outside pipe wall temperatures were measured using platinum resistance thermometers. The objective of this appendix is to show that, even under the most extreme experimental conditions, no significant error is introduced by this apparent inconsistency.

III.2 GOVERNING EQUATIONS

Assuming negligible axial conduction (this is justified by results presented in Chapter 5) the pipe wall radial temperature distribution is given by the solution to the Fourier heat conduction equation with uniform heat generation :

$$\frac{d^2 T_w}{dr^2} + \frac{1}{r} \frac{dT_w}{dr} + \frac{q''}{\lambda_T} = 0 \quad (\text{III.2})$$

Integrating the above equation twice gives the general form of the temperature distribution :

$$T_w = \frac{q_r}{2\pi r} + C_1 \ln r + C_2$$

It can be noted that the above equation allows for the temperature on the outside wall surface to be higher than on the inside wall surface in the case where the pipe is perfectly insulated on the outside, for example, or lower than on the inside wall in the cases where radial losses are high with respect to heat flux toward the suspension.

The constants C_1 and C_2 can be determined using the following two boundary conditions:

$$\frac{q_r}{2\pi r} = -k \frac{dT}{dr} \bigg|_{r=r_o}$$

The above condition relates the heat losses to the atmosphere to the heat conduction at the outer pipe wall surface. This allows determination of the first constant C_1 as:

$$C_1 = \frac{r_o^2 q_r}{2\lambda_m} = \frac{q_r}{2\pi \lambda_m}$$

The second boundary condition is simply:

$$T_w = T_{wi} \text{ at } r = r_i$$

and leads to:

$$C = T_{wi} + \frac{r_i^2 q''}{4\lambda_T} + \left[\frac{q''}{2\pi L \lambda_T} \frac{r_0^2 q''}{2\lambda_T} \right] (\ln r_i) \quad (\text{III.6})$$

Substituting the constants into Equation III.3 and making use of the additional relation :

$$q_i/L = U_0 r_0 (T_{wo} - T_\infty) \quad (\text{III.7})$$

gives the radial temperature profile as :

$$T_{wo} - T_{wi} = (r_i^2 - r_0^2) \left[\frac{q''}{4\lambda_T} \right] + \left[\frac{r_0^2 q''}{\lambda_T} - \frac{U_0 r_0 (T_{wo} - T_\infty)}{\lambda_T} \right] \ln(r_0/r_i) \quad (\text{III.8})$$

III.3 RESULTS

The maximum difference between the two temperatures occurs when either $T_{wo} = T$ and $q'' = q''_{MAX}$ or when $(T_{wo} - T_\infty) = (T_{wo} - T_\infty)_{MAX}$ and $q'' = 0$. Substituting the following numerical values in the above equation :

$$r_i = 10 \times 10^{-3} \text{ m}$$

$$r_0 = 10.5 \times 10^{-3} \text{ m}$$

$$\lambda_T = 16.3 \text{ W/m}^\circ\text{C}$$

$$U_0 = 1.9 \text{ W/m}^2 \text{ }^\circ\text{C}$$

leads to the following results :

$$\text{Case 1 : } T_{wo} = T_{\infty} \quad q'' = q''_{MAX} = 7.7 \times 10^6 \text{ W/m}^3$$

(Power input = 1000 W)

$$T_{wo} - T_{wi} = 6.06 \times 10^{-2} \text{ (}^{\circ}\text{C)}$$

$$\text{Case 2 : } (T_{wo} - T_{\infty}) = (T_{wo} - T_{\infty})_{MAX} = 100^{\circ}\text{C}$$

$$q'' = 0$$

$$T_{wo} - T_{wi} = -5.97 \times 10^{-3} \text{ }^{\circ}\text{C}$$

In both cases the difference is negligible.



APPENDIX IV

HYDRODYNAMIC DATA

Hydrodynamic data for all experiments carried out with sand and glass beads are listed in the tables given in this Appendix. The data are grouped into Series A, B, C and D, the objectives of which are listed in Table 6.1.

Solids and gas flowrates are listed in (g/s). W_{g1} refers to the gas flowrate measured by rotameter at the disengaging section outlet; W_{g2} is the gas flowrate down the return line. The in-line gas mass flowrate is the sum of these two terms.

The temperatures and pressures listed in the tables allow the in-line gas velocities to be calculated from the gas mass flowrate, recalling that the inside transport line pipe diameter was 20 mm in all cases. The hydrodynamic data summaries obtained in the heat transfer runs (Series C) list two temperatures: at the heat transfer test section entry point (T(4086)) and at the test section outlet (T(8410)).

All pressure gradient data is given relative to the pressure in the disengaging zone P(CY). Absolute pressures at different points can be easily determined by simply summing P(CY) and the relative pressure listed. The pressure gradient data are listed in the tables as $P(n)-P(CY)$ where n is the transport line position as indicated in Figure 5.3.

"Valve closing time" refers to the time lapsed between the closing of the lower and upper slide valves. The error that this introduces in the mean solids concentration measurements is discussed in Section 5.2.5. The solids hold-up listed can be converted to mean

solids concentrations using Eq. 5.7.

Note finally that the solids hold-up measurements in the glass bead experiments (Series D) are subject to errors discussed in Chapter 6.

TABLE IV.1
 HYDRODYNAMIC DATA : SERIES A-1, W_s 1 R/S
 PARTICLE SIZE DISTRIBUTION : P.S.D: 1 (SAAD), P_s 2620 KR/m

Run number	A-1.1	A-1.2	A-1.3	A-1.4	A-1.5	A-1.6	A-1.7
W _g (g/s)	2.65	2.18	2.17	1.93	1.70	1.43	1.74
Temperature (°C)	14.1	14.0	14.1	14.1	14.1	14.2	14.1
P (CY) (bar abs.)	1.06	1.05	1.02	1.01	1.01	1.01	1.00
Line pressures (mm H ₂ O)							
P (4676) - P (CY)	30	24	27	22.5	20.5	15	20
P (5176) - P (GY)	27	21.5	24.5	20	18.5	13	18
P (5676) - P (CY)	24	19.5	21.5	18.5	17	12	16.5
P (6176) - P (CY)	21	18	19.5	16.5	15	11	14.5
P (6676) - P (CY)	19	16	17.5	15	13.5	10.5	13
P (7176) - P (CY)	16	13	14.5	12.5	11	8.5	10.5
P (7676) - P (CY)	14	11	12.5	10.5	9.5	7.5	9

TABLE IV.1 (continued)
 HYDRODYNAMIC DATA : SERIES A-1 W_s 1 g/s
 PARTICLE SIZE DISTRIBUTION : P.S.D. 1 (SAND) ρ_s 2620 kg/m³

Run number	A-1.8	A-1.9	A-1.10	A-1.11	A-1.12	A-1.13	A-1.14
W _s (g/s)	1.54	1.25	1.07	0.842	0.75	0.703	0.584
Temperature (°C)	14.1	14.2	14.1	14.1	14.1	14.1	14.1
P (CY) (bar abs.)	1.00	1.00	0.99	0.99	0.99	1.00	1.00
Line pressures (mm H ₂ O)							
P (4676) - P (CY)	16.5	17.5	19	27	33.5	38.5	48
P (5176) - P (CY)	14.5	15.5	17	23.5	30	34.5	43
P (5676) - P (CY)	13.5	14	15	20.5	26.5	31	38
P (6176) - P (CY)	11.5	13	13.5	18	23	27	34
P (6676) - P (CY)	10.5	11	12	16	21	23.5	29.5
P (7176) - P (CY)	8	9	10	13.5	17	20	25
P (7676) - P (CY)	7	7.5	8.5	11	14.5	16.5	21

TABLE IV.2
 HYDRODYNAMIC DATA : SERIES A-2 $W_s = 2 \text{ g/s}$
 PARTICLE SIZE DISTRIBUTION : P.S.D. 1 (SAND) $\rho_s = 2620 \text{ kg/m}^3$

Run number	A-2.1	A-2.2	A-2.3	A-2.4	A-2.5	A-2.6	A-2.7
W_s (g/s)	2.33	2.80	3.43	2.58	1.85	2.28	2.01
Temperature (°C)	16.6	16.7	16.6	16.6	16.6	16.6	16.7
P (CY) (bar abs.)	1.08	1.09	1.10	1.08	1.07	1.05	1.04
Line pressures (mm H ₂ O)							
P (4676) - P (CY)	27	36	46	32.5	24	30	26.5
P (5176) - P (CY)	25	32	41.5	29	21	27	24
P (5676) - P (CY)	22.5	28.5	39	26	19	24	21.5
P (6176) - P (CY)	20	25.5	33	23	17	21.5	19
P (6676) - P (CY)	17.5	22.5	29	20.5	15.5	19	17
P (7176) - P (CY)	15	19	25	17.5	13	16	14.5
P (7676) - P (CY)	12	16	21	15	11	13.5	12.5

TABLE IV.2 (continued)
 HYDRODYNAMIC DATA : SERIES A-2 $W_s = 2 \text{ g/s}$
 PARTICLE SIZE DISTRIBUTION : P:S.D. 1 (SAND) $\rho_s = 2620 \text{ kg/m}^3$

Run number	A-2.8	A-2.9	A-2.10	A-2.11	A-2.12	A-2.13	A-2.14
W_g (g/s)	1.75	1.54	1.35	1.08	0.892	0.768	0.718
Temperature (°C)	16.7	16.8	16.9	16.9	16.9	16.9	16.9
P (CY) (bar abs.)	1.03	1.03	1.03	1.03	1.03	1.03	1.03
Line pressures (mm.H ₂ O)							
P (4676) - P (CY)	23.5	21	22	25	34	41.5	52
P (5176) - P (CY)	21	18.5	20	23	30.5	37.5	46
P (5676) - P (CY)	19.5	17	18	20.5	27	33.5	41
P (6176) - P (CY)	17	15.5	16	18.5	24	29.5	36
P (6676) - P (CY)	15.5	14	14.5	16.5	21.5	26	31
P (7176) - P (CY)	13.1	11.5	12.5	13.5	18	21.5	25
P (7676) - P (CY)	11.5	10	11	12	15	18.5	20

TABLE IV.3
 HYDRODYNAMIC DATA : SERIES A-3 $W_s = 5 \text{ g/s}$
 PARTICLE SIZE DISTRIBUTION : P.S.D. 1 (SAND) $\rho_s = 2620 \text{ kg/m}^3$

Run number	A-3.1	A-3.2	A-3.3	A-3.4	A-3.5	A-3.6	A-3.7	A-3.8
W_g (g/s)	3.18	3.69	4.12	3.54	2.57	2.05	2.18	1.68
Temperature (°C)	17.8	17.8	17.8	17.9	17.9	17.9	17.9	17.9
P (CY) (bar abs.)	1.10	1.11	1.12	1.11	1.09	1.08	1.05	1.04
Line pressures (mm H ₂ O)								
P (4676) - P (CY)	60	65	82	62.5	50	41.5	44	44.5
P (5176) - P (CY)	54	58	74	56.5	45	37.5	40	40
P (5676) - P (CY)	49	52.5	67	51	41.5	33.5	36	36.5
P (6176) - P (CY)	44	47	60	45.5	37	30.5	32	32.5
P (6676) - P (CY)	39	41.5	54	41	34	28	29.5	29.5
P (7176) - P (CY)	34	36	47.5	35	29	24	25	24.5
P (7676) - P (CY)	29.5	31.5	41.5	30.5	25.5	20.5	22	21.5

TABLE IV.3 (continued)
 HYDRODYNAMIC DATA : SERIES A-3 $W_s = 5 \text{ g/s}$
 PARTICLE SIZE DISTRIBUTION : P.S.D. 1 (SAND) $\rho_s = 2620 \text{ kg/m}^3$

Run number	A-3.9	A-3.10	A-3.11	A-3.12	A-3.13	A-3.14	A-3.15
W_g (g/s)	1.35	1.06	0.902	2.72	2.06	2.00	1.66
Temperature ($^{\circ}\text{C}$)	17.9	17.9	17.9	21.0	21.0	21.0	21.0
P (CY) (bar abs.)	1.04	1.04	1.04	1.06	1.05	1.02	1.01
Line pressures (mm H_2O)							
P (4676) - P (CY)	49.5	63	86	47	44	40.5	43
P (5176) - P (CY)	44.5	57.5	77	42	39	36.5	38.5
P (5676) - P (CY)	41	51	69	38.5	35.5	33	35
P (6176) - P (CY)	36	46	62	34	31.5	29.5	31
P (6676) - P (CY)	31.5	39.5	54	30	28	26.5	28
P (7176) - P (CY)	26.5	33.5	46	26	24	22.5	24
P (7676) - P (CY)	23	28.5	39	22	20	19.5	20

TABLE IV.4

HYDRODYNAMIC DATA : SERIES A-4 $\dot{W}_s = 50 \text{ g/s}$

PARTICLE SIZE DISTRIBUTION : P.S.D. 2 (SAND) $\rho_s = 2620 \text{ kg/m}^3$

Run number	A-4.1	A-4.2	A-4.3	A-4.4	A-4.5	A-4.6
$W_g \text{ (g/s)}$	5.74	4.49	3.50	3.04	2.20	1.90
Temperature ($^{\circ}\text{C}$)	19.0	17.0	16.0	18.1	18.1	16.0
P (CY) (bar abs.)	1.16	1.11	1.10	1.09	1.09	1.11
Line pressures (mm H_2O)						
P (1700) - P (CY)	404	334	316	320	401	490
P (1950) - P (CY)	382	315	297	301	381	465
P (2450) - P (CY)	349	289	270	275	346	435
P (2700) - P (CY)	336	276	256	263	338	417
P (2950) - P (CY)	322	266	246	255	323	397
P (3200) - P (CY)	308	253	236	245	309	380
P (3400) - P (CY)	301	247	227	236	299	365
P (3780) - P (CY)	286	233	213	220	276	340
P (4676) - P (CY)	212	172	162	168	220	265
P (5176) - P (CY)	174	143	139	140	185	220
P (5676) - P (CY)	147	122	121	122	160	185
P (6176) - P (CY)	124	101	100	100	130	153
P (6676) - P (CY)	102	81	78	78	100	123
P (7176) - P (CY)	78	62	56	56	73	90
P (7676) - P (CY)	57	43	37	37	48	55

TABLE IV.4 (continued)
 HYDRODYNAMIC DATA : SERIES A-4 W_s 50 g/s
 PARTICLE SIZE DISTRIBUTION : P.S.D. 2 (SAND) ρ_s 2620 kg/m³

Run number	A-4.7	A-4.8	A-4.9	A-4.10	A-4.11
W _g (g/s)	6.79	8.59	5.40	3.79	9.57
Temperature (°C)	16.0	18.5	17.0	19.5	20.5
P (CY) (bar abs.)	1.19	1.25	1.14	1.10	1.30
<u>Line pressures (mm H₂O)</u>					
P (1700) - P (CY)	440	510	357	303	547
P (1950) - P (CY)	414	481	335	284	515
P (2450) - P (CY)	379	439	306	259	474
P (2700) - P (CY)	363	421	293	248	454
P (2950) - P (CY)	349	405	282	236	436
P (3200) - P (CY)	335	388	270	227	417
P (3400) - P (CY)	325	378	262	220	409
P (3780) - P (CY)	307	356	255	205	382
P (4676) - P (CY)	226	255	189	152	275
P (5176) - P (CY)	187	210	139	136	228
P (5676) - P (CY)	156	173	116	116	188
P (6176) - P (CY)	129	139	93	86	153
P (6676) - P (CY)	105	110	74	66	121
P (7176) - P (CY)	80	82	54	47	91
P (7676) - P (CY)	58	56	35	29	62

TABLE IV.5
 HYDRODYNAMIC DATA : SERIES A-5 U_g 25 g/s
 PARTICLE SIZE DISTRIBUTION : P.S.D. 2 (SAND) ρ_s 2620 kg/m³

Run number	A-5.1	A-5.2	A-5.3	A-5.4	A-5.5	A-5.6	A-5.7
W (g/s)	2.76	2.23	1.82	3.01	4.19	2.20	1.98
Temperature (°C)	26.0	17.0	18.5	18.0	17.5	16.0	17.0
Rel. humidity (%)	24	56	31	38	44	23	31
P (CY) (bar abs.)	1.08	1.07	1.07	1.07	1.09	1.03	1.03
Line pressures (mm H ₂ O)							
P (1700) - P (CY)	173	192	236	182	205	185	211
P (1950) - P (CY)	163	184	225	174	195	176	200
P (2450) - P (CY)	150	169	206	158	179	160	185
P (2700) - P (CY)	145	163	200	153	172	155	178
P (2950) - P (CY)	138	156	191	146	165	149	171
P (3200) - P (CY)	132	150	181	139	158	143	164
P (3400) - P (CY)	129	146	177	136	155	138	157
P (3780) - P (CY)	120	135	164	128	146	128	146
P (4676) - P (CY)	91	104	127	96	108	99	115
P (5176) - P (CY)	78	90	110	81	90	85	102
P (5676) - P (CY)	66	75	94	68	75	73	86
P (6176) - P (CY)	55	63	77	57	63	61	71
P (6676) - P (CY)	44	50	62	45	50	48	58
P (7176) - P (CY)	32	37	44	33	37	35	41
P (7676) - P (CY)	22	24	30	22	26	23	27
Solids hold-up (g)	24.922	26.603	38.979	21.029	14.989	25.214	28.729
Valve closing first	Bottom	Top	Top	Top	Top	Bottom	Bottom
Valve closing time (s)	0.01	0.07	0.06	0.04	0.07	0.03	0.10

TABLE IV.5 (continued)
 HYDRODYNAMIC DATA: SERIES A-5 W_s = 25 g/s.
 PARTICLE SIZE DISTRIBUTION: P.S.D. 2 (SAND) ρ_s = 2620 kg/m³

Run number	A-5.8	A-5.9	A-5.10	A-5.11	A-5.12	A-5.13
W _g (g/s)	1.44	5.50	3.59	4.95	6.32	9.27
Temperature (°C)	20.0	18.0	24.5	23.0	23.0	21.0
Rel. humidity (%)	19	31	34	19	19	28
P (CY) (bar abs.)	1.03	1.13	1.10	1.07	1.17	1.29
Line pressure (mm H ₂ O)						
P (1700) - P (CY)	345	250	187	239	301	433
P (1950) - P (CY)	333	237	178	226	284	410
P (2450) - P (CY)	305	217	161	206	261	376
P (2700) - P (CY)	293	209	157	198	250	361
P (2950) - P (CY)	280	201	149	190	241	348
P (3200) - P (CY)	265	191	139	183	231	332
P (3400) - P (CY)	255	187	137	178	225	323
P (3780) - P (CY)	235	176	131	167	211	306
P (4676) - P (CY)	190	130	98	124	157	226
P (5176) - P (CY)	165	108	82	102	131	189
P (5676) - P (CY)	145	90	69	85	108	157
P (6176) - P (CY)	120	74	57	70	89	129
P (6676) - P (CY)	100	59	46	56	71	103
P (7176) - P (CY)	75	44	34	41	53	78
P (7676) - P (CY)	50	31	25	28	37	53
Solids hold-up (g)	64.508	11.471	21.740	14.158	11.205	8.497
Valve closing first	Bottom	Top	Top	Top	Top	Top
Valve closing time (s)	0.09	0.02	0.08	0.03	0.02	0.09

TABLE IV.6

HYDRODYNAMIC DATA : SERIES B-1 $U_g = 1.48$ m/sPARTICLE SIZE DISTRIBUTION : P.S.D. 1 (SAND) $\rho_s = 2620$ kg/m³

Run number	B-1.1	B-1.2	B-1.3	B-1.4	B-1.5	B-1.6	B-1.7	B-1.8
W_1 (g/s)	0.549	0.551	0.551	0.553	0.558	0.549	0.551	0.561
W_2 (g/s)	0.0012	0.0011	0.0013	0.0010	0.0011	0.0012	0.0013	0.0014
W_s (g/s)	1.2	0.63	0.92	0.78	0.25	0.40	0.32	0.10
Temperature (°C)	36.7	25.0	29.2	27.3	25.3	32.0	30.0	23.2
P (CY) (bar-abs)	1.024	1.025	1.024	1.025	1.020	1.023	1.022	1.019
Line pressures (mm H ₂ O)								
P (1700) - P (CY)	132	113	125	71	76	89	78	54
P (1950) - P (CY)	128	110	121	69	75	86	75	53
P (2450) - P (CY)	123	103	114	65	70	81	70	50
P (2700) - P (CY)	119	98	110	62	66	78	67	49
P (2950) - P (CY)	116	96	107	60	64	75	65	48
P (3200) - P (CY)	112	92	104	57	61	73	64	47
P (3400) - P (CY)	109	89	102	55	59	71	61	46
P (3780) - P (CY)	103	84	93	52	55	67	57	44
P (4676) - P (CY)	90	71	79	45	47	55	50	38
P (5176) - P (CY)	80	63	68	39	41	48	44	32
P (5676) - P (CY)	71	55	59	34	36	42	39	28
P (6176) - P (CY)	61	46	50	28	30	35	32	24
P (6676) - P (CY)	51	38	41	24	25	29	27	21
P (7176) - P (CY)	40	30	31	18	19	21	20	15
P (7676) - P (CY)	29	21	25	13	14	14	14	11
Solids, hold-up (g)	30.935	25.701	27.312	16.699	17.507	19.890	17.285	12.354
Valve closing first	Top	-	Top	Bottom	Top	Bottom	Bottom	Top
Valve closing time (s)	0.04	0.00	0.03	0.02	0.01	0.04	0.01	0.03

5 5

OF / DE

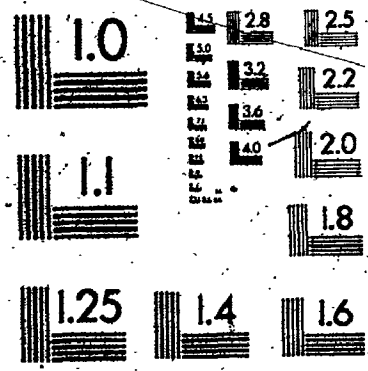


TABLE IV.6 (continued)
 HYDRODYNAMIC DATA: SERIES B-1 U_g = 1.48 m/s
 PARTICLE SIZE DISTRIBUTION: P.S.D. 1 (SAND) ρ_s = 2620 kg/m³

Run number	B-1.9	B-1.10	B-1.11	B-1.12	B-1.13	B-1.14	B-1.15	B-1.16
W ₈₁ (g/s)	0.559	0.557	0.555	0.557	0.556	0.556	0.555	0.555
W ₈₂ (g/s)	0.0012	0.0011	0.0013	0.0012	0.0013	0.0013	0.0013	0.0012
W ₅ (g/s)	0.39	0.65	0.62	0.88	0.63	0.89	0.76	0.79
Temperature (°C)	23.8	25.0	27.2	26.1	24.7	25.1	26.0	26.2
P (CY) (bar abs)	1.021	1.033	1.033	1.022	1.023	1.023	1.025	1.025
Line pressures (mm H ₂ O)								
P (1700) - P (CY)	43	62	44	45	53	69	83	73
P (1950) - P (CY)	42	60	42	43	51	66	80	70
P (2450) - P (CY)	41	56	39	40	48	62	75	67
P (2700) - P (CY)	40	55	38	39	47	61	74	66
P (2950) - P (CY)	39	53	37	37	45	58	70	64
P (3200) - P (CY)	38	51	35	35	43	56	68	62
P (3400) - P (CY)	37	50	34	34	41	55	65	60
P (3780) - P (CY)	35	47	33	32	38	52	61	57
P (4676) - P (CY)	31	39	26	27	33	44	51	48
P (5176) - P (CY)	27	34	23	24	30	40	45	42
P (5676) - P (CY)	24	30	21	21	27	36	39	38
P (6176) - P (CY)	21	26	18	18	23	31	34	33
P (6676) - P (CY)	18	22	15	15	19	26	28	28
P (7176) - P (CY)	14	17	12	13	16	21	22	22
P (7676) - P (CY)	11	13	9	10	13	16	16	16
Solids hold-up (g)	9.382	13.538	6.783	6.968	9.037	13.036	16.494	14.850
Valve closing first	Top	Top	Top	Top	Top	Top	Top	Top
Valve closing time (s)	0.03	0.01	0.01	0.01	0.03	0.00	0.04	0.02

TABLE IV.7

HYDRODYNAMIC DATA : SERIES B-2 U_g 1.72 m/s

PARTICLE SIZE DISTRIBUTION : P.S.D. 1 (SAND) ρ_s = 2620 kg/m³

Run number	B-2.1	B-2.2	B-2.3	B-2.4	B-2.5	B-2.6	B-2.7	B-2.8	B-2.9
W ₁ (g/s)	0.660	0.660	0.661	0.659	0.658	0.659	0.656	0.657	0.658
W ₂ (g/s)	0.0015	0.0016	0.0013	0.0013	0.0013	0.0014	0.0016	0.0016	0.0013
W _s (g/s)	1.1	1.2	0.63	0.58	0.59	1.1	1.5	1.6	1.1
Temperature (°C)	23.0	24.2	23.8	24.0	27.0	24.2	27.3	25.4	24.8
P (CY) (bar abs.)	1.023	1.022	1.022	1.021	1.021	1.023	1.023	1.021	1.020
Line pressures (mmH ₂ O)									
P (1700) - P (CY)	54	60	35	28	26	60	67	69	51
P (1950) - P (CY)	53	58	33	26	24	58	64	66	48
P (2450) - P (CY)	49	55	32	25	22	54	61	62	46
P (2700) - P (CY)	47	53	31	24	22	53	58	60	44
P (2950) - P (CY)	46	52	30	23	21	51	56	58	42
P (3200) - P (CY)	44	50	29	22	21	49	54	55	40
P (3400) - P (CY)	42	49	28	21	19	48	51	53	39
P (3780) - P (CY)	40	46	27	21	18	46	49	50	37
P (4676) - P (CY)	36	41	22	17	17	40	44	43	30
P (5176) - P (CY)	33	38	20	15	15	37	40	39	26
P (5676) - P (CY)	30	35	18	13	13	34	36	35	23
P (6176) - P (CY)	27	32	16	12	12	31	32	30	20
P (6676) - P (CY)	24	29	14	11	10	27	28	26	17
P (7176) - P (CY)	21	25	12	9	8	24	24	20	14
P (7676) - P (CY)	17	21	11	7	7	21	19	17	11
Solids hold-up (g)	8.610	10.567	5.227	3.227	3.489	10.045	10.943	11.128	7.979
Valve closing first	Top	Top	Top	Top	Bottom	Top	-	Bottom	Bottom
Valve closing time (s)	0.02	0.01	0.04	0.03	0.01	0.01	0.00	0.03	0.02

TABLE IV.7 (continued)

HYDRODYNAMIC DATA : SERIES B-2 U = 1.72 m/s

PARTICLE SIZE DISTRIBUTION : P.S.D. 1 (SAND) $\rho_s = 2620 \text{ kg/m}^3$

Run number	B-2.10	B-2.11	B-2.12	B-2.13	B-2.14	B-2.15	B-2.16	B-2.17
W ₁ (g/s)	0.662	0.661	0.667	0.663	0.663	0.663	0.663	0.663
W ₂ (g/s)	0.0015	0.0014	0.0016	0.0018	0.0018	0.0020	0.0020	0.0020
W _s (g/s)	1.6	1.9	2.1	2.4	2.5	3.1	2.9	3.4
Temperature (°C)	21.5	22.3	20.3	26.0	23.0	24.8	24.7	25.0
P (G) (bar abs.)	1.021	1.022	1.034	1.033	1.033	1.034	1.031	1.034
Line pressures (mm H ₂ O)								
P (1700) - P (CY)	81	98	105	117	125	158	142	175
P (1950) - P (CY)	77	93	100	113	118	154	136	169
P (2450) - P (CY)	73	88	92	106	110	142	127	156
P (2700) - P (CY)	71	85	90	102	106	136	123	149
P (2950) - P (CY)	69	81	86	98	102	130	118	147
P (3200) - P (CY)	66	78	83	93	98	124	112	137
P (3500) - P (CY)	63	75	79	90	95	119	108	131
P (3780) - P (CY)	59	70	74	85	88	111	101	120
P (4676) - P (CY)	51	59	62	72	74	92	85	103
P (5176) - P (CY)	45	52	56	64	66	83	76	91
P (5676) - P (CY)	40	47	50	57	59	74	68	81
P (6176) - P (CY)	35	41	43	49	51	65	59	69
P (6676) - P (CY)	29	35	37	42	44	54	49	58
P (7176) - P (CY)	24	29	30	35	38	45	41	48
P (7676) - P (CY)	19	23	24	28	30	35	33	36
Solids hold-up (g)	13.270	15.842	16.663	19.558	20.183	30.697	24.650	29.859
Valve closing first	Top	Bottom	Top	Top	Top	Top	Bottom	Top
Valve closing time (s)	0.05	0.03	0.06	0.05	0.05	0.03	0.05	0.05

TABLE IV.8

HYDRODYNAMIC DATA : SERIES B-3 $U_g = 2.0$ m/s
 PARTICLE SIZE DISTRIBUTION : P.S.D. 1 (SAND) $\rho_s = 2620$ kg/m³

Run number	B-3.1	B-3.2	B-3.3	B-3.4	B-3.5	B-3.6	B-3.7	B-3.8
W ₁ (g/s)	0.745	0.759	0.747	0.746	0.747	0.753	0.746	0.751
W ₂ (g/s)	0.0020	0.0023	0.0027	0.0024	0.0023	0.0023	0.0017	0.0017
W _s (g/s)	1.9	3.2	4.4	3.3	2.6	2.6	1.5	1.7
Temperature (°C)	26.0	19.0	24.0	26.4	24.3	22.1	24.5	26.5
P (CY) (bar abs)	1.021	1.022	1.022	1.023	1.023	1.018	1.021	1.023
Line pressures (mm H ₂ O)								
P (1700) - P (CY)	70	112	153	118	88	86	60	54
P (1950) - P (CY)	68	109	147	114	85	84	59	52
P (2450) - P (CY)	61	100	137	107	79	78	54	49
P (2700) - P (CY)	62	99	134	103	77	76	53	48
P (2950) - P (CY)	58	94	130	99	74	72	51	46
P (3200) - P (CY)	56	90	124	96	70	70	48	45
P (3400) - P (CY)	55	88	121	93	69	68	47	43
P (3780) - P (CY)	54	83	113	88	64	64	43	40
P (4676) - P (CY)	43	70	97	73	55	53	38	35
P (5176) - P (CY)	39	63	88	65	50	48	34	31
P (5676) - P (CY)	34	55	78	58	45	43	30	28
P (6176) - P (CY)	30	48	67	51	39	38	26	25
P (6676) - P (CY)	27	42	59	44	35	33	22	22
P (7176) - P (CY)	21	35	48	37	28	28	18	19
P (7676) - P (CY)	17	28	39	29	23	23	15	16
Solids hold-up (g)	9.694	16.999	26.929	18.192	13.203	12.750	8.459	7.023
Valve closing first	Top	Bottom	Bottom	Bottom	Top	Top	Top	Top
Valve closing time (s)	0.04	0.08	0.02	0.02	0.06	0.05	0.11	0.08

TABLE IV.8 (continued)
 HYDRODYNAMIC DATA : SERIES B-3 $U_g = 2.0$ m/s
 PARTICLE SIZE DISTRIBUTION : P.S.D. 1 (SAND) $\rho_s = 2620$ kg/m³

Run number	B-3.9	B-3.10	B-3.11	B-3.12	B-3.13	B-3.14	B-3.15	B-3.16
W_{g1} (g/s)	0.742	0.740	0.745	0.741	0.747	0.743	0.750	0.754
W_{g2} (g/s)	0.0017	0.0016	0.0022	0.0023	0.0026	0.0023	0.0022	0.0021
W_s (g/s)	1.5	1.2	3.7	4.1	4.8	4.2	1.5	1.4
Temperature (°C)	31.4	32.0	31.0	32.5	32.5	31.8	26.0	23.0
P (CY) (bar abs)	1.022	1.021	1.022	1.024	1.023	1.020	1.022	1.023
Line pressures (mm H ₂ O)								
P (1700) - P (CY)	57	44	134	148	162	147	58	51
P (1950) - P (CY)	55	43	130	143	157	142	56	49
P (2450) - P (CY)	50	40	120	136	149	134	54	47
P (2700) - P (CY)	51	39	116	130	142	128	51	45
P (2950) - P (CY)	47	37	112	125	138	124	50	44
P (3200) - P (CY)	46	36	109	122	132	120	48	40
P (3400) - P (CY)	46	35	105	117	128	115	46	40
P (3780) - P (CY)	43	34	101	111	120	109	42	38
P (4676) - P (CY)	36	27	83	93	102	92	36	32
P (5176) - P (CY)	32	24	74	84	92	81	32	29
P (5676) - P (CY)	28	22	66	74	83	71	28	26
P (6176) - P (CY)	24	19	58	66	72	62	25	23
P (6676) - P (CY)	22	17	51	57	62	55	22	20
P (7176) - P (CY)	17	14	42	48	52	47	18	16
P (7676) - P (CY)	14	12	34	37	43	37	15	13
Solids hold-up (g)	7.957	5.746	22.199	24.207	29.402	24.341	8.663	7.222
Valve closing first	Bottom	Top	Bottom	Top	Top	Top	Bottom	Top
Valve closing time (s)	0.05	0.05	0.01	0.03	0.04	0.06	0.01	0.02

TABLE IV.9

HYDRODYNAMIC DATA : SERIES B-4 U = 4.3 m/s
 PARTICLE SIZE DISTRIBUTION : P.S.D. I (SAND) $\rho_s = 2620 \text{ kg/m}^3$

Run number	B-4.1	B-4.2	B-4.3	B-4.4	B-4.5	B-4.6	B-4.7	B-4.8
W ₁ (g/s)	1.66	1.67	1.67	1.66	1.67	1.67	1.68	1.68
W _{g1} (g/s)	0.0071	0.0072	0.0058	0.0061	0.0083	0.0031	0.0051	0.0046
W _{g2} (g/s)	23.0	20.0	15.0	17.0	25.0	3.0	10.0	8.0
Temperature (°C)	19.4	19.6	21.4	22.2	21.4	16.6	16.4	18.4
P (CY) (bar abs.)	1.018	1.028	1.029	1.029	1.030	1.011	1.033	1.032
Line pressures (mm H ₂ O)								
P (0) - P (CY)	347	287	232	260	382	74	182	143
P (590) - P (CY)	293	243	196	219	323	59	147	117
P (810) - P (CY)	288	238	193	215	317	58	145	115
P (1185) - P (CY)	273	225	183	203	302	57	141	113
P (1700) - P (CY)	253	208	169	189	280	51	130	105
P (1950) - P (CY)	243	201	162	180	268	49	125	100
P (2450) - P (CY)	227	188	152	170	252	46	118	94
P (2700) - P (CY)	221	182	147	166	243	45	115	92
P (2950) - P (CY)	214	178	143	159	236	43	111	88
P (3200) - P (CY)	208	172	138	155	230	41	107	85
P (3400) - P (CY)	203	168	135	152	223	41	104	83
P (3780) - P (CY)	191	158	128	143	211	40	99	79
P (4676) - P (CY)	160	132	106	118	176	34	83	67
P (5176) - P (CY)	144	120	96	107	158	29	75	58
P (5676) - P (CY)	129	107	86	96	142	26	68	53
P (6176) - P (CY)	114	95	76	85	127	24	60	47
P (6676) - P (CY)	105	82	66	74	108	21	52	41
P (7176) - P (CY)	86	70	56	63	93	18	44	35
P (7676) - P (CY)	72	59	47	52	78	15	38	30
P (8595) - P (CY)	46	37	29	32	49	9	23	17
Solids hold-up (g)	30.832	25.095	18.787	22.763	34.673	4.078	13.721	10.260
Valve closing first	Top	Top	Top	Top	Top	Top	Top	Top
Valve closing time (s)	0.03	0.01	0.03	0.01	0.05	0.04	0.09	0.12

TABLE IV.9 (continued)
 HYDRODYNAMIC DATA : SERIES B-4 $U = 4.3 \text{ m/s}$
 PARTICLE SIZE DISTRIBUTION : P.S.D. 1 (SAND) $\rho_s = 2620 \text{ kg/m}^3$

Run number	B-4.9	B-4.10	B-4.11	B-4.12	B-4.13	B-4.14	B-4.15	B-4.16
W_1 (g/s)	1.67	1.68	1.67	1.69	1.69	1.68	1.69	1.65
W_2 (g/s)	0.0036	0.0026	0.0027	0.0030	0.0033	0.0035	0.0039	0.0039
W_3 (g/s)	5.0	1.0	2.0	3.0	4.0	5.0	6.0	7.0
Temperature (°C)	14.6	19.0	21.6	16.4	14.0	15.6	13.8	25.5
P (CY) (bat abs.)	1.016	1.036	1.024	1.038	1.033	1.032	1.028	1.030
Line pressures (mm H ₂ O)								
P (0)	94	46	60	65	83	89	110	119
P (590)	76	36	48	50	67	71	88	96
P (810)	74	35	47	49	66	69	86	94
P (1185)	73	34	46	48	65	68	85	92
P (1790)	66	30	41	43	60	63	78	86
P (1950)	162	27	39	42	54	60	74	82
P (2450)	59	25	37	39	51	57	69	76
P (2700)	55	25	36	38	50	55	68	74
P (2950)	54	24	35	37	49	54	66	73
P (3200)	52	23	34	36	47	51	64	70
P (3500)	50	22	34	35	46	50	62	68
P (3780)	49	22	32	34	44	49	60	65
P (4676)	42	19	23	28	37	41	49	55
P (5176)	36	16	20	25	35	36	44	50
P (5676)	32	14	18	23	33	33	40	45
P (6176)	28	13	17	21	26	30	35	40
P (6676)	25	11	15	19	23	27	31	35
P (7176)	21	9	13	15	20	22	27	30
P (7676)	17	8	10	13	16	18	22	25
P (8595)	11	5	5	8	10	11	14	15
Solids hold-up (g)	5.743	1.648	2.806	3.887	5.275	5.855	7.887	8.806
Valve closing first	Top	Top	Top	Top	Bottom	Top	Bottom	Top
Valve closing time (s)	0.07	0.05	0.03	0.04	0.02	0.05	0.03	0.05

TABLE IV.9 (continued)
 HYDRODYNAMIC DATA : SERIES B-4 U = 4.3 m/s
 PARTICLE SIZE DISTRIBUTION : P.S.D. 1 (SAND) $\rho_s = 2620 \text{ kg/m}^3$

Run number	B-4.17	B-4.18	B-4.19	B-4.20	B-4.21	B-4.22	B-4.23	B-4.24
W ₁ (g/s)	1.65	1.68	1.65	1.66	1.67	1.67	1.67	1.66
W _{S1} (g/s)	0.0045	0.0053	0.0098	0.0075	0.0088	0.0093	0.0051	0.0030
W _{S2} (g/s)	9.0	12.0	30.5	20.0	25.0	27.0	10±0	3.0
Temperature (°C)	25.8	16.8	19.0	19.4	14.8	15.8	18.6	20.6
P (CY) (bar abs.)	1.028	1.029	1.008	1.017	1.020	1.017	1.021	1.023
Line pressures (mm H ₂ O)								
P (O) - P (CY)	149	185	437	310	390	417	165	72
P (590) - P (CY)	122	154	362	260	325	355	137	55
P (810) - P (CY)	120	151	354	255	320	345	134	53
P (1185) - P (CY)	117	147	338	243	308	327	128	50
P (1700) - P (CY)	109	138	313	222	284	302	119	47
P (1950) - P (CY)	104	130	299	213	274	289	113	44
P (2450) - P (CY)	97	123	278	200	258	271	108	42
P (2700) - P (CY)	95	120	271	195	248	264	104	41
P (2950) - P (CY)	92	116	264	190	241	256	100	40
P (3200) - P (CY)	88	112	256	182	233	248	97	39
P (3400) - P (CY)	84	108	248	176	225	241	93	37
P (3780) - P (CY)	81	103	234	168	216	229	90	35
P (4676) - P (CY)	70	87	199	141	180	183	73	30
P (5176) - P (CY)	64	79	179	126	160	166	66	26
P (5676) - P (CY)	57	72	160	115	145	148	60	23
P (6176) - P (CY)	51	63	144	101	130	133	53	21
P (6676) - P (CY)	44	54	125	87	110	114	46	18
P (7176) - P (CY)	38	46	106	75	95	97	38	15
P (7676) - P (CY)	32	39	88	62	80	81	32	13
P (8595) - P (CY)	19	24	67	39	50	48	19	8
Solids hold-up (g)	11.435	15.196	41.411	21.721	38.384	38.692	13.752	3.914
Valve closing first	Top	Top	Bottom	Bottom	Top	Bottom	Bottom	Bottom
Valve closing time (s)	0.09	0.05	0.02	0.03	0.04	0.01	0.03	0.01

TABLE IV.10

HYDRODYNAMIC DATA : SERIES B-5 U = 5.22 m/s
 PARTICLE SIZE DISTRIBUTION : M.S.D. 1 (SAND) $\rho_s = 2620 \text{ kg/m}^3$

Run number	B-5.1	B-5.2	B-5.3	B-5.4	B-5.5	B-5.6	B-5.7
Wg1 (g/s)	2.06	2.04	2.04	2.06	2.05	2.04	2.05
Wg2 (g/s)	0.0032	0.0041	0.0046	0.0055	0.0063	0.0069	0.0085
W _s (g/s)	3.0	5.0	7.0	9.0	10.0	15.0	20.0
Temperature (°C)	15.6	16.2	15.8	12.2	15.2	16.4	14.0
P (CY) (bar abs.)	1.036	1.027	1.027	1.026	1.026	1.026	1.028
Line pressures (mm H ₂ O)							
P (O)	74	98	119	144	178	205	254
P (590)	55	75	92	141	142	163	204
P (810)	54	73	90	109	139	160	201
P (1185)	53	72	89	108	134	155	194
P (1700)	50	68	83	101	125	145	181
P (1950)	46	64	78	96	117	137	173
P (2450)	44	59	73	90	110	129	161
P (2700)	43	58	71	87	108	127	157
P (2950)	42	56	69	85	105	122	153
P (3200)	41	54	66	82	100	117	147
P (3400)	39	53	64	79	98	115	143
P (3780)	38	52	62	77	92	110	137
P (4676)	32	43	53	65	79	92	115
P (5176)	30	38	48	58	71	83	104
P (5676)	27	35	43	53	65	75	95
P (6176)	23	31	38	47	58	67	84
P (6676)	20	28	34	42	51	59	73
P (7176)	17	24	29	36	44	50	62
P (7676)	14	20	25	30	37	42	52
P (8595)	8	12	15	18	22	25	32
Solids hold-up (g)	3.159	5.297	7.101	9.770	12.444	14.837	19.797
Valve closing first	Bottom	Top	Bottom	Bottom	Bottom	Bottom	Bottom
Valve closing time (s)	0.04	0.05	0.01	0.05	0.03	0.01	0.03

TABLE IV.10 (continued)

HYDRODYNAMIC DATA: SERIES B-5 U_g 5.22 m/s
 PARTICLE SIZE DISTRIBUTION: P.S.D. 1 (SAND) ρ_s 2620 kg/m³

Run number	B-5.8	B-5.9	B-5.10	B-5.11	B-5.12	B-5.13	B-5.14
W ₁ (g/s)	2.07	2.05	2.64	2.05	2.03	2.04	2.03
W ₂ (g/s)	0.0076	0.0081	0.0044	0.0032	0.0111	0.0098	0.0087
W ₂ (g/s)	16.0	18.0	6.0	4.0	31.0	27.0	23.0
Temperature (°C)	14.6	15.6	19.2	14.8	19.8	18.8	22.8
P (CY) (bar abs.)	1.048	1.034	1.033	1.031	1.027	1.026	1.030
Line pressures (mm H ₂ O)							
P (Q) - P (CY)	216	243	413	86	410	366	318
P (590) - P (CY)	174	193	85	64	324	303	261
P (810) - P (CY)	171	189	83	63	316	295	255
P (1185) - P (CY)	162	181	79	61	302	281	243
P (1700) - P (CY)	152	168	74	56	278	254	224
P (1950) - P (CY)	145	160	70	54	267	242	214
P (2450) - P (CY)	136	151	66	51	248	226	199
P (2700) - P (CY)	133	147	65	49	240	219	194
P (2950) - P (CY)	128	142	63	48	233	214	189
P (3200) - P (CY)	124	138	60	46	225	207	183
P (3400) - P (CY)	120	134	58	44	220	201	178
P (3780) - P (CY)	116	128	57	42	210	192	170
P (4676) - P (CY)	96	107	47	37	176	156	138
P (5176) - P (CY)	86	96	42	33	160	140	124
P (5676) - P (CY)	78	87	38	30	145	127	112
P (6176) - P (CY)	70	77	34	27	129	113	100
P (6676) - P (CY)	61	67	30	24	111	97	86
P (7176) - P (CY)	52	57	29	21	95	82	74
P (7676) - P (CY)	44	47	22	18	79	69	62
P (8595) - P (CY)	27	28	12	11	51	43	38
Solids hold-up (g)	15,546	18,593	5,562	4,352	30,610	27,499	26,522
Valve closing first	Top	Bottom	Top	Bottom	Top	Top	Bottom
Valve closing time (s)	0.02	0.02	0.03	0.04	0.04	0.06	0.04

TABLE IV.11
 HYDRODYNAMIC DATA : SERIES B-6 U_g 6.16 m/s
 PARTICLE SIZE DISTRIBUTION : P.S.D. 1 (SAND) ρ_s = 2620 kg/m³

Run number	B-6.1	B-6.2	B-6.3	B-6.4	B-6.5	B-6.6	B-6.7
W ₁ (g/s)	2.42	2.41	2.44	2.43	2.39	2.44	2.40
W ₁ (g/s)	0.0094	0.0081	0.0070	0.0063	0.0040	0.0056	0.0049
W ₂ (g/s)	23.0	19.0	12.0	9.0	3.0	5.0	7.0
Temperature (°C)	13.2	16.4	11.0	13.8	20.8	10.4	17.6
P (CY) (bar abs.)	1.025	1.025	1.035	1.035	1.028	1.039	1.027
Line pressures (mm H ₂ O)							
P (O) - P (CY)	262	206	178	159	106	113	137
P (590) - P (CY)	202	158	136	120	80	83	102
P (810) - P (CY)	198	155	133	117	78	81	100
P (1185) - P (CY)	188	150	128	114	77	80	98
P (1700) - P (CY)	176	140	120	108	73	71	93
P (1950) - P (CY)	168	134	114	101	69	71	88
P (2450) - P (CY)	157	126	107	95	65	67	83
P (2700) - P (CY)	152	122	104	93	64	66	80
P (2950) - P (CY)	149	119	101	90	62	64	78
P (3200) - P (CY)	143	115	97	87	60	61	76
P (3400) - P (CY)	140	112	94	85	59	59	74
P (3780) - P (CY)	134	108	91	82	57	57	72
P (4676) - P (CY)	113	90	76	68	50	49	60
P (5176) - P (CY)	101	81	69	61	46	44	53
P (5676) - P (CY)	92	73	62	55	43	40	47
P (6176) - P (CY)	83	65	56	50	39	36	43
P (6676) - P (CY)	73	58	49	44	36	33	39
P (7176) - P (CY)	63	50	43	38	32	28	33
P (7676) - P (CY)	53	43	37	33	29	24	29
P (8595) - P (CY)	33	26	23	20	22	15	18
Solids hold-up (g)	16.346	11.634	10.182	7.992	3.177	4.734	6.074
Valve closing first	Bottom	Top	Bottom	Bottom	Top	Top	Top
Valve closing time (s)	0.02	0.05	0.06	0.06	0.05	0.05	0.02

TABLE IV.11 (continued)
 HYDRODYNAMIC DATA : SERIES B-6 U_g = 6.16 m/s
 PARTICLE SIZE DISTRIBUTION : P.S.D. 1 (SAND) ρ_s = 2620 kg/m³

Run number	B-6.8	B-6.9	B-6.10	B-6.11	B-6.12	B-6.13	B-6.14
W _{g1} (g/s)	2.40	2.40	2.39	2.41	2.39	2.40	2.40
W _{g2} (g/s)	0.0084	0.0116	0.0057	0.0051	0.0047	0.0104	0.0098
W _s (g/s)	17.0	30.5	8.0	6.0	4.0	27.0	23.0
Temperature (°C)	-19.2	19.4	20.6	15.0	19.4	19.8	19.8
P (CY) (bar abs.)	1.025	1.034	1.031	1.027	1.027	1.031	1.029
Line pressures (mm.H ₂ O)							
P (O) - P (CY)	231	366	175	125	105	344	300
P (590) - P (CY)	177	283	117	93	78	272	238
P (810) - P (CY)	173	276	115	91	76	265	234
P (1185) - P (CY)	168	263	110	88	73	252	224
P (1700) - P (CY)	157	243	102	82	69	230	207
P (1950) - P (CY)	149	231	98	78	65	216	196
P (2450) - P (CY)	140	217	92	74	62	202	184
P (2700) - P (CY)	137	211	90	71	61	197	178
P (2950) - P (CY)	132	204	87	69	59	191	173
P (3200) - P (CY)	127	197	84	67	56	185	167
P (3400) - P (CY)	124	192	81	65	54	180	162
P (3780) - P (CY)	120	184	79	63	53	173	155
P (4676) - P (CY)	100	152	66	53	44	139	127
P (5176) - P (CY)	90	138	59	48	39	124	113
P (5676) - P (CY)	81	126	53	43	35	113	103
P (6176) - P (CY)	73	113	48	39	31	102	93
P (6676) - P (CY)	65	98	43	35	28	88	82
P (7176) - P (CY)	56	82	37	30	24	74	70
P (7676) - P (CY)	47	69	32	26	20	63	59
P (8595) - P (CY)	30	42	20	16	11	38	36
Solids hold-up (g)	12.902	23.443	6.342	4.813	3.677	20.612	19.562
Valve closing first	Top	Top	Top	Bottom	Top	Top	Top
Valve closing time (s)	0.03	0.03	0.04	0.03	0.03	0.07	0.07

TABLE IV.12
 HYDRODYNAMIC DATA : SERIES B-7 U = 10.2 m/s
 PARTICLE SIZE DISTRIBUTION : P.S.D. 1 (SAND), $\rho_s = 2620 \text{ kg/m}^3$

Run number	B-7.1	B-7.2	B-7.3	B-7.4	B-7.5	B-7.6	B-7.7
W ₁ (g/s)	4.21	4.21	4.22	4.24	4.25	4.22	4.22
W ₈₁ (g/s)	0.0134	0.0162	0.0194	0.0201	0.0207	0.0239	0.0223
W ₈₂ (g/s)	3.0	5.0	10.0	15.0	20.0	35.0	30.0
Temperature (°C)	20.8	21.9	22.8	21.2	19.8	23.4	23.4
P (CY) (bar abs.)	1.026	1.102	1.114	1.115	1.113	1.112	1.114
Line pressures (mm H ₂ O)							
P (O) - P (CY)	176	199	267	308	355	484	491
P (590) - P (CY)	117	136	194	221	260	352	354
P (810) - P (CY)	116	134	192	218	256	343	345
P (1185) - P (CY)	110	128	184	208	244	323	325
P (1700) - P (CY)	101	117	170	191	226	295	296
P (1950) - P (CY)	96	111	162	183	216	281	282
P (2450) - P (CY)	91	105	152	173	204	264	265
P (2700) - P (CY)	88	102	148	168	199	256	257
P (2950) - P (CY)	86	99	144	164	194	249	250
P (3200) - P (CY)	83	95	140	159	180	242	243
P (3400) - P (CY)	80	92	137	155	176	238	239
P (3780) - P (CY)	76	89	133	150	160	226	228
P (4676) - P (CY)	64	73	105	119	134	181	181
P (5176) - P (CY)	58	65	94	106	118	161	159
P (5676) - P (CY)	50	58	84	95	107	143	144
P (6176) - P (CY)	45	50	76	85	97	130	130
P (6676) - P (CY)	39	44	67	76	87	116	116
P (7176) - P (CY)	33	40	58	66	77	102	101
P (7676) - P (CY)	27	32	51	59	67	89	88
P (8595) - P (CY)	18	21	33	38	43	57	58
Solids hold-up (g)	2.645	3.452	5.913	7.455	9.576	16.162	18.256
Valve closing first	Top	Bottom	Top	Top	Bottom	Top	Bottom
Valve closing time (s)	0.02	0.03	0.04	0.06	0.01	0.03	0.04

TABLE IV.12 (continued)
 HYDRODYNAMIC DATA : SERIES B-7 U = 10.2 m/s
 PARTICLE SIZE DISTRIBUTION : P.S.D. 1 (SAND) $\rho_s = 2620 \text{ kg/m}^3$

Run number	B-7.8	B-7.9	B-7.10	B-7.11	B-7.12	B-7.13
W _{g1} (g/s)	4.23	4.21	4.22	4.21	4.24	4.25
W _{g2} (g/s)	0.0207	0.0216	0.0168	0.0200	0.0143	0.0107
W _s (g/s)	25.0	27.0	7.0	23.0	5.0	3.0
Temperature (°C)	23.4	20.8	20.2	20.8	20.4	18.8
P (CY) (bar abs.)	1.112	1.097	1.101	1.098	1.109	1.111
Line pressures (mm H ₂ O)						
P (0) - P (CY)	411	449	227	386	212	196
P (590) - P (CY)	303	321	157	280	147	137
P (810) - P (CY)	298	314	155	275	145	136
P (1185) - P (CY)	282	296	149	260	140	131
P (1700) - P (CY)	260	271	138	240	130	124
P (1950) - P (CY)	248	259	131	229	124	118
P (2450) - P (CY)	233	243	125	216	117	112
P (2700) - P (CY)	226	236	120	209	114	108
P (2950) - P (CY)	220	230	118	204	111	106
P (3200) - P (CY)	214	224	114	199	108	103
P (3400) - P (CY)	210	219	112	196	106	101
P (3780) - P (CY)	201	210	108	186	101	98
P (4676) - P (CY)	160	168	86	147	83	72
P (5176) - P (CY)	142	149	77	130	73	64
P (5676) - P (CY)	127	134	70	118	66	57
P (6176) - P (CY)	115	121	61	106	59	51
P (6676) - P (CY)	103	108	55	94	52	45
P (7176) - P (CY)	91	95	47	84	45	39
P (7676) - P (CY)	79	83	41	73	38	33
P (8595) - P (CY)	52	54	26	48	14	21
Solids held-up (g)	11.829	13.987	3.557	11.410	3.0163	2.436
Valve closing first	Top	Top	Top	Top	Top	Top
Valve closing time (s)	0.03	0.02	0.03	0.05	0.06	0.06

TABLE IV.13
 HYDRODYNAMIC DATA : SERIES C-1 U = 4.63 m/s
 PARTICLE SIZE DISTRIBUTION : P.S.D. 2 (SAND) $\rho_s = 2620 \text{ kg/m}^3$

Run number	C-1.1	C-1.2	C-1.3	C-1.4	C-1.5	C-1.6	C-1.7
W (g/s)	1.74	1.74	1.76	1.76	1.78	1.75	1.79
W _{B1} (g/s)	0.0044	0.0035	0.0038	0.0032	0.0026	0.0040	0.0039
W _{B2} (g/s)	9.1	7.0	7.0	5.3	3.0	7.3	8.0
T (4086) (°C)	23.7	21.7	21.2	24.0	21.9	22.7	19.2
T (8410) (°C)	44.3	41.4	41.4	45.8	42.9	41.8	42.2
P (CY) (bar abs.)	1.00	1.01	1.03	1.02	1.03	1.02	1.03
Line pressures (mm H ₂ O)							
P (O) - P (CY)	179	138	155	133	78	141	165
P (590) - P (CY)	152	114	132	113	64	117	138
P (810) - P (CY)	148	112	128	110	63	115	136
P (1185) - P (CY)	143	108	123	105	61	111	129
P (1700) - P (CY)	134	102	116	97	58	106	121
P (1950) - P (CY)	130	98	112	94	56	103	116
P (2450) - P (CY)	124	93	106	90	53	98	109
P (2700) - P (CY)	121	91	103	88	52	95	106
P (2950) - P (CY)	118	89	101	86	51	93	103
P (3200) - P (CY)	115	87	99	84	50	91	101
P (3400) - P (CY)	112	84	96	82	49	88	98
P (3780) - P (CY)	108	81	93	79	47	85	94
Solids hold-up (g)	12,470	10,644	10,629	8,007	4,250	9,397	11,723
Valve closing first	Bottom	Top	Top	Bottom	Top	Bottom	Top
Valve closing time (s)	0.04	0.08	0.03	0.01	0.03	0.01	0.03

TABLE IV.13 (continued)
 HYDRODYNAMIC DATA : SERIES C-1 $U_g = 4.63 \text{ m/s}$
 PARTICLE SIZE DISTRIBUTION : P.S.D. 2 (SAND) $\rho_s = 2620 \text{ kg/m}^3$

Run number	C-1.8	C-1.9	C-1.10	C-1.11	C-1.12	C-1.13
W ₁ (g/s)	1.79	1.79	1.78	1.77	1.77	1.78
W ₈₁ (g/s)	0.0032	0.0029	0.0027	0.0031	0.0049	0.0036
W ₈₂ (g/s)	5.0	4.0	3.0	4.0	10.0	6.0
T (4086) (°C)	19.8	21.2	20.1	23.6	26.2	23.7
T (8410) (°C)	43.6	44.3	44.2	39.4	39.8	40.4
P (CY) (bar abs.)	1.04	1.04	1.03	1.02	1.04	1.04
Line pressures (mm H ₂ O)						
P (0)	111	94	69	86	165	118
P (590)	90	76	53	70	136	98
P (810)	89	75	52	68	134	96
P (1185)	86	72	51	65	128	91
P (1700)	82	68	49	59	120	85
P (1950)	78	65	47	57	115	82
P (2450)	73	61	43	53	108	77
P (2700)	71	59	42	52	105	75
P (2950)	70	58	41	50	103	73
P (3200)	69	57	40	49	100	71
P (3400)	67	55	39	47	97	68
P (3780)	65	53	37	45	93	65
Solids hold-up (g)	6.743	4.953	3.718	5.330	11.706	7.424
Valve closing first	Top	Bottom	Bottom	Top	Top	Bottom
Valve closing time (s)	0.04	0.04	0.02	0.03	0.02	0.01

TABLE IV.14
 HYDRODYNAMIC DATA : SERIES C-2 U = 5.23 m/s
 PARTICLE SIZE DISTRIBUTION : P.S.D. 2 (SAND) $\rho_s = 2620 \text{ kg/m}^3$

Run number	C-2.1	C-2.2	C-2.3	C-2.4	C-2.5	C-2.6	C-2.7	C-2.8	C-2.9
W (g/s)	1.99	2.00	2.02	2.03	2.03	2.02	2.02	2.04	2.04
W _{g1} (g/s)	0.0032	0.0041	0.0046	0.0058	0.0033	0.0039	0.0025	0.0036	0.0030
W _s (g/s)	4.3	7.3	10.0	15.0	4.0	7.0	3.0	5.0	8.0
T (4086) (°C)	23.1	21.5	20.2	20.4	19.4	20.8	21.3	19.5	20.9
T (8410) (°C)	43.7	41.7	40.7	40.7	42.8	44.2	44.9	38.5	42.0
P (CY) (bar abs.)	1.03	1.03	1.03	1.03	1.03	1.03	1.03	1.04	1.04
Line pressures (mm H ₂ O)									
P (0) - P (CY)	107	146	194	249	99	144	89	95	142
P (590) - P (CY)	86	119	160	202	78	117	70	74	115
P (810) - P (CY)	85	118	157	198	77	115	69	73	113
P (1185) - P (CY)	82	114	151	189	74	111	67	71	109
P (1700) - P (CY)	78	109	143	177	70	105	64	68	103
P (1950) - P (CY)	75	106	138	171	68	102	61	66	99
P (2450) - P (CY)	72	101	131	163	65	96	57	62	93
P (2700) - P (CY)	70	98	128	158	63	93	56	61	91
P (2950) - P (CY)	69	96	125	156	62	91	55	59	89
P (3200) - P (CY)	67	94	123	153	60	89	54	58	87
P (3400) - P (CY)	65	92	120	147	58	87	52	56	84
P (3780) - P (CY)	63	89	116	142	56	84	51	54	81
Solids hold-up (g)	5.183	8.941	13.665	18.111	5.004	8.941	3.869	4.246	8.770
Valve closing first	Top	Top	Top	Top	Top	Top	Top	Bottom	Bottom
Valve closing time (s)	0.01	0.08	0.07	0.03	0.01	0.03	0.02	0.07	0.01

TABLE IV.14 (continued)
 HYDRODYNAMIC DATA : SERIES C-2 U = 5.23 m/s
 PARTICLE SIZE DISTRIBUTION : P.S.D. 2 (SAND) $\rho_s = 2620 \text{ kg/m}^3$

Run number	C-2.10	C-2.11	C-2.12	C-2.13	C-2.14	C-2.15	C-2.16	C-2.17	C-2.18
W ₁ (g/s)	2.05	2.05	2.05	2.04	2.04	2.03	2.03	2.03	2.00
W ₂ (g/s)	0.0056	0.0059	0.0065	0.0069	0.0090	0.0031	0.0042	0.0052	0.0042
W _s (g/s)	12.0	15.0	15.0	18.0	23.0	4.0	7.0	10.0	6.0
T (4086) (°C)	20.1	22.1	15.1	19.1	23.2	22.3	23.0	22.3	25.2
T (8410) (°C)	40.2	37.6	31.6	34.4	39.0	39.0	38.8	37.6	39.7
P (CY) (bar abs.)	1.06	1.06	1.04	1.04	1.05	1.05	1.05	1.05	1.02
Line pressures (mm H ₂ O)									
P (0)	191	238	252	269	346	93	138	161	118
P (590)	157	196	207	222	287	72	113	132	95
P (840)	154	192	203	218	282	71	111	129	93
P (1185)	146	183	193	208	268	68	106	123	89
P (1700)	137	171	181	193	249	64	99	115	83
P (1950)	133	164	172	187	240	62	95	112	81
P (2450)	125	155	162	176	226	59	90	106	76
P (2700)	122	150	157	171	219	57	87	103	74
P (2950)	119	146	154	167	213	56	85	100	73
P (3200)	166	143	150	162	208	54	83	97	71
P (3400)	113	139	146	159	203	53	81	95	69
P (3780)	108	133	138	151	194	51	78	92	66
Solids hold-up (g)	13.218	16.478	19.722	19.184	25.985	4.017	7.604	9.916	6.691
Valve closing first	Top	Bottom	Top	Bottom	Bottom	Bottom	Bottom	Top	Top
Valve closing time (s)	0.03	0.02	0.15	0.01	0.10	0.10	0.04	0.02	0.02

TABLE IV.15
 HYDRODYNAMIC DATA : SERIES C-3 $U_g = 3.37 \text{ m/s}$
 PARTICLE SIZE DISTRIBUTION : P.S.D. Z (SAND) $\rho_s = 2620 \text{ kg/m}^3$

Run number	C-3.1	C-3.2	C-3.3	C-3.4	C-3.5	C-3.6	C-3.7
W ₁ (g/s)	1.28	1.28	1.28	1.28	1.29	1.28	1.29
W _{B1} (g/s)	0.0021	0.0025	0.0027	0.0035	0.0025	0.0026	0.0032
W _S (g/s)	3.0	5.0	7.0	9.0	5.3	5.0	4.8.0
T (4086) (°C)	24.1	23.8	25.3	23.0	22.2	21.1	20.5
T (8410) (°C)	44.8	44.9	46.0	43.2	41.6	42.6	42.2
P (CY) (bar abs.)	1.03	1.03	1.03	1.02	1.03	1.02	1.02
Line pressures (mm H ₂ O)							
P (0) - P (CY)	82	127	182	231	142	130	218
P (590) - P (CY)	69	109	158	199	120	109	188
P (810) - P (CY)	68	107	153	193	117	107	182
P (1185) - P (CY)	66	103	147	183	112	103	173
P (1700) - P (CY)	63	97	139	170	106	98	163
P (1950) - P (CY)	60	93	134	164	103	95	158
P (2450) - P (CY)	57	88	126	155	97	89	148
P (2700) - P (CY)	55	85	122	150	94	86	144
P (2950) - P (CY)	54	83	117	145	92	85	140
P (3200) - P (CY)	53	80	115	140	89	81	136
P (3400) - P (CY)	51	78	112	136	86	78	131
P (3780) - P (CY)	50	74	107	129	83	74	125
Solids hold-up (g)	7.095	11.588	17.109	21.453	12.916	12.688	22.346
Valve closing first	Bottom	Bottom	Top	Bottom	-	Top	Top
Valve closing time (s)	0.08	0.03	0.05	0.01	0.00	0.02	0.03

TABLE IV.16
 HYDRODYNAMIC DATA : SERIES C-4
 U = 6.19 m/s
 PARTICLE SIZE DISTRIBUTION : P.S.D. 2 (SAND) p_s = 2620 kg/m³

Run number	C-4.1	C-4.2	C-4.3	C-4.4	C-4.5	C-4.6	C-4.7
W ₁ (g/s)	2.37	2.36	2.37	2.37	2.37	2.37	2.41
W _{g1} (g/s)	0.0067	0.0062	0.0041	0.0043	0.0052	0.0034	0.0039
W _{g2} (g/s)	14.0	12.0	5.0	7.0	9.0	3.0	4.0
T (4086) (°C)	20.9	21.5	19.5	20.0	19.1	19.0	21.2
T (8410) (°C)	41.0	43.9	43.4	41.7	39.9	40.5	43.1
P (CY) (bar abs.)	1.02	1.01	1.01	1.01	1.02	1.01	1.06
Line pressures (mm H ₂ O)							
P (0) - P (CY)	244	213	127	145	170	99	123
P (590) - P (CY)	197	171	99	115	136	75	99
P (810) - P (CY)	194	168	97	112	134	74	98
P (1185) - P (CY)	186	160	93	107	128	71	95
P (1700) - P (CY)	175	151	88	101	121	67	87
P (1950) - P (CY)	168	145	85	97	117	64	85
P (2450) - P (CY)	159	138	80	92	111	61	81
P (2700) - P (CY)	154	134	78	89	108	59	79
P (2950) - P (CY)	151	132	76	88	105	58	78
P (3200) - P (CY)	147	127	75	86	103	57	76
P (3400) - P (CY)	144	125	72	84	101	56	75
P (3780) - P (CY)	140	122	70	81	97	55	72
Solids hold-up (g)	13.135	11.370	4.822	6.812	8.253	2.865	4.013
Valve closing first	Top	Top	Top	Top	Top	Top	Top
Valve closing time (s)	0.04	0.10	0.07	0.08	0.05	0.05	0.04

TABLE IV.16 (continued)
 HYDRODYNAMIC DATA : SERIES C-4 U = 6.19 m/s
 PARTICLE SIZE DISTRIBUTION : P.S.D. 2 (SAND) $\rho_s = 2620 \text{ kg/m}^3$

Run number	C-4.8	C-4.9	C-4.10	C-4.11	C-4.12	C-4.13	C-4.14
W ₁ (g/s)	2.41	2.41	2.41	2.37	2.41	2.41	2.40
W ₂ (g/s)	0.0042	0.0044	0.0058	0.0068	0.0082	0.0083	0.0093
W _s (g/s)	5.0	6.0	12.0	15.0	20.0	18.0	22.0
T (4086) (°C)	21.1	21.1	22.2	21.7	18.5	21.4	24.7
T (8410) (°C)	44.6	44.0	43.0	36.8	32.9	38.0	40.6
P (CY) (bar abs.)	1.05	1.05	1.06	1.02	1.04	1.05	1.05
Line pressures (mm H ₂ O)							
P (0) - P (CY)	129	139	211	240	296	279	340
P (590) - P (CY)	101	110	169	193	238	225	274
P (810) - P (CY)	99	109	166	189	233	220	269
P (1185) - P (CY)	95	105	159	181	221	207	255
P (1700) - P (CY)	90	99	150	170	206	196	237
P (1950) - P (CY)	87	95	144	164	200	188	228
P (2450) - P (CY)	82	90	136	155	189	178	217
P (2700) - P (CY)	80	88	132	151	184	173	210
P (2950) - P (CY)	79	86	130	147	180	169	206
P (3200) - P (CY)	77	84	126	144	175	165	201
P (3400) - P (CY)	75	82	124	141	171	163	196
P (3780) - P (CY)	73	80	120	135	166	156	188
Solids hold-up (g)	5.232	6.022	10.297	12.462	18.202	14.481	18.951
Valve closing first	Top	Top	Bottom	Bottom	Top	Bottom	Bottom
Valve closing time (s)	0.10	0.07	0.08	0.05	0.07	0.03	0.08

TABLE IV.17
 HYDRODYNAMIC DATA : SERIES C-5 U_g = 10.2 m/s
 PARTICLE SIZE DISTRIBUTION : P.S.D. 2 (SAND) ρ_s = 2620 kg/m³

Run number	C-5.1	C-5.2	C-5.3	C-5.4	C-5.5	C-5.6	C-5.7	C-5.8
W ₁ (g/s)	4.14	4.15	4.18	4.18	4.18	4.16	4.23	4.22
W _{B2} (g/s)	0.0139	0.0138	0.0130	0.0138	0.0165	0.0239	0.0124	0.0153
W _S (g/s)	3.0	5.0	7.0	9.0	12.0	16.0	5.0	12.0
T (4086) (°C)	22.8	22.8	20.2	22.2	23.8	27.0	21.7	21.2
T (8410) (°C)	43.0	42.7	63.1	66.2	66.9	61.6	36.4	37.2
P (CY) (bar abs.)	1.06	1.09	1.10	1.10	1.11	1.10	1.13	1.12
Line pressures (mm H ₂ O)								
P (0) - P (CY)	203	236	252	324	358	418	221	329
P (590) - P (CY)	146	176	189	255	279	329	161	253
P (810) - P (CY)	144	173	186	251	274	323	158	248
P (1185) - P (CY)	139	167	179	242	263	309	152	237
P (1700) - P (CY)	131	157	168	223	247	291	143	223
P (1950) - P (CY)	126	151	162	218	239	281	138	215
P (2450) - P (CY)	120	144	154	208	228	267	132	203
P (2700) - P (CY)	117	140	149	203	222	160	128	198
P (2950) - P (CY)	115	137	147	200	218	254	126	194
P (3200) - P (CY)	112	135	144	195	213	250	122	190
P (3400) - P (CY)	109	132	141	192	209	245	120	186
P (3780) - P (CY)	106	127	136	187	204	238	116	181
Solids hold-up (g)	2.662	3.484	4.588	6.805	7.915	10.592	4.029	7.215
Valve closing first	Bottom	Top	Top	Top	Top	Top	Bottom	Top
Valve closing time (s)	0.20	0.11	0.04	0.09	0.02	0.08	0.01	0.02

TABLE IV.17 (continued)
 HYDRODYNAMIC DATA : SERIES C-5 U = 10.2 m/s
 PARTICLE SIZE DISTRIBUTION : P.S.D. 2 (SAND) $\rho_s = 2620 \text{ kg/m}^3$

Run number	C-5.9	C-5.10	C-5.11	C-5.12	C-5.13	C-5.14	C-5.15
W (g/s)	4.21	4.27	4.27	4.26	4.17	4.14	4.16
W ₈₁ (g/s)	0.0210	0.0215	0.0173	0.0213	0.0241	0.0233	0.0187
W ₈₅ (g/s)	15.0	20.0	18.0	32.0	29.0	25.0	6.0
T (4086) (°C)	23.6	23.0	19.8	24.0	33.0	29.4	24.0
T (8410) (°C)	39.1	38.3	35.3	37.4	47.4	42.7	39.3
P (CY) (bar abs.)	1.12	1.14	1.14	1.14	1.12	1.13	1.09
Line pressures (mm H ₂ O)							
P ₁ (O) - P (CY)	360	442	409	571	564	469	234
P (590) - P (CY)	284	344	317	444	440	365	172
P (810) - P (CY)	278	336	310	437	430	357	169
P ₁ (1185) - P (CY)	265	320	294	410	407	339	161
P (1700) - P (CY)	249	299	273	378	378	315	150
P (1950) - P (CY)	239	289	265	364	364	304	145
P (2450) - P (CY)	227	273	251	344	345	288	138
P (2760) - P (CY)	222	268	245	336	337	281	135
P (2950) - P (CY)	217	262	240	330	329	275	132
P (3200) - P (CY)	212	256	235	322	322	269	128
P (3400) - P (CY)	208	251	231	315	317	264	125
P (3780) - P (CY)	202	244	224	306	308	256	120
Solids hold-up (g)	8.246	12.410	9.546	17.841	15.571	12.815	4.486
Valve closing first	Bottom	Top	Bottom	Top	Bottom	Top	Top
Valve closing time (s)	0.08	0.02	0.08	0.04	0.04	0.00	0.12

TABLE IV.18

HYDRODYNAMIC DATA : SERIES D-1 U = 4.61 m/s $\rho_s = 2410 \text{ kg/m}^3$
 PARTICLE SIZE DISTRIBUTION : P.S.D.. 3 (GLASS)

Run number	D-1.1	D-1.2	D-1.3	D-1.4	D-1.5	D-1.6	D-1.7	D-1.8	D-1.9	D-1.10
W ₅ (g/s)	1.77	1.75	1.76	1.76	1.75	1.76	1.75	1.76	1.77	1.76
W ₈₂ (g/s)	0.0045	0.0083	0.0053	0.0067	0.0068	0.0044	0.0054	0.0073	0.0097	0.0035
W ₅ (g/s)	3.5	9.4	2.6	5.0	8.7	1.6	4.6	6.2	10.3	7.5
Temperature (°C)	19.8	26.0	22.8	22.8	25.0	23.2	26.0	23.4	20.0	22.4
P (CY) (bar abs.)	1.04	1.03	1.03	1.03	1.03	1.03	1.03	1.03	1.03	1.03
Line pressures (mmH ₂ O)										
P (CY)	76	149	72	95	156	60	103	117	160	136
P (CY)	56	117	52	71	124	43	81	90	125	106
P (CY)	55	115	51	69	120	42	79	88	122	103
P (CY)	53	108	48	61	97	36	73	82	108	94
P (CY)	49	103	44	59	95	35	65	77	103	89
P (CY)	47	100	43	57	92	33	62	74	100	85
P (CY)	45	94	40	54	87	31	59	70	94	81
P (CY)	43	92	39	52	84	30	57	68	91	78
P (CY)	42	88	38	51	81	30	56	66	88	76
P (CY)	41	86	37	50	79	29	55	64	85	74
P (CY)	40	84	36	50	76	28	53	62	82	72
P (CY)	38	80	33	48	74	27	52	60	79	69
P (CY)	32	66	29	40	61	22	42	49	64	57
P (CY)	28	59	24	35	55	19	38	44	58	52
P (CY)	25	52	22	31	52	17	34	41	53	47
P (CY)	23	47	20	28	46	15	32	36	47	42
P (CY)	21	41	18	25	39	13	30	31	40	37
P (CY)	17	35	15	21	34	11	25	27	33	32
P (CY)	14	29	12	17	27	9	23	21	28	26
P (CY)	9	15	7	9	14	5	12	11	16	14
Solids hold-up (g)	3.342	9.406	2.357	5.012	7.695	2.878	4.613	6.261	9.117	8.064
Valve closing first	Bottom	Bottom	Bottom	Bottom	Bottom	Bottom	Bottom	Bottom	Top	Bottom
Valve closing time (s)	0.08	0.08	0.07	0.06	0.06	0.01	0.05	0.07	0.02	0.02

TABLE IV.19
 HYDRODYNAMIC DATA : SERIES D-2 U^R 3.40 m/s
 PARTICLE SIZE DISTRIBUTION : P.S.D. 3 (GLASS) p_s 2410 kg/m³

Run number	D-2.1	D-2.2	D-2.3	D-2.4	D-2.5	D-2.6	D-2.7	D-2.8
W ₁ (g/s)	1.29	1.30	1.29	1.29	1.30	1.29	1.30	1.30
W ₈₁ (g/s)	0.0026	0.0038	0.0048	0.0046	0.0029	0.0035	0.0032	0.0042
W ₈₂ (g/s)	1.9	7.2	10.6	4.5	3.1	1.1	5.9	8.9
Temperature (°C)	23.0	20.0	22.0	24.2	20.4	22.2	19.6	20.6
P (CY) (bar abs.)	1.02	1.02	1.02	1.02	1.02	1.02	1.02	1.02
Line pressures (mm H ₂ O)								
P (0)	50.5	130	181	92	74	44.5	114	143
P (590)	39.5	101	147	71	54	32.5	93	116
P (810)	38.5	100	144	70	53	31.5	91	113
P (1185)	36.5	95	139	66	49	29.5	87	106
P (1700)	33.5	90	130	62	47	26.5	77	101
P (1950)	32.5	87	126	58	45	24.5	75	98
P (2450)	30.5	82	119	56	43	23.5	69	91
P (2700)	29.5	79	115	54	41	23.5	66	88
P (2950)	29	77	112	53	40	22	64	85
P (3200)	28.5	74	108	52	38	21.5	62	82
P (3400)	28	72	105	49	37	21.5	60	80
P (3780)	27.5	70	102	47	36	21	59	78
P (4676)	19	57	81	40	30	17	49	64
P (5176)	17	50	73	34	27	15	44	57
P (5676)	15.5	45	66	32	24	14	40	51
P (6176)	13.5	40	57	29	22	12	34	45
P (6676)	12	35	49	25	19	11	29	38
P (7176)	10	29	42	21	16	7	24	33
P (7676)	8	24	35	18	14	7	20	27
P (8595)	5	15	21	10	8	4	12	15
Solids hold-up (g)	3.149	11.013	17.131	7.022	4.407	3.122	8.943	12.681
Valve closing first	Top	-	Top	Bottom	Top	Bottom	Top	Top
Valve closing time (s)	0.03	0.00	0.09	0.06	0.07	0.06	0.08	0.06

TABLE IV.20

HYDRODYNAMIC DATA : SERIES D-3 U = 2.0 m/s

PARTICLE SIZE DISTRIBUTION : P.S.D. 3 (GLASS) $\rho_s = 2410 \text{ kg/m}^3$

Run number	D-3.1	D-3.2	D-3.3	D-3.4	D-3.5	D-3.6	D-3.7	D-3.8
W ₁ (g/s)	0.758	0.756	0.759	0.756	0.750	0.749	0.754	0.753
W ₂ (g/s)	0.0624	0.0075	0.0059	0.0025	0.0022	0.0031	0.0027	0.0031
W _s (g/s)	5.0	2.5	6.6	3.0	4.1	1.8	3.3	2.6
Temperature (°C)	20.6	22.2	20.2	22.8	27.2	28.2	23.8	24.8
P (CY) (bar abs.)	1.02	1.02	1.02	1.02	1.02	1.02	1.02	1.02
Line pressures (mm H ₂ O)								
P (0)	120	61	127	76	105	45	74	65
P (590)	100	50	103	62	86	38	64	53
P (810)	96	49	100	60	83	36	63	51
P (1185)	92	45	95	57	79	34	60	48
P (1700)	84	42	86	52	74	29	56	44
P (1950)	82	40	83	50	72	28	54	42
P (2450)	77	38	76	47	67	27	51	39
P (2700)	75	37	73	45	65	26.5	50	38
P (2950)	72	36	70	44	63	25.5	49	37
P (3200)	70	35	67	43	61	25	48	36
P (3400)	68	34	65	41	60	24.5	46	35
P (3780)	65	33	61	40	58	23.5	45	33
P (4676)	54	28	61	36	47	20	37	29
P (5176)	48	25	54	31	42	18	32	25.5
P (5676)	43	22	48	28	37	16	29	23
P (6176)	37	19	40	25	32	14	26	20
P (6676)	32	16	33	22	27	12	22	17
P (7176)	27	14	27	18	23	11	19	15
P (7676)	22	11.5	21	15	20	8	15	12
P (8595)	13	6	10	9	12	5	9	8
Solids hold-up (g)	14.914	7.286	18.682	10.693	12.912	5.499	11.584	8.491
Valve closing first	Top	Top	Top	Bottom	Bottom	Top	Bottom	-
Valve closing time (s)	0.09	0.05	0.06	0.02	0.06	0.08	0.07	0.0

APPENDIX V

HEAT TRANSFER DATA

Data from the suspension heat transfer experiments is listed in the tables in this appendix.

The overall length of the heat transfer test section was, as is reported in Chapter 5, 4 m. Surface temperatures measured along its length are noted at positions relative to the test section entry point. Heat transfer coefficients h_{ss} are calculated using the equations given in Section 5.3.5.

The pressure and suspension temperatures are given at the heat transfer test section entry and exits: P(4086), P(8410); T(4086), T(8410). The entry temperature was measured with a thermocouple as the gas and the solids were at thermal equilibrium at that point. The outlet temperature, given as the mixed mean temperature of the suspension, was calculated via the overall heat balance.

Ambient temperatures are included since they are necessary to calculate radial heat losses along the test section using the results given in Section 5.3.3.

TABLE V.1 (continued)

HEAT TRANSFER DATA : SERIES C-1 $U_g = 4.63 \text{ m/s}$ PARTICLE SIZE DISTRIBUTION : P.S.D. 2 (SAND) $\rho_s = 2620 \text{ kg/m}^3$

Run number	C-1.6	C-1.7	C-1.8	C-1.9	C-1.10					
W (g/s)	1.75	1.79	1.79	1.79	1.78					
W_s^g (g/s)	7:3	8.0	5.0	4.0	3.0					
Power input (W)	154.4	197.2	148.3	125.6	110.9					
P(4086) (bar abs.)	1.03	1.04	1.04	1.04	1.03					
P(8410) (bar abs.)	1.02	1.03	1.04	1.04	1.03					
T (4086) ($^{\circ}\text{C}$)	22.7	19.2	19.8	21.2	20.1					
T_{ss}^{ss} (8410) ($^{\circ}\text{C}$)	41.8	42.2	43.6	44.3	44.2					
T (ambient) ($^{\circ}\text{C}$)	24.4	19.8	22.2	23.8	23.2					
Position (mm)	T_w	h_{ss}	T_w	h_{ss}	T_w	h_{ss}	T_w	h_{ss}	T_w	h_{ss}
30	31.6		29.9		28.7		29.3		27.7	
		42.3		46.6		41.0		38.6		35.9
250	44.6		44.2		41.8		41.0		39.2	
		26.4		29.6		25.4		23.9		21.8
500	47.7		48.0		45.4		44.4		42.9	
				27.8		23.7		22.2		20.1
750	-	24.5	49.9		47.6		46.6		44.9	
				28.0		23.5		22.0		20.2
1000	51.1		50.4		48.4		47.4		45.4	
				28.1		23.5		21.9		20.8
1250	-		52.5		50.4		49.4		46.7	
				27.2		22.8		21.2		21.0
1500	-	23.2	54.6		52.4		51.3		47.9	
				27.8		23.3		21.7		22.1
1750	-		54.1		52.3		51.2		47.8	
				28.6		23.9		22.3		22.9
2000	56.7		55.9		54.1		53.0		49.5	
				28.0		23.2		21.6		22.3
2500	-	22.7	59.2		57.6		56.3		52.7	
3000	60.7		-	27.6	-	22.6	-	21.2	-	21.7
3250	-		63.2		61.9		60.2		57.0	
				27.9		22.7		21.3		22.0
3500	-	24.6	64.0		62.7		61.2		57.8	
				28.4		23.1		21.5		22.4
3750	-		65.0		63.9		62.3		59.0	
				30.4		25.4		23.6		25.0
3950	61.9		63.7		63.9		60.8		57.6	

 T_w in $^{\circ}\text{C}$, h_{ss} in ($\text{W}/\text{m}^2\text{ }^{\circ}\text{C}$)

TABLE V.1
HEAT TRANSFER DATA : SERIES C-1 $U_g = 4.63 \text{ m/s}$
PARTICLE SIZE DISTRIBUTION : P.S.D. 2 (SAND) $\rho_s = 2620 \text{ kg/m}^3$

Run number	C-1.1	C-1.2	C-1.3	C-1.4	C-1.5					
W (g/s)	1.74	1.74	1.76	1.76	1.78					
W_s^g (g/s)	9.1	7.0	7.0	5.3	3.0					
Power input (W)	95.6	152.9	157.0	141.9	98.3					
P(4086) (bar abs.)	1.01	1.01	1.03	1.02	1.03					
P(8410) (bar abs.)	1.00	1.01	1.02	1.02	1.03					
T (4086) (°C)	23.7	21.7	21.2	24.0	21.9					
T_{ss}^{ss} (8410) (°C)	44.3	41.4	41.4	45.8	42.9					
T (ambient) (°C)	25.2	23.0	22.9	25.8	24.6					
Position (mm)	T_w	h_{ss}	T_w	h_{ss}	T_w	h_{ss}	T_w	h_{ss}	T_w	h_{ss}
30	34.7	44.7	30.7	41.9	30.3	42.4	33.0	39.3	28.4	35.3
250	49.6	28.3	43.5	26.6	43.4	26.9	45.6	24.8	39.5	21.1
500	53.0	26.4	46.1	25.5	46.1	25.6	48.7	23.5	42.4	19.7
750	55.4	26.0	47.6	25.0	47.7	25.1	50.4	23.0	44.2	19.0
1000	56.2	26.3	49.1	24.8	49.3	24.5	52.0	22.4	46.0	18.4
1250	57.2	26.0	50.3	-	51.1	-	54.0	-	47.8	-
1500	59.2	26.1	-	24.8	-	24.8	-	22.6	-	18.3
1750	59.4	26.6	-	-	-	-	-	-	-	-
2000	60.7	26.0	53.6	24.4	53.5	25.0	56.7	22.8	50.8	18.3
2500	64.2	25.7	56.6	-	56.5	-	59.9	-	53.8	-
3000	65.9	-	-	-	-	-	-	-	-	-
3250	-	-	-	24.4	-	25.0	-	22.7	-	18.0
3500	-	26.0	-	-	-	-	-	-	-	-
3750	-	-	-	-	-	-	62.2	-	60.0	-
3950	70.4	-	62.2	-	62.3	-	-	-	-	-

T_w in °C, h_{ss} in (W/m²°C)

TABLE V.1 (continued)
 HEAT TRANSFER DATA : SERIES C-1 $U_g = 4.63 \text{ m/s}$
 PARTICLE SIZE DISTRIBUTION : P.S.D. 2 (SAND) $\rho_s = 2620 \text{ kg/m}^3$

Run number	C-1.11		C-1.12		C-1.13	
W (g/s)	1.77		1.77		1.78	
W _s ^B (g/s)	4.0		10.0		6.0	
Power input (W)	86.7		136.7		116.5	
P(4086) (bar abs.)	1.02		1.05		1.05	
P(8410) (bar abs.)	1.02		1.04		1.04	
T (4086) (°C)	23.6		26.2		23.7	
T _{ss} ^{ss} (8410) (°C)	39.4		39.8		40.4	
T (ambient) (°C)	35.7		28.4		27.0	
Position (mm)	T _w	h _{ss}	T _w	h _{ss}	T _w	h _{ss}
30	30.1		32.1		31.3	
		35.1		55.1		40.2
250	38.0		41.7		40.7	
		22.5		33.1		25.9
500	40.6		44.5		43.4	
		20.6		30.4		24.0
750	42.2		45.9		45.1	
		20.3		30.2		23.6
1000	42.9		46.3		45.8	
		20.0		30.1		23.5
1250	44.4		47.6		47.3	
		19.4		29.0		22.7
1500	45.6		49.1		48.9	
		19.6		29.2		21.9
1750	45.9		48.9		48.9	
		19.6		29.7		23.2
2000	47.4		50.2		50.3	
		18.9		28.6		22.5
2500	49.6		52.5		52.9	
3000	-	18.6	-	27.8	-	21.9
3250	52.2		55.1		55.8	
		18.7		27.7		22.0
3500	52.9		55.7		56.5	
		18.9		27.8		22.2
3750	53.6		56.4		57.3	
		20.5		29.3		23.5
3950	52.6		55.7		56.5	

T_w in °C, h_{ss} in (W/m²°C)

TABLE V.2

HEAT TRANSFER DATA : SERIES C-2 $U_g = 5.23 \text{ m/s}$ PARTICLE SIZE DISTRIBUTION : P.S.D. 2 (SAND) $\rho_s = 2620 \text{ kg/m}^3$

Run number	C-2.1		C-2.2		C-2.3		C-2.4		C-2.5	
W (g/s)	1.99		2.00		2.02		2.03		2.03	
W _s ^B (g/s)	4.3		7.3		10.0		15.0		4.0	
Power input (W)	123.3		162.5		212.7		291.0		132.7	
P(4086) (bar abs.)	1.03		1.04		1.04		1.04		1.04	
P(8410) (bar abs.)	1.03		1.03		1.03		1.03		1.03	
T ₄₀₈₆ (°C)	23.1		21.5		20.2		20.4		19.4	
T _{ss} ^{SS} (8410) (°C)	43.7		41.7		40.7		40.7		42.8	
T (ambient) (°C)	24.8		23.3		22.3		21.0		22.4	
Position (mm)	T _w	h _{ss}	T _w	h _{ss}	T _w	h _{ss}	T _w	h _{ss}	T _w	h _{ss}
30	30.6	-	30.3	44.1	30.8	48.9	34.2	52.4	27.6	35.42
250	42.5	23.8	44.0	27.1	46.4	30.5	53.0	33.5	40.3	24.0
500	45.6	-	47.2	-	49.9	-	56.7	-	43.7	-
750	-	21.9	-	25.1	-	28.5	-	31.6	-	22.4
1000	49.2	-	50.8	-	53.4	-	60.2	-	47.2	-
1250	-	-	-	-	-	-	-	-	-	-
1500	-	20.8	-	25.0	-	27.6	-	30.5	-	22.0
1750	-	-	-	-	-	-	-	-	-	-
2000	54.7	-	56.4	-	58.9	-	66.2	-	52.4	-
2500	-	20.7	-	24.8	-	27.8	-	30.6	-	22.7
3000	58.7	-	60.4	-	62.5	-	69.4	-	56.7	-
3250	-	-	-	-	-	-	-	-	-	-
3500	-	23.0	-	27.2	-	-	-	-	-	-
3750	-	-	-	-	-	30.2	-	33.1	-	25.4
3950	60.0	-	61.7	-	-	-	-	-	-	-
3950	-	-	-	-	64.0	-	70.7	-	58.9	-

T_w in °C, h_{ss} in (W/m²°C)

TABLE V.2 (continued)

HEAT TRANSFER DATA : SERIES C-2 $U_g = 5.23 \text{ m/s}$ PARTICLE SIZE DISTRIBUTION : P.S.D. 2 (SAND) $\rho_s = 2620 \text{ kg/m}^3$

Run number	C-2.6	C-2.7	C-2.8	C-2.9	C-2.10					
W (g/s)	2.02	2.02	2.04	2.04	2.06					
W _s ^B (g/s)	7.0	3.0	5.0	8.0	12.0					
Power input (W)	189.0	113.6	122.7	187.8	241.8					
P(4086) (bar abs.)	1.03	1.04	1.05	1.05	1.06					
P(8410) (bar abs.)	1.03	1.03	1.04	1.04	1.06					
T (4086) (°C)	20.8	21.3	19.5	20.9	20.1					
T _{ss} ^{ss} (8410) (°C)	44.2	44.9	38.5	42.0	40.2					
T (ambient) (°C)	22.7	23.8	22.3	22.1	20.2					
Position (mm)	T _w	h _{ss}	T _w	h _{ss}	T _w	h _{ss}	T _w	h _{ss}	T _w	h _{ss}
30	31.0		28.9		27.3		33.5		32.0	
		44.5		38.1		38.7		44.6		50.8
250	46.7		39.4		38.7		47.7		48.4	
		27.4		24.1		23.9		28.2		31.6
500	50.5		42.5		41.8		49.5		52.5	
		25.4		23.7		22.8		26.2		29.5
750	53.2		42.7		42.6		51.4		54.6	
		25.3		25.8		23.8		26.0		29.4
1000	53.3		42.7		42.5		52.4		55.1	
		25.4		26.9		24.5		25.7		29.2
1250	55.8		44.2		43.9		54.7		57.4	
		24.9		26.6		24.0		24.7		28.1
1500	57.1		45.8		45.4		56.8		59.6	
		25.2		27.6		24.3		25.0		28.5
1750	57.9		46.0		45.6		56.5		58.9	
		25.0		28.6		24.6		25.4		28.9
2000	60.1		47.6		47.2		58.5		61.0	
		24.6		28.1		23.7		24.5		28.0
2500	62.7		50.6		50.2		61.8		64.4	
3000	-	25.0	-	27.9	-	22.6	-	23.9	-	27.3
3250	66.0		54.5		54.2		65.9		68.3	
		25.3		28.7		22.3		23.7		27.2
3500	67.4		55.3		54.9		66.9		69.2	
		25.2		29.5		22.4		23.8		27.3
3750	68.8		56.4		56.0		68.1		70.3	
		28.3		32.5		23.9		25.0		28.5
3950	65.3		55.8		55.1		66.9		69.1	

T_w in °C, h_{ss} in (W/m²°C)

TABLE V.2 (continued)

HEAT TRANSFER DATA : SERIES C-2 $U_g = 5.23 \text{ m/s}$ PARTICLE SIZE DISTRIBUTION : P.S.D. 2 (SAND) $\rho_s = 2620 \text{ kg/m}^3$

Run number	C-2.11		C-2.12		C-2.13		C-2.14		C-2.15	
W (g/s)	2.06		2.06		2.05		2.05		2.03	
W_s^g (g/s)	15.0		15.0		18.0		23.0		4.0	
Power input (W)	222.9		232.2		253.2		324.4		92.9	
P(4086) (bar abs.)	1.06		1.04		1.05		1.06		1.05	
P(8410) (bar abs.)	1.06		1.04		1.04		1.05		1.05	
$T_{(4086)}$ ($^{\circ}\text{C}$)	22.1		15.1		19.1		23.2		22.3	
T_{ss}^{ss} (8410) ($^{\circ}\text{C}$)	37.6		31.6		34.4		39.0		39.0	
T (ambient) ($^{\circ}\text{C}$)	22.3		16.1		19.1		21.0		26.6	
Position (mm)	T_w	h_{ss}	T_w	h_{ss}	T_w	h_{ss}	T_w	h_{ss}	T_w	h_{ss}
30	32.4	53.7	25.5	54.9	29.7	57.2	35.9	61.8	28.1	39.0
250	46.5	33.3	40.2	33.9	45.6	35.2	54.2	38.1	37.2	23.5
500	50.6	31.1	44.5	31.7	49.4	32.8	59.1	35.6	40.1	22.3
750	51.7	31.6	45.4	32.4	51.1	32.9	60.2	35.8	40.6	23.6
1000	51.6	31.8	45.4	32.6	51.0	33.2	58.9	38.3	40.5	24.6
1250	53.2	30.9	46.9	31.8	52.5	32.3	59.7	38.2	41.4	24.4
1500	55.0	31.3	48.7	32.4	54.3	32.8	60.9	39.3	42.7	24.8
1750	54.3	31.8	47.8	33.2	53.4	33.4	59.9	39.4	42.9	25.3
2000	56.0	30.7	49.6	31.9	55.2	32.1	62.6	36.8	44.1	24.5
2500	58.8	30.0	52.6	31.2	58.2	31.3	66.8	37.0	46.6	24.0
3000	-	30.0	-	31.2	-	31.3	-	37.0	-	24.0
3250	61.6	30.1	55.6	31.4	61.0	31.6	66.9	39.3	49.4	24.3
3500	62.2	30.4	56.0	31.9	61.3	31.9	67.0	39.6	50.0	24.7
3750	63.0	31.7	56.8	33.5	62.2	33.2	68.2	40.1	50.8	26.9
3950	62.1	31.7	55.6	33.5	61.1	33.2	68.1	40.1	50.0	26.9

 T_w in $^{\circ}\text{C}$, h_{ss} in ($\text{W/m}^2\text{ }^{\circ}\text{C}$)

TABLE V.2 (continued)
 HEAT TRANSFER DATA : SERIES C-2. $U_g = 5.23 \text{ m/s}$
 PARTICLE SIZE DISTRIBUTION : P.S.D. 2 (SAND) $\rho_s = 2620 \text{ kg/m}^3$

Run number	C-2.16		C-2.17		C-2.18	
W (g/s)	2.03		2.04		2.00	
W_s^g (g/s)	7.0		10.0		6.0	
Power input (W)	126.1		158.9		105.3	
P(4086) (bar abs.)	1.05		1.05		1.03	
P(8410) (bar abs.)	1.05		1.05		1.02	
T_{ss} (4086) ($^{\circ}\text{C}$)	23.0		22.3		25.2	
T_{ss} (8410) ($^{\circ}\text{C}$)	38.8		37.6		39.7	
T (ambient) ($^{\circ}\text{C}$)	25.7		25.0		27.7	
Position (mm)	T_w	h_{ss}	T_w	h_{ss}	T_w	h_{ss}
30	29.5		30.2		32.0	
		46.4		49.1		40.5
250	39.8		41.9		40.4	
		28.3		29.8		26.1
500	42.5		45.5		42.8	
		26.4		27.6		24.1
750	43.9		46.7		44.3	
		26.4		27.7		23.8
1000	44.3		47.2		45.0	
		26.4		27.5		23.6
1250	45.8		48.8		46.2	
		25.5		26.5		23.0
1500	47.3		50.4		47.4	
		25.8		26.9		23.3
1750	47.2		50.0		47.5	
		26.2		27.3		23.8
2000	48.6		51.6		48.4	
		24.7		26.3		23.1
2500	51.9		54.2		50.9	
3000	-	24.2	-	25.3	-	22.5
3250	53.7		57.4		53.3	
		25.1		25.2		22.3
3500	54.3		58.0		54.4	
		25.4		25.3		22.4
3750	55.0		58.8		54.8	
		27.3		26.7		23.3
3950	54.0		57.8		54.7	

T_w in $^{\circ}\text{C}$, h_{ss} in ($\text{W}/\text{m}^2\text{C}$)

TABLE V.3

HEAT TRANSFER DATA : SERIES C-3 $U_g = 3.37 \text{ m/s}$ PARTICLE SIZE DISTRIBUTION : P.S.D: 2 (SAND) $\rho_s = 2620 \text{ kg/m}^3$

Run number	C-3.1		C-3.2		C-3.3		C-3.4		C-3.5	
W (g/s)	1.28		1.28		1.28		1.28		1.29	
W_s^B (g/s)	3.0		5.0		7.0		9.0		5.3	
Power input (W)	85.7		119.8		150.6		177.6		115.5	
P(4086) (bar abs.)	1.03		1.03		1.04		1.03		1.03	
P(8410) (bar abs.)	1.03		1.03		1.03		1.02		1.03	
T (4086) ($^{\circ}\text{C}$)	24.1		23.8		25.3		23.0		22.2	
T_{ss} (8410) ($^{\circ}\text{C}$)	44.8		44.9		46.0		43.2		41.6	
T (ambient) ($^{\circ}\text{C}$)	26.5		26.0		26.9		25.0		24.0	
Position (mm)	T_w	h_{ss}	T_w	h_{ss}	T_w	h_{ss}	T_w	h_{ss}	T_w	h_{ss}
30	30.8		31.2		34.5		32.8		29.6	
		32.5		39.4		41.9		46.3		39.3
250	40.0		42.5		46.4		45.6		39.8	
		20.8		24.9		28.2		31.6		25.5
500	42.2		46.6		47.8		46.3		41.7	
		20.1		24.4		28.5		32.4		
750	43.5		45.7		48.5		47.1			24.8
		19.8		24.3		28.6		32.1		
1000	45.1		47.2		50.1		49.0		44.2	
		19.2		23.7		27.7		30.8		
1250	46.8		49.0		52.1		51.1			
1500										23.9
		19.2		23.8		27.5		30.7		
1750										
2000	49.7		52.0		55.2		53.9		49.7	
		19.2		23.8		27.6		31.1		
2500	52.7		55.0		58.0		56.5			23.6
3000									53.4	
3250										
3500		18.8		28.6		27.6		31.2		
3750										26.8
3950	58.9		61.3		64.2		62.8		54.7	

 T_w in $^{\circ}\text{C}$, h_{ss} in ($\text{W/m}^2\text{ }^{\circ}\text{C}$)

TABLE V.3 (continued)
 HEAT TRANSFER DATA : SERIES C-3 $U_g = 3.37$ m/s
 PARTICLE SIZE DISTRIBUTION : P.S.D. 2 (SAND) $\rho_s = 2620$ kg/m³

Run number	C-3.6		C-3.7	
W (g/s)	1.28		1.29	
W_s^B (g/s)	5.0		8.0	
Power input (W)	121.3		172.9	
P(4086) (bar abs.)	1.03		1.03	
P(8410) (bar abs.)	1.03		1.02	
T_{ss} (4086) (°C)	21.1		20.5	
T_{ss} (8410) (°C)	42.5		42.2	
T (ambient) (°C)	23.4		22.4	
Position (mm)	T_w	h_{ss}	T_w	h_{ss}
30	28.9	39.7	30.1	47.1
250	39.4	26.1	42.0	32.3
500	41.3		43.2	
750	-	25.6	-	32.0
1000	43.9		46.3	
1250	-		-	
1500	-	25.1	-	31.0
1750	-		-	
2000	49.5		52.1	
2500	-	25.5	-	31.5
3000	53.3		55.9	
3250	-		-	
3500	-	30.3	-	35.6
3750	-		-	
3950	54.4		57.9	

T_w in °C; h_{ss} in (W/m²°C)

TABLE V.4

HEAT TRANSFER DATA : SERIES C-4 $U_g = 6.19 \text{ m/s}$ PARTICLE SIZE DISTRIBUTION : P.S.D.: 2 (SAND) $\rho_s = 2620 \text{ kg/m}^3$

Run number	C-4.1	C-4.2	C-4.3	C-4.4	C-4.5					
W (g/s)	2.37	2.36	2.37	2.37	2.38					
W_s^B (g/s)	14.0	12.0	5.0	7.0	9.0					
Power input (W)	279.2	277.1	161.7	182.7	208.1					
P(4086) (bar abs.)	1.02	1.02	1.01	1.01	1.02					
P(8410) (bar abs.)	1.02	1.01	1.01	1.01	1.01					
T (4086) ($^{\circ}\text{C}$)	20.9	21.5	19.5	20.0	19.1					
T_{ss}^{SS} (8410) ($^{\circ}\text{C}$)	41.0	43.9	43.4	41.7	39.9					
T (ambient) ($^{\circ}\text{C}$)	20.4	21.0	20.8	20.9	19.4					
Position (mm)	T_w	h_{ss}	T_w	h_{ss}	T_w	h_{ss}	T_w	h_{ss}	T_w	h_{ss}
30	33.8	52.7	34.7	51.3	28.6	43.8	29.9	44.8	29.4	48.5
250	52.3	33.3	53.5	32.0	41.9	28.1	44.5	27.9	45.0	29.9
500	55.8	31.9	58.5	30.5	44.3	28.2	48.1	26.5	48.8	28.2
750	57.3	31.4	59.0	31.1	44.6	29.8	49.3	27.2	50.3	28.5
1000	59.1	31.3	59.7	30.8	44.9	30.4	49.5	27.6	50.7	28.5
1250	59.9	30.9	62.2	29.8	46.8	29.6	51.2	27.0	52.8	27.8
1500	62.1	31.6	64.4	30.5	48.7	30.4	53.0	27.6	54.4	28.4
1750	61.0	32.3	63.5	31.2	48.7	31.2	52.7	28.2	54.1	28.8
2000	63.1	31.3	65.6	30.2	50.5	30.4	54.7	27.3	56.2	27.8
2500	66.6	30.8	69.4	29.4	53.8	29.6	57.9	26.4	59.5	26.9
3000	-	30.8	-	29.4	-	29.6	-	26.4	-	26.9
3250	69.9	31.0	73.7	29.3	58.4	29.8	62.5	26.2	63.9	26.7
3500	70.7	31.2	74.8	29.4	59.0	30.6	63.1	26.6	64.6	27.0
3750	71.9	32.3	76.0	30.9	60.2	33.2	64.2	28.5	65.6	28.6
3950	70.2	32.3	74.6	30.9	59.1	33.2	62.9	28.5	64.4	28.6

 T_w in $^{\circ}\text{C}$, h_{ss} in ($\text{W/m}^2\text{ }^{\circ}\text{C}$)

TABLE V.4 (continued)
 HEAT TRANSFER DATA : SERIES C-4 $U_g = 6.19 \text{ m/s}$
 PARTICLE SIZE DISTRIBUTION : P.S.D. 2 (SAND) $\rho_s = 2620 \text{ kg/m}^3$

Run number	C-4.6		C-4.7		C-4.8		C-4.9		C-4.10	
W (g/s)	2.37		2.41		2.41		2.41		2.41	
W _s ^B (g/s)	3.0		4.0		5.0		6.0		12.0	
Power input (W)	111.8		131.5		159.6		173.9		257.4	
P(4086) (bar abs.)	1.02		1.06		1.06		1.06		1.06	
P(8410) (bar abs.)	1.01		1.06		1.06		1.06		1.06	
T (4086) (°C)	19.0		21.2		21.1		21.1		22.2	
T _{ss} ^B (8410) (°C)	40.5		43.1		44.6		44.0		43.0	
T (ambient) (°C)	20.0		23.8		23.2		23.2		23.2	
Position (mm)	T _w	h _{ss}	T _w	h _{ss}	T _w	h _{ss}	T _w	h _{ss}	T _w	h _{ss}
30	25.4		29.2		29.9		30.8		34.0	
		45.4		42.4		44.5		44.8		53.4
250	34.0		39.8		43.0		44.4		51.0	
		30.1		28.0		28.0		28.5		33.5
500	35.8		41.8		45.9		47.5		54.9	
		29.4		28.1		27.8		27.8		31.6
750	37.2		42.3		46.2		48.1		56.7	
		29.9		29.6		29.5		29.1		31.7
1000	38.0		42.8		46.4		48.3		57.3	
		29.7		29.9		30.1		29.6		31.4
1250	39.9		44.6		48.2		50.1		59.6	
		28.4		28.9		29.4		29.1		30.3
1500	41.7		46.4		50.0		51.8		61.7	
		28.8		29.5		30.2		29.7		31.0
1750	42.1		46.6		50.0		51.8		60.8	
		29.5		30.3		31.4		30.4		31.6
2000	43.6		48.1		51.7		53.7		63.0	
		28.3		29.5		30.4		29.6		30.6
2500	46.9		51.3		54.9		56.8		66.2	
3000		26.8		28.5		29.9		29.0		30.0
3250	51.2		55.4		59.1		61.1		70.3	
		26.5		28.5		30.2		29.1		29.9
3500	52.0		56.3		59.9		61.9		71.2	
		26.8		28.9		30.8		29.6		30.1
3750	53.3		57.4		61.1		63.0		72.2	
		28.7		31.1		33.2		31.5		31.6
3950	52.7		56.8		60.3		62.3		71.0	

T_w in °C, h_{ss} in (W/m²°C)

TABLE V.4 (continued)
 HEAT TRANSFER DATA : SERIES C-4 $U_g = 6.19 \text{ m/s}$
 PARTICLE SIZE DISTRIBUTION : P.S.D. 2 (SAND) $\rho_s = 2620 \text{ kg/m}^3$

Run number	C-4.11	C-4.12	C-4.13	C-4.14				
W (g/s)	2.37	2.42	2.42	2.41				
W_s^g (g/s)	15.0	20.0	18.0	22.0				
Power input (W)	221.5	267.0	284.0	322.5				
P(4086) (bar abs.)	1.03	1.05	1.06	1.06				
P(8410) (bar abs.)	1.02	1.04	1.05	1.05				
T_{4086} (°C)	21.7	18.5	21.4	24.7				
T_{ss}^{8410} (°C)	36.8	32.9	38.0	40.6				
T (ambient) (°C)	22.1	17.5	20.4	22.2				
Position (mm)	T_w	h_{ss}	T_w	h_{ss}	T_w	h_{ss}	T_w	h_{ss}
30	31.9	54.1	29.2	59.8	33.6	57.5	37.7	61.6
250	45.7	34.3	45.1	37.1	50.4	36.2	55.2	38.8
500	48.9	32.3	48.6	34.7	54.3	33.9	59.6	36.2
750	50.4	32.2	50.3	34.6	56.1	33.8	61.4	36.2
1000	50.8	31.9	50.5	34.4	56.5	33.4	61.4	36.3
1250	52.7	30.7	52.4	33.1	58.8	32.2	63.2	35.3
1500	54.4	31.2	54.3	33.7	60.7	32.8	65.0	36.2
1750	53.6	31.9	53.1	34.5	59.5	33.5	63.4	37.4
2000	55.2	30.7	54.8	33.2	61.5	32.3	65.0	36.1
2500	58.1	30.7	57.7	33.2	64.6	32.3	68.3	36.1
3000	-	29.8	-	32.2	-	31.4	-	35.3
3250	61.0	29.7	60.7	32.1	68.0	31.3	71.2	35.4
3500	61.7	30.0	61.2	32.4	68.7	31.5	71.8	35.7
3750	62.4	31.2	61.9	33.6	69.6	32.4	72.4	36.7
3950	61.5	31.2	61.0	33.6	69.3	32.4	72.0	36.7

T_w in °C, h_{ss} in ($W/m^2 \cdot ^\circ C$)

TABLE V.5

HEAT TRANSFER DATA : SERIES C-5 $U_g = 10.2 \text{ m/s}$ PARTICLE SIZE DISTRIBUTION : P.S.D. 2 (SAND) $\rho_s = 2620 \text{ kg/m}^3$

Run number	C-5.1	C-5.2	C-5.3	C-5.4	C-5.5					
W (g/s)	4.15	4.16	4.19	4.19	4.19					
W_s^g (g/s)	3.0	5.0	7.0	9.0	12.0					
Power input (W)	140.5	170.9	441.8	523.9	615.4					
P(4086) (bar abs.)	1.09	1.09	1.11	1.11	1.12					
P(8410) (bar abs.)	1.09	1.09	1.10	1.10	1.11					
T (4086) (°C)	22.8	22.8	20.2	22.2	23.8					
T_{ss} (8410) (°C)	43.0	42.7	63.1	66.2	66.9					
T (ambient) (°C)	24.5	24.2	21.7	22.0	22.3					
Position (mm)	T_w	h_{ss}	T_w	h_{ss}	T_w	h_{ss}	T_w	h_{ss}	T_w	h_{ss}
30	29.1	65.1	30.8	62.0	37.4	67.9	38.5	65.8	46.0	69.3
250	35.4	45.9	38.4	43.8	58.9	44.7	69.8	43.3	77.0	45.5
500	37.5	43.7	40.7	41.3	64.8	42.5	74.4	42.4	81.1	45.4
750	39.0	43.7	42.5	41.1	67.8	42.7	77.1	42.7	82.5	46.4
1000	39.9	43.8	43.3	40.7	69.5	41.8	79.0	42.2	84.2	45.9
1250	41.4	43.4	45.2	39.7	74.6	40.7	83.5	41.4	88.8	44.4
1500	42.5	43.5	46.4	39.6	76.7	41.0	85.8	41.8	92.7	44.6
1750	43.8	42.4	47.7	38.7	79.2	40.1	88.0	41.8	91.3	46.5
2000	45.5	41.7	49.4	37.8	83.4	39.3	92.4	41.5	95.8	45.7
2500	47.8	41.9	52.0	37.4	88.5	39.1	96.9	41.4	100.8	45.5
3000	51.3	41.9	55.5	37.2	96.4	38.8	104.4	41.2	109.0	45.5
3250	52.5	41.7	56.8	37.0	99.0	38.8	107.0	41.4	111.0	45.9
3500	53.7	45.8	58.0	39.2	101.5	41.8	113.2	44.0	112.0	48.1
3750	52.9	57.4	57.4	39.2	99.3	41.8	107.0	44.0	112.0	48.1

 T_w in °C, h_{ss} in ($\text{W/m}^2 \cdot ^\circ\text{C}$)

TABLE V.5 (continued)
 HEAT TRANSFER DATA : SERIES C-5 $U_g = 10.2 \text{ m/s}$
 PARTICLE SIZE DISTRIBUTION : P.S.D. 2 (SAND) $\rho_s = 2620 \text{ kg/m}^3$

Run number	C-5.6	C-5.7	C-5.8	C-5.9	C-5.10					
W (g/s)	4.17	4.24	4.23	4.23	4.29					
W_s^g (g/s)	16.0	5.0	12.0	15.0	20.0					
Power input (W)	604.5	129.9	224.1	254.5	312.4					
P(4086) (bar abs.)	1.11	1.13	1.13	1.13	1.15					
P(8410) (bar abs.)	1.10	1.13	1.12	1.12	1.14					
$T_{(4086)}$ (°C)	27.0	21.7	21.2	23.6	23.0					
T_{ss}^{ss} (8410) (°C)	61.6	36.9	37.2	39.1	38.3					
T (ambient) (°C)	22.9	23.4	21.8	23.2	20.4					
Position (mm)	T_w	h_{ss}	T_w	h_{ss}	T_w	h_{ss}	T_w	h_{ss}	T_w	h_{ss}
30	49.5		27.7		38.8		32.8		33.3	
		67.7		64.6		68.9		70.0		75.0
250	79.4		33.0		40.4		45.1		47.7	
		45.4		46.8		46.1		46.5		48.9
500	81.9		34.5		42.0		46.6		49.6	
		45.6		45.2		45.1		45.8		47.0
750	83.0		35.6		43.1		47.6		50.5	
		46.6		45.0		45.4		46.2		48.6
1000	84.0		36.4		43.7		48.1		50.8	
		46.1		44.7		44.9		45.6		48.0
1250	88.3		37.6		45.4		50.0		52.9	
		44.5		43.3		43.3		43.8		46.1
1500	91.4		38.9		47.0		51.6		54.6	
		45.5		43.9		43.8		44.4		46.9
1750	90.4		39.1		46.8		51.2		53.9	
		46.3		45.3		44.8		45.1		47.7
2000	93.9		40.1		48.2		52.8		55.7	
		45.6		44.2		43.6		44.0		46.1
2500	98.1		42.3		50.6		55.1		58.2	
3000	-	45.4	-	43.1	-	42.3	-	43.0	-	45.2
3250	104.6		45.1		54.0		58.3		61.3	
		45.3		43.2		42.2		43.0		45.2
3500	106.5		45.8		54.5		58.3		62.1	
		45.5		43.8		42.8		43.5		44.9
3750	108.2		46.6		55.3		59.6		62.7	
		46.6		45.1		44.1		44.5		46.7
3950	108.2		46.9		54.8		59.5		62.5	

T_w in °C, h_{ss} in ($W/m^2 \text{ } ^\circ\text{C}$)

TABLE V.5 (continued)
 HEAT TRANSFER DATA : SERIES C-5 $U_g = 10.2 \text{ m/s}$
 PARTICLE SIZE DISTRIBUTION : P.S.D. 2 (SAND) $\rho_s = 2620 \text{ kg/m}^3$

Run number	C-5.11	C-5.12	C-5.13	C-5.14	C-5.15					
W (g/s)	4.28	4.28	4.19	4.17	4.18					
W_s^g (g/s)	18.0	32.0	29.0	25.0	6.0					
Power input (W)	289.5	399.0	400.0	325.5	142.5					
P(4086) (bar abs.)	1.15	1.15	1.13	1.14	1.10					
P(8410) (bar abs.)	1.14	1.14	1.12	1.13	1.09					
T_{4086} ($^{\circ}\text{C}$)	19.8	24.0	33.0	29.4	24.0					
T_{ss}^{8410} ($^{\circ}\text{C}$)	35.3	37.4	47.4	42.7	39.3					
T (ambient) ($^{\circ}\text{C}$)	19.0	19.5	27.4	26.6	25.2					
Position (mm)	T_w	h_{ss}	T_w	h_{ss}	T_w	h_{ss}	T_w	h_{ss}	T_w	h_{ss}
30	29.0		35.4		44.5		38.5		29.9	
		75.6		83.8		83.6		83.6		67.9
250	43.1		52.5		61.6		53.2		36.2	
		48.5		52.9		52.9		52.5		47.1
500	44.8		55.3		64.4		55.3		37.8	
		47.5		51.2		51.4		51.0		45.1
750	45.9		56.0		65.0		56.1		39.0	
		47.8		51.8		52.2		51.5		45.3
1000	46.4		56.3		65.3		56.5		39.6	
		47.0		50.9		51.3		50.6		44.6
1250	48.5		58.5		67.7		58.5		41.2	
		45.0		48.9		49.1		48.3		42.6
1500	50.2		60.4		69.6		60.3		42.5	
		45.7		49.6		50.0		49.0		43.2
1750	49.7		59.1		68.3		59.4		42.7	
		46.4		50.5		50.8		49.6		44.2
2000	51.3		61.0		70.4		61.3		43.8	
		45.0		48.9		49.4		48.0		42.9
2500	53.9		63.4		72.6		63.4		46.1	
3000	-	43.6	-	47.5	-	48.4	-	46.7	-	41.3
3250	57.3		66.7		75.8		66.6		49.2	
		43.3		47.2		48.1		46.2		40.9
3500	57.9		67.0		76.4		67.1		49.9	
		43.9		47.8		48.6		46.7		41.4
3750	58.5		67.5		76.9		67.6		50.7	
		44.9		48.7		49.6		47.7		42.3
3950	58.7		67.5		76.9		67.7		51.1	

T_w in $^{\circ}\text{C}$, h_{ss} in ($\text{W/m}^2\text{C}$)

REFERENCES

- 1 Anderson, T.B.; Jackson, R., "A fluid mechanical description of fluidized beds", *Ind. Eng. Chem. Fundam.*, 6 (4), 527-39 (1967).
- 2 Arastoopour, H., Gidaspow, D., "Vertical pneumatic conveying using four hydrodynamic models", *Ind. Eng. Chem. Fundam.*, 18, 123-30 (1979).
- 3 Arastoopour, H., Lin, S.C., Weil, S.A., "Analysis of vertical pneumatic conveying using multiphase flow models", *A.I.Ch.E. J.*, 28 (3), 467-73 (1982).
- 4 Arundel, P.A.; Bibb, S.D.; Boothroyd, R.G., "Dispersed density distribution and extent of agglomeration in a polydisperse fine particle suspension flowing turbulently upward in a duct" *Powder Technol.*, 4, 302-312 (1970-71).
- 5 Barth, W.; "Physikalische und Wirtschaftliche Probleme des Transportes von Festteilchen in Flüssigkeiten und Gasen", *Chem. Ing. Techn.*, 32 (3), 164-71 (1960).
- 6 Batchelor, G.K.; "The stress system in a suspension of force free particles", *J. Fluid Mech.*, 41 (3), 545-70 (1970).
- 7 Bean, H.S., "Fluid meters: Their theory and applications", ASME, New-York, (1971).
- 8 Belden, D.H., Kassel, L.S., "Pressure drops encountered in conveying particles of large diameter in vertical transfer lines", *Ind. Eng. Chem.*, 41 (6), 1174-78 (1949).
- 9 Birchenough, A., Mason, J.S., "Particle wall velocity measurements in a densely flowing gas-solids suspension", *Pneumotransport 3*, BHRA, Cranfield (1976).
- 10 Boothroyd, R.G., "Pressure drop in duct flow of gaseous suspensions of fine particles", *Trans. Instn. Chem. Engrs.*, 44, T306-T313 (1966).
- 11 Boothroyd, R.G., "Turbulence characteristics of the gaseous phase in duct flow of a suspension of fine particles", *Trans. Instn. Chem. Engrs.*, 45, T297-T310 (1967).
- 12 Boothroyd, R.G., "Heat transfer in flowing gaseous suspensions", *Chem. Process Eng.*, 50 (10), 108-114 (1969).
- 13 Boothroyd, R.G., Haque, H., "Fully developed heat transfer to a gaseous suspension of particles flowing turbulently in ducts of different sizes", *J. Mech. Eng. Sci.*, 12 (3), 191-200 (1970).

- 14 Boothroyd, R.G., Haque, H., "Experimental investigation of heat transfer in the entrance region of a heated duct conveying fine particles", *Trans. Instn. Chem. Engrs.*, 48, T109-T120 (1970).
- 15 Boothroyd, R.G., "Flowing gas solids suspensions", Chapman and Hall, London (1971).
- 16 Bouré, J.A., Delhaye, J.M., "General equations and two-phase flow modeling", in *Handbook of Multiphase Systems* (Ed. G. Hetsroni), Hemisphere, New-York (1982).
- 17 Brewster, B.S., Seader, J.D., "Measuring temperature in a flowing gas-solids suspension with a thermocouple", *A.I.Ch.E. J.*, 30 (4), 676-679 (1984).
- 18 Briller, R., Peskin, R.L., in "Augmentation of Convective Heat Transfer" (Eds: A.E. Bergles, R.L. Webb), A.S.M.E, New-York 1970).
- 19 Brötz, W.J., Hiby, J.W., Müller, K.G., "Wärmeübergang auf eine Flugstaubströmung im Senkrechten Rohr sowie auf eine durchströmte Schüttgutsschicht", *Chemie. Ing. Techn.*, 30 (3), 138-143 (1958).
- 20 Capes, C.E., Nakamura, K., "Vertical pneumatic conveying: An experimental study with particles in the intermediate and turbulent flow regimes", *Can. J. Chem. Eng.*, 51, 31-38 (1973).
- 21 Chandock, S.S., Pei, D.C.T., "Particle dynamics in solids-gas flow in a vertical pipe"; *Proc. Pneumotransport 1*, BHRA, Cranfield (1971).
- 22 Chao, B.T., Sha, W.T., Soo, S.L., "On inertial coupling in dynamic equations of components in a mixture", *Int. J. Multiphase Flow*, 4, 219-223 (1978).
- 23 Chatley, H., "The pumping of granular solids in fluid suspension", *Engineering*, 230-31. (1940).
- 24 Chu, N.C., "Turbulent heat transfer of gas-solid two-phase flow in circular tubes", Ph. D. Thesis, Univ. of Washington, Seattle (1971).
- 25 Cramp, W.J., *J. Royal Soc. Arts*, 69, 283 (1920/21).
- 26 Cramp, W.J., Priestley, A., "Pneumatic grain elevators", *The Engineer*, 137, 34-36. (1924).
- 27 Curievici, D.P., Horia, D., "Experimental investigation of local heat transfer from a tube wall to a turbulently flowing gas-graphite suspension", *Buletinul Institutului Politehnic*, 16 (20), 53-64 (1970).

- 28 Danziger, W.J., "Heat transfer to fluidized gas-solids mixtures in vertical transport", *Ind. Eng. Chem. Process Des. Dev.*, 2 (4), 269-76 (1963).
- 29 Danziger, W.J., "Heat transfer to air-solids suspensions in turbulent flow", *Ind. Eng. Chem. Process Des. Dev.*, 11, 634 (1972).
- 30 Danziger, W.J., "Heat transfer to air-solids suspensions in turbulent flow: Modified correlation", *Ind. Eng. Chem. Process Des. Dev.*, 12, 396-97 (1973).
- 31 de Jong, J.A.H., "Aerated solids flow through a vertical stand-pipe below a pneumatically charged bunker", *Powder Technol.*, 12, 197-200 (1975).
- 32 Delhaye, J.M., "Equations fondamentales des écoulements diphasiques", CEA-R-3429 (1968).
- 33 Delhaye, J.M., Achard, J.L., "On the averaging operators introduced in two phase flow modeling", *Trans. Specialists Meeting on Transient Two-Phase Flow, Toronto* (1976).
- 34 Depew, C.A., Farbar, L., "Heat transfer to pneumatically conveyed glass particles of fixed size", *J. Heat Trans.*, 85, 164-69 (1963).
- 35 Depew, C.A., Kramer, T.J., "Heat transfer to flowing gas-solids mixtures", in *Advances in Heat Transfer, Vol. 9* (Eds. T.F. Irvine, J.P. Hartnett), Academic Press, New-York (1973).
- 36 Dixon, G., "Particle velocities in vertical pneumatic conveying systems", *Int. J. Multiphase Flow*, 2, 465-70 (1976).
- 37 Doig, I.D., Roper, G.H., "Air velocity profiles in the presence of cocurrently transported particles", *Ind. Eng. Chem. Fundament.*, 6 (2), 247-256 (1967).
- 38 Doig, I.D., Roper, G.H., "Contribution of the continuous and dispersed phases to the suspension of spheres by a bounded gas-solids stream", *Ind. Eng. Chem. Fundament.*, 7 (3), 459-471 (1968).
- 39 Drew, D.A., "Averaged field equations for two-phase media", *Studies in Appl. Math.*, L (2), 133-165 (1971).
- 40 Drew, D.A., Segal, L.A., "Averaged equations for two-phase flows", *Studies in Appl. Math.*, L (3), 205-231 (1971).
- 41 Duckworth, R.A., "Pressure gradient and velocity correlation and their application to design", *Proc. Pneumotransport 1, BHRA, Cranfield* (1971).

- 42 Duckworth, R.A., Kakka, R.S., "The influence of particle size on the frictional pressure drop caused by the flow of a solid-gas suspension in a pipe", Proc. Pneumotransport 1, BHRA, Cranfield (1971).
- 43 Farbar, L., "Flow characteristics of solids-gas mixtures in horizontal and vertical circular conduit", Ind. Eng. Chem., 41 (6), 1184-90 (1949).
- 44 Farbar, L., Morley, M., "Heat transfer to flowing gas-solids mixtures in a circular tube", Ind. Eng. Chem., 49 (7), 1143-50 (1957).
- 45 Farbar, L., Depew, C.A., "Heat transfer effect to gas-solids mixtures using solids spherical particles of uniform size", Ind. Eng. Chem. Fundam., 2, 134-135 (1963).
- 46 Fitremann, J.M., "Ecoulements diphasiques : théorie et application à quelques régimes d'écoulement verticaux ascendants d'un mélange gaz-liquide", Thèse de Doctorat d'Etat, Université Pierre et Marie Curie, Paris VI (1977).
- 47 Fortier, A., "Mecanique des suspensions", Masson, Paris (1967).
- 48 Fortier, A., Chen, C.P., "Ecoulement turbulent stationnaire biphasique air-solide dans un tube cylindrique à forte concentration massique", J. de Mécanique, 15 (1), 155-83 (1976).
- 49 Gasterstadt, H., "Die Experimentelle Untersuchung des Pneumatischen Förder.- Vorganges, V.D.I. Forschungsarbeiten, (265), (1924).
- 50 Ghosh, D.P., Prem Chand, J., Agr. Eng. Res., 13 (1), 29 (1968).
- 51 Gidasow, D., "Hyperbolic compressible two-phase flow equations based on stationary principles", in Two-phase transport and reactor safety (Eds T.N. Veziroglu, S. Kakac), Hemisphere, Washington, 283-298 (1976).
- 52 Gidasow, D., "A set of hyperbolic incompressible two-phase flow equations for two components", Chem. Eng. Sym. Sér., 74 (174), 186-90 (1978).
- 53 Gorbis, Z.R., Bakhtiozin, R.A., "Convective heat transfer of a graphite-in-gas suspension during internal flow through vertical canals", Sov. At. Energy, 12, 378-84 (1962).
- 54 Govier, G.W., Aziz, K., "The flow of complex mixtures in pipes", Van Nostrand, New-York (1972).
- 55 Hair, A.R., Smith, K.L., "The behavior of mixed size particles in pneumatic conveying", Mech. Chem. Eng. Trans., 8 (1), 19-23 (1972).

- 56 Hariu, O.H., Molstad, M.C., "Pressure drop in vertical transport of solids by gases, *Ind. Eng. Chem.*, 41 (6), 1148-60 (1949).
- 57 Heyde, M., "Heat transfer and minimum pressure drop in pneumatic conveying", *Ger. Chem. Eng.*, 3, 203-209 (1980).
- 58 Himmelblau, D.M., "Basic principles and calculations in Chemical Engineering", Prentice-Hall, Englewood Cliffs, N.J. (1974).
- 59 Hinkle, B.L., "Acceleration of particles and pressure drops encountered in horizontal pneumatic conveying", Ph. D. Thesis, Georgia Institute of Technology (1953).
- 60 Hinze, J.O., "Momentum and mechanical energy balance equations for a flowing homogeneous suspension with slip between the two phases", *Appl. Sci. Res.*, A11, 33-46 (1962).
- 61 Hirshfelder, J.O., Curtis, C.F., Bird, R.B., "Molecular theory of gases and liquids", John Wiley, New-York (1964).
- 62 Ishii, M., "Thermo-fluid dynamic theory of two-phase flow", Eyrolles, Paris (1975).
- 63 Jackson, R., "The mechanics of fluidized beds, Part 1: The stability of uniform fluidization", *Trans. Instn. Chem. Engrs.*, 41, 13-25 (1963).
- 64 Jepson, G., Poll, A., Smith, W., "Heat transfer from gas to wall in a gas-solids transport line", *Trans. Instn. Chem. Engrs.*, 41, T207-T211 (1963).
- 65 Jodlowski, G., "Study of minimum transport velocities for upward flow in vertical pipes", *Proc. Pneumotransport 3*, BHRA, Cranfield (1976).
- 66 Jodlowski, C., Etablissements NEU, Personal Communication (1982).
- 67 Jones, J.H., Braun, W.G., Daubert, T.E., Allendorf, H.D., "Slip velocity of particulate solids in vertical tubes", *A.I.Ch. E. J.*, 12 (6), 1070-74 (1966).
- 68 Jones, J.H., Braun, W.G., Daubert, T.E., Allendorf, H.D., "Estimation of pressure drop for vertical pneumatic transport of solids", *A.I.Ch.E. J.*, 13 (3), 608-11 (1967).
- 69 Julian, F.M., Dukler, A.E., "An eddy viscosity model for friction in gas-solids flow", *A.I.Ch.E. J.*, 11 (5), 853-58 (1965).

- 70 Kane, R.S., Weinbaum, S., Pfeffer, R., "Characteristics of dilute gas-solids suspensions in drag reducing flow", Proc. Pneumotransport 2, BHRA, Cranfield (1972).
- 71 Kays, W.H., Perkins, H.C., "Forced convection internal flow in ducts", in Handbook of Heat Transfer (Eds. W.M. Rohsenow, J.P. Hartnett), Mc Graw-Hill, New-York (1973).
- 72 Khan, J.I., Pei, D.C., "Pressure drop in vertical solid-gas suspension flow", Ind. Eng. Chem. Process Des. Dev., 12 (4), 428-31 (1973)
- 73 Kim, J.M., "Pressure drop and heat transfer in cocurrent down-flow of gas-solids suspensions", Ph. D Thesis, University of Utah, Salt Lake City (1979).
- 74 Kim, J.M., Seader, J.D., "Heat transfer to gas-solids suspensions flowing cocurrently downward in a circular tube", A.I.Ch.E J., 29 (2), 306-312 (1983).
- 75 Klinzig, G.E., "Gas-solids transport", Mc Graw-Hill, New-York (1981).
- 76 Knowlton, T.M., Bachovchin, D.M., "The determination of gas-solids pressure drop and choking velocity as a function of gas density in a vertical pneumatic conveying line" in Fluidization Technology (Ed. D.L. Keairns), Hemisphere, Washington (1976).
- 77 Konchesky, J.L., George, T.J., Craig, J.G., "Air and power requirements for the pneumatic transport of crushed coal in vertical pipelines", Trans. A.S.M.E. J. Eng. for Industry, 101-106 (1975).
- 78 Konno, H., Saito, S., "Pneumatic conveying of solids through straight pipes", J. Chem. Eng. Japan, 2 (2), 211-217 (1969).
- 79 Kramer, T.J., "A study of the mean flow characteristics of gas-solids suspension flowing in vertical tubes", Ph. D. Thesis, University of Washington (1970).
- 80 Kraus, M.N., "Pneumatic conveying of bulk materials", Ronald Press, New-York (1968).
- 81 Kunii, D., Levenspiel, O., "Fluidization Engineering", Krieger, Huntington, New-York (1977).
- 82 Lapple, C.E., Shepard, C.B., "Calculation of particle trajectories", Ind. Eng. Chem., 32, 605-617 (1940).
- 83 Leung, L.S., Wiles, R.J., "A quantitative design procedure for vertical pneumatic conveying systems", Ind. Eng. Chem. Process Des. Dev., 15 (4), 552-57 (1976).

- 84 Maeda, M., Saigusa, T., Ikai, S., "Study of heat transfer to gas-solids suspension - Part 1 : Influence of free turbulence on heat transfer", Bull. J.S.M.E., 19 (137), 1317-1325 (1976).
- 85 Mamaev, V.V., Nosov, V.S., Syromyatnikov, N.I., Barbolin, V.S., "Heat transfer of gas-suspension flow in horizontal and vertical tubes", Inzhenero-Fizicheskii Zhurnal, 31 (4), 613-618 (1976).
- 86 Matsumoto, S., Ohnishi, S., Maeda, S., "Heat transfer to vertical gas-solids suspension flows", J. Chem. Eng. Japan, 11 (2), 89-95 (1978).
- 87 Matsumoto, S., Takahashi, A., Suzuki, M., Maeda, S., "Gas temperature distribution and eddy diffusivity of heat in gaseous suspension flow", J. Chem. Eng. Japan, 12 (3), 183-89 (1979).
- 88 Mehta, N.C., Smith, J.M., Comings, E.W., "Pressure drop in air-solids flow systems", Ind. Eng. Chem., 49 (6), 986-992 (1957).
- 89 Mickley, H.S., Trilling, C.A., "Heat transfer characteristics of fluidized beds", Ind. Eng. Chem., 41, 1135-47 (1949).
- 90 Molodtsov, Y., "General equations of gas-solids flow", Université de Compiègne Publication, Compiègne (1982).
- 91 Molodtsov, Y., Muzyka, D.W., "General probabilistic multiphase flow equations", Université de Compiègne Publication, Compiègne (1983).
- 92 Molodtsov, Y., Muzyka, D.W., Large, J.F., Bergougnou, M.A., "The use of asymptotic similar solutions to probabilistic multiphase flow equations to predict heat transfer rates to dilute gas-solids suspension", 16th Int. Centre for Heat and Mass Transfer Symp., Dubrovnik, (Sept. 1984).
- 93 Molodtsov, Y., "Equations generales probabilistes des mélanges polyphasiques et application aux systèmes gaz-solides", Thèse de Doctorat d'Etat, Université de Compiègne, Compiègne (1985).
- 94 Murray, J.D., "On the mathematics of fluidization, Part 1 : Fundamental equations and wave propagation", J. Fluid Mech., 21 (2), 465-93 (1963).
- 95 Nag, P.K., Rao, D.N., "Heat transfer from gas-solids suspensions", Proc. 4th Nat. Heat Mass Trans. Conf., Prakashan, India (1977).
- 96 Nakamura, K., Capes, C.E., "Vertical pneumatic conveying : a theoretical study of uniform and annular flow models", Can. J. Chem. Eng., 51, 39-46 (1973).

- 97 Nakamura, K., Capes, C.E., "Vertical pneumatic conveying of binary particle mixtures", in Fluidization Technology (Ed. D.L. Keairns), Hemisphere, Washington (1976).
- 98 Ottjes, J.A., Meeuse, G.C., van Kuijk, G.J.L., "Particle velocity and pressure drop in horizontal and vertical pipes", Proc. Pneumotransport 3, BHRA, Bath (1976).
- 99 Panton, R., "Flow properties for the continuum point of view of a non-equilibrium gas-particle mixture", J. Fluid Mech., 31 (2), 273-303 (1968).
- 100 Perry, R., Chilton, C., "Chemical Engineers' Handbook", Mc Graw-Hill, New-York (1973).
- 101 Peters, L.K., Klinzig, G.E., "Friction in turbulent flow of solids-gas systems", Can. J. Chem. Eng. 50, 441-444 (1972).
- 102 Pfeffer, R., Rossetti, S., Lieblein, S., "Analysis and correlation of heat transfer coefficient and friction factor data for dilute gas-solid suspensions", NASA TN D-3603, N66 35647 (1966).
- 103 Ranz, W.E., Marshall, W.R., "Evaporation from drops", Chem. Eng. Progr., 48, 141-45 (A52).
- 104 Rao, C.S., "Study of the mechanism of turbulent gas-solids flow pressure drop : Reynolds equations for solids laden gas streams and solids phase momentum equations for turbulent flow", Indian J. Technol., 14, 361-68 (1976).
- 105 Razumov, I.M., "Calculating pneumatic transport of solid catalysts", Int. Chem. Eng., 2 (4), 539-43 (1962).
- 106 Reddy, K.V.S., Pei, D.C.T., "Particle dynamics in solids-gas flow in vertical pipes", Ind. Eng. Chem. Fundam., 8 (3), 490-97 (1969).
- 107 Richards, P.C., Wierma, S., "Pressure drop in vertical pneumatic conveying", Proc. Pneumotransport 2, BHRA, Cranfield (1972).
- 108 Richardson, J.F., Zaki, W.N., "Sedimentation and fluidization", Trans. Instn. Chem. Engrs., 32, 35-53 (1954).
- 109 Rose, H.E., Barnacle, H.E., "Flow of suspensions of non-cohesive spherical particles in pipes", The Engineer, 898-901, 939-940 (1957).
- 110 Rose, H.E., Duckworth, R.A., "Transport of solid particles in liquids and gases", The Engineer, 227, 393-97, 430-33, 478-83 (1969).

- 111 Rosetti, S.J., Pfeffer, R., "Drag reduction in dilute flowing gas-solids suspensions", A.I.Ch.E. J., 18, 31-36 (1972).
- 112 Sadek, S.E., "Heat transfer to air-solids suspensions in turbulent flow", Ind. Eng. Chem. Process Des. Dev., 11 (1), 133-135 (1972).
- 113 Sadek, S.E., "Heat transfer to air-solids suspensions in turbulent flow: Modified correlation", Ind. Eng. Chem. Process Des. Dev., 11, 635 (1972).
- 114 Sadek, S.E., "Heat transfer to air-solids suspensions in turbulent flow: Modified equations", Ind. Eng. Chem. Process Des. Dev., 12, 397-98 (1973).
- 115 Schluderberg, D.C., Whitelaw, R.L., Carlson, R.W., "Gaseous suspensions: A new reactor coolant", Nucleonics, 19 (8), 67-94 (1961).
- 116 Schuchart, P., "Pneumatic Conveying" Chem. Eng. Sym. Series (27), 65-72 (1968).
- 117 Segler, W., "Untersuchungen an Kornergebläsen und Grundlagen für ihre Berechnung", Weibold, Mannheim (1934).
- 118 Sha, W.T., Soo, S.L., "Multidomain multiphase fluid mechanics", Int. J. Heat Mass Transfer, 21, 1581-1595 (1978).
- 119 Shimizu, A., Echigo, R., Hasegawa, S., "Experimental study on the pressure drop and entry length of the gas-solid suspension flow in a circular tube", Int. J. Multiphase Flow, 4, 53-64 (1978).
- 120 Singh, B., "Analysis of pressure drop in vertical pneumatic conveying: Generalized approach for gas-particle and liquid-particle systems", Powder Technol., 32 (2), 179-182 (1982).
- 121 Solbrig, C.W., Hughes, E.D., "Governing equations for serialized continuum: an unequal velocity model for two phase flow", in Two-Phase Transport and Reactor Safety (Eds. T.M. Veziroglu, S. Kakac), Hemisphere, Washington (1976).
- 122 Soo, S.L., Trezek, G.J., "Turbulent pipe flow of magnesia particles in air", Ind. Eng. Chem. Fundam., 5, 388-392 (1966).
- 123 Soo, S.L., "Fluid dynamics of multiphase systems", Blaisdell, Waltham, Mass. (1967).
- 124 Soo, S.L., "On the nature of equations of multiphase multidomain mechanics", Proc. 2nd Multiphase Flow and Heat transfer Workshop, Miami (1979).

- 125 Soo, S.L., "Design of pneumatic conveying systems", J. Powder Bulk Solids Technol., 4, 33-43 (1980).
- 126 Stermerding, S., "The pneumatic transport of cracking catalyst in vertical risers", Chem. Eng. Sci., 17, 599-608 (1962).
- 127 Stockburger, D., "Transfert thermique entre une paroi tubulaire et un mélange gaz-solides en écoulement turbulent", VDI Cahier de Recherches, 518 (1966).
- 128 Teo, C.S., Chong, Y.O., "Pressure drop in vertical pneumatic conveying", Powder Technol., 38(2), 175-76 (1984).
- 129 Tien, C.L., "Heat transfer by a turbulently flowing fluid-solids mixtures in a pipe", J. Heat Transfer, 5, 183-88 (1961).
- 130 Tien, C.L., Quan, V., "Local heat transfer characteristics of air-glass and air lead mixtures in turbulent pipe flow", A.S.M.E. 62-HT-15, 1-9 (1962).
- 131 Tomita, Y., Yatanni, S., Jotaki, T., "Pressure drop in vertical transport lines of powdery material at high solids loading", Powder Technol., 25, 101-107 (1980).
- 132 Torobin, L.B., Gauvin, W.H., "Fundamental aspects of solids-gas flow", Can. J. Chem. Eng., 37, 29-41 (1959)
- 133 Tsuji, Y., Morikawa, Y., Shiomi, H., "LDV measurements of an air-solid two phase flow in a vertical pipe", J. Fluid Mech., 139, 417-434 (1984).
- 134 Van Deemter, J.J., Van der Laan, E.T., "Momentum and energy balances for dispersed two-phase flow", Appl. Sci. Res., A10, 102-108 (1961).
- 135 Van Swaaij, W.P.M., Buurman, C., Van Breugel, J.W., "Shear stresses on the wall of a dense gas-solids riser", Chem. Eng. Sci., 25, 1818-20 (1970).
- 136 Van Zoonen, D., "Measurements of diffusional phenomena and velocity profiles in a vertical riser", Proc. Sym. Interaction between Fluids and Particles, London (1962).
- 137 Vogt, E.G., White, R.R., "Friction in the flow of suspensions: Granular solids in gases through pipe", Ind. Eng. Chem., 40 (9), 1731-38 (1948).
- 138 Wahi, M.K., "Heat transfer to flowing gas-solid mixtures", J. Heat Transfer, 2, 145-48 (1977).
- 139 Wen, C.Y., Yu, Y.H., Chem. Eng. Progr. Sym. Series, 62 (62), 101 (1966).

- 140 Wen, C.Y., Galli, A.F., in Fluidization, (Eds. J.F. Davidson, D. Harrison), Academic Press, London (1971).
- 141 Wen, C.Y., O'Brien, W.S., "Pneumatic conveying and transport" in Gas-Solids Handling in the Process Industries, (Eds. J.M. Marchello and A. Gometplata), Marcel Dekker, New-York, 89-134 (1976).
- 142 Wen, C.Y., in Bulk materials handling, (Ed. M.C. Hawk), University of Pittsburgh Engineering Publishing Series, Pittsburgh (1971).
- 143 Whitaker, S., "The transport equations for multiphase systems", Chem. Eng. Sci., 28, 139-147 (1973).
- 144 Wilkinson, B.E.; Norman, J.R., "Heat transfer to a suspension of solids in a gas", Trans. Instn. Chem. Engrs., 45, T314-T318 (1967).
- 145 Wood, S.A., Bailey, A., Proc. Instn. Mech. Engrs., 142, 149 (1939).
- 146 Yang, W.C., "Estimating the solid particle velocity in vertical pneumatic conveying lines", Ind. Eng. Chem. Fundam., 12 (3), 349-52 (1973).
- 147 Yang, W.C., "Correlations for solid friction factors in vertical and horizontal pneumatic conveyings", A.I.Ch.E. J., 20 (3), 605-607 (1974).
- 148 Yang, W.C., "A unified theory on dilute phase pneumatic transport", J. Powder Bulk Solids Technol., 1, 89-95 (1977).
- 149 Yang, W.C., "A correlation for solid friction factor in vertical pneumatic conveying lines", A.I.Ch.E. J., 24 (3), 548-551 (1978).
- 150 Yousfi, Y., "Contribution a l'étude d'un réacteur à transport pneumatique : Hydrodynamique et transfert de chaleur", Thèse de Doctorat d'Etat, Université de Nancy (1973).
- 151 Yousfi, Y., Gau, G., Le Goff, P., "Heat transfer to an air-solid suspension at high concentration and low velocity", Heat Transfer, 5, 218-222 (1974).
- 152 Yousfi, Y., Gau, G., "Aérodynamique de l'écoulement vertical de suspensions concentrées gaz-solides", Chem. Eng. Sci., 29, 1939-1954 (1974).
- 153 Zenz, F.A., "Two-phase fluid-solid flow", Ind. Eng. Chem., 41 (12), 2801-2806 (1979).

- 154 Zenz, F.A., Othmer, D.F., "Fluidization and fluid-particle systems", Reinhold, New-York (1960).
- 155 Zuber, N., "On the dispersed flow in the laminar flow regime", Chem. Eng. Sci., 19, 897-902 (1964).

END

1 | 1 | 0 | 3 | 8 | 6

FIN